Defining the heterogeneity of steroid responses, and their safety in glioblastoma

Kathryn Amy McGinnis

Submitted in accordance with the requirements for the degree of
Doctor of Philosophy

The University of Leeds

School of Medicine

September 2020

Copyright Declaration

Acknowledgements

A page isn't enough space to thank all of the people who have contributed to this thesis, but here goes. Firstly, to my supervisor Laura Matthews, for her endless enthusiasm and ideas on the project. More than that though, thank you for your encouragement, your patience, and for building my confidence as a scientist, and as a person. To my co-supervisor, Jacquelyn Bond, thank you for your support, and for reading over some very rough drafts of what follows. Also thanks to Graham Cook, and the Cook group for great questions and advice during weekly lab meetings. Thank you to Syed Murtaza Baker, Bharat Rash and Andy Hayes at the University of Manchester for their help in the sequencing experiments.

More broadly, thank you to the Matthews group, past and present, in particular Fiona Leslie and Freya Leif. We have been, and hopefully will continue to be, a great team. I'm so sorry for the continual mess on my lab bench. Thanks also to Level 5 as a whole – I started on the floor without any other PhD students or post-docs in my group, and you all took me under your collective wing and showed me the ropes, gave me tips, and made me laugh about even my most embarrassing mistakes. Some of my most enlightening conversations, scientific and otherwise, were spent during morning coffee, lunch breaks, and 3pm coffee time (although in writing that down, how did we have time to do any science?!). I could not have done it without you all.

And to my family – there are not enough words to explain my love and gratitude. To Mum, thank you for always being available for a chat, and for fighting the world on my behalf. We have been through hell together, and I hope you know that your love and support have propelled me here. Your care packages of cards and

chocolate mean more than you could ever know. Dad, thank you for always making me laugh, in particular, for "if you keep accidentally killing your cells, surely that means you've cured cancer?" Sadly, if that were true, this thesis would be much shorter. You have been a pillar of strength over recent months, and an eternal example of kindness and strength. Thank you both for instilling the importance of education, however, I do realise 8 years of higher education is taking it a bit far. I love you both so very much. To Laura, my big sister and my best friend. You have always forged the way for us both, in education and in so many other ways, and have been able to empathise with me at every stage of this process, even though I ignored your advice not to do a PhD. Finishing a thesis during a global lockdown has been difficult for many reasons, but the hardest by far has been not being able to see you all. Just know you three have been with me at every moment of this journey.

Finally, I would like to thank my fiancé Luke. You have contributed to this thesis in more ways than I can count – you have let me cry when experiments haven't worked, have come to the lab with me on weekends, and listened to me practice presentations until you almost knew them by heart. Thank you for the hugs, the encouragement, and for believing in my abilities even when I didn't. You have been a constant source of confidence, love, and food. I wouldn't have finished this without you.

There are countless others who have helped along this journey, both knowingly and unknowingly. Thank you. When the world has returned to normal, I look forward to celebrating with all of you.

Abstract

Synthetic glucocorticoids (Gc) are anti-inflammatory agents, which are commonly used in cancer treatment. Glioblastoma (GBM) is an aggressive form of brain cancer with a median survival of 15 months. Dexamethasone, a potent Gc, is used to reduce oedema, however, patients prescribed high doses of Dexamethasone have reduced survival times. Despite the widespread use of Gc, much of their mechanism of action is still unclear, and their effects are tissue-specific. This project has therefore aimed to investigate Gc function in the context of GBM.

Gc activate the glucocorticoid receptor (GR), a ligand activated transcription factor. Through RNA sequencing, Gc were predicted to affect DNA repair pathways in GBM, through control of p53 effectors. We demonstrated that Gc treatment increased DNA repair within GBM cells. This is relevant in the context of GBM treatment, as radiotherapy and chemotherapy both rely on the induction of DNA damage to induce GBM cell death. Screening selective steroids which fail to induce these transcriptional targets shows promise in maintaining beneficial anti-inflammatory effects while maintaining efficacy of standard treatments.

Evidence is emerging that tumour cell populations show plasticity and can therefore adapt their response over time, and evade cancer treatment. Understanding the underlying mechanisms that control Gc responses at the single cell level is therefore essential to understand Gc action *in vivo*. Single cell RNA sequencing revealed that even within a clonal cell population, gene expression was variable. While the expression of GR correlated with the expression of GR target genes, there was less correlation between GR target genes suggesting importance of other unidentified factors.

This work uncovered a new mechanism of GR action through DNA repair, and revealed for the first time how Gc responses are controlled at a single cell level. These insights will lead to improved treatment strategies for GBM and allow for the further study of factors which modulate the Gc response in individual cells.

Table of Contents

List of Figures

List of Tables

Abbreviations

ACTB	β-actin
ACTH	Adrenocorticotrophin hormone
ADPRHL1	ADP-ribosylhydrolase like 1
AF-1	Activation Function-1
AF-2	Activation Function-2
AMIGO2	Adhesion molecule with Ig-like domain 2
ANKRD1	Ankyrin repeat domain 1
ANOVA	Analysis of variance
AP-1	Activator protein-1
AR	Androgen receptor
ARL4C	ADP ribosylation like GTPase 4C
ARMC8	Armadillo repeat containing 8
ATM	Ataxia telangiectasia mutated
ATR	Ataxia telangiectasia Rad3-related
B3GNT5	Beta-1,3-N-acetylglucosaminyltransferase 5
BBB	Blood-brain barrier
BCA	Bicinchonic Acid
BCL2L1	B-cell lymphoma 2 like protein 1
BCL6	B-cell lymphoma 6
BIRC3	Baculoviral IAP repeat containing 3
BRCA1	Breast cancer type 1 susceptibility protein
BRCA2	Breast cancer type 2 susceptibility protein
BSA	Bovine serum albumin
c-src	Proto-oncogene tyrosine-protein kinase Src
CBP	CREB binding protein
CDKN1A	Cyclin dependent kinase inhibitor 1A
CDKN2A	Cyclin dependent kinase inhibitor 2A
CEBPB	CCAAT enhancer binding protein β
CEBPD	CCAAT enhancer binding protein δ
ChIP-seq	Chromatin immunoprecipitation-sequencing
Chk1	Checkpoint kinase 1
Chk2	Checkpoint kinase 2

CpA	Compound A
CRH	Corticotrophin releasing hormone
CSS	Charcoal stripped serum
CtIP	C terminal binding protein 1 interacting protein
CTGF	Connective tissue growth factor
DBD	DNA binding domain
DDIT4	DNA damage inducible transcript 4
DE	Differentially expressed
Dex	Dexamethasone
DMEM	Dulbecco's modified eagle medium
DMSO	Dimethyl sulfoxide
DNAJB4	DNaJ homolog subfamily B member 4
DNA-PK	DNA-dependent protein kinase
DNA-PKcs	DNA-dependent protein kinase catalytic subunit
DPBS	Dulbecco's phosphate buffered saline
DSB	Double stranded breaks
DUSP1	Dual specificity protein phosphatase 1
E2F7	E2F transcription factor 7
EGFR	Epidermal growth factor receptor
ERRFI1	ERBB receptor feedback inhibitor 1
FACS	Fluorescence activated cell sorting
FCS	Foetal calf serum
FDR	False discovery rate
FKBP5	FK506 binding protein 5
FSTL3	Follistatin Like 3
GAPDH	Glyceraldehyde 3-phosphate dehydrogenase
GBM	Glioblastoma
Gc	Glucocorticoid
GILZ	Glucocorticoid-induced leucine zipper
GR	Glucocorticoid receptor
GRE	Glucocorticoid response element
GRIP1	Glucocorticoid receptor interacting protein 1
H2AX	H2A family member X
HBEGF	Heparin binding EGF like growth factor

HC	Hydrocortisone
HDAC	Histone deacetylase
HDAC6	Histone deacetylase 6
HNF	Hepatocyte nuclear factor
HOXC13	Homeobox C13
HPA axis	Hypothalamic–pituitary–adrenal axis
HR	Homologous recombination
HRP	Horseradish peroxidase
HSP	Heat shock protein
IF	Immunofluorescence
IHC	Immunohistochemistry
IL1β	Interleukin 1β
IL2	Interleukin 2
IL6	Interleukin 6
IL7	Interleukin 7
IL8	Interleukin 8
IR	Irradiation
JNK	c-JUN N-terminal kinases
KLF6	Kruppel like factor 6
KLF9	Kruppel like factor 9
LBD	Ligand binding domain
LE	Loteprednol etabonate
MAD	Median absolute deviations
MAPK	Mitogen activated protein kinase
MGMT	O^6-methylguanine–DNA methyltransferase
MMR	Mismatch repair
MR	Mineralocorticoid receptor
MRN	MRE11-Rad50-NBS1
mRNA	Messenger RNA
MT2A	Metallothionein 2A
MTT	3-(4,5-dimethylthiazol-2-yl)-2,5-diphenyltetrazolium bromide
NCoR	Nuclear receptor corepressor
NFκB	Nuclear factor kappa B

NFKBIA	NFκB inhibitor alpha
nGRE	Negative glucocorticoid response element
NHEJ	Non homologous end joining
NNMT	Nicotinamide N-methyltransferase
NR	Nuclear receptor
NR3C1	Nuclear receptor subfamily C member 1 (glucocorticoid receptor)
NR3C2	Nuclear receptor subfamily C member 2 (mineralocorticoid receptor)
NRE	NFκB response element
NRS	Nuclear retention signal
NTD	N-terminal transactivation domain
PBS	Phosphate buffered saline
PCA	Principal component analysis
PER1	Period circadian regulator 1
PI	Propidium iodide
PI3K	Phosphoinositide 3-kinase
PIKK	Phosphatidyl inositol 3' kinase-related kinase
PKA	Protein kinase A
PKB	Protein kinase B
PKC	Protein kinase C
PLAU	Plasminogen activator urokinase
PR	Progesterone receptor
PTM	Post-translational modification
PVN	Paraventricular nucleus
QC	Quality control
RGCC	Regulator of cell cycle
RIPA	Radioimmunoprecipitation assay
ROI	Region of interest
RNA	Ribonucleic acid
RNA-seq	RNA sequencing
RPA	Replication protein A
RQ	Relative quantification
RT	Reverse transcriptase

SAPK	Stress activated protein kinase
SCID	Severe combined immunodeficiency
SCN	Superchiasmatic nucleus
scRNA-seq	Single cell RNA sequencing
SDS	Sodium dodecyl sulfate
SEGRM	Selective GR modulators
SEM	Standard error of the mean
SERPINE1	Serpin family E member 1
siNT	Small interfering RNA, non-targeting
siRNA	Small interfering RNA
smFISH	Single molecule fluorescence In Situ hybridization
SMRT	Silencing mediator for retinoid or thyroid-hormone receptors
SNAI2	SNAIL family transcriptional repressor 2
SRC	Steroid receptor coativator
SSB	Single stranded break
ssDNA	Single stranded DNA
TBP	TATA binding protein
TCGA	The Cancer Genome Atlas
TERT	Telomerase reverse transcriptase
TFIIB	Transcription factor II B
TNF-α	Tumour necrosis factor
t-sne	T-distributed Stochastic Neighbour Embedding
TF	Transcription factor
TMZ	Temozolomide
TNFRSF11B	TNF receptor subfamily member 11b
TTFields	Tumour-treating alternating fields
VCAM1	Vascular Cell Adhesion Molecule 1
VEGF	Vascular endothelial growth factor
WB	Western blotting
WRN	Werner syndrome ATP-dependent helicase
XLF	XRCC4-like factor
XRCC4	X-Ray Repair Cross Complementing 4

Chapter 1 Introduction

1.1 Glucocorticoids

Homeostasis is defined as the maintenance of multiple processes within the body within a defined optimal range. This can include maintaining glucose levels, salt concentrations, and temperature (1). Constraining physiology within these optimal ranges safeguards against extremes, and is a highly regulated process. Tissue homeostasis requires the coordination and integration of a complex network of cues that range from individual signalling pathways, intracellular responses, autocrine and paracrine signals and endocrine systems. Glucocorticoids (Gc) are a class of steroid hormones discovered in the 1940s, which play a key role in the maintenance of homeostasis (1). They were originally named for their role in gluconeogenesis, and thus in controlling glucose levels, but in the decades that followed, their effects have been shown to be wide-ranging and complex. Indeed, we now know they affect every tissue within the body, often driving variable effects depending on the tissue in question, and the tissue microenvironment. Cortisol is the endogenous Gc found within humans, and its circulating levels rise and fall within a 24-hour cycle. As this cycle is synchronised to the day/night cycle, this is known as a diurnal rhythm. Peak cortisol occurs at the onset of waking, and so peak cortisol is measured in the morning in humans, and late evening in rodents (2). Cortisol regulates various aspects of physiology including mood, sleep, vascular tone, feeding, energy metabolism and immune function. Diurnal changes in circulating cortisol drive diurnal rhythms in these process, which underlies the circadian rhythm observed

across many tissues. Cortisol is also released under conditions of psychological or physical stress. While the magnitude of this response is greater, the purpose is the same, to mobilise energy, coordinate (and constrain) the immune response and restore balance. For over 60 years, these potent anti-inflammatory effects have been harnessed through the development of synthetic Gc which are a common first-line treatment for many inflammatory conditions. A range of synthetic Gc are in widespread clinical use, depending on their delivery, efficacy and side effect profiles, and several are listed within the World Health Organisation's list of Essential Medicines (3).

1.1.1 Hypothalamic–pituitary–adrenal axis

Due to the broad effects of cortisol on multiple tissues, production is tightly controlled at multiple levels of regulation. Much of this regulation is controlled by the hypothalamic–pituitary–adrenal (HPA) axis (Fig. 1.1). The first step of cortisol production requires either the uptake of cholesterol in the adrenal glands from dietary cholesterol, transported via low-density lipoproteins, or the *de novo* production of cholesterol within the adrenal cortex (4). The suprachiasmatic nucleus (SCN), the central circadian pacemaker in the brain, is capable of stimulating the paraventricular nucleus (PVN) within the hypothalamus. The PVN is stimulated to release both corticotrophin-releasing hormone (CRH) and arginine vasopressin (5). Both hormones then act on the anterior pituitary to release adrenocorticotrophin hormone (ACTH), the key regulator of cortisol production. Finally, within the adrenal cortex, ACTH stimulates cortisol production from cholesterol within the zona fasciculata via a series of stepwise enzymatic reactions (6, 7). Cortisol cannot be stored prior to activation, and so upon synthesis, is immediately released into the circulation. Once in the circulation,

cortisol then acts upon multiple tissues to modulate physiology and also switches off its own production by targeting the HPA axis, as part of a negative feedback loop. Cortisol inhibits release of both CRH and ACTH, preventing excessive cortisol production and resulting in a pulsatile pattern of cortisol release (8). Once in the circulation there is another level of control as cortisol availability to tissues is further determined by levels of corticosteroid binding globulin and albumin, which bind to approximately around 95% of circulating cortisol, restricting its uptake into target cells (9).
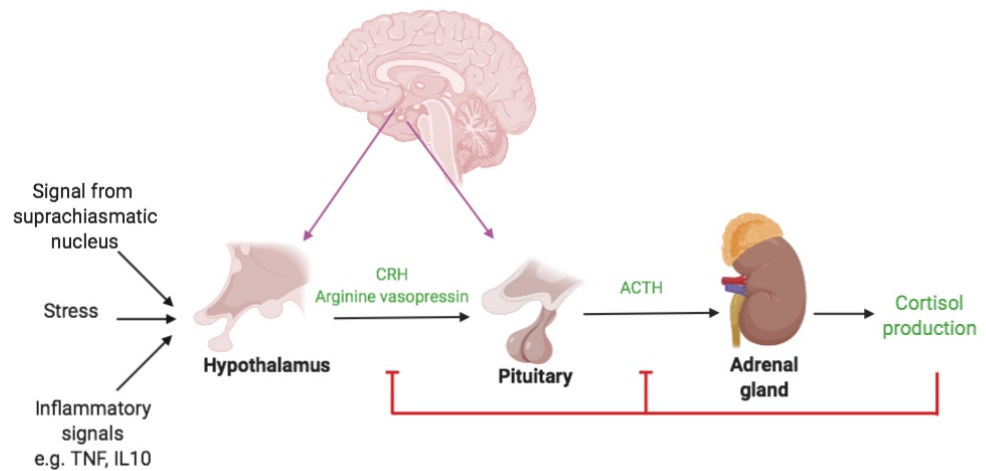
Figure 1.1: Cortisol production is controlled by the HPA axis. Signals converge within the hypothalamus to increase production of CRH and arginine vasopressin, which in turn induce ACTH production from the anterior pituitary. ACTH then stimulates cortisol production from the adrenal glands, which then inhibits multiple steps within the HPA axis. Information obtained from (1, 8, 10).

As previously mentioned, cortisol levels fluctuate with a diurnal rhythm, however, they are also under dynamic control, and can rapidly increase following a stressor, whether physical or psychological. Cortisol is therefore a primary mediator of the stress response. Stress can be defined as a factor, internal or external, which poses a threat to homeostasis, for example, infection, extreme

temperature, or injury (8, 11). These signals are interpreted at the level of the hypothalamus, activating the HPA axis, leading to increased cortisol production. As cortisol must first be synthesised prior to release, this causes a time delay, meaning that cortisol levels peak relatively late in the stress response. In this context cortisol plays an essential role to limit the physiological response to the stressor and facilitate tissue repair, i.e. to restore tissue homeostasis.

1.1.2 Synthetic Gc in clinical applications

As previously mentioned, Gc are widely used within the clinic. These have revolutionised the treatment of a multitude of inflammatory conditions, and studies have shown that 0.9% of the UK population were prescribed a Gc treatment in a single year (12). Synthetic Gc are capable of rapidly reducing inflammation in a range of inflammatory disorders, however, they are not controlled in the same manner as endogenous cortisol. Cortisol, for instance, has a biological half-life of 8 - 12 hours, whereas for Dexamethasone (Dex), a potent synthetic Gc, this is increased to 36 – 72 hours (13, 14). Whilst cortisol levels are therefore capable of fluctuating throughout a 24 hour cycle, synthetic Gc administration can lead to constitutive activation of the Gc response, and its downstream functions. Synthetic Gc administration is also not under the control of the HPA axis. This means that the homeostasis of the system is removed, resulting in hyperactivation of Gc functions.

For this reason, many of the side effects of Gc treatment are extremes of homeostatic cortisol functions. For instance, hyperactivation of the wake/sleep cycle leads to insomnia in Gc-administered patients, and neural effects result in mood disorders, such as depression and psychosis (15). Effects on vascular tone

result in side effects of hypertension and glaucoma (16, 17). Finally, even when the suppression of inflammation is the reason for Gc prescription, this can also lead to unwanted side effects. Immune system suppression increases risk of secondary infections for chronic Gc patients, and wound healing is impaired (18). In order to understand these side effects, it is necessary to understand the effects of cortisol within homeostatic conditions.

1.1.3 Effects of Gc on metabolism

Glucocorticoids were originally named based on their effects on glucose metabolism, and they form a key level of control on circulating glucose levels. Cortisol levels are increased under conditions of physiological stress, such as fasting, and its effects lead to the production of glucose, and changes to glucose uptake within tissues in order to preserve energy (19).

Within the liver, GR activation leads to gluconeogenesis through upregulation of key glucose metabolism genes, increasing the conversion of precursors such as lactate to glucose via the production of pyruvate (10, 20). This increase in glucose production results in increased plasma glucose levels, preventing hypoglycaemia. These increased glucose levels are maintained through the effects of cortisol in peripheral tissue. Glucose uptake is reduced within skeletal muscle and adipose tissue (21, 22). These tissues may use alternative energy sources, whereas the brain can only utilise glucose for metabolism. By tipping these balances, cortisol may keep safeguard the glucose supply for the brain. In addition, Gc can also exert effects on lipid metabolism through multiple mechanisms. Gc increase lipid mobilization within skeletal muscle, and increase

expression of fatty acid synthase in hepatocytes, resulting in *de novo* lipid production (23, 24).

Another important mechanism by which Gc can alter metabolism is through effects on mitochondrial function. The glucocorticoid receptor (GR), the receptor by which Gc modulate the majority of their effects, is capable of translocation to the mitochondria (25, 26). Human mitochondrial genes have been shown to contain sequences similar to nuclear Gc response elements, suggesting GR is capable of controlling mitochondrial gene expression (27). Indeed expression of GRγ, an isoform of GR, has been shown to increase mitochondrial mass, suggesting GR may play a key role in determining ATP production and metabolism (28). Through these complex mechanisms, Gc are capable of increasing energy supplies to tissue, in order to ensure metabolic demands can be met.

1.1.4 Immune effects of Gc

One of the hallmarks of the immune response is the multiple, redundant mechanisms by which the immune system may be activated. These mechanisms include the direct recognition of foreign organisms, recognition of infected cells, or cells undergoing other forms of stress. These varied signals are recognised by a spectrum of receptors, such as Toll-like receptors, and NOD-like receptors. The activation of these receptors leads to the eventual activation of proinflammatory transcription factors, such as Nuclear Factor κB (NFκB) and mitogen/stress activated protein (MAP/SAP) kinases, such as ERK and JNK (29). These transcription factors ultimately drive the production of proinflammatory mediators, such as interferons chemokines and cytokines. These mediators lead to the

recruitment and activation of both innate and adaptive immune cells, and destruction of the pathogen. Whilst this system protects the body from potentially dangerous infections, an inflammatory response, when out of control, can lead to the destruction of tissue, and the development of autoimmune conditions or chronic inflammatory disease. It is therefore imperative that this inflammation can be quickly and effectively controlled. Gc are a robust, conserved mechanism by which inflammation can be limited, and homeostatic balance restored.

The effects of Gc in inhibiting proinflammatory gene expression through the inhibition of NFκB and Activator Protein-1 (AP-1) have been well documented, and are a major point of control within many tissues (30). Glucocorticoids also affect immune cells directly to inhibit or alter their function.

Within the innate immune system, glucocorticoids inhibit the recruitment of macrophages and neutrophils to the site of inflammation, by inhibiting the expression of chemokines, such as CXCL-1 and CXCL-2 (31, 32). At the site of injury, the functions of macrophages and neutrophils are inhibited through increased expression of Annexin A1 and GILZ, resulting in inhibition of macrophage cytokine secretion, and inhibition of neutrophil degranulation (33, 34). In turn, this reduction in expression of inflammatory mediators reduces the activation of adaptive immunity, and drives the immune system towards a reparative, tolerant phenotype.

1.1.5 Effects of Gc in the brain

GR expression is relatively abundant in the brain, however, its expression does vary between regions. GR expression is high within the hypothalamus as part of

the feedback loops required to restrict activation of the HPA axis (Section 1.1.1). GR also plays a critical role in controlling memory and learning through its expression in the limbic system. Within the amygdala, for instance, Gc treatment has been shown to lead to neuronal hypertrophy, a phenomenon usually associated with a reduction in memory and increased stress (35). These effects, however, appear to be dose- and time-dependent, as a timed, low dose of corticosterone reduced anxiety in rats, and treatment of patients with Gc within an hour of traffic accidents was correlated with reduced PTSD symptoms (36, 37).

In addition, patients with Cushing's syndrome, who have elevated circulating cortisol experience psychiatric symptoms such as anxiety and depression, and hyperactivation of GR has been linked to the development of mood disorders (38, 39). This is also a side effect of patients taking synthetic Gc long term. This can be alleviated through treatment with mifepristone, a GR antagonist, highlighting the direct importance of Gc in maintaining homeostasis within the brain.

In contrast, Addison's disease, also known as primary adrenal insufficiency, is characterised as a disease caused by adrenal failure, commonly caused through the production of autoantibodies against 21-hydoxylase, an enzyme required for cortisol production (40). This results in reduction of cortisol production, ultimately resulting in adrenal failure. Symptoms are often non-specific, but commonly include fatigue, hypotension and weight loss (41). These symptoms highlight the complex and wide-ranging effects of Gc.

Highest expression of GR is found within the cerebellum within both the human and mouse brain, and this appears to be critical for brain development. In particular, Gc administration within pre-term babies leads to a stunting of cerebellum development (42). Further study is required to fully elucidate the complex roles of GR within different regions of the brain.

1.1.6 Nuclear receptor superfamily

As previously mentioned, Gc exert their effects through binding to GR. GR is a member of the nuclear receptor (NR) superfamily of 48 ligand-activated transcription factors (TF). NR ligands include various classes of steroid hormones, such as progesterone and oestrogen, and vitamins including vitamin D_3 and retinoids, and lipid soluble metabolites such as oxysterols (43). The NR family can be classified into subfamilies (NR0-NR6), depending on structural homology (Fig 1.2). GR (NR designation *NR3C1*), is part of NR subfamily 3 or NR3, a closely related group of NRs that respond to steroid hormones and includes receptors that respond to circulating mineralocorticoids, progestins, oestrogens, and androgens.

1.1.7 GR isoforms

The *GR* gene is located on chromosome 5, and consists of 9 exons (44). The first of these exons is not translated, whilst exons 2 – 9 form the GR protein. Alterations in the translation of exon 9 result in several splice variants (Fig. 1.3). GRα and GRβ are highly homologous, however, GRα, the most common splice variant, considered full length GR, contains an additional 50 amino acids.
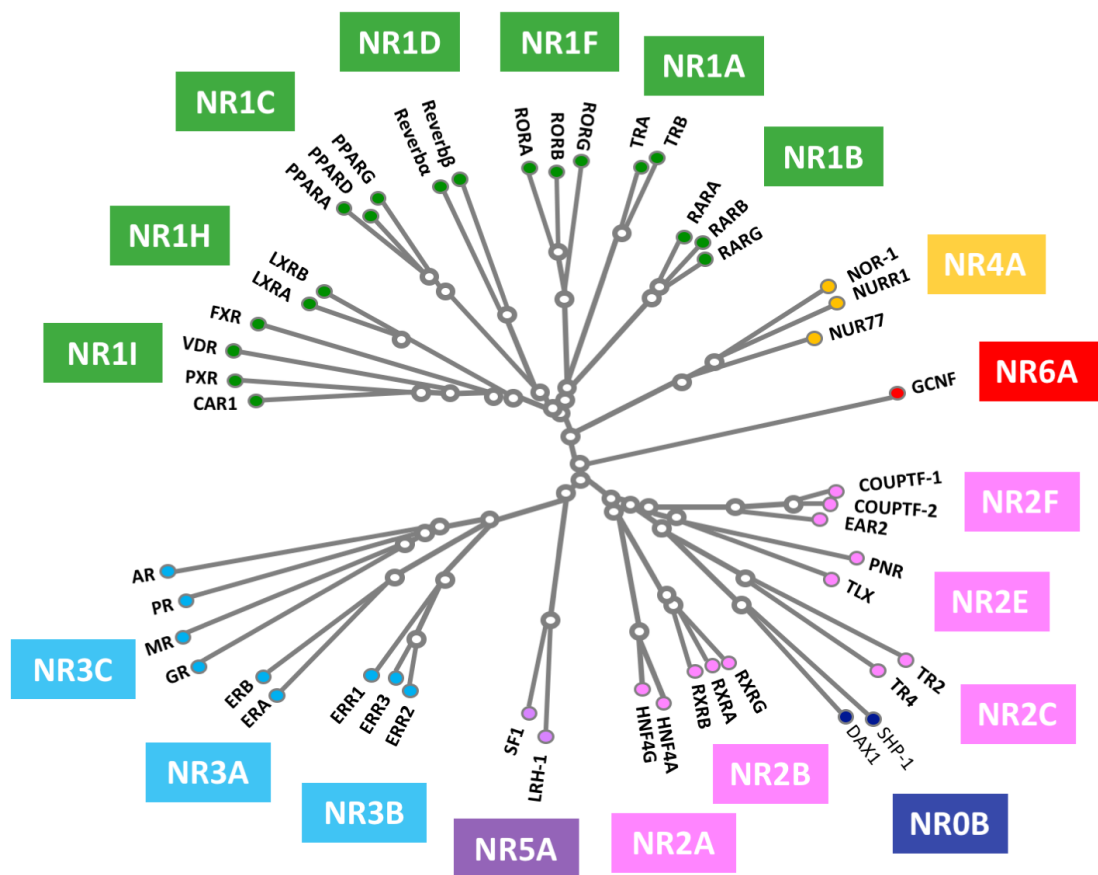
Figure 1.2: Diagram of the nuclear receptor superfamily. Hierarchical illustration of the nuclear receptor superfamily within humans, and its subfamilies. Subfamilies, namely NR0 – NR3, can then be further divided into groups, such as NR3A – NR3C. Individual receptors within these groups are then shown. Information drawn from (43, 45, 46).

These amino acids form the full length ligand binding domain (LBD), allowing it to bind Gc. GRβ, however, contains 15 nonhomologous amino acids, which do not confer ligand binding properties (5). These differences in structure predict differences in protein function. Whilst GRα is largely sequestered to the cytoplasm in the absence of ligand, GRβ is found predominantly within the nucleus (47). GRβ is also unable to bind to and regulate expression of traditional GR target genes through direct binding at GREs. It is able to regulate transcription, however, as an inhibitor of GRα and through the recruitment of histone deacetylases to repress selected genes (48). Due to its ability to inhibit

GRα function, the ratio of GRα:GRβ expression has been linked to Gc resistance (49). Further research is required to fully understand the effects of GRβ.

GRγ, another splice variant, contains an additional arginine residue within the DNA binding domain (DBD), altering its specificity and resulting in the capability to bind to a smaller subset of GR target genes (50). Two further isoforms also exist, GR-A and GR-P. Both lack functional ligand binding domains, and are commonly found within cancer cells (51). The relative abundance of both GRγ and GR-P have been linked to Gc resistance in several malignancies, however, their functional relevance is still unlear(52-54).

1.1.8 GR structure

All NRs share a common modular structure and contain three functional domains; an N-terminal regulatory domain (NTD), and a C-terminal ligand binding domain (LBD), joined to the central DNA binding domain (DBD) by a flexible linker or hinge region (HR).
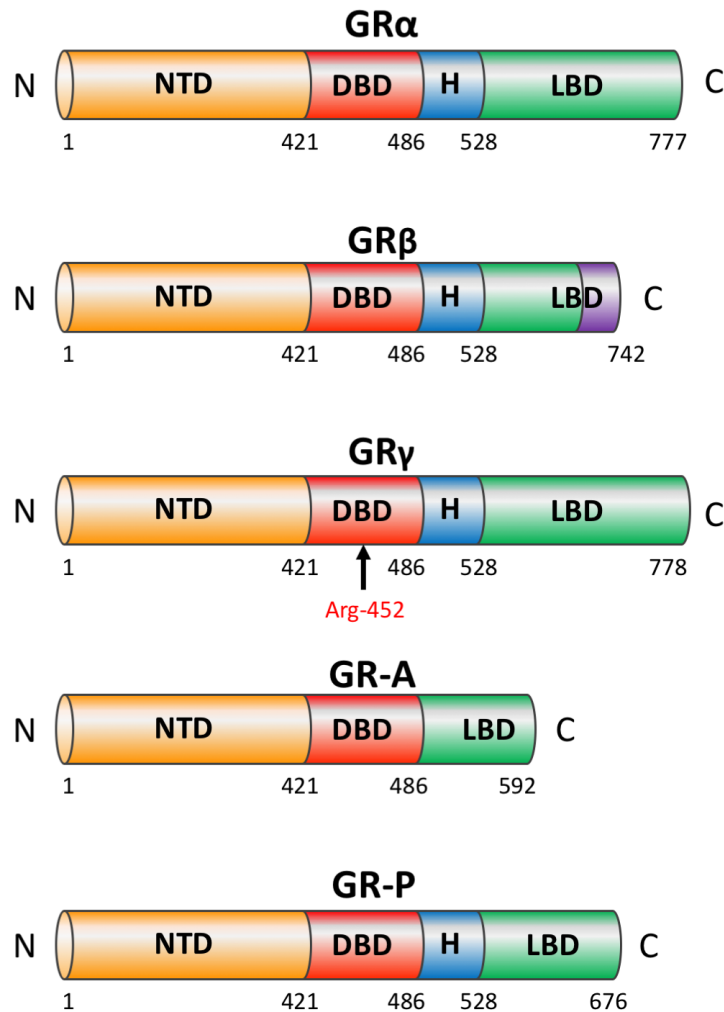
Figure 1.3: Splice variants of the GR gene result in several different isoforms. All slice variants share a close structural homology, with several key differences. GRβ does not share the same final 50 amino acids as GRα, but contains an additional 15 non-homologous amino acids, indicated in purple. GRγ is highly homologous to GRα, but contains an additional arginine residue within the DBD. GR-A is missing a 184 amino acid portion comprising the hinge region and part of the LBD. GR-P does not contain the 8th and 9th exons of the LBD. N and C denote N- and C- terminal domains. Key - NTD- N-terminal domain; DBD – DNA binding domain; H – hinge region; LBD – Ligand binding domain. Data obtained from (55).

The LBD contains 12 α-helices and 4 β-sheets, which form a central hydrophobic pocket capable of binding ligand. Within GR, this pocket is highly adaptable compared with other nuclear receptors, and can bind to a wide variety of ligands, both steroidal and non-steroidal (43). It is also capable of binding hsp90, allowing the pocket to maintain its conformation in the absence of ligand (56). The DBD also contains activation function-2 (AF-2), which enhances protein-protein

interactions with coregulators and other transcription factors following ligand binding (Fig. 1.4A) (57). Whilst AF-2 is around 5 – 10 times less active than AF-1, its structure is more defined, suggesting it may be responsible for binding a select group of ligands with higher affinity (58, 59). The DBD is linked to the LBD via a short hinge region (HR). The HR allows for flexibility within the protein, aiding dimerization and DNA binding.

The DBD is highly conserved between NRs, and consists of two zinc finger domains (29). The first of these zinc finger motifs is critical for recognising target sequences, or response elements, within DNA, whilst the second stabilises interactions between the protein and DNA (60). The DBD is also required for other GR functions, such as dimerization of the receptor, and repression of other transcription factors, such as NFκB (61).

The NTD is the least conserved region amongst nuclear receptors, allowing for large variations in both size and function (62). The NTD region is intrinsically disordered, where the conformational changes induced in the LBD by ligand engagement recruits transcriptional cofactors, such as NCoA-2, with low binding affinity, which modulate GR function (63). Some NRs, including GR, contain an additional domain within the NTD, known as activation function-1 (AF-1) (Fig. 1.4A). AF-1 is capable of binding multiple GR coactivators, resulting in maximal activation of the receptor (29). It is also required for docking of the basal transcriptional machinery, for example, the TATA box, and is a common site for regulation by post-translational modifications, such as phosphorylation at Ser-203 and Ser-211 in response to ligand binding (Fig. 1.4B) (64, 65).
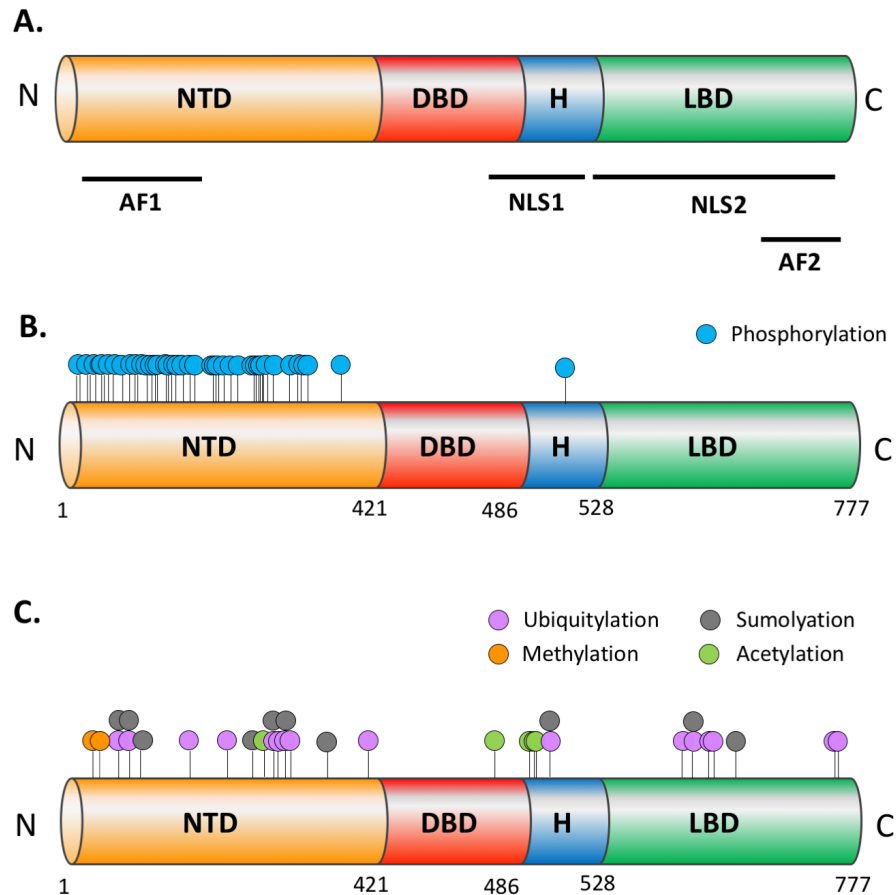
Figure 1.4: Key regions of GRα, and the post-translational modifications which can alter its function. The key sequences which alter GR structure and function, and their location within GRα. GR is also subject to a high number of post-translational modifications (PTM), and these modifications can alter its affinity for localisation and for binding other proteins, such as corepressors and coactivators. It is subject to several types of PTM, most commonly phosphorylation (B), but also ubiquitylation, sumolyation, methylation and acetylation (C). AF – Activation Function 1, NLS – Nuclear Localisation Sequence, NTD – N terminal domain, DBD – DNA binding domain, H – hinge region, LBD – ligand binding domain. Data obtained from (62, 66, 67).

Finally, GR also contains several sequences which determine its localisation. These include nuclear localisation sequences (NLS), NLS1 and NLS2, which drive nuclear translocation (Fig. 1.4A). NLS1 is contained between the DBD and LBD, whilst NLS2 is located within the LBD. These sequences enable nuclear localization, and are therefore critical for GR function (68). GR also contains a nuclear retention signal (NRS), which overlaps with NLS1 within the hinge region of the DBD. This sequence prevents nuclear export whilst GR mediates

transcription (69). The combination of these domains enables the GR to bring together a wide range of signals, from Gc along with a range of cofactors, and exert their effects on gene expression.

1.1.9 Mechanism of cortisol action

It is important to note that cortisol does not function only through GR. Cortisol can also bind to the mineralocorticoid receptor (MR). Depending on the tissue, cortisol can function through one or both of these receptors. MR, for instance, is expressed by neurons within the hippocampus, but is absent from other brain regions (70). The endogenous ligand of MR is aldosterone, however, MR also has a higher affinity for cortisol, approximately 10-fold greater than GR (71). It should be noted, however, that some synthetic Gc, such as Dex, are not capable of activating MR, and thus their effects may be considered MR-independent, even in MR-positive tissues (70). The primary role of MR is in the control of fluid and electrolyte homeostasis, ultimately controlling blood pressure.

Due to the higher circulating concentrations of cortisol, however, MR in the brain is also commonly activated by circulating cortisol. Within the brain, GR and MR have closely related effects, and MR is capable of binding to glucocorticoid response elements (GREs) within the genome, although its effects are distinct due to the differential recruitment of corepressors and coactivators (72). Together, the receptors are believed to play a key role in orchestrating the stress response within the brain, and thus the rest of the body.

1.1.10 Mechanisms of GR Action

GR is both an intracellular receptor and transcription factor, expressed in virtually all tissues within the body. In its unliganded state, GR is localised in the cytoplasm, bound to a chaperone complex, which maintain it in a ligand-ready conformation but also maintain its inactive state. These chaperones include Hsp70, Hsp40 and Hsp90, and when bound to GR, this forms the GR foldosome (73). Formation of the GR foldosome is also critically dependent on interactions with several other cochaperones, including histone deacetylase 6 (HDAC6), resulting in a stable complex in which GR is stable and ready to bind Gc (74). In order to activate GR, ATP hydrolysis by Hsp90 leads to the dissociation of Hsp70, allowing the ligand binding pocket to open and bind the ligand (75).

1.1.10.1 Non-genomic effects of GR

GR is capable of exerting profound changes on the transcriptome of cells. These transcriptional effects, however, often take hours before they are observed (76). This seems at odds with previous observations that some Gc responses can be observed within minutes and do not require new transcription. These effects are termed non-genomic GR effects (Fig. 1.5).

In contrast to genomic GR effects, the rapid non-genomic effects are much less clearly understood. These effects include increases in intracellular calcium levels, increased reactive oxygen species production in breast cancer and increased nitric oxide production in endothelial cells, resulting in vasodilation (77-79). They may also directly affect inflammation through a number of key mechanisms.

Within immune cells, GR was shown to inhibit neutrophil degranulation within minutes of Gc treatment (80). NFκB activation was also inhibited in macrophages, just 30 minutes after Dexamethasone (Dex) treatment (81). In A549 adenocarcinoma cells, epidermal growth factor receptor (EGFR) signalling was rapidly inhibited following GR activation (82). These effects appear to be due to GR inhibition of kinase activation, such as MAPK, within these inflammatory signalling pathways (83). GR has also been shown to be interact directly with calveolin-1, a membrane protein which serves as a component of caveolae lipid rafts within many cell types. The interaction of GR with caveolin has downstream effects on the immune response within a lung inflammation model (84). In addition, in the presence of caveolin, GR has been shown to colocalize with c-src. Following GR activation, c-src is released from this complex, and is capable of exerting its effects, including the activation of protein kinase B (PKB) (85). PKB activation can result in a range of cellular effects, including effects on apoptosis, proliferation, and cell growth (86). Through rapid PKB activation, within 5 minutes of Dex addition, GR is thus able to affect a wide range of cellular process before it has begun affecting transcription.

In addition, Dex has been shown to activate both protein kinase A (PKA) and protein kinase C (PKC) rapidly following Dex treatment (87). This results in a rapid inhibition of calcium signalling within airway epithelial cells.
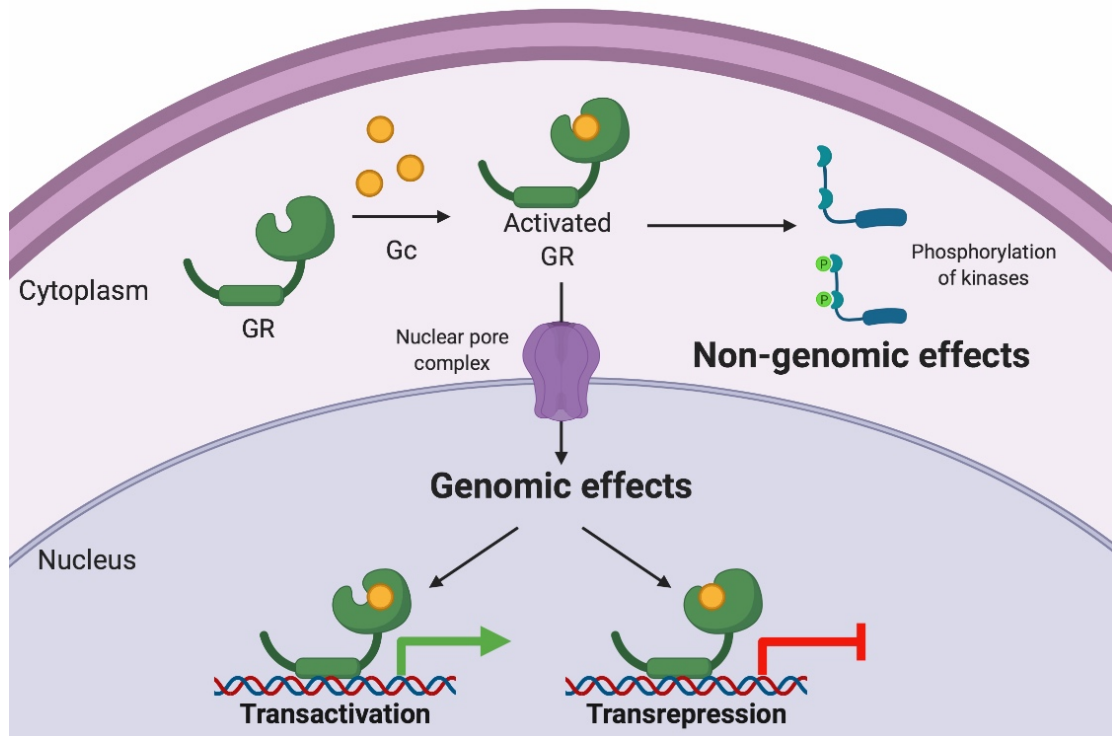
Figure 1.5: GR affects cell function through both genomic and non-genomic mechanisms. Upon Gc entry to the cell, GR binds to Gc and becomes activated. Within the cytoplasm, GR can modulate the activation of multiple kinases, resulting in complex, rapid signalling cascades. GR activation also allows for the exposure of nuclear localisation sequences, enabling GR translocation to the nucleus through the nuclear pore complex. Within the nucleus, GR can transactive or transrepress expression of individual genes. Gc – glucocorticoid, GR – glucocorticoid receptor. Data from (76, 83). Diagram created using Biorender.com.

1.1.10.2 Genomic mechanism of GR action

Following ligand binding, GR undergoes a conformational change which leads to the exposure of the bipartite nuclear localisation signal (NLS1 and NLS2) on the outside surface. These domains enable rapid nuclear translocation through the nuclear pore complex (88, 89) (Fig. 1.5). Once in the nucleus, liganded GR can bind to DNA directly to modulate transcription, or to other DNA bound transcription factors to modulate their function. With increasing numbers of high throughput sequencing studies, literature has shown that GR can activate or inhibit gene transcription via either mechanism – although there is a bias which will be discussed later.

GR binds DNA directly at sites containing GREs. GREs were originally thought to consist of 2 hexamer palindromic sequences, joined by a three-nucleotide spacer. Recent genomic analysis, however, has shown that relatively few GREs consist of this sequence, and sequences show much more variation than was originally expected (90). It may be that these differences in GRE may alter the affinity of GR to bind particular sites, residence time on chromatin, or the recruitment of coregulators, ultimately regulating the type and strength of the response (65). The GR binding site may also dictate the recruitment of other complex proteins, as negative GREs (nGREs) have been shown to lead to the specific recruitment of corepressors and histone deacetylases, resulting in chromatin modification and gene repression (91). Therefore, the specific sequence of the binding site, or DNA motif, is thought to have a key role in determining GR function.

1.1.10.3   GR effects on transcription

GR can modulate transcription by both inducing expression of target genes (transactivation), and repressing expression of others (transrepression) (Fig. 1.6). These effects often work synergistically to create the same phenotype. For instance, GR can increase the expression of anti-inflammatory and pro-repair genes, while simultaneously repressing the expression of pro-inflammatory mediators and injurious genes.

GR can also affect transcription without directly binding to DNA via a process known as tethering. GR may bind a range of transcription factors, such as NFκB, and AP-1, and modulate their effects (5). In many cases, this allows GR to target the same pathway in multiple, redundant ways; for instance, in the case of NFκB,

GR can transactivate and increase the expression of IκBa, an NFκB inhibitor, bind to DNA at the promoter region of NFκB target genes directly to suppress expression, and bind to NFκB directly whilst it is bound to DNA to inhibit its function (92). These effects are complex, complementary, and difficult to understand independently of each other.
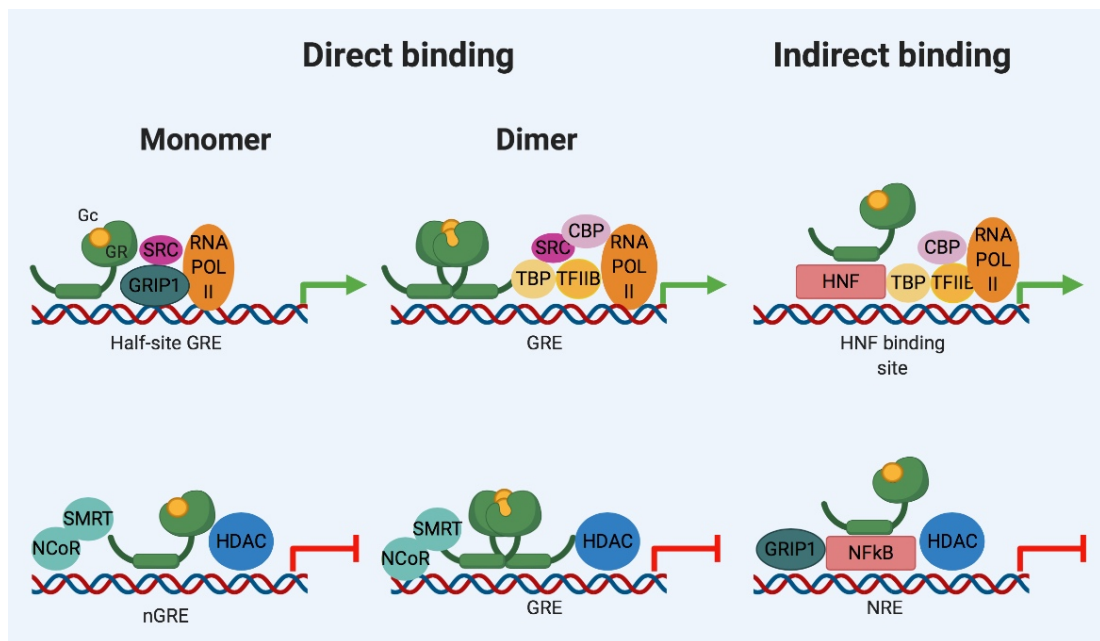
Figure 1.6: GR can modulate transcription through multiple mechanisms. GR can bind to DNA as a monomer or a dimer, or can modulate transcription indirectly through tethering to other transcription factors. Each of these forms can either activate or repress transcription of the bound gene, depending on the response element, and the recruitment of other cofactors. Green arrows indicate increased gene expression, whilst red arrows represent gene inhibition. CBP – CREB binding protein, GRE - glucocorticoid response element, GRIP1 – Glucocorticoid receptor interacting protein, HDAC – histone deacetylase, HNF – Hepatocyte nuclear factor, NCoR – nuclear receptor corepressor, NFκB – nuclear factor kappa B, nGRE - negative Gc response element, NRE - NFκB response element, RNA Pol II – RNA polymerase II, SMRT – silencing mediator for retinoid or thyroid-hormone receptors, SRC - steroid receptor coactivator, TBP – TATA binding protein, TFIIB – Transcription factor II B. Data from (51, 93-95). Created using Biorender.com.

GR may also bind as a monomer at "half-site" GREs, which do not contain the the 3 nucleotide spacer, or the second palindromic sequence found within a full GRE, as explained above (96). GR can bind at these sites alongside other transcription factors, such as NFκB and AP-1 which are themselves bound to a

nearby target sequence. From these half-sites, GR can either activate or repress transcription. This is a relatively novel mechanism of GR action, and its abundance and clinical significance is as yet unclear (65, 97).

For many years, dogma stipulated that GR dimerization and the DNA binding mechanism dictated the effect of GR activation on the transcriptional response. Tethering of monomeric GR was believed to be largely responsible for transrepression of inflammatory genes, therefore orchestrating the beneficial effects of Gc therapy. In contrast, direct DNA binding of dimerized GR was believed to be responsible for transactivation of genes, such as those involved in gluconeogenesis, and many of those responsible for the damaging side effects of Gc therapy. This hypothesis appeared to be confirmed by *in vitro* studies using GR mutants incapable of forming dimers, however, *in vivo* work using GR mutant mice containing the same point mutation showed that GR dimerization is essential for a full anti-inflammatory response (98, 99). In addition, other side effects, such as osteoporosis, have since been shown to be caused independently of dimerization (100). As research has progressed, this clean monomer/dimer model of activation/repression has been shown to be overly simplistic, and the positive and negative effects of Gc therapy are much more inextricably linked than initially believed.

1.1.11   Selective GR modulators (SEGRMs)

Based on the traditional dogma of transactivation/transrepression, it was hypothesised that if GR ligands could be designed which retained the transrepressive effects of Gc, but limited transactivation, it would be possible to produce ligands with efficacy in reducing inflammation, whilst minimising side

effects (101). It was hoped that these ligands, referred to as SEGRM, would revolutionise the treatment of inflammatory conditions, by providing effective control of inflammation, but without affecting metabolism, and other side effects. There have been many of these ligands designed over the past several decades, however, none have lived up to their original promise.

Several SEGRMs which showed initial promise *in vitro* and *in vivo* have undergone clinical trials, and some have even reached Phase II trials (102). None, however, have been approved for oral use. It is probable that this lack of success at the clinical trial stage, at least in part, is due to the complexity of GR function. As discussed above, GR function goes beyond the original dichotomy, and there are multiple layers of complexity of GR signalling which are not yet understood. It may therefore be necessary to further understand Gc function more thoroughly before selective ligands can be used successfully.

1.2 Glioblastoma Multiforme

Glioblastoma multiforme (GBM) accounts for 15.6% of primary brain tumours, and is the most lethal brain tumour in adults (103). Median survival time remains less than 15 months with standard treatment, and the 5-year survival rate is just 5% (103, 104). After diagnosis, standard treatment consists of tumour resection, followed by 6 weeks of concomitant radiotherapy and Temozolomide (TMZ), the most effective chemotherapeutic drug used for GBM. This is followed by a period of adjuvant TMZ. This treatment is aggressive, often with severe side effects, and on average only extends life by approximately 3 months (104). Despite advances in our understanding of the molecular mechanisms underlying glioblastoma in the

past 15 years, this has not transferred to new standard treatments since the current standards were published in 2005 (105).

1.2.1 Classification

Gliomas are defined as tumours arising from glial cells, or glial precursors, and can be further divided into Grades I – IV according to both histological and morphological features. Using the World Health Organisation nomenclature, all Grade IV gliomas are classified as GBM (106). Within this broad classification, molecular profiling has allowed us to further define subtypes according to common mutations and epigenetic changes. Some of the most common of these include mutations in telomere length genes, such as TERT, and RB pathway genes, such as CDKN2A, and the DNA repair effector, p53 (107-109). The most commonly used prognostic marker, however, has arguably been O^6-methylguanine–DNA methyltransferase (MGMT) methylation. Methylation of the MGMT gene, resulting in gene silencing, is associated with increased efficacy of chemotherapy, and in turn, increased survival times (110).

1.2.2 Current Treatments

As previously mentioned, the current standard of care for GBM consists of surgical resection, followed by radiotherapy and chemotherapy. Due to the often diffuse nature of the tumour, and its sensitive location within the brain, the maximum possible resection is carried out, depending on factors such as health status, age, and precise location within the brain (111). The remaining tumour will be targeted by radiotherapy, at a dose advised at 60Gy, divided into doses of 2Gy/day for 5 days per week alongside concomitant, daily Temozolomide

($75mg/m^2$) for 6 weeks, followed by Temozolomide alone ($150 – 200mg/m^2$) for up to six four-week cycles. This schedule, originally described by Stupp et al, may be deemed unsuitable for many patients due to severe side effects, but was shown to increase survival to 14.6 months, compared with 12.1 months with radiotherapy alone (104).

1.2.3 Therapeutic mechanism of action

Radiotherapy has long been a stalwart of treatment in a broad range of cancers, and despite many therapeutic advances, it still remains a first-line treatment for many. Radiotherapy is effective in many cancer types due to its broad mechanism of action; namely through the induction of DNA damage, which, when unrepaired, leads to apoptosis of cells, resulting in tumour shrinkage and in some cases elimination. However, cell destruction by radiotherapy is not specific to cancer cells. Instead, it is more effective in rapidly dividing cells. This includes cancer cells, but also a range of other healthy cells. The efficacy within certain cancers, including GBM, is also limited by the development of radioresistance, meaning the best-case scenario is the shrinkage of tumour, allowing only for extension of life span until inevitable tumour recurrence or regrowth.

IR produces a number of different types of lesions within DNA, such as single-stranded breaks (SSBs), nucleotide damage, and double stranded breaks (DSBs) (112). It is estimated that IR leads to approximately 25 times more SSBs than DSB, however, DSBs are much more damaging, and require more complex repair mechanisms (113). The main mechanisms of DSB repair are outlined in Figure 1.7.
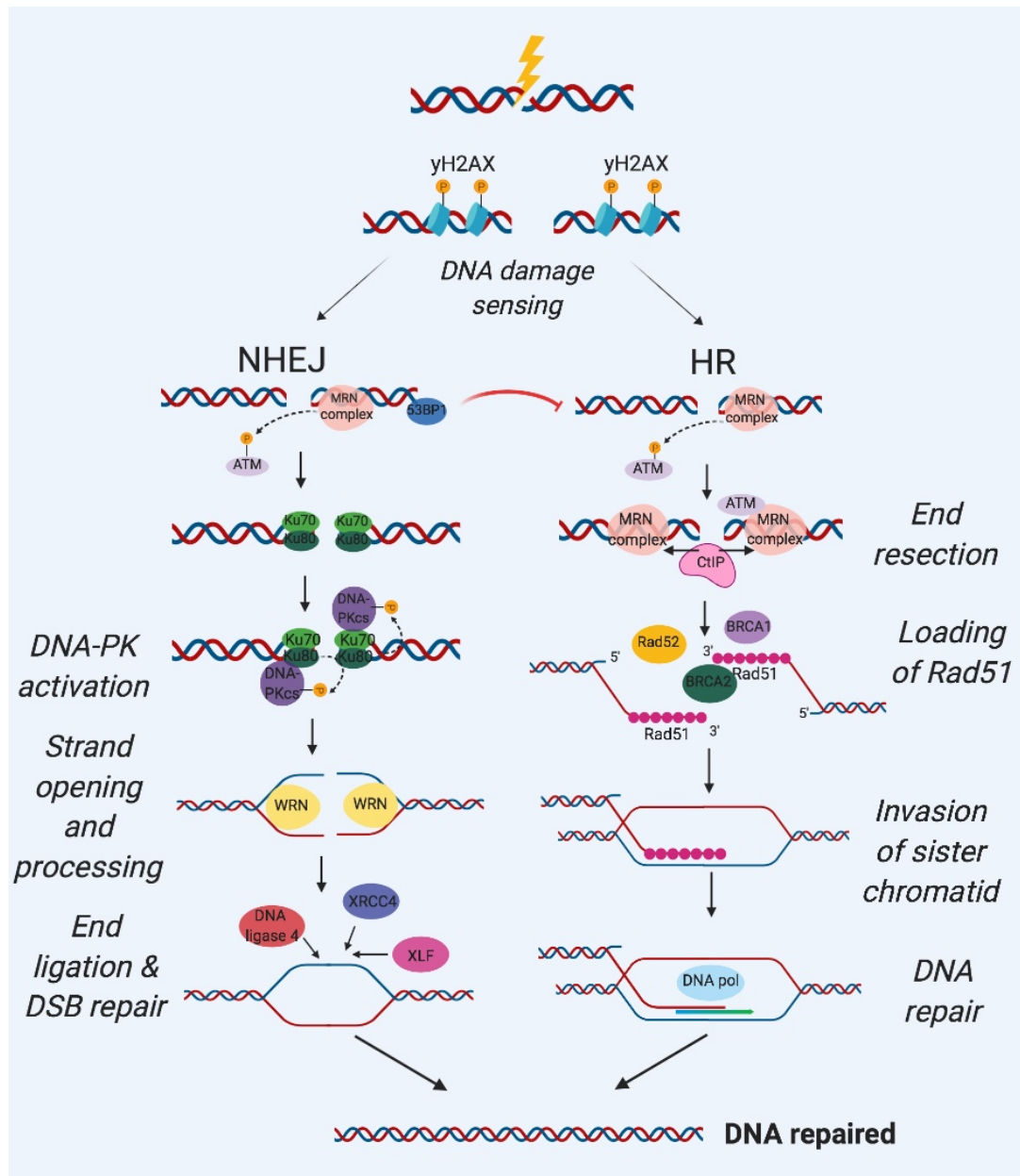
Figure 1.7: Double strand breaks are repaired by multiple mechanisms, including NHEJ and HR. Double stranded breaks are incurred by agents such as irradiation, then immediately sensed by yH2AX. Damage can then be repaired by two main mechanisms: non-homologous end joining (NHEJ), or homologous recombination (HR). NHEJ required DNA-PKcs, which enables the recruitment of the MRN complex, enabling ligation proteins such as DNA ligase IV to enter the break and ligate the ends. Alternatively, HR required the presence of a sister chromatid, which can be used as a template by Rad51 to ensure accurate repair. ATM - ataxia telangiectasia mutated, ATR - ataxia telangiectasia Rad3-related, BRCA1 – breast cancer type 1 susceptibility protein, BRCA2 – breast cancer type 2 susceptibility protein, CtIP – C terminal binding protein 1 interacting protein, DNA-PKcs - DNA-PK catalytic subunit, DNA pol – DNA polymerase, HR – homologous recombination, MRN complex - MRE11-Rad50-NBS1 complex, NHEJ – non homologous end joining, WRN – Werner syndrome ATP-dependent helicase, XLF – XRCC4-like factor, XRCC4 - X-Ray Repair Cross Complementing 4. Data adapted from (114-117). Created using Biorender.com

1.2.4 Non-homologous end joining

The most common mechanism of DSB repair is non-homologous end joining (NHEJ), which is responsible for repairing up to 85% of DSB caused by IR (118). This mechanism is rapid, but more error-prone than homologous recombination (HR), the other common mechanism of DSB repair. NHEJ requires a number of key DNA repair proteins, and the most critical comprise the DNA-dependent protein kinase (DNA-PK) complex. This complex is made up of 3 subunits; DNA-PK catalytic subunit (DNA-PKcs), and Ku70 and Ku80. DNA-PKcs is a PI3K-related protein kinase (PIKK), whilst the Ku70/80 heterodimer is capable of binding DNA directly (119). Together, DNA-PKcs, Ku70/80 and DNA form a sequence-independent complex, known as the DNA-PK complex, or DNA-PK. It has been shown that Ku70/80 binds to ends of DNA at sites of DSB, recruiting DNA-PKcs, and activating its kinase activity (120). DNA-PKcs is then capable of phosphorylating many components of the DNA repair machinery, such as H2A family member X (H2AX), Artemis, and itself (121). Activation of DNA-PK also results in the recruitment of a complex comprised of DNA ligase IV, along with XRCC4, and XRCC4-like factor (XLF) (122). This complex is required for ligation of broken ends, resulting in the repair of DSB (123). This process leads to rapid, efficient DNA repair, and DNA-PKcs inhibition results in increased sensitivity to radiation within GBM cells (124). The functional impact of this is emphasised by the correlation of increased DNA-PK expression with reduced overall survival in GBM patients (125). Given the clear importance of DNA-PK, and NHEJ in general in rendering cells radioresistant, inhibition of DNA-PK is a potential new target for cancer therapy. For instance, a phase Ib/II trial is currently being planned using a DNA-PK small molecule inhibitor, CC-115, to increase radiation efficacy in GBM (126).

1.2.4.1 Alternative roles of DNA-PK

The function of DNA-PK is not just limited to the repair of damage caused by IR; DNA-PKcs deficient mice are severe combined immune deficient (SCID), due to the critical role of DNA-PK in V(D)J recombination, the process by which a wide repertoire of B and T cell receptors are formed during the development of lymphocytes (127-129). Aside from these critical roles, however, DNA-PK may have even more wide-ranging effects. For instance, DNA-PK has been suggested to play a role in inflammation. Induction of NFκB target genes, such as *VCAM-1*, *IL7* and *IL-1β* was inhibited in GBM cells lacking DNA-PKcs (in the M059J cell line) following TNF treatment (130). Within immune cells, DNA-PK inhibition was shown to block IL2 production from T cells, potentially limiting the adaptive immune response (131). This may translate to a functional impact, as DNA-PK inhibition was shown to inhibit the development of murine asthma models, without affecting lymphocyte maturation (132). Finally, M059J cells were unable to form tumours within SCID mice, unlike their DNA-PK proficient counterpart cell line (M059K) (133). DNA-PKcs knockdown within melanoma cells was also shown to inhibit their ability to form tumours *in vivo*, and knockdown *in vitro* inhibited their ability to migrate within transwell assays (133). Together, these results suggest that DNA-PK may have complex roles outside DNA repair which must be further understood before it can be considered as a cancer therapy target.

1.2.5 Homologous recombination

The other common mechanism used to repair DSB induced by IR is HR. HR is a slow, but more accurate mechanism of repair, however, due to the requirement of a template DNA strand, its usage is limited to S and G2 phases of the cell cycle (134). HR also requires single-strand DNA (ssDNA) ends. DSB result in blunt

DNA ends, so the first stage of HR requires the processing of the blunt 5' ends of DSB to produce ssDNA ends, a process known as DSB end resection. This process is carried out by the MRE11-Rad50-NBS1 (MRN) complex (135). This complex is sensed by replication protein A (RPA), which orchestrates the recruitment of other DNA repair-related proteins, including BRCA2. BRCA2 enables the loading of RAD51 onto the broken DNA ends, replacing RPA, which in turn leads to strand invasion of the sister chromatid (117, 136). Using this sister chromatid as a template, the broken DNA is repaired. The choice between the use of HR or NHEJ is complex, and depends on factors such as cell cycle phase, as discussed, and the relative abundance of factors such as BRCA1 and 53BP1 (116). A key determinant of repair fate is the resection of DSB ends, and Ku70/80 binding to DSB ends prevents the binding of the MRN complex, and vice versa (137).

1.2.6 ATM, ATR and the wider effects of DNA damage

In addition to the direct mechanisms of repair described above, both NHEJ and HR lead to the activation of a number of other PI3K enzymes; namely, ataxia telangiectasia mutated (ATM) and ataxia telangiectasia Rad3-related (ATR). Both enzymes are phosphorylated in response to DNA damage: ATM is activated in the presence of DSB, whilst ATR is activated by ssDNA, and in particular, ssDNA with an RPA coating (134). This means that within the context of DSB, ATM is preferentially activated in response to NHEJ, and ATR is activated predominantly in HR. Their roles, however, are not fully independent; it has been suggested, for instance, that ATM is activated by the MRN complex, and that ATR may be capable of phosphorylating ATM in the context of UV damage (138-140).

ATM is capable of phosphorylating hundreds of substrates in response to DNA damage. Some of these substrates, in turn, may phosphorylate other targets, resulting in a wide-ranging signalling cascade. For instance, ATM may directly phosphorylate H2AX, a key DNA damage sensor, Checkpoint Kinase 2 (Chk2), and p53 (141). ATR, meanwhile, phosphorylates a related, but distinct, group of substrates (141). ssDNA is formed in response to a broad range of genotoxic stressors, and also at sites of stalled replication forks. The substrates of ATR include many proteins involved in pathways which lead to the repair of replication forks, and substrates which result in the stalling of cell cycle phase (142). The phosphorylation of Checkpoint Kinase 1 (Chk1) is key to the induction of cell cycle arrest, allowing cells time to repair DNA before replication occurs.

Through the activation of ATM and ATR, DNA damage leads to a comprehensive, robust response, resulting in cell cycle arrest to allow DNA repair to occur, and activation of multiple other pathways, including p53 and the Fanconi Anaemia pathway of DNA repair (143, 144). The importance of this system in preventing the formation of cancer is underlined by the redundancy found within these pathways, as multiple substrates lead to the same cellular effects. Even within this redundancy, however, certain proteins are critical, as evidenced by the high incidence of p53 mutations within a broad range of cancers.

1.2.7 Effects of p53 within DNA repair

p53 is a transcription factor which is activated downstream of many DNA repair pathways. P53 activation is essential in the safeguarding against the survival of mutations, and for this reason, mutations of the *p53* gene has been reported in close to every cancer type (145, 146). Within GBM, *p53* itself is mutated in 27.3%

of tumours, but the wider p53 pathway was mutated in 85% of tumours (147). This suggests that p53, and DNA repair as a whole, are a key pathway dysregulated within GBM. Following activation of either NHEJ or HR, ATM and ATR both induce p53 activation. Both ATM and ATR can directly phosphorylate p53 at serine-15, resulting in increased p53-mediated gene transcription (148). In addition, ATM can also phosphorylate and repress MDM2, a key p53 repressor, and both mitotic checkpoint genes Chk1 and Chk2 can phosphorylate p53 at multiple sites (149, 150).

Once activated, p53 can affect the transcription of thousands of genes through both direct and indirect mechanisms. Upon activation, p53 may directly induce cell cycle arrest through the upregulation of genes such as *p21 (151)*. This allows the cell time to repair DNA damage within the cell, before progressing through cell division. Alternatively, p53 also upregulates various apoptosis-related genes, including *Bad* and *Bax*, *caspase 6* and *Fas* (152, 153). This means that in cells with catastrophic DNA damage, apoptosis will be induced to prevent the propagation of potentially dangerous DNA mutations.

1.2.8 Temozolomide

TMZ is the current standard chemotherapeutic used to treat GBM. TMZ is a lipophillic prodrug which is metabolised to its active form at a pH of 7 – 9 (154). This allows TMZ to act with a modicum of specificity; due to its lipophilic properties, it may cross the blood brain barrier (BBB), and as brain tissue is more alkaline than surrounding tissue, TMZ is broken down within the brain to form 5-aminoimidazole-4-carboxamide (AIC) and methyldiazonium cation (155, 156). This cation is then capable of methylating DNA at numerous residues, including

O^6 guanine residues (O^6-MeG). The addition of this methyl group may be repaired

quickly and directly by O^6-methylguanine DNA methyltransferase (MGMT). The

methyl group is transferred from the guanine base to the MGMT molecule, which

results in the degradation of MGMT, and the DNA strand is repaired. If MGMT is

not present, the O^6-methylguanine adduct leads to the mispairing of guanine with

thymine instead of cystine during DNA replication (113, 157). This mispairing is

recognised by conserved DNA repair mechanisms, and in particular the

mismatch repair (MMR) system. MMR attempts to repair this damage through the

removal of the thymine base, but the original alkylated guanine residue is left

intact. Through multiple failed rounds of MMR during replication, DSBs are

eventually formed, which are repaired by the mechanisms listed previously (158).

If these mechanisms are unsuccessful, GBM cells eventually undergo apoptosis

(159). Therefore, reduced MGMT activity results in increased DSB formation, and

can therefore lead to increased GBM cell apoptosis. Whilst the Stupp protocol is

undoubtedly the most effective current treatment, and can increase survival times

as a whole, there is a high level of variability in the response rate within individual

patients. Differences in response can, in part, be explained by differences in

MGMT methylation. In patients with methylated MGMT, median survival was 21.7

months for patients receiving IR and TMZ, compared with just 12.7 months for

patients with unmethylated MGMT receiving the same treatment (160, 161).

1.2.9 MGMT methylation as a prognostic marker

As described above, MGMT comprises a one-step repair mechanism for the most

damaging lesions caused by TMZ. Methylation of the promoter region of the

MGMT gene results in epigenetic silencing, preventing transcription of the MGMT

protein. Without MGMT, TMZ-treated GBM cells are forced to undertake MMR,

leading to the production of DSB. When these breaks cannot be repaired, cells undergo apoptosis. As expected, therefore, increased MGMT methylation has been repeatedly correlated with improved TMZ treatment efficacy within GBM, resulting in reduced survival times within patients (162-164). In fact, this is considered such a strong indicator of prognosis that MGMT gene methylation has been used as a stratification tool within clinical trials (165).

Interestingly, there has been previous literature suggesting that Dex is capable of inducing MGMT methylation, and this has been hypothesised as a mechanism of Dex reducing therapeutic efficacy. This was due to the discovery that the MGMT gene contains multiple GRE sites, along with NFκB and AP-1 binding sites, suggesting that the gene is under some form of inflammatory control (166-168). This was furthered by a study which demonstrated that MGMT mRNA was induced following Dex treatment (169). This work, however, has been limited by several methodological problems. Most importantly, the Dex dosage used within the work was 10µM, many times higher than physiological levels, and 100 times what is commonly used *in vitro*. Similarly, Dex was shown to inhibit apoptosis following TMZ treatment in GBM cells, but this was shown at doses of 100µM and 200µM Dex, once again far higher than would be physiologically relevant (170).

Recently, however, using doses of 100nM Dex, MGMT transcriptional activity was increased in several GBM cell lines, assessed using MGMT cloned into GBM cells, using the dual luciferase reporter assay (171). Whilst this demonstrates the ability of GR to bind and regulate MGMT under synthetic conditions, this does not

confirm the ability of Dex to regulate the endogenous MGMT gene within GBM cells, particularly given the complex nature of epigenetic GR regulation.

Further evidence of GR effects on TMZ efficacy comes from work with a GR antagonist, mifepristone. Mifepristone is used to induce abortion due to its ability to antagonise both glucocorticoid and progesterone actions through their respective receptors (172). Recent work, however, has demonstrated that mifepristone administration alongside TMZ and radiation is capable of increasing survival in several rat models of GBM (173, 174). In addition, mifepristone usage was shown to decrease levels of MGMT expression within tumour cells (173). These effects are presumably mediated through effects on either GR or progesterone receptor (PR), but further work is required to determine a specific mechanism of action.

1.2.10 Use of Dexamethasone

Treatment with Gc is considered the gold standard in the control of cerebral oedema caused by brain tumours (175). Dex is a high affinity, highly potent Gc, which was first synthesised in 1958. Dex is routinely administered for relatively few conditions due to the high risks of severe side effects, however, it is the preferred corticosteroid in treating cerebral oedema, due to its low mineralocorticoid activity and high efficacy (176). Dex usage within patients with cerebral metastases and primary tumours reduced symptoms in over 70% of patients, across multiple Phase III trials (175, 177). Despite this high efficacy, and common usage, the mechanisms by which Dex reduces cerebral oedema have not been fully explored. Importantly, however, Gc have failed to show similar efficacy in the treatment of oedema caused by stroke, suggesting that they repair

specific dysregulated mechanisms within brain tumours (178). In particular, it has previously been demonstrated that the BBB is dysregulated within GBM, which leads to the influx of fluid into the brain, causing oedema and symptoms such as migraine and nausea. This can often lead to more severe neurological symptoms, such as confusion and increase the risk of stroke. This dysregulation of the BBB is due in part to an upregulation of inflammatory mediators, released from immune cells within the tumour microenvironment, resulting in immune cell infiltration, and tumour-associated factors such as vascular endothelial growth factor (VEGF), which lead to the breakdown of tight junctions between cells (179). Gc lead to an upregulation of tight junction components within endothelial cells in the BBB, and dampen the damaging effects of inflammation (179, 180). Both of these effects lead to improved BBB function through increased junctional integrity, resulting in the reduction of fluid and immune cell influx (181). Whilst these effects of Dex on endothelial cells have been relatively well-described, the effects of Dex on GBM cells has been less well characterised. This has become particularly controversial, as the effects on GBM cell survival have recently gained attention (182).

1.2.11   Effects of Dex on GBM patient survival

There has been an increasing awareness of Dex as a potential confounding factor within clinical trials for novel treatments within GBM. As previously discussed by Millar et al, this is complicated by the fact that, due to an underestimation of Dex effects, previous studies have often omitted steroid usage and dosage entirely from published results, making it impossible to determine whether steroids may have caused differences in response (183). This was discussed by Millar et al in the context of metastatic brain disease, but within our

experience, the same is also true within GBM trial results. Whilst it is recommended to taper Dex usage following surgery, and prior to radiotherapy, chemotherapy, and other novel treatments, the efficacy of Dex in reducing treatment-related side effects such as nausea mean that Dex is often continued at a maintenance dose throughout chemotherapy and radiotherapy, however, this is often unreported within clinical trial data (182). Within trials that have reported Dex usage, Dex has been shown to interfere with the efficacy of immunotherapies, such as ipilimumab, an immune checkpoint inhibitor (184). This may be expected, due to the well-known immunosuppressive effects of Gc, however, Dex has also been shown to interfere with other therapies, such as tumour-treating alternating fields (TTFields) and standard chemotherapy (185). Given that the effects of standard chemotherapy, such as TMZ, are not primarily mediated by an immune response, this would suggest that it may be reducing survival through other mechanisms.

In light of these growing concerns within the GBM community, Pitter et al demonstrated that higher Dex usage within GBM patients is associated with reduced survival time, independent of other factors, such as tumour size and other therapies (182). Their work suggested that within a mouse model of glioma, Dex was capable of reducing tumour cell proliferation, which may render cells more radioresistant, however, their work did not confirm if similar effects were found within human tissue or cells. Similar effects of Dex on survival were reported in a retrospective analysis by Shields et al, who showed Dex usage was a significant predictor of reduced survival (186). A consistent criticism of these studies has been the relationship between severity of disease and Dex dependency; cases which require consistent Dex usage are more likely to consist

of more severe disease. Therefore, it is essential we understand the mechanisms of Dex action, both positive and negative, within GBM to ensure their safe usage.

1.3 Stochasticity in the Transcriptional Response

When a population of cells are treated with Gc, the expression of GR target genes is altered. This can be measured by qPCR or bulk RNA sequencing, which can be used to compare the population average of an untreated and treated population. What this does not describe, however, is the variation of response between cells within each population. It has therefore been hypothesised that there may be an inherent level of heterogeneity within responses.

The process of transcription is complex and therefore inherently noisy or 'stochastic'. This property is beneficial from an evolutionary perspective, as identical cells do not respond in exactly the same way, which increases the robustness of the signal across a cell population.

In order to understand how factors can alter the variability within a response, these differences can be modelled mathematically. A large degree of variation comes from the inherent complexity of the transcriptional response. For instance, in the glucocorticoid response, GR translocates to the nucleus, then must bind to the appropriate GRE and recruit the appropriate corepressors or coactivators, then recruit factors such as RNA polymerase II to the promoter region of the gene (187). A pre-initiation complex is formed, allowing transcription to begin. These steps, each relying on the interaction of multiple proteins, must all occur sequentially before transcription can occur. It is therefore not surprising that even

within a clonal population, each stage will occur at different rates in different cells (62, 188). We must then consider the added complexity of cells at different stages in the cell cycle, which will alter transcriptional output, the rates of promoter transition, and the chromatin landscape of individual cells (189, 190). For instance, if the chromatin state must change from closed to open before a gene may be transcribed, this will further delay transcription and increase the stochasticity of the system. Factors such as these, when multiplied across a large population, can theoretically lead to vast differences between individual cells.

The concept of transcriptional heterogeneity is not a new one – many studies have shown this heterogeneity between cells within a population, using fluorescent reporters tagged to promoters within bacterial cells (191, 192). Fluorescence can be used as a readout of transcription, however, this synthetic system lacks the complexity of *in vivo* regulation and cell state. Even within a relatively simple, artificial system such as this, however, different promoters were shown to result in different levels of stochasticity. For instance, the activation of stress-related promoters was more heterogenous than those promoters found in "essential" genes, for example, those genes involved in cellular structure (193). This suggests that heterogeneity, rather than an unavoidable result of complex systems, may be an additional layer of regulation for gene responses (194).

With the advent of single cell technologies, it is now beginning to be possible to study differences at a single cell level in more realistic systems. Specifically, single cell RNA-seq allows us to measure expression of individual genes in single cells without the need for fluorescent tags or insertion of genes. So far, single cell RNA-seq has been used within a large variety of lineage studies, and to highlight

inherent heterogeneity within populations (195, 196). Notably, this has included studies within primary GBM tissue, which has further highlighted the heterogeneity within individual tumours, and has increased knowledge of the development of subtypes, including the presence of GBM stem cells, within tumours (197-200).

Thus far, however, there has been little study of how this underlying heterogeneity in gene expression is changed following the addition of a ligand, such as Gc. Through understanding cell-specific heterogeneity in response to a ligand, we aim to understand how the response may be controlled, either at a cell- or gene-specific level. Through this, we aim to shed new light on how resistance to Gc may develop.

1.3.1 Modelling stochasticity within the transcriptional response

Until relatively recently, technological limitations mean it was necessary to infer single cell responses from the population response, however, with the advent of single cell technologies, it has become possible to analyse the transcriptional output and phenotype of individual cells within a population. This technology also allows us to validate mathematic modelling of single cell responses in the most physiologically relevant ways yet.

Two models have been proposed for eukaryotic gene expression within individual cells across time: these are binary and rheostat, or graded, responses (188). Binary models dictate that promoter regions of genes can be in either an active or inactive state (201). Both are discrete and defined states, with no points in between. In the inactive state, gene expression is completely repressed, whilst in

the active state, the gene is expressed at a single, constant level between cells (Fig. 1.8A). Thus, within a population of cells, it may be possible that some cells will contain promoters in the inactive state, and not express the gene, whilst others will be active, and exhibit a relatively consistent level of expression. In the case of a transcription factor, such as GR, by increasing the ligand , or inducer, concentration, for a GR-induced gene, we would expect that more cells would be "switched" from an inactive promoter to an active promoter. This would increase the proportion of cells exhibiting high expression of the gene, at the same maximal level of expression (Fig. 1.8A-B).

Alternatively, graded responses theorise that there is a spectrum of activation for promoter regions, resulting in a broad spectrum of mRNA expression. With little to no activation, expression within a population of cells would be clustered around the low end of the expression spectrum. Upon ligand addition, however, TF binding would increase expression beyond the original maximum expression. Therefore, the entire population of cells would shift upwards in expression towards this new maximum (Fig. 1.8C-D).
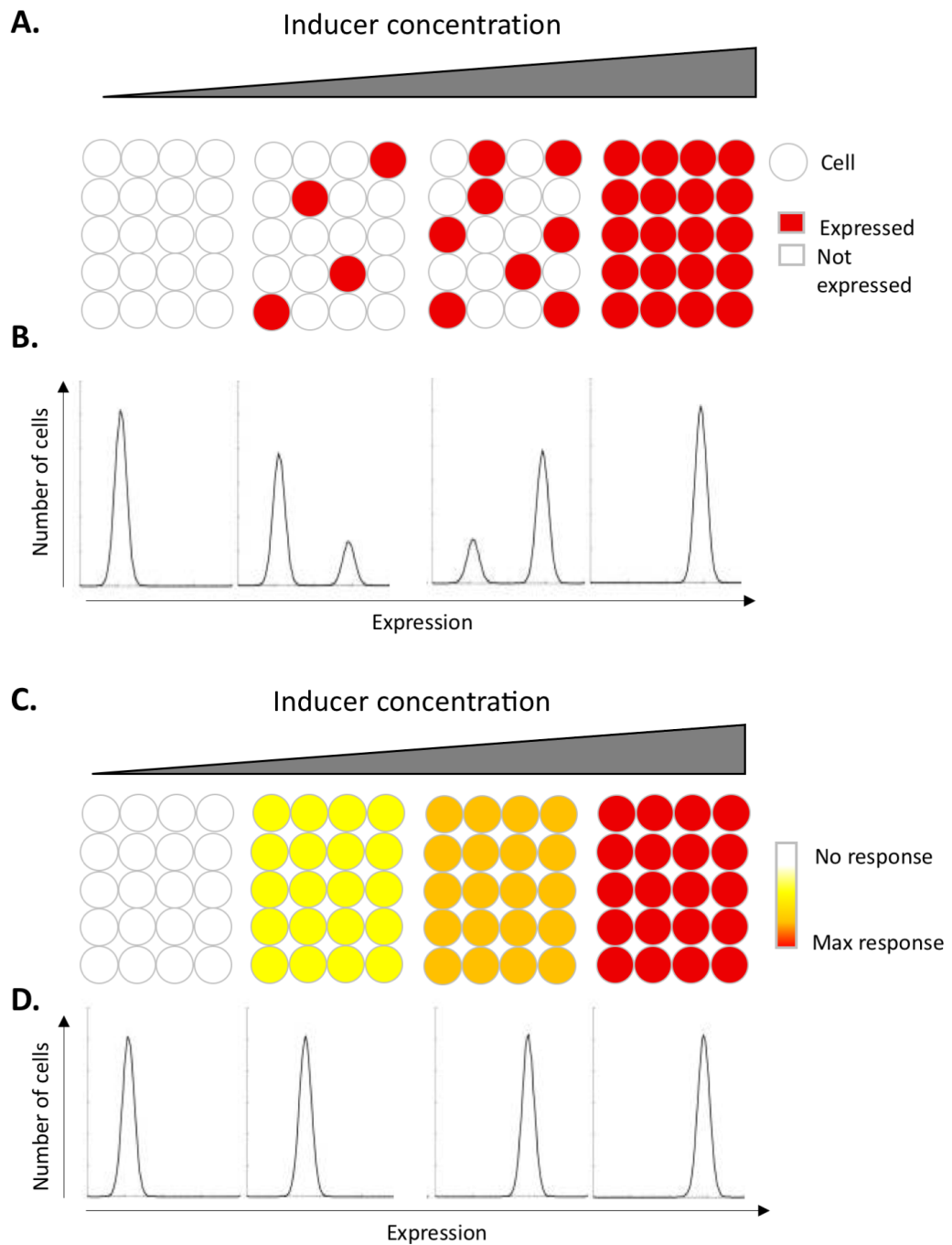
Figure 1.8: Binary and graded models show different patterns of gene expression within a cell population. As the concentration of the inducer, such as a Gc, increases, the population level response has been modelled to increase in two distinct methods. A) In a binary response, as the concentration of the inducer increases, individual cells begin to respond through expression of the gene (strong gene expression indicated in red), within a population of cells. As the inducer concentration increases, more cells within that population respond to the same level. B) When expression for individual cells was shown in graph form, 2 distinct peaks form, corresponding to cells which either express or do not express the gene. C) In a graded response, expression between individual cells is more homogeneous. Instead, as the inducer concentration is increased, the expression within individual cells increased in a graded manner. D) When expression is quantified, this is seen as a single peak, which shifts as the inducer concentration increases. Figure includes components from Zhang et al (201).

Importantly, both models have been well modelled mathematically, and have been validated, as well as possible, within transfected model systems (188, 202). Several technical problems, however, have limited the usefulness of these results. Firstly, using transfected reporter systems relies on the activation of an artificially inserted promoter. These assays also rely on the induction of expression of a reporter protein, and results have been shown to vary according to the reporter gene chosen, such as luciferase and β-galactosidase (201). This is critical as it relies on the accumulation of a protein, which can be altered by factors such as protein half-life, or translational efficiency. This therefore confers very little information on the original transcription event. Further, by analysing accumulation of protein at a defined end point on a bulk level, this gives no information on single cell responses (203).

Some research has hinted at the complexity of inflammatory signalling using population-level techniques. For instance, Reddy et al demonstrated using ChIP-seq analysis that the sensitivity of GR binding at GR-responsive genes was highly variable (204). For instance, genes such as *PER1* showed GR binding at Dex doses as low as 0.5nM, whilst the majority of GR-responsive genes (75.5%) were bound only at higher doses of 50nM. This work has suggested that multiple factors determine this variability in GR binding between genes, including chromatin state, and the presence of other binding factors. This suggests a further level of complexity in the GR response, at the point of GR control of a single gene.

Through the use of single cell RNA-seq, it is now possible to investigate both binary and rheostat models in single cells at the mRNA level, without the confounding factors related to translation and protein half-life. It is also possible to investigate gene expression at a single cell resolution, across thousands of genes. One of the aims of this research project is therefore to investigate which model, if either, can be used to predict the response to Gc addition within GR target genes. This will be the first time single cell RNA-seq technologies have been used to investigate the mechanics of the nuclear receptor response.

Chapter 2 Aims and Objectives

2.1 Summary

The role of Gc in the treatment of GBM is without question essential, but remains controversial. Studies that have investigated Gc responses at the transcriptional level in GBM to date have been over long time courses, and so the primary underlying mechanism explaining adverse effects of Gc are still unclear. Defining these, and screening for better alternatives provides an essential route to improve patient outcome in GBM.

2.2 Hypothesis

Defining acute effects of Gc on gene transcription will identify primary GR targets that influence the efficacy of chemotherapy and radiotherapy which can be used as screening tool for alternative drugs. Exploring transcriptional effects, and the influence of inflammatory cues present in the inflammatory tumour environment at the single cell level will be important in defining how the efficient use of Gc can be maximised in vivo.

2.3 Aims and Objectives

1. **To characterise a GBM cell line to explore GR function:**
   a. Quantify GR expression and posttranslational activation in response to ligand in a panel of GBM cell lines
   b. Confirm nuclear GR translocation upon ligand binding, as a marker of activation

   c. Determine whether there is a GR-dependent transcriptional effect in response to ligand binding

   d. Complete endpoint assays to compare Gc effects in different cell lines and select a single cell line to take forward

2. **To determine the effects of Gc on GBM cell function:**

   a. Complete bulk RNA-seq using different doses and affinities of GR ligands in the selected GBM cell line

   b. Analyse differentially expressed genes, to identify pathways regulated by steroids in GBM cells relevant to cancer progression and treatment

   c. Determine how Gc can affect GBM cell function, and possible effects on the response to chemotherapy and radiotherapy

   d. Test whether selective steroids mediate the same effects as conventional steroids to identify safer alternatives

3. **To identify the heterogeneity of the steroid response in GBM cells**

   a. Complete single cell RNA-seq using different doses and affinities of GR ligands in the selected GBM cell line

   b. Analyse differentially expressed genes, to identify pathways regulated by steroids in GBM cells relevant to cancer progression and treatment

   c. Define the type of transcriptional response for individual genes, and define heterogeneity in the transcriptional response

   d. Develop an optimal assay to validate findings from the scRNA-seq, and explore the effects of inflammatory cues at single cell level

Chapter 3 Materials and Methods

3.1 Preparation of stock solutions

Dexamethasone, progesterone and RU486 were stored as a 20mM stock solution using dimethyl sulfoxide (DMSO). Hydrocortisone (HC) was stored as a 100mM stock solution, also solubilised in DMSO. Compound A (CpA), Deflazacort and Loteprednol etabonate (LE) were made up to a 10mM stock in DMSO, and all were stored at -20°C until required. Temozolomide (TMZ) was resuspended in DMSO to prepare a 50mM stock solution. Stocks were stored at -20ºC. TNFα was resuspended in high purity water to a final concentration of 10ng/ml. Stocks were stored at -80ºC. Catalogue numbers for each reagent are listed in Table 3.1.

Table 3.1: Reagents prepared for stock solutions. Compounds are listed below, alongside catalogue numbers and preferred suppliers. Solutions were prepared according to manufacturer's recommendations.

Reagent	Supplier	Catalogue No.
Compound A	Abcam	ab144525
Deflazacort	Selleck	S1888-SEL
Dexamethasone	Sigma-Aldrich	D4902
Human TNFα	Peprotech	300-01A
Hydrocortisone	Sigma-Aldrich	H0888
Loteprednol etabonate	Sigma-Aldrich	SML0547
Progesterone	Sigma-Aldrich	P8783
RU486	Sigma-Aldrich	M8046
Temozolomide (TMZ)	Selleck chemicals	S1237-SEL

3.2 Cell Culture

3.2.1 Cell passage

Cells were routinely passaged before reaching 80% confluency. Cells were washed using 3ml sterile Dulbecco's phosphate buffered saline (DPBS), then Trypsin-EDTA solution was added (1ml/75cm^2 flask). Cell culture reagents are shown in Table 3.2. Cells were incubated until detached, then trypsin neutralised with appropriate media and centrifuged at 300g x 5mins. Cells were split as appropriate and reseeded in 75cm^2 or 150cm^2 flasks, or into dishes or plates for experiments. Cell lines and their culture requirements are summarised (Table 3.3). Representative images of each cell line are shown (Fig. 3.1).

Table 3.2: List of reagents used within cell culture procedures. Reagents used during cell culture procedures, and their catalogue numbers are provided.

Reagent	Supplier	Catalogue No.
Charcoal stripped serum (CSS)	Gibco	12676029
DMSO	Honeywell	D5879
DPBS	Sigma-Aldrich	D8662
Dulbecco's modified eagle medium (DMEM)	Sigma-Aldrich	D6429
DMEM/Nutrient Mixture F12 Ham (DMEM/F12)	Sigma-Aldrich	D8437
Foetal calf serum (FCS)	Gibco	10500064
Non-essential amino acids	Thermo Fisher	11140035
Sodium pyruvate	Thermo Fisher	11360039
Trypan blue	Sigma-Aldrich	T8154
10x Trypsin-EDTA solution	Sigma-Aldrich	T4174

Table 3.3: Cell lines used within this work, and their required growth conditions. Suppliers for cell lines are shown, and the basal media used for cell culture conditions was used, according to supplier recommendations. For experimental conditions, FCS was replaced with charcoal stripped serum. All other supplements were unchanged.

Cell Line	Catalogue No.	Supplier	Basal Media	Supplier	Supplements
A172	CRL-1620	ATCC	DMEM, high glucose	Sigma	10% FCS
M059J	CRL-2366	ATCC	DMEM/F12 (1:1)	Gibco	10% FCS Sodium pyruvate (1mM) Non-essential amino acids (1mM)
M059K	CRL-2365	ATCC	DMEM/F12 (1:1)	Gibco	10% FCS Sodium pyruvate (1mM) Non-essential amino acids (1mM)
U87	HTB-14	ATCC	DMEM, high glucose	Sigma	10% FCS
U251	09063001	Merck	DMEM, high glucose	Sigma	10% FCS
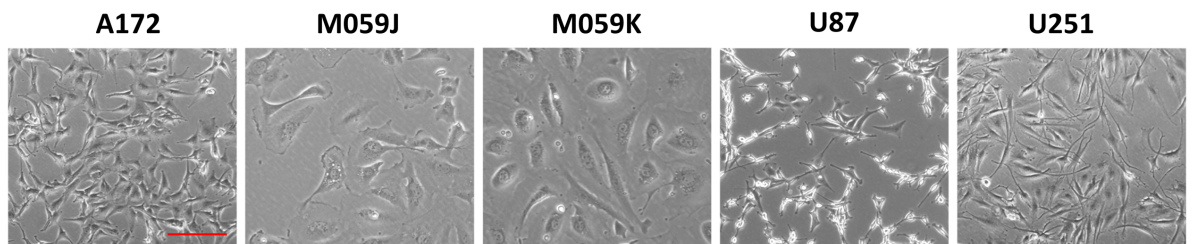
Figure 3.1: Morphology of GBM cell lines used within this thesis. Cells were untreated, cultured in a 6 well plate and imaged at a 10x objective on an Evos microscope. Scale bar denotes 200µm.

3.2.2 Cell freezing and thawing

Cells were frozen in media containing 10% DMSO. Cells were frozen at a density of 1×10^6 cells/ml, and 1 ml was added to each cryovial. Vials were frozen in a Mr Frosty freezing container in a -80ºC freezer, then transferred to liquid nitrogen for long term storage.

To thaw cells, vials were warmed slightly in a 37ºC water bath, then contents were added to 12ml prewarmed media. Cells were then centrifuged at 300g for 5 minutes, media aspirated and replaced with 10ml fresh media. This cell suspension was then added to a T75. Media was replaced after 24 hours, then cultured as described above.

3.2.3 Cell counting

In order to determine cell number, 20µl of cell suspension was mixed with 20µl Trypan Blue solution. 10µl of this mixture was added to a haemocytometer and counted. The number of cells in the 4 outer corners of the haemocytometer were counted and concentration was calculated as follows:

$$Concentration = \frac{Cell\ count}{4} \ x\ 2\ x\ 10^4\ cells/ml$$

In order to determine the dilution required for experiments, the dilution factor was calculated:

$$Dilution\ factor = \frac{Current\ concentration}{Required\ concentration}$$

Finally, the dilution factor was used to calculate the volume of cell suspension required:

$$Volume\ of\ cell\ suspension = \frac{Required\ volume}{Dilution\ factor}$$

Fresh media was then added to make up the required volume.

3.3 Cell treatment

For all experiments, cells were cultured overnight in steroid depleted media prior to experiments (growth media supplemented with 10% CSS). Dex, progesterone, and RU486 were diluted to 1mM in DMSO, and HC was diluted to 5mM. CpA, Deflazacort and LE were diluted to 100µM in DMSO. All of these solutions were then diluted as required in steroid depleted media. TMZ was diluted from the 50mM stock in steroid depleted media as required before addition. TNF-α was diluted to a concentration of 1µg/ml in steroid depleted media and added to cells as required. All solutions were prepared immediately before addition. For IR treatments, cells were irradiated using a RADSOURCE RS-2000 X-ray irradiator, and irradiation was delivered at a dose of 0.11Gy/minute.

3.4 Cell growth assay

Cells were plated in 6 well plates at a density of 1×10^5 cells/well and treated as described in the results. Media and treatments were replaced every 24 hours, and cell counts were carried out at 24 hour intervals. Cell number was calculated as follows:

$$Total\ cell\ number = Cell\ suspension\ volume\ (ml) \times Live\ cell\ count\ (\frac{cells}{ml})$$

3.5 MTT assays

Cells were plated at a density of 1×10^3 cells/well in a 96 well plate. Cells were incubated overnight, then treated with Gc and incubated overnight once again. Cells were then subjected to irradiation or Temozolomide as described. Cells were incubated for a further 5 days, then incubated with 3-(4,5-dimethylthiazol-2-yl)-2,5-diphenyltetrazolium bromide (MTT) (cat. no. 6494, Thermo Fisher) at a final concentration of 0.5mg/ml for 4 hours. Media was removed and replaced with 100µl DMSO. Colour change was measured using a plate reader at 540nm and the average blank value was subtracted from each well. For Gc treatments, survival was calculated relative to each Gc treatment at 0Gy/0µM TMZ.

3.6 qPCR

3.6.1 RNA extraction

Cells were cultured in 10cm dishes until confluent, and treated as indicated. RNeasy kits were used to extract RNA, according to manufacturer's instructions (cat. no. 74104, Qiagen). Briefly, media was removed, and dishes were washed twice using 5ml PBS. PBS was removed, then 600µl of Buffer RLT containing 1% β-mercaptoethanol was added to each dish. Cell scrapers were used to remove lysate, and lysates were transferred to Qiashredders, then centrifuged at 12000g for 15 seconds (cat no. 79654, Qiagen). 600µl 70% ethanol was added to each sample, mixed thoroughly, and mixture was added to RNeasy spin columns. Columns were centrifuged at 12000g for 15 seconds. Supernatant was discarded, 350µl Buffer RW1 was added to each column, and centrifuged as described. On column DNase digestion was carried out, and 10µl DNase was added to each column, diluted in 70µl Buffer RDD (cat. no. 79254, Qiagen).

Columns were incubated at room temperature for 15 minutes, then 350µl Buffer RW1 was added, and centrifuged. 700µl Buffer RPE added to each sample, centrifuged at 12000g for 15 seconds, then 500µl Buffer RPE was added and centrifuged. 500µl Buffer RPE was again added, and centrifuged at 12000g for 2 minutes. Columns were transferred to fresh collection tubes, then centrifuged at 12000g for 1 minute. Columns were finally transferred to 1.5ml Eppendorf tubes, 30µl RNase free water was added, and centrifuged at 12000g for 1 minute. The elute was then transferred to the column and centrifuged again. Samples were then stored at -80ºC until required.

3.6.2 cDNA synthesis

1µl of each sample was used to estimate RNA concentration using a Nanodrop spectrophotometer (Thermo Fisher). 2µg of each sample was diluted to a final volume of 9µl in RNase free water. 10µl of reverse transcriptase (RT) buffer mix, and 1µl of RT Enzyme mix were added to each sample (both high capacity RNA to cDNA kit, cat no. 4387406, Applied Biosystems). Samples were added to a thermal cycler, and incubated at 37ºC for 1 hour, then heated to 95ºC for 5 minutes, before being held at 4 ºC until required. 180µl of RNase free water was added to each sample, then transferred to storage at -20 ºC.

3.6.3 qPCR

qPCR was carried out using Taqman Advanced Master Mix (Thermo Fisher) and Taqman assay probes, according to manufacturer's instructions. 10µl Taqman Advanced Master Mix, 7µl of RNase free water, and 1µl of the appropriate Taqman probe was added to each well of a 96 well plate (Table 3.4). 2µl of cDNA

was then added, to give a final cDNA concentration of 1µg/µl. Plates were run on a QS5 machine (Applied Biosystems) with an initial 2 minute incubation at 50ºC, then 95ºC for 20 seconds. 40 cycles of 1 second at 95ºC, followed by 20 seconds at 60ºC, were used to detect gene expression. Relative gene expression was quantified using the $2^{-\Delta\Delta CT}$ method, and target gene expression was calculated relative to GAPDH. Samples were then normalised to the vehicle control.

Table 3.4 qPCR probes used for RNA-seq validation. qPCR probes were purchased from Thermo Fisher. All probes were specific to the human gene of interest.

Gene target	Catalogue number	Supplier
CDKN1A	Hs00355782_m1	Thermo Fisher
DDIT4	Hs01111686_g1	Thermo Fisher
DUSP1	Hs00610256_g1	Thermo Fisher
FKBP5	Hs01561006_m1	Thermo Fisher
GAPDH	Hs02786624_g1	Thermo Fisher
GILZ	Hs00608272_m1	Thermo Fisher
IL6	Hs00174131_m1	Thermo Fisher
IL8	Hs00174103_m1	Thermo Fisher
PER1	Hs00242988_m1	Thermo Fisher

3.7 Western blotting

3.7.1 Protein extraction

Cells were cultured in 10cm dishes until confluent, and treated as indicated. Cells were lysed in Radioimmunoprecipitation assay (RIPA) buffer (50 mM Tris-HCl pH 7.4, 1% NP40 (Igepal), 0.25% Na-deoxycholate 150 mM NaCl, 1 mM EDTA), supplemented with protease (cat. no. 539134, Merck) and phosphatase inhibitors (cat. no. P5726 and P0044, both Sigma). Insoluble cellular debris was pelleted

by centrifugation at 12,000g at 4°C for 20 minutes and the cleared supernatant retained for protein quantification. 10µl of each sample was added, in triplicate, to a 96 well plate, alongside known bovine serum albumin (BSA) protein standards. 190µl of bicinchonic acid (BCA) reagent was added to each well, and incubated at 37 ºC for 30 minutes (cat. no. 23227, Thermo Fisher). The colorimetric change was measured using a plate reader at a wavelength of 540nm. BSA standards were used to produce a line of best fit, and the equation for this line was used to estimate the protein concentration of the samples. All lysates were diluted using PBS and sodium dodecyl sulfate (SDS) loading dye (250mM TrisHCl, 10% SDS, 30% glycerol, 5% β-mercaptoethanol, 0.02% bromophenol blue) to give a final concentration of 0.5µg/µl. Samples were boiled at 95°C for 5 mins, and then stored at -20°C until required.

3.7.2 Western blotting

A minimum of 5µg protein were electrophoresed on 4–15% polyacrylamide gels (cat. no. 4561086, Bio-Rad Laboratories) and transferred to 0.45µm nitrocellulose membranes (cat. no. 10600002, GE Healthcare) overnight at 4°C. Membranes were blocked for 6 hours (0.15 M NaCl, 1% skimmed milk powder, 0.1% Tween 20) and incubated with primary antibodies (1:1000, diluted in TBST containing 5% BSA) overnight at 4°C with agitation (primary antibodies listed in Table 3.5). After three 10 minute washes (88 mM Tris pH 7.8, 0.1% Tween 20), membranes were incubated with a species-specific horseradish peroxidase (HRP)-conjugated secondary antibody (1:5,000, diluted in wash buffer) for 1 hour at RT, and washed a further three times, each for 10 minutes. Immunoreactive proteins were visualised using enhanced chemiluminescence Super Signal Kit

(cat. no. 34087, Thermo Fisher). ImageJ was used to quantify densitometry compared to loading control.

Table 3.5: Antibodies used for western blotting. Primary and secondary antibodies used for western blotting, and their supplier. Dilutions used are listed, and the species each antibody was produced within. Secondary antibodies for both rabbit and mouse were used depending on the species of the primary antibody. CST – Cell Signalling Technology.

Target	Species	Specificity	Dilution	Supplier	Catalogue No.
B-actin	Mouse	Monoclonal	1:10,000	Sigma-Aldrich	A5441
DNA-PKcs (3H6)	Mouse	Monoclonal	1:1,000	CST	12311
Mineralocorticoid receptor (MR)	Mouse	Monoclonal	1:1,000	Santa Cruz Biotechnology	sc-53000
Glucocorticoid receptor (GR)	Rabbit	Monoclonal	1:1,000	Sigma-Aldrich	3660
p53	Rabbit	Polyclonal	1:1,000	Santa Cruz Biotechnology	sc6243
Phospho-ATM (Ser1981)	Rabbit	Monoclonal	1:1,000	CST	5883
Phospho-ATR (Ser428)	Rabbit	Polyclonal	1:1,000	CST	2853
Phospho-BRCA1 (Ser1524)	Rabbit	Polyclonal	1:1,000	CST	9009
Phospho-Chk1 (Ser345)	Rabbit	Monoclonal	1:1,000	CST	2348
Phospho-Chk2 (Thr68)	Rabbit	Monoclonal	1:1,000	CST	2197
Phospho-p53	Mouse	Monoclonal	1:1,000	CST	9286
Progesterone receptor (PR)	Rabbit	Monoclonal	1:1,000	CST	8757
Rad51	Mouse	Monoclonal	1:1,000	Invitrogen	MA123271
Rad51	Rabbit	Monoclonal	1:1,000	CST	8875
Rad51	Rabbit	Polyclonal	1:1,000	Abcam	ab63801
Anti-rabbit HRP-linked	Donkey	Monoclonal	1:5,000	GE Healthcare	NA934
Anti-mouse HRP-linked	Sheep	Monoclonal	1:5,000	GE Healthcare	NA931

3.7.3 Densitometry analysis

Scanned images of western blots were opened in ImageJ. For each antibody, a box was drawn around the first lane of the blot (Fig. 3.2A). The gel tool was used to mark the first lane of the blot, then the box was copied to the second lane, and so on. The final lane was marked using the tool, allowing the histograms of each lane to be visualised. The "draw line" tool was used to mark off each side of the histogram (Fig. 3.2B). The "wand" tool was then used to measure the size of the area under the histogram. This enables the quantification of the intensity of the band as a numerical value (Fig. 3.2C). This process was repeated for each band, for each antibody. The value for each target antibody was then divided by the β-actin value for each lane, to normalise for variations in gel loading. Values were then normalised to the vehicle control for each experiment.

3.8 Immunofluorescence

3.8.1 Slide preparation

Cells were plated into 12 well plates containing 13mm coverslips overnight, and treated as indicated in the results section. Cells were washed twice with 1ml PBS, and fixed in 1ml 4% paraformaldehyde for 1 hour at room temperature. Cells were washed twice with PBS, then blocked for 4 hours in 1ml blocking buffer (1% FCS and 0.1% Triton-X in DPBS). 220µl primary antibody (diluted 1:200 in blocking buffer) was added to each well, and incubated overnight at room temperature with agitation. Coverslips were washed three times with 1ml DPBS. Wells were treated with 220µl secondary antibody (diluted 1:500) and Alexa647-phalloidin (diluted 1:1000, both in blocking buffer) for a further 2 hours in the dark with agitation.

A. Raw image

B. Bands defined

C. Histogram of individual band

D. Line added to create a single area

E. Area of histogram measured

F. Readout for histogram area
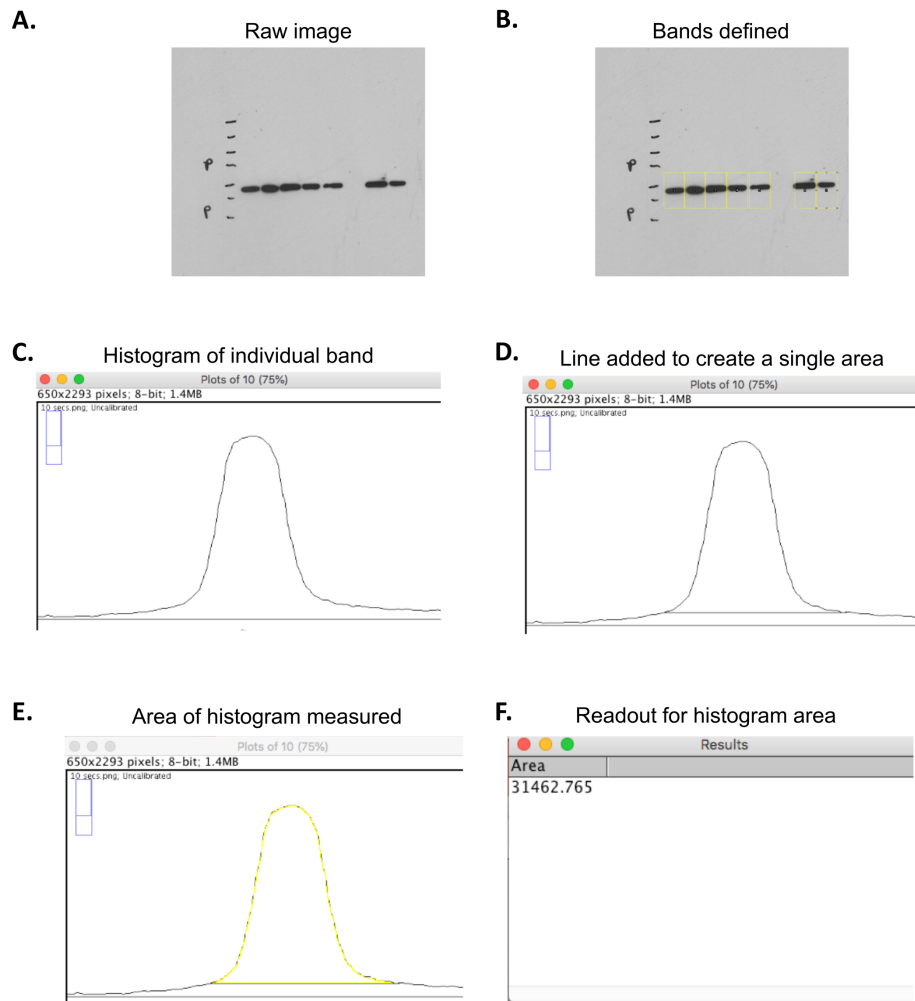
Figure 3.2: Densitometry analysis of western blot images. A) Images of western blot bands were opened in ImageJ. B) The gel tool was used to add a rectangle around the first band. This rectangle was copied to each band, and final band marked. C – D) After marking the final band, the histograms for each band were opened, and the line tool was used to fill in the bottom of the peak. E) The wand tool was used to measure the area of the histogram. F) This result can then be copied to Excel. The value for each target of interest can then be divided by the housekeeping control for the same sample.

Solution was removed and coverslips were washed with 1ml PBS, then incubated with 1ml Hoescht (diluted 1:10,000 in PBS) for 10 mins. Hoescht was then removed, and coverslips were washed three times in 1ml PBS, then mounted onto slides using hard set aqueous mountant (Vectamount, Vectashield).

3.8.2 Imaging

For GR translocation, and Rad51, 53BP1 and γH2AX staining, slides were imaged using Nikon Widefield at 40x objective. Z-stacks were taken, with a minimum of 4 slices, and 10 fields of view were captured for each condition. Imaging conditions were kept consistent between experiments.

3.8.3 Quantification of γH2AX, Rad51 and 53BP1 staining

Z-stacks of images were opened in ImageJ, and the most in-focus slice was chosen for analysis. Images were converted to greyscale, and the Hoescht channel was used to apply a threshold around nuclei, and the Analyse Particle tool was used to create nuclear masks (Fig. 3.3A). This mask was applied to the channels of γH2AX, Rad51 and 53BP1 staining. The mean grey value of each mask was measured using the Region of Interest (ROI) Manager to indicate the mean staining across the nucleus of each cell (Fig. 3.3B). The Find Maxima tool was then used to determine points within the nucleus which reached saturation, seen as foci (Fig. 3.3C). The mask was then applied to this maxima map, to count the number of foci within each nucleus. A minimum of 50 cells were analysed for each condition.

A.

| Raw image of nuclei channel | Threshold used to identify nuclei | Masks added to ROI manager |

B.

Raw image of protein of interest – mean grey value analysed of each mask

	Area	Mean	StdDev	Min	Max	IntDen	RawIntDen
1	176.057	410.305	123.797	150	971	72236.891	2778175
2	228.112	334.261	87.032	144	1074	76248.776	2932469
3	155.177	337.801	94.340	151	688	52419.124	2015999
4	164.694	579.964	204.109	146	1823	95516.610	3673495
5	135.338	268.375	87.006	137	1541	36321.427	1396894.000
6	231.804	378.083	118.143	144	1712	87641.231	3370614.000
7	111.079	1292.192	526.720	272	3231	143534.969	5520244.000
8	265.346	1064.445	376.367	180	2584	282446.081	10862658.000
9	136.144	430.412	188.483	156	2963	58598.135	2253639.000
10	98.884	427.955	206.044	164	2688	42317.829	1627511.000
11	126.706	1224.035	508.347	216	3410	155092.144	5964724.000
12	107.282	580.688	206.131	177	1396	62297.638	2395919.000
13	104.370	347.726	117.914	158	1536	36292.279	1395773.000

C.

Find maxima tool used to determine the number of foci in each nucleus

	Area	Mean	StdDev	Min	Max	IntDen	RawIntDen
1	176.057	1.544	19.784	0	255	271.846	10455
2	228.112	1.541	19.761	0	255	351.411	13515
3	155.177	0.684	13.187	0	255	106.086	4080
4	164.694	2.295	24.083	0	255	377.933	14535.000
5	135.338	1.029	16.166	0	255	139.238	5355.000
6	231.804	2.832	26.724	0	255	656.409	25245.000
7	111.079	2.865	26.881	0	255	318.259	12240.000
8	265.346	4.473	33.476	0	255	1186.841	45645.000
9	136.144	2.386	24.555	0	255	324.890	12495.000
10	98.884	2.012	22.562	0	255	198.912	7650.000
11	126.706	3.663	30.345	0	255	464.128	17850.000
12	107.282	4.079	31.996	0	255	437.606	16830.000
13	104.370	2.668	25.951	0	255	278.477	10710.000

Figure 3.3: Quantification of nuclear staining using ImageJ. A) The Hoescht channel was opened, and the thresholding tool used to create a mask over each nucleus. The analyse particle tool was then used to create a mask to add ROI manager for each nucleus. B) The measure function of the ROI manager was used to measure the mean grey value (staining intensity) within each nucleus. C) The find maxima tool was used to identify foci of staining within each nucleus. The raw integrated density value can be divided by 255 to determine the number of foci.

3.8.4 GR translocation quantification

To determine GR translocation to the nucleus from the cytoplasm, images were converted to greyscale, then thresholded using the nuclear (Hoechst) and cytoplasmic (phalloidin) channels to create nuclear and cytoplasmic masks (Fig. 3.4A). 3 random points were selected within the nucleus or the cytoplasm on the GR (FITC) channel, and added to the ROI manager (Fig. 3.4B). The mean grey

value of the 3 nuclear and cytoplasmic regions was calculated, and the nuclear/cytoplasmic staining ratio was calculated, then expressed as a percentage (Fig. 3.4C). 5 cells were selected at random for each field of view, and 6 fields of view were analysed for each condition. The results of 3 independent experiments were pooled.

A.

Raw image of nuclei channel   Threshold used to identify nuclei   Masks added to ROI manager

B.

3 random points picked within the nucleus & cytoplasm in the GR channel and mean grey value measured

	Area	Mean	StdDev	Min	Max	IntDen	RawIntDen
73	6.188	125.546	7.616	111	151	776.927	29880.000
74	3.328	175.094	12.097	154	202	582.747	22412.000
75	1.820	183.343	11.981	163	214	333.704	12834.000
76	2.054	175.051	9.637	155	195	359.576	13829.000
77	2.990	191.522	10.199	169	223	572.684	22025.000
78	3.536	136.897	9.968	122	171	484.097	18618.000
79	4.264	174.524	11.737	149	209	744.217	28622.000
80	2.184	174.488	7.673	156	191	381.105	14657.000
81	2.912	160.562	10.346	141	187	467.586	17983.000
82	1.560	184.517	9.888	157	209	287.863	11071.000
83	2.704	147.740	9.872	124	178	399.514	15365.000
84	3.536	123.890	6.614	111	147	438.100	16849.000
85	3.458	136.902	7.883	118	155	473.436	18208.000
86	1.794	156.986	4.178	149	170	281.649	10832.000
87	1.794	151.841	5.622	138	169	272.418	10477.000
88	1.560	152.483	5.245	140	164	237.888	9149.000
89	4.056	144.449	10.311	124	178	585.919	22534.000

C.

$$Translocation\ (\%) = \frac{Mean\ grey\ value\ (nucleus)}{Mean\ grey\ value\ (nucleus) + mean\ grey\ value\ (cytoplasm)}\ x\ 100$$

Figure 3.4: Measurement of GR translocation using ImageJ. A) Images were opened in ImageJ, and nuclear masks created using the thresholding tool in the Hoescht channel. B) Within the GR channel, 3 circles were created in a random pattern within the nucleus, following the demarcation of the nuclear masks. Three random points were also selected within the cytoplasm, following the demarcation of the cytoplasmic mask. C) The mean grey value of each three points is calculated, and the translocation to the nucleus is calculated using the equation above.

3.9 Flow Cytometry

3.9.1 Cell viability

Samples were treated as required, then trypsinised and centrifuged at 300g for 5 mins. Cell pellets were resuspended in media and cell counts carried out to ensure equal cell numbers within each cell number. Samples were then transferred to fluorescence activated cell sorting (FACS) tubes, and centrifuged at 300g for 5 mins. Supernatant was removed, and cells were resuspended in 1ml DPBS. Cells were washed once, resuspended in 100µl Zombie NIR viability dye (1:500, cat. no 423105, Biolegend) and incubated for 15 mins, before neutralisation in 2ml FACS buffer (0.5% bovine serum albumin). Cells were washed, resuspended in 100µl FACS buffer, then processed on a Cytoflex (Beckman Coulter), and analysed using CytExpert software (Beckman Coulter). Cells were not gated for single/doublets/viability to test the conditions of single cell RNA-seq (scRNA-seq).

3.9.2 Cell cycle

Samples were cultured in 6 well plates in media supplemented with CSS. Cells were treated for 24 or 48 hours, as required, using Dex and HC. Cells were then trypsinised, resuspended in PBS and counted. 1×10^5 cells were transferred to a FACS tube and analysed for each condition. Samples were washed twice using PBS, then resuspended in 1ml 70% ethanol overnight at 4°C. Cells were then washed twice using PBS, then stained with 5µg RNase A (cat. no. EN0531, Thermo Fisher) and 50µg propidium iodide (PI) (cat. no. P4864, Sigma). Samples were incubated for 1 hour, then analysed by flow cytometry. Signal was

thresholded using an unstained control. Results were analysed using Modfit Software v3.2 (Verity Software House).

3.10 Cell straining and cell counting

Cells were plated into 10cm dishes overnight. Cells were trypsinised and resuspended in 5ml media. Cells were passed through a 70µm cell strainer, and cell counts were carried out before and after straining. Cell counts were carried out using Trypan Blue, as described above. Cell counts were normalised relative to unstrained cell number for each sample. Samples were processed for flow cytometry as described above, and gated for doublet discrimination using side scatter height and area. Gating strategies were kept consistent throughout samples.

3.11 Metaphase Spread Assay

3.11.1　Cell preparation

Cells were plated in 10cm dishes overnight to reach 70 – 80% confluency. Fresh media was added, containing colcemid (cat. no. 234109, Merck) at a final concentration of 100ng/ml. Cells were incubated for 90 minutes at 37°C, then harvested by typsinisation and centrifuged at 250g for 5 minutes. Cells were resuspended in 100µl media, then 4ml pre-warmed 75mM potassium chloride was added in a dropwise manner. Following incubation for 20 minutes at 37°C, cells were centrifuged at 250g for 5 minutes and resuspended in a dropwise manner in 4ml pre-chilled fixative (3:1 methanol:acetic acid). Cells were then centrifuged again at 300 g for 5 minutes and resuspended again in 4ml fixative.

Cells were centrifuged, then supernatant was aspirated until approximately 200µl remained. Samples were then stored at -20ºC.

3.11.2   Metaphase drop

Samples were thawed on ice and tapped to resuspend. Slides were breathed on to create moisture, and 7.5µl cell suspension was immediately pipetted from a 30cm height onto slide. 2 drops were added to each per slide, then dried at room temperature for 1 hour. Hoescht was diluted in mounting solution 1:1000, and add 100µl of this solution was added to each spread before adding coverslip.

3.11.3   Imaging and quantification

Slides were imaged using Nikon Widefield at a 60x objective and processed using ImageJ. The counting tool was used to manually count the chromosome number within each metaphase spread. 20 spreads were quantified for each cell line per replicate.

3.12 Comet assays

3.12.1   Sample preparation

M059K cells were plated in 10cm dishes and treated overnight using Gc as described. Cells were irradiated or treated with TMZ, then incubated for 24 hours. Trevigen Comet Assay Kit (cat. no. 4250-050-K, Trevigen) was used, with a modified alkaline electrophoresis protocol as described below.

3.12.2   Comet assay

Slides were prepared by adding 50μl molten agarose to each well, then stored at 4ºC while samples were prepared. 10cm dishes were scraped using a cell scraper, then contents transferred to centrifuge tubes and centrifuged at 700g for 5 minutes. Cell pellets were resuspended in 5ml chilled DPBS, then centrifuged again. Samples were resuspended in 100μl DPBS, then passed through 70μm cell strainers to limit doublets. Cell counts were performed and cells were resuspended at 2.25×10^5 cells/ml. 10μl of each sample was mixed with 90μl agarose, and 75μl added to each well of the slides. Care was taken not to disturb the base layer of agarose. Slides were incubated at 4ºC to set the agarose. Slides were then immersed in chilled lysis solution at 4ºC for 3 hours, then transferred to chilled alkaline electrophoresis solution (300mM NaOH, 1mM EDTA) for 30 minutes in the dark at room temperature. Slides were transferred to the comet tank in the cold room and alkaline electrophoresis solution was added to cover the slides. Voltage was set to 25V and buffer volume adjusted to reach a current of 300mA. Slides were run for 1 hour, submerged twice within chilled distilled water, then immersed in chilled 70% ethanol for 5 minutes. Ethanol was removed and slides left to dry. 100μl of SYBR green DNA dye solution was added to each well for 15 minutes in the dark at room temperature. Slides were then stored overnight at 4°C prior to imaging.

3.12.3   Imaging

Slides were imaged using a Nikon Widefield. Slides were imaged at a 10x objective, and Z-stack images were acquired for each field of view. Z-stacks contained a minimum of 30 slices, at a slice size of 1μm. A minimum of 10 fields of view were captured for each condition. Exposure time was kept consistent

between repeats of the same experiments. Images were all acquired within 48 hours of staining.

3.12.4 Quantification

OpenComet (v 1.3.1), an ImageJ plugin, was used to quantify comets (205). Maximum intensity projections were created from each z-stack image (Fig. 3.5A). These projections were added to OpenComet, and analysed using background correction and auto head finding (Fig. 3.5B). Output images were analysed manually for outliers, such as doublets, and outliers removed from analysis (Fig. 3.5C). A minimum of 50 cells were analysed for each condition per replicate. Tail moment and olive moment were automatically calculated by the software.

A. Raw image of comets

B. OpenComet interface

C. Image following OpenComet analysis

D. Measurements following OpenComet analysis
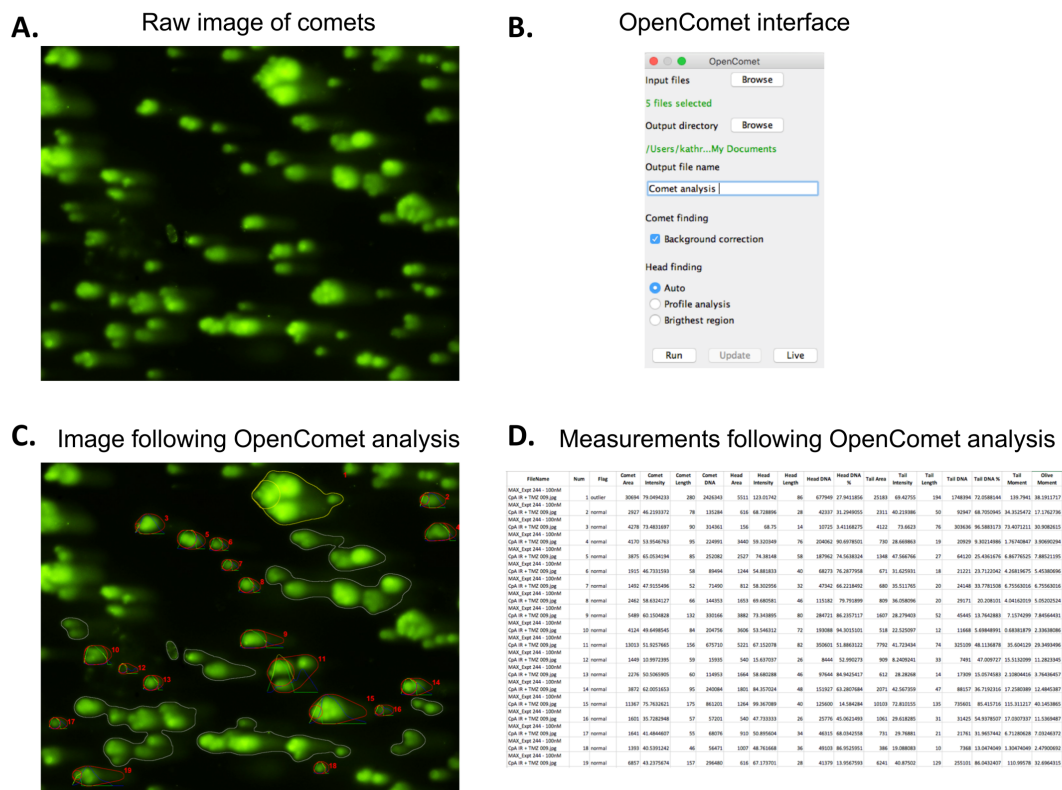
Figure 3.5: Comet assay analysis using OpenComet software. A) Maximum projections of each image were created in ImageJ. B) These projections were uploaded to the OpenComet plugin within ImageJ, and auto head finding option selected. C - D) An output file of detected comets, and a spreadsheet of quantification of individual comets were created. Outliers identified within the images were removed from further analysis.

3.13 siRNA knockdown

3.13.1   Western blotting to assess siRNA knockdown efficiency

M059K cells were plated at a density of 1.15 x 10^5 cells/well of a 6 well plate. 1 well was plated for each small interfering RNA (siRNA). Plates were incubated for 4 hours to allow cells to attach, then transfected using RNAiMAX (cat. no. 13778075, Thermo Fisher). For each well, 150µl serum-free RPMI was mixed with 9µl RNAiMAX. Each siRNA was also added to another 150µl serum-free media to a final concentration of 200nM (Table 3.6). The RNAiMAX and siRNA mixtures were combined, and incubated for 5 minutes. 250µl of this mixture was added to each well. Cells were incubated for 48 hours, then lysed in 100µl RIPA buffer. Western blotting was carried out as described above.

3.13.2   siRNA knockdown for MTT assay

Cells were plated at a concentration of 1 x 10^3 cells/well of 5 96 well plates, then incubated for 4 hours to allow cells to attach. 12 wells were transfected with each siRNA in each plate. For each siRNA, 120µl RNAiMAX was added to 400µl serum-free RPMI. Each siRNA was diluted in 400µl serum-free RPMI to a final concentration of 200nM (Table 3.6). The RNAiMAX and siRNA mixtures were combined, then incubated for 5 minutes. 10µl of this mixture was added to each well. Plates were incubated for 24 hours, then treated with Gc. 6 wells of each knockdown were treated with a vehicle control, and 6 were treated with 100nM Dex. Cells were incubated overnight, then treated with 0, 0.25, 1, 5, or 10Gy irradiation. Cells were incubated for 5 days, then MTT assay carried out as described above. Relative survival was analysed relative to the 0Gy value for each siRNA.

Table 3.6: siRNA used within the scope of this thesis. siRNA probes are listed, alongside catalogue numbers. For DNA-PKcs, Rad51 and p53, Flexitube products were purchased, containing each of the listed probes. Within the results section, probes are referred to by the clone numbers listed.

Target	Clone No.	Manufacturer	Catalogue No.
DNA-PKcs	5	Qiagen	SI0222423
DNA-PKcs	6	Qiagen	SI02224229
DNA-PKcs	8	Qiagen	SI02663633
DNA-PKcs	14	Qiagen	SI04436705
GR	3	Qiagen	SI00003759
GR	4	Qiagen	SI02654757
Non-targeting control	N/A	Qiagen	SI03650318
Rad51	6	Qiagen	SI02629837
Rad51	7	Qiagen	SI02663682
Rad51	8	Qiagen	SI03061338
Rad51	9	Qiagen	SI03072272
TP53	7	Qiagen	SI02623747
TP53	8	Qiagen	SI02623754
TP53	9	Qiagen	SI02655170
TP53	13	Qiagen	SI04384079

3.14 Luciferase assays

3.14.1   Plasmid transfection

M059K cells were plated in 10cm dishes in media supplemented with 10% FCS and incubated overnight. For each 10cm dish, 3.75µl of Fugene transfection reagent was added to 100µl of serum-free RPMI media and incubated for 2 minutes (Cat no. E2691, Promega). All plasmids had previously been prepared within the Matthews group (85, 206). 1µg of either the TAT3-luc or NFκB-luc plasmid, and 0.25µg Renilla plasmid were combined in a separate tube, then added to the Fugene mix. This mixture was incubated at room temperature for

15 minutes, then 100µl was added in a dropwise fashion to the 10cm dish. Cell were incubated overnight to enable efficient transfection.

3.14.2   Cell treatment

10cm dishes were trypsinised and centrifuged at 300g for 5 minutes. If multiple dishes were transfected with the sample plasmid, dishes were pooled. Each dish was resuspended in 25ml of CSS media, and 500µl of cell suspension was added to each well of 2 24-well plates. These plates were incubated for 1 hour, then treated with GR ligands, or a vehicle control for 4 hours. Cells were then treated with TNF, if required, and incubated overnight. Conditions were carried out in triplicate.

3.14.3   Luciferase assay

Wells were washed twice using DPBS, then 100µl passive lysis buffer (included with dual luciferase kit, cat. no. E1910, Promega) was added to each well. Plates were incubated at room temperature on a rocker for 30 minutes. 95µl of lysate from each well was transferred to a white bottomed 96-well plate (cat. no. 655074, Grenier). A dual injector luminometer (Berthold) was used. The luminometer was programmed to dispense 25µl of LARII into each well, followed by a 2 second shake, then 2 second wait time, followed by a 10 second read time. 25µl of Stop & Glo reagent was then dispensed, with a 2 second shake, a 2 second wait time, and a 5 second read time. The LARII (NRE-luc, or TAT3-luc) value for each well was divided by the Stop & Glo (Renilla value) to create a ratio. A mean for the triplicate of each condition was then calculated. This ratio was then normalised to the vehicle control, with no TNF.

3.15 Bulk RNA-seq preparation and analysis

3.15.1   Preparation of samples for bulk RNA-seq

Samples were treated in parallel with single cell RNA-seq samples. RNA was extracted as previously described for qPCR preparation, and an ethanol clean-up kit was used to maximise RNA quality. Samples were prepared in triplicate for each treatment and transferred to sequencing staff at the University of Manchester. Samples were run on a single lane, and a read depth of 300 million reads was used for the 12 samples processed.

3.15.2   Analysis of bulk RNA-seq

Analysis was carried out by Syed Murtaza Baker at the University of Manchester. Trimmomatic 0.36 was used to carry out quality and adapter trimming to fastq files (207). Star 2.5.1a was then used to map the reads to the GRCh38 human genome (208). Following this, HTSeq was used to quantify read counts for each gene (209). Differential expression was determined using DEseq2 (210). During this analysis, sample LM18_S44, one of the high HC replicates, was analysed as an outlier using principal component analysis. Due to this, this sample was removed from downstream analysis. Using DEseq2, differentially expressed (DE) gene lists were created for each Gc treatment relative to the vehicle control. Genes were selected with a log2fold change of 1.5, and a False Discovery Rate (FDR) of <0.05 was used to signify significantly differentially expressed genes. Variation was tested between vehicle and Dex treated samples. BCV analysis was used within EdgeR (211).

3.16 Single cell RNA-seq preparation and analysis

3.16.1   Preparation of samples for single cell RNA-seq

Cells were plated into 10cm dishes and left to adhere overnight. The media was changed to steroid depleted media and cells left overnight. Cells were treated for 4 hours, then trypsinised using TrypLE Express (Gibco), and centrifuged at 95g for 5 minutes. Cell counts were completed using a BioRad TC20 automated cell counter and the cell concentration was adjusted to 1.0×10^6 cells/ml in culture media. 1ml cell suspension for each sample was stained using 160μl Hoescht and PI solution, mixed 1:1 (Wafergen) and cells incubated for 20mins at 37°C. Solution was neutralised using 1ml warmed PBS. Cells were centrifuged at 95g for 5 minutes and resuspended in 1ml warmed PBS. Cell counts were repeated and adjusted to 5×10^5 cells/ml and 1ml was given to the Genomic Technologies Core Facility at the University of Manchester. Staff transferred equal volumes of samples into each well of the 5,000 well barcoded plate (ICell8, Wafergen). Tiled images were captured and wells containing single, live cells determined using Hoescht to mark all cells, and PI to mark dead cells. A plate map was determined from this data, and 1,000 wells containing live, single cells selected for library preparation and sequencing.

3.16.2   Single cell RNA-seq analysis

Analysis was carried out by Syed Murtaza Baker at the University of Manchester. Sequence files were mapped to GRChg38 genome using STAR-2.5.1a. The uniquely mapped read counts were quantified using htseq-0.6.1. Methods for cell filtering, normalisation and classification of cell cycle phase are described within Chapter 5. DE analysis was carried out using edgeR. Cells were grouped into

their respective samples, then data was normalised using trimmed means of m values (212). An exact test was used to identify differentially expressed genes between each Gc treatment, and the vehicle control. Genes with an FDR of <0.01 were considered differentially expressed.

3.17 Gene ontology analysis

Differentially expressed gene lists were uploaded to Enrichr (https://amp.pharm.mssm.edu/Enrichr), a free-to-use gene ontology analysis tool. The pathways tool was used to predict pathways affected by the differentially expressed genes. KEGG 2019 Human and NCI-Nature 2016 databases were analysed to determine pathways affected by DE genes. Combined z-score was used to determine significance.

3.18 ChIP-seq analysis

Publicly available datasets were accessed using Cistrome DB (http://cistrome.org/db/). Datasets were downloaded and the top 5,000 hits were analysed. An online venn diagram tool (http://bioinformatics.psb.ugent.be/webtools/Venn) was used to compare lists and gene tracks were also imported into UCSC genome browser to visualise binding peaks. ChIP-seq datasets accessed are listed in Table 3.7.

Table 3.7: ChIP-seq databases accessed for this thesis. ChIP-seq databases were accessed via Cistrome DB. Data was downloaded for further analysis, and peaks were visualised using UCSC browser to compare peaks between transcription factors.

Cell line	Treatment	Transcription factor	GEO accession number	CistromeDB ID
A549	100nM Dex for 4 hours	GR	ENCSR660RYY	64155
MDA-MB-231	100nM Dex for 1 hour	GR	GSM1350529	56103
MDA-MB-231	Untreated	P53	GSM2501568	75042
U20S	100nM Dex for 1 hour	GR	GSM1607528	58057
U20S	Untreated	P53	GSM545807	2796

3.19 Single Molecule Fluorescence In Situ Hybridization (smFISH)

3.19.1   Sample preparation

Cells were plated in glass-bottomed 96 well plates at a density of 6×10^3 cells/well and incubated overnight. Samples were treated using 10ng/ml TNF-α for 1 hour or 20 hours, then treated for 4 hours with a vehicle control, 50nM HC, 500nM HC or 100nM Dex. Cells were then stained using the ViewRNA Plus smFISH assay kit (cat. no. 88-19000-99, Thermo Fisher). Media was removed from wells, and replaced with 50μl permeabilization/fixation solution. The plate was incubated for 30 minutes at room temperature in a humidified chamber. Wells were then washed 3 times using 100μl/well of PBS containing RNase inhibitor. Care was taken to ensure that no more than 2 wells were aspirated at a time. After aspirating the third wash, 50μl fixation solution was added to each well. The plate was incubated for 1 hour at room temperature in a humidified chamber. Probes

were diluted 1:100 in probe diluent, and wells were washed 3 times using PBS, as described previously (probes listed in Table 3.8). 50µl of probe mixture was then added to each well, and incubated within a humidified chamber for 1 hour in a 40°C incubator. Wells were then washed 5 times using 100µl wash buffer. After adding the final wash, the plate was stored at 4°C overnight.

Diluents were pre-warmed at 40°C for 30 minutes, then preamplifier mix was diluted 1:25 in amplifier diluent. Wash buffer was removed and 50µl of this mixture was added to each well. The plate was incubated at 40°C for 1 hour in a humidified chamber. Amplifier mix was then diluted 1:25 in preamplifier diluent. Wells were then washed 5 times using 100µl wash buffer, before adding 50µl amplifier mix. The plate was then incubated in a humidified chamber at 40°C for 1 hour. Wells were washed again 5 times using 100µl wash buffer. 50µl probe label mix was then added, diluted 1:25 in label probe diluent. The plate was then incubated for 1 hour at 40°C in a humidified chamber. Wells were washed five times with 100µl wash buffer. Following washes, 50µl Dapi, diluted 1:100 in PBS was added to each well. The plate was then incubated in the dark at room temperature for 5 minutes. Wells were washed with 100µl/well of PBS, then replaced with 150µl/well of PBS for imaging.

Table 3.8: smFISH probes used for single cell RNA-seq validation. Table summarises details of smFISH probes used. Catalogue number, type (defined by excitation wavelength), and optimal detection wavelength, as shown for each probe.

Target	Species	Catalogue number	Type	Detection Wavelength
B-actin	Human	VA4-10293-VCP	4	488
DUSP1	Human	VA4-3083868-VC	4	488
GILZ	Human	VA1-20469-VC	1	546
GR	Human	VA6-3169256-VC	6	647
IL6	Human	VA4-15969-VC	4	488
IL8	Human	VA1-13103-VC	1	546

3.19.2 Imaging

All images were taken within 24 hours of staining in order to prevent loss of signal. For images taken on Nikon widefield, images were taken a 40x magnification. Z-stacks were taken with a minimum of 6 slices, with slices of 1μm. A minimum of 20 fields of view were taken for each condition. When using Operetta High Content Imaging System (Perkin Elmer), 15 fields of view were taken within each well, and 10 planes were taken within each z-stack. For confocal imaging, z-stacks were taken at 40x magnification of slices of 0.25μm, using an A1R confocal microscope (Nikon). 10 z-stacks were taken for each well. Imaging conditions were kept consistent between experiments.

3.19.3   Quantification using ImageJ

Z-stack images were opened within ImageJ, and maximum projections were created for each channel. Initially, cytoplasmic thresholding was attempted using the mRNA staining, and brightfield images of the field of view, however, neither method provided widespread enough staining to create a cytoplasmic mask. Instead, the freehand tool was used using brightfield imaging to manually draw around each cell. The find maxima tool was then used to detect foci, and the number of foci was quantified within each cell. A minimum of 50 cells were analysed for each condition.

3.19.4   Quantification using FishQuant

In order to provide unbiased analysis of foci, FishQuant software (v3) was used on the Matlab platform (version R2019a). The FQ segmentation tool (opened through the FQ_seg command in Matlab) was used to create maximum projections of both the Dapi and FITC channels to provide a reference point for nuclear and cytoplasmic masks respectively. These maximum projections were then imported to CellProfiler (v 2.1.1), using the pipeline provided within the FishQuant software package. This pipeline was used to create segmentation masks for each field of view, for all required channels (Fig. 3.6A). The batch processing tool within FishQuant was then used to detect foci throughout the z-stack for each cell in each field of view (Fig. 3.6B). Each mask was manually examined to ensure cells were accurately segregated (Fig. 3.6C). Inaccurate masks were removed from further analysis. 5 fields of view were analysed for each condition, and the experiment was repeated 3 times.

A.

Z-projections made using FQ seg

Z projections added to CellProfiler pipeline

Nuclear and cytoplasmic masks created for each cell

B. Outlines added to each channel's z-stack

Outlines added to FishQuant batch processing tool

C. Spots thresholded using quality scores

Images manually analysed for outliers
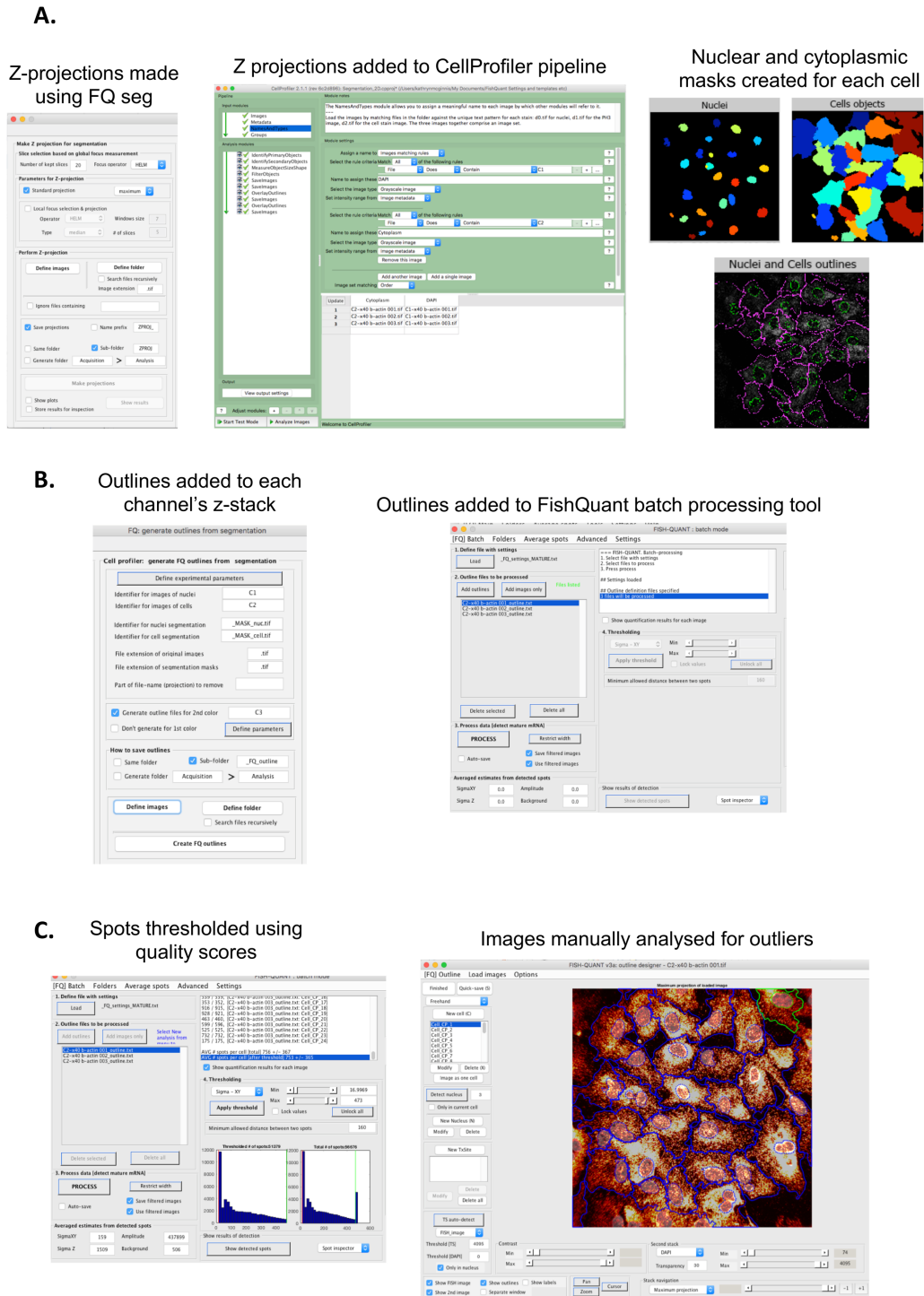
Figure 3.6: Analysis of smFISH staining using FishQuant. A) Z-stacks of individual channels were uploaded to the FQ segmentation tool, and maximum projections were created for each image. These maximum projections were uploaded to CellProfiler, and masks for both nuclei and cytoplasm were created using the pipeline found within the FishQuant software package. B) These masks were added to each channel of each image using the FQ segmentation tool to create both nuclear and cytoplasmic outlines for each. These outlines were then added to the batch processing tool in the FishQuant software, and processed. C) Outliers were removed through removing cells with low quality scores, and by manually analysing images.

3.19.5   Correlation analysis for smFISH

Expression of each mRNA was correlated within individual cells, for each condition. Line of best fit for each graph was calculated using simple linear regression, and correlation was tested using a Pearson's correlation coefficient. R^2 value is shown for each correlation.

3.20 Statistics

Statistical analysis was carried out using Prism (version 8.4.1). GR and γH2AX immunofluorescence results were analysed using a 1-way analysis of variance (ANOVA) with Tukey's multiple comparisons test. Comet assays, growth assays, smFISH, qPCR and MTT results were analysed using a 2-way ANOVA with Dunnett's multiple comparisons test. All results were analysed compared to vehicle control. Results of $p < 0.05$ were considered statistically significant. All error bars indicate $\pm$ standard error of the mean (SEM). All experiments were carried out 3 times, unless otherwise stated.

Chapter 4 – Glucocorticoid effects on therapeutic efficacy in glioblastoma

4.1 Introduction

Gc are potent anti-inflammatory drugs, prescribed to patients with GBM to reduce oedema and inflammation (156, 181). Recent reports suggest that high doses of Gc can be detrimental, thus reducing survival times of patients (182, 186). Despite their wide clinical use, the specific effects that Gc have directly on GBM cells are not well characterised. This is particularly important given that Gc effects are tissue-specific. In some leukemias for example, Gc are prescribed as a chemotherapeutic agent, and can be very potent inducers of apoptosis (213, 214). In small cell lung cancer, the GR promoter is hypermethylated, resulting in reduced GR expression, and restoring GR expression is strongly apoptotic (215-217). In contrast, in non-small cell lung cancers such as adenocarcinomas, which comprise more than 80% of lung cancers, Gc induce cell cycle arrest (216, 218). This potential effect is particularly important in the context of GBM, as radiotherapy and some chemotherapeutics, such as TMZ, rely on the targeting of rapidly dividing cells, and therefore induction of cell cycle arrest may reduce the efficacy of cancer treatment (219).

The aims of this chapter were therefore two-fold:

1) To characterise GR expression, activation and modulation of cell function in a panel of GBM cell lines.

2) To determine how Gc treatment reduces the efficacy of radiotherapy and chemotherapy in GBM cells.

4.2 Results

4.2.1 GR expression within GBM

Firstly the expression of GR within GBM tumours was investigated by accessing The Cancer Genome Atlas (TCGA) RNA-seq data from primary GBM tissue, various low grade glioma subtypes, or normal brain tissue, accessed through the GlioVis database (220). This data is derived from tumour tissue, however, an important caveat is that there is no data provided for whether patients had been treated with Dexamethasone prior to surgery. GR expression showed no significant difference between GBM tissue and normal brain (Fig. 4.1A), however, expression was significantly lower in GBM tissue when compared with the low grade glioma subtypes of oligodendroma, oligoastrocytoma and astrocytoma (Fig. 4.1B). In addition, within astrocytoma and GBM tumours, low GR expression was associated with significantly reduced survival (Fig. 4.1C). For astrocytoma patients, at 75 months, survival for patients with low GR expression was 25%, whilst for patients with high GR expression, survival was 55%. GBM patients show a markedly reduced survival due to the aggressive nature of the tumour, however, a similar pattern is also seen. At 25 months, survival for patients with high GR expression was 30%, whilst this was reduced to 9% in patients with low GR expression. As previously mentioned, information regarding Dex treatment is not recorded, and it has previously been well demonstrated that Gc treatment leads to a reduction in GR expression – through protein turnover, but also at the transcriptional level (221). It is therefore possible that reduced GR expression within GBM patients is caused by Dex treatment itself, and patients with low GR expression indicate those receiving the highest doses of Dex, thus correlating with reduced survival.
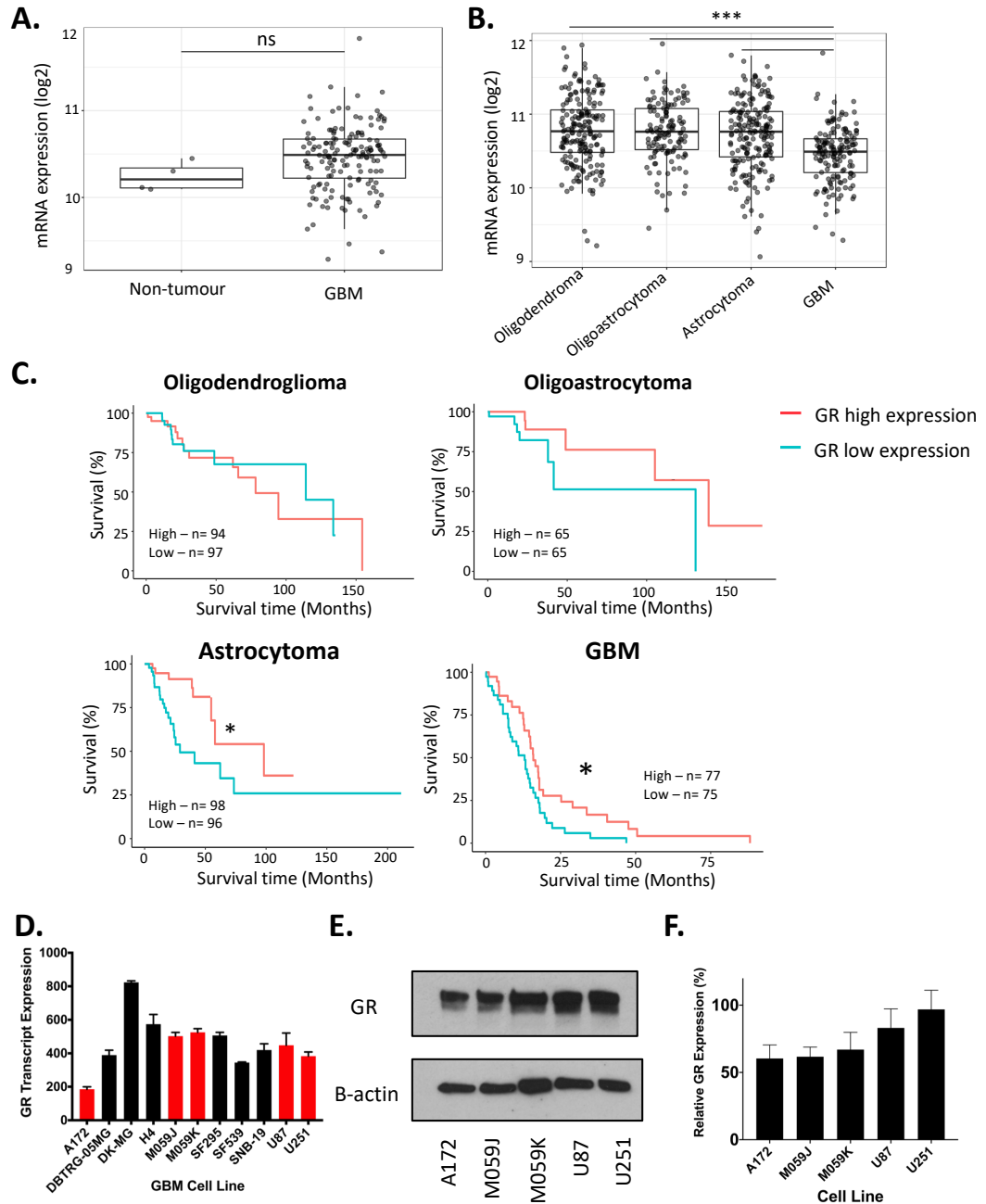
Figure 4.1: NR3C1 (GR) expression was significantly decreased in GBM tissue, and reduced expression correlates with shorter survival. GR expression within primary brain tumour tissue were analysed using GlioVis, with publicly available RNA-seq data from The Cancer Genome Atlas. Expression of GR within GBM was compared with normal brain tissue (A), and types of low grade glioma (B). C) Patient survival was plotted, correlated with high and low NR3C1 expression. D) Expression of GR transcript within multiple GBM cell lines is shown. Data was provided by GSK as part of a previous group collaboration. E) Protein expression of GR was analysed within 5 selected GBM cell lines, compared with β-actin as a housekeeping control. F) Expression was quantified, relative to MCF7, and normalised to b-actin. Western blot images are representative of n=2, and quantification indicated the mean of n=2. Error bars denote SEM. Significance for A) and B) was tested using Tukey's Honest Significant Difference test. Significance for C) was tested using the log rank p value. * = p ≤ 0.05, and *** = p ≤ 0.001.

After confirming that GR was expressed within GBM primary tissue, expression was then investigated in a panel of GBM cell lines. Gene expression data was first analysed, which indicated GR RNA transcript expression within ten well-characterised GBM cell lines (Fig. 4.1D). The expression between cell lines was highly variable. Five cell lines were identified for further analysis – A172 cells which showed low expression, and U87, U251, M059J and M059K cells, which showed higher expression.

A172 cells have been used in previous papers used to investigate the effects of Dex within GBM (222, 223). U87 and U251 cell lines have often been described as the most commonly used GBM cell lines. A PubMed search for U87 and U251 retrieved 3,546 and 2,477 results respectively (224). Therefore, through the use of these cell lines, this work will fit into the existing field of GBM research. Two further GBM cell lines, both derived from single cell clones from within the same GBM tumour were also utilised for this research; M059J and M059K cells. As mentioned within Section 1.2.4.1, M059J cells are commonly used, not just within GBM research, but more broadly as a model for understanding DNA-PK effects due to its effective DNA-PKcs deletion (225). This renders the M059J cell line radiosensitive, whilst M059K cells remain relatively radioresistant (226). These 5 GBM cell lines were therefore chosen to reflect the heterogeneity of GR expression between GBM tumours.

GR protein expression within the five selected cell lines was next analysed using western blotting (Fig. 4.1E). Following labelling with the GR antibody, two bands of a similar size were seen. The antibody used was capable of binding to both GRα and GRβ, two isoforms of GR. GRα is known to have a molecular weight of

94kDa, and may represent the larger band, whilst the smaller, lighter band may represent GRβ, which has a molecular weight of 90kDa. This expression of both bands was quantified, relative to β-actin as an internal housekeeping protein control (Fig. 4.1F). All five cell lines showed GR expression, and differences in protein expression were not as marked as those seen in transcript expression. All five cell lines were therefore taken forward for further analysis.

4.2.2 Gc increase GBM cell survival following IR and TMZ

As Dex has been shown to reduce GBM patient survival, it was hypothesised that this may be due to a reduction in therapeutic efficacy. Therefore the effect of Gc on GBM cell survival following irradiation (IR) and Temozolomide (TMZ), the standard chemotherapeutic drug used in the treatment of GBM, was analysed. Previous work has estimated that Dex concentration within the brain tissue of GBM patients may reach up to 530 - 573nM, although values were highly variable (227, 228). An important caveat is that these studies contained patients receiving Dex doses of between 12–32mg daily. Recent guidelines have advised a dose of 16mg/day, divided into 4 doses of 4mg (229). These values are far higher than concentrations commonly used within mechanistic studies of Gc action. Therefore a dose of 100nM Dex has been utilised in this study, which is in line with doses used in the study of GR, and should well exceed the saturating dose for *in vitro* studies. The effects of endogenous cortisol within GBM cells was investigated through the use of hydrocortisone (HC), the synthetic equivalent of cortisol in order to understand what effects synthetic and endogenous Gc could have on GBM cells. A high and low dose of HC was selected to represent maximum and minimum circulating levels.

Cells were pre-treated overnight with either a vehicle control, 50nM HC, 500nM HC, or 100nM Dex. Cells were then subjected to IR doses of 0.25Gy – 10Gy, TMZ doses of 0.3µM – 300µM, or a combination of 5Gy irradiation, and increasing doses of TMZ. Cells were incubated for 5 days following treatment to reach confluence, then MTT cell viability assays were performed. MTT is converted by living, metabolising cells to formazan, a purple substrate. By measuring the colorimetric change, it is possible to gain a relative estimate of the number of metabolising (live) cells for each condition. The number of surviving cells were calculated relative to untreated cells.

A172 cells showed high levels of resistance to both IR and TMZ treatment (Fig. 4.2A). After 10Gy IR and 300µM TMZ, survival was still approximately 50%. There was also no discernible effect of Gc addition. When the treatments were combined, however, Dex caused a significant increase in cell survival following 5Gy IR and both 30µM and 300µM TMZ. This may be of interest as previous research has shown that doses of TMZ within patient brain reached approximately 30µM, and treatment regimens usually consist of concurrent radiotherapy and TMZ, so the protective effect seen at this dose is physiologically relevant (230).

As previously reported, M059J cells demonstrated high radiosensitivity, with a significant reduction in survival with radiation doses as low as 1Gy (Fig. 4.2B). M059K cells, meanwhile, show higher survival even at higher doses of irradiation (Fig. 4.2C). Both cell lines, however, show significantly increased survival when cells were pre-treated with Gc compared with the vehicle control. This response appears to be both dose- and affinity-dependent. A small increase in survival is

seen with a dose of 50nM HC, reaching significance in M059J cells, but not M059K cells. 500nM HC led to increased survival in both cell lines at a dose of 5Gy, whilst pre-treatment with 100nM Dex led to a significant increase in cell survival with all 4 irradiation doses. M059K cells showed 20.98% survival in vehicle treated samples, but with Dex treatment this rose to 39.98%, resulting in an almost doubling of cell survival. Similarly, M059J cells had a survival of 15.27% with 10Gy irradiation, but this rose to 27.78% with Dex addition.

Following TMZ treatment, for both M059J and M059K cells, there appeared to be a dose- and affinity- dependent protective effect when pre-treated using Gc. This effect was small with 50nM HC, and only reached significance with a dose of 3µM TMZ in M059K cells, and 30µM TMZ in M059J cells. When pre-treated with 500nM HC, once again this effect was larger, and reached significance at doses of 0.3µM – 30µM in M059J cells, and at 30µM in M059K cells. A similar effect was seen with 100nM Dex addition, reaching significance in M059J cells at doses of 3 and 30µM TMZ, and 30µM and 300µM in M059K cells.

When the treatments were combined, both cell lines showed a significant increase in cell number following both 500nM HC and 100nM Dex when subjected to 5Gy IR and 30µM TMZ, as was seen for A172 cells.
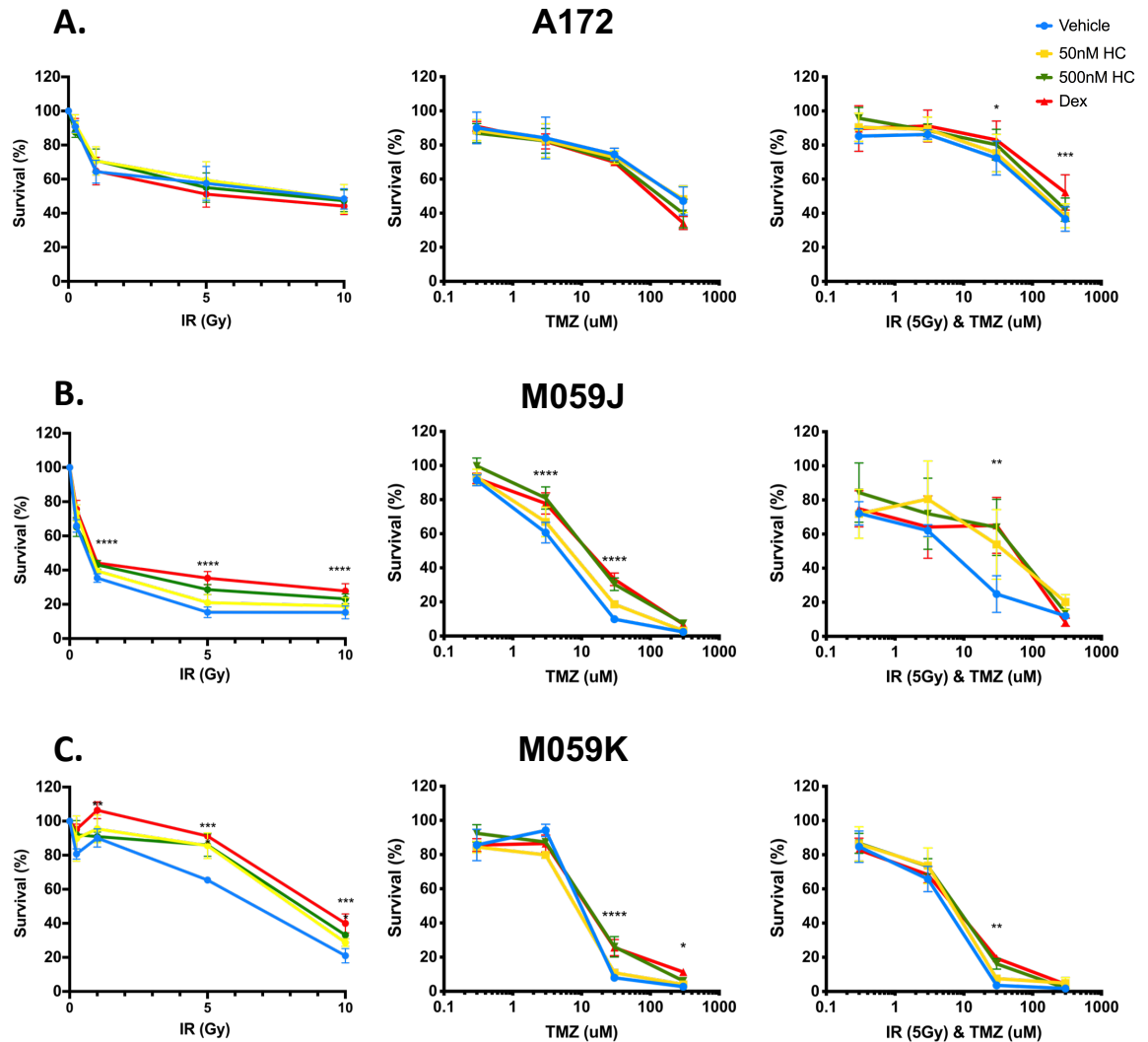
Figure 4.2: Dex treatment increases GBM cell survival following both irradiation and chemotherapy. A172, M059J, and M059K cells were pre-treated overnight with 50nM HC, 500nM HC, 100nM Dex or a vehicle control. Cells were then subjected to increasing doses of irradiation, the chemotherapeutic Temozolomide, or a combined dose of irradiation (5Gy), and increasing doses of Temozolomide. Cells were incubated for 5 days, then metabolic activity was analysed using MTT. Survival was quantified relative to untreated control. Results shown are the mean of 3 independent experiments. Error bars denote SEM. Statistical significance was tested using 2-way ANOVA with Dunnett's multiple comparison test. Stars denote significance between Dex treated samples and the vehicle control. For simplicity, significance is not shown for 50nM and 500nM HC doses. * = $p \leq 0.05$, ** = $p \leq 0.01$, *** = $p \leq 0.001$, and **** = $p \leq 0.0001$.

U251 cells were also highly resistant to both treatments in isolation, however, Dex treatment did lead to significantly higher survival when cells were subjected to 5Gy IR alongside 0.3 – 30µM TMZ (Fig. 4.3A). Finally, Gc addition appeared to exhibit no effect on cell survival in U87 cells, however, Dex addition caused noticeable changes to cell morphology (Fig. 4.3B - C). Images in Fig. 4.3C show cells following MTT addition at endpoint at doses of 0Gy and 10Gy. Dex treated wells showed similar large spheroid-like structures at all IR and TMZ doses. These changes to cell morphology may suggest that Dex is exerting different effects within U87 cells compared to A172, M059J, M059K and U251 cells. Previous research has demonstrated 512 homozygous mutations within the U87 cell genome, and many of these genes were linked to cell adhesion (231). This mutational signature may result in the altered Gc response seen within U87 cells.

Overall, four out of five GBM cell lines tested showed that Dex was able to increase cell survival following therapy. This increase in cell survival *in vitro* may suggest a mechanism by which Gc could render GBM cells more radio- and chemo-resistant within patients. This could in turn allow a larger proportion of the tumour to survive following therapy, allowing the tumour mass to regrow more quickly, ultimately resulting in the reduced survival times seen in previous research.
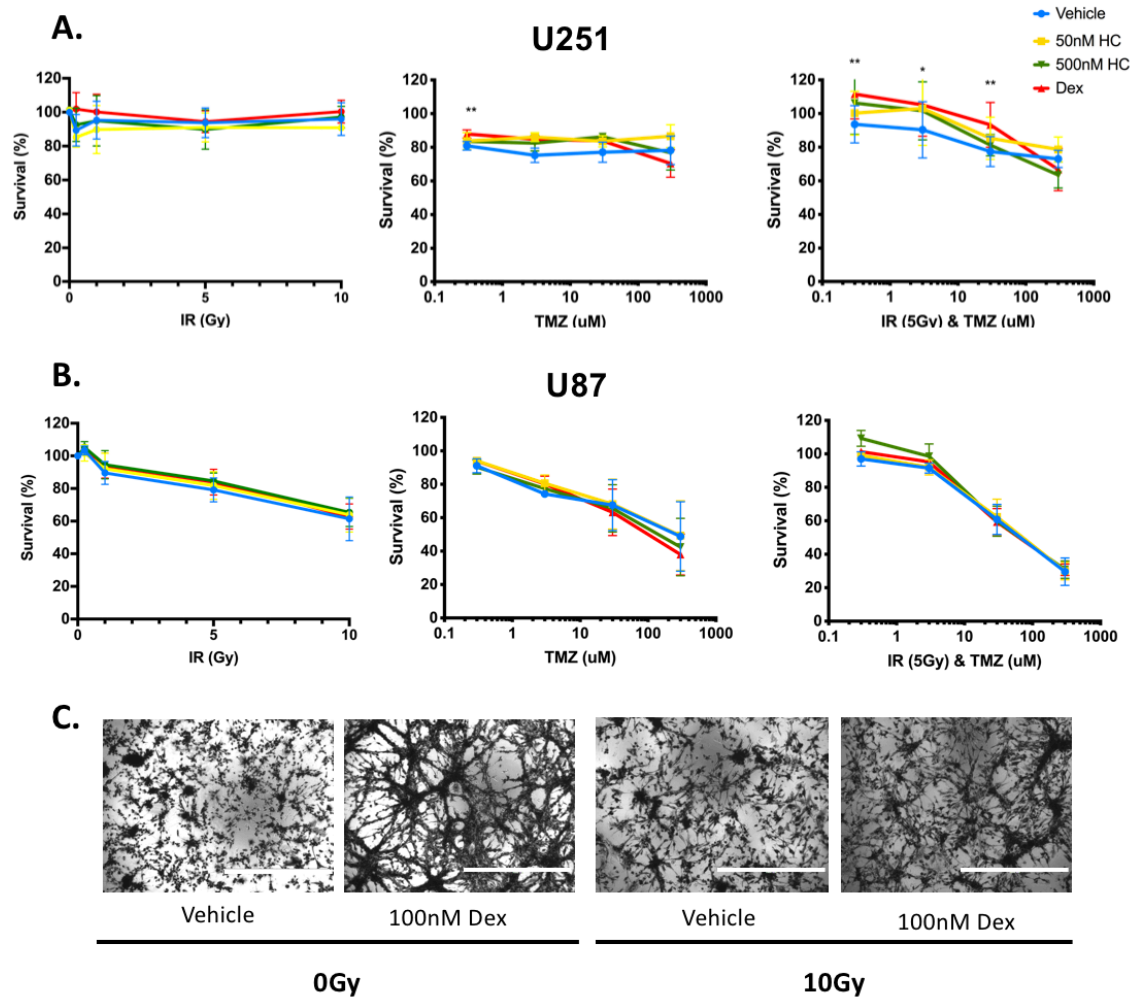
Figure 4.3: Dex treatment increases GBM cell survival in some, but not all, GBM cell lines. U251 (A) and U87 (B) cells were pre-treated overnight with 50nM HC, 500nM HC, 100nM Dex or a vehicle control. Cells were then subjected to increasing doses of irradiation, the chemotherapeutic Temozolomide, or a combined dose of irradiation (5Gy), and increasing doses of Temozolomide. Cells were incubated for 6 days, then metabolic activity was analysed using MTT. Survival was quantified relative to untreated control. Images of U87 cells at the end of the experiment are also shown (C). Scale bar denotes 1mm. Results shown are the mean of 3 independent experiments. Error bars denote SEM. Statistical significance was tested using 2-way ANOVA with Dunnett's multiple comparison test, Stars denote significance between Dex treated samples and the vehicle control. For simplicity, significance is not shown for 50nM and 500nM HC doses. * = $p \leq 0.05$, and ** = $p \leq 0.01$.

4.2.3 GR antagonist RU486 restores radiosensitivity and chemosensitivity

M059K cells were then pre-treated for 1 hour with 100nM RU486, an antagonist for GR, and treated with either 100nM Dex or a vehicle control, then subjected to IR or TMZ (Fig. 4.4A & B). Once again, 100nM Dex led to a significant increase in cell survival following both 10Gy IR and 30µM TMZ, compared with the vehicle control. Pre-treatment with RU486 abrogated this increase in survival, as cells treated with RU486 and 100nM Dex showed no significant difference in survival compared with the vehicle control.

RU486 is also able to bind and modulate the activity of a related steroid receptor, progesterone receptor (PR). To exclude a possible effect through PR expression in GBM was examined using data from the human protein atlas (232), which suggested that PR was not expressed in GBM tissue (Fig. 4.4C).

PR expression levels were therefore quantified by western blotting relative to MCF7, a breast cancer cell line known to express both GR and PR. MDA-MB-231, a triple negative breast cancer cell line, was included as a negative control for PR expression (Fig. 4.4D). PR was expressed in MCF7 cells, but was not expressed in any of the GBM cell lines, suggesting that modulation of the Dex response in the MTT assays was due to antagonism of GR.
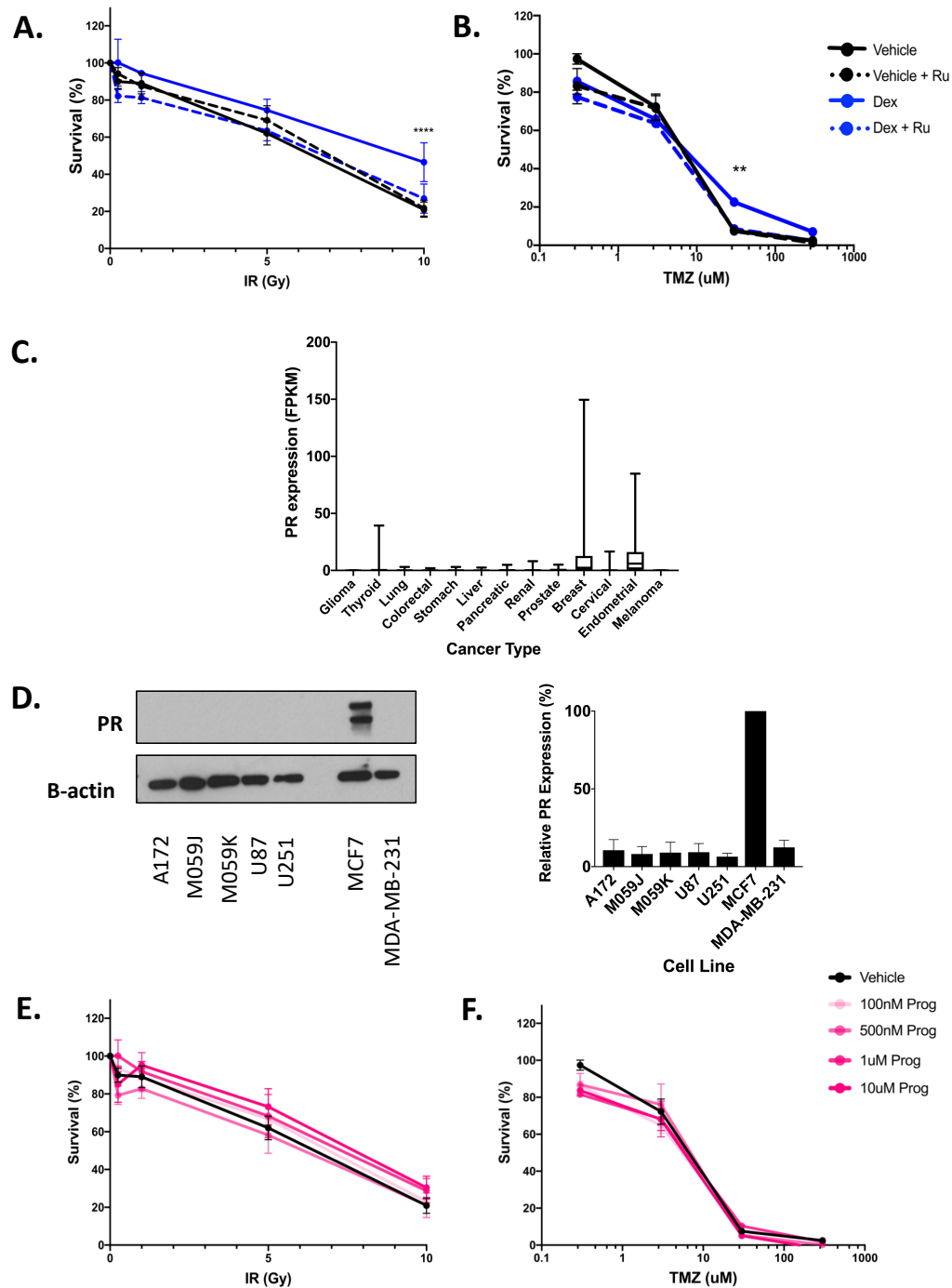
Figure 4.4: GR antagonist RU486 restores radiosensitivity and chemosensitivity, suggesting GR specificity. M059K cells were pre-treated for 1 hour with RU486, then treated overnight with 100nM Dex or a vehicle control, then subjected to IR (A), or TMZ (B). Cells were incubated for 6 days, and survival was analysed by MTT assay. (C) PR expression was analysed using The Human Protein Atlas. (D) Expression of PR was analysed in GBM cell lines by western blotting, and results were quantified normalised to β-actin control. M059K cells were pre-treated overnight with various doses of progesterone or a vehicle control, then subjected to increasing doses of IR (E), or TMZ (F). All experiments are n=3, and error bars denote SEM. Statistical significance was tested using 2-way ANOVA with Dunnett's multiple comparison test, where * = p ≤ 0.05, and ** = p ≤ 0.01.

4.2.4 Progesterone does not affect GBM cell survival following therapy

As an additional control, the role of progesterone in GBM cell survival was analysed as part of an undergraduate research project of which I was co-supervisor, and which was completed by Alexandra Schofield. As PR was not expressed in either primary tissue, or the cell lines tested, it was unlikely that progesterone could exert protective effects on GBM cell survival. This was confirmed using doses of 100nM – 10μM progesterone prior to both IR and TMZ. M059K cell survival was analysed using MTT assay, as previously discussed for Gc addition (Fig. 4.4E & F). There was no significant difference in GBM cell survival with the addition of any progesterone doses then treatment with either IR or TMZ. This confirmed that progesterone addition could not mimic the protective effects of Gc addition within M059K GBM cells.

Another possible confounder is that HC can also bind another steroid receptor, the mineralocorticoid receptor (MR). As previously discussed (section 1.1.9), low affinity GR ligands, such as hydrocortisone, bind MR with higher affinity than GR at low concentrations, however, Dex can bind to GR with high affinity, and has no binding affinity for MR. Data from the human protein atlas suggests both GR and MR were likely expressed in GBM (Fig. 4.5 A & B). MR was quantified using western blotting relative to Caco2, a colorectal adenocarcinoma cell line, as colon tissue is known to express high levels of MR (Fig. 4.5C). MR was highly expressed across all five GBM cell lines, exceeding the positive control, and correlating with the expression data from within primary tumour tissue (Fig. 4.5B).
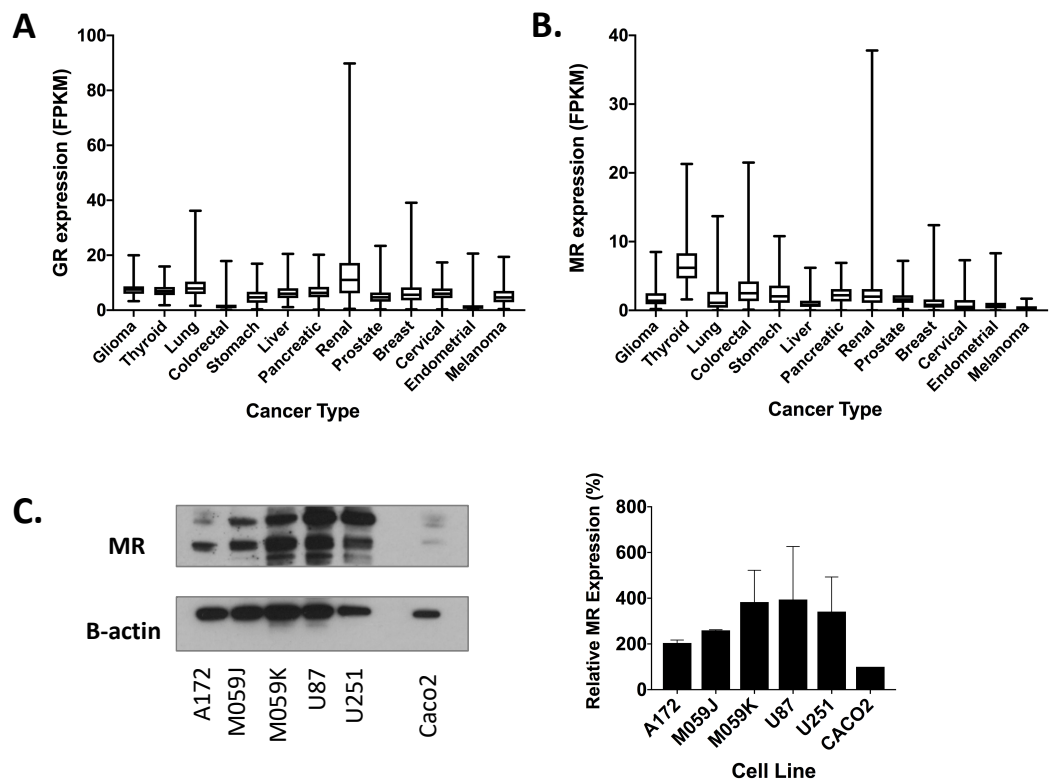
Figure 4.5 : Glioma tissue and cell lines express GR and MR. (A) GR and (B) MR expression were analysed in cancer tissues using Human Protein Atlas data. (C) MR expression in 5 GBM cell lines was analysed compared with a positive control cell line (CACO2). MR expression was quantified, relative to CACO2, normalised to b-actin expression. Western blots are representative of n=2, and quantification shows the mean of n=2. Error bars denote SEM.

This data suggested that MR expression could be a confounding factor in HC treatment. It is important to note that the protective effects seen with Dex were MR-independent, however, further steps were taken to ensure these effects were GR specific. The next step would therefore be to demonstrate loss of the Gc effect following specific knockdown of GR using siRNA. For further analysis, it was necessary to reduce the number of cell lines used. Cell lines were required which were sensitive to both radiation and chemotherapy in order to model differences in therapeutic efficacy, and both A172 and U251 cells were almost completely resistant to both treatments in isolation. This is not representative of patient response. U87 cells were also problematic due to the differences in morphology

seen following Dex treatment, and the difference in response seen compared with the other cell lines. Both M059J and M059K cells were shown to be Gc-responsive, and in addition, the use of both cell lines in parallel enables the study of potential interaction of DNA-PKcs and GR function. These cell lines were therefore used for further analysis, and the results were also compared with the broader panel of cell lines whenever this was feasible.

4.2.5 Effects of Gc on GBM cell survival is GR-dependent

GR was knocked down using two well-characterised GR specific siRNAs, previously used within the Matthews group (233). Transfection with either GR targeting siRNA reduced M059K cell survival relative to the negative control (Fig. 4.6A). Cells were treated with siRNA overnight, then plated for MTT assays, treated overnight with Dex, or a vehicle control, and subjected to increasing doses of IR. Cells were then incubated for 5 days before an MTT assay performed. When treated with a non-targeting siRNA (siNT) control, Dex pre-treatment resulted in significantly increased survival compared with the vehicle control, at both 5Gy and 10Gy (Fig. 4.6B). Alternatively, when treated with a GR targeting siRNA, there was no significant difference in survival between Dex and vehicle-treated cells at any IR dosage (Fig. 4.6C & D). It is important to note that according to manufacturer's instructions, this siRNA knockdown is transient, and expression can be expected to increase again approximately 72 – 96 hours following treatment. Therefore, during the course of the MTT assays, GR can be assumed to be re-expressed approximately 2 days after IR was performed. This suggests that GR is required at the point of IR to increase survival, and expression after this point is not sufficient to increase survival. These results confirm that the protective effect of Dex treatment prior to IR is dependent on GR.
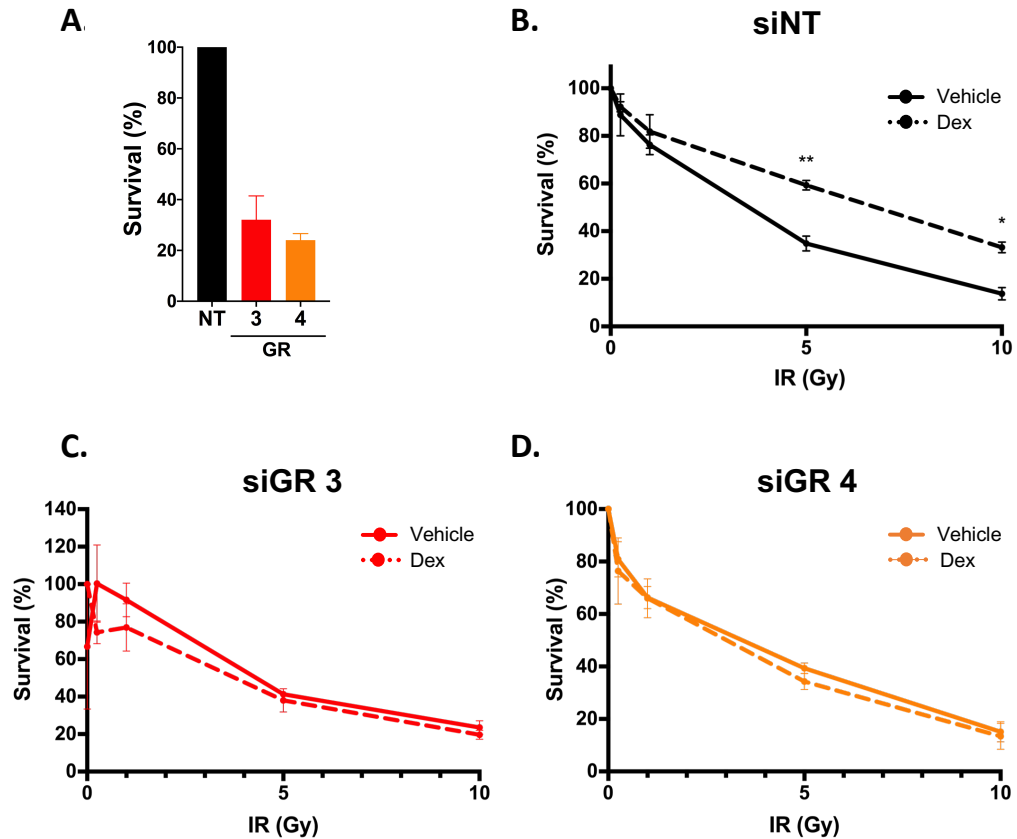
Figure 4.6: GR knockdown reverses the protective effect of Dex upon irradiation. The effect of 2 GR siRNA on M059K cell survival was analysed by MTT assay, compared with a negative control (siNT), at 6 days following treatment. B) M059K cells were treated for 24 hours using siRNA, then treated overnight with Dex or vehicle. Cells were then subjected to IR, and survival analysed by MTT assay. Cells were treated with a not targeting (NT) siRNA control (B), siGR 3 (C), or siGR 4 (D). Results shown are n=3, and error bars denote SEM. Statistical significance was tested using 2-way ANOVA with Dunnett's multiple comparison test. * = p ≤ 0.05 ** = p ≤ 0.01.

4.2.6 Glucocorticoids control an anti-inflammatory phenotype in GBM cells

To understand the transcriptional targets regulated by GR in GBM, cells were analysed by transcriptome profiling. M059K cells were treated for 4 hours with a vehicle control or the 3 Gc doses as previously described. Cells were treated in parallel for single cell RNA-seq in triplicate, then lysed and RNA extracted.

Using a False Discovery Rate of 0.05, as this has commonly been used within the literature, 266 genes were differentially expressed across all 3 treatment groups, relative to the vehicle control (Fig. 4.7A) (234, 235). 37 genes were differentially expressed across all 3 treatment groups. 1 gene was expressed in response to both HC doses, whilst 16 were expressed in response 500nM HC only. A large proportion, 72 genes, were differentially expressed following both 500nM HC and 100nM Dex. These results suggest a robust response within M059K cells in response to endogenous or synthetic Gc. The largest proportion of genes, however, was expressed only following Dex treatment, suggesting that a high affinity ligand leads to a defined gene signature, even when potency matched to a lower affinity Gc. Interestingly, when compared with a dataset analysing A549 adenocarcinoma cells in response to an equivalent dose of Dex, there are only 43 genes which overlap (Fig. 4.7B) (235). This suggests that Gc may regulate different subsets of genes within both tissues. This is to be expected, as GR effects are known to be highly tissue specific.

The response was strongest using Dex, which is to be expected, as this is the highest affinity ligand. What is interesting, however, is that with the 50nM HC dose a distinct, MR-specific response was not observed. Instead, all but one of the genes differentially expressed in response to 50nM HC were also regulated by 500nM HC and 100nM Dex (Fig. 4.7A).

A.

Gc regulated genes (>1.5 fold, <0.05 FDR)

B.

C.
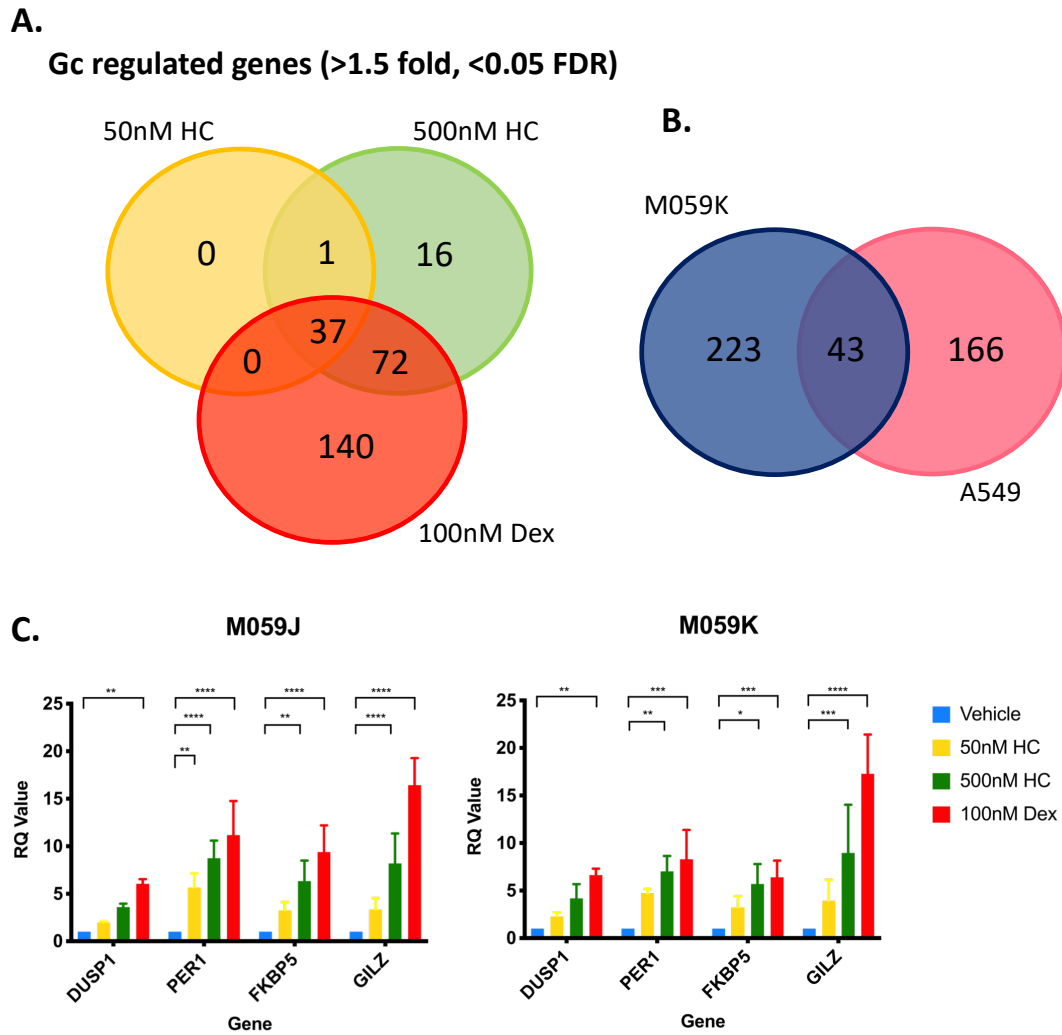
Figure 4.7: Gc regulate expression of target genes in a dose- and affinity-dependent manner. M059K cells were treated for 4 hours using 50nM HC, 500nM HC, 100nM Dex, or a vehicle control. RNA was extracted and libraries were prepared for bulk RNA-seq. Genes differentially expressed in response to each Gc treatment, relative to the vehicle control, were analysed. DE genes were compared between Gc treatment groups (A). DE genes in response to 100nM Dex were compared with DE genes in A549 cells following 100nM Dex (B). Results were validated by analysing expression of 4 DE genes, in both M059J and M059K cells (C). Cells were pre-treated for 4 hours with Gc, or a vehicle control, then RNA extracted and qPCR carried out using Taqman probes for the genes listed. Gene expression was normalised to GAPDH and analysed relative to the vehicle control. For qPCR, results shown are the mean of 3 independent experiments, and error bars denote SEM. Statistical significance was tested using a 2-way ANOVA with a Dunnett's multiple comparison test. ** = $p \leq 0.01$, *** = $p \leq 0.001$, **** = $p \leq 0.0001$.

In order to validate these results, qPCR was used to analyse expression of four genes which were significantly upregulated in response to all 3 Gc treatments.

These genes were *DUSP1, PER1, FKBP5* and *GILZ* (Fig. 4.7C)*. All 4 genes are well-characterised GR target genes within the literature, and were in the top 25 most highly upregulated genes within our dataset (204, 236-238). This was completed in M059K cells as a direct repeat of the RNA-seq conditions, and also in M059J cells in parallel. Both cell lines were treated for 4 hours with a vehicle control, 50nM HC, 500nM HC and 100nM Dex. RNA was extracted and qPCR was performed. Optimisation experiments showed both *GAPDH* and *β-actin,* two common housekeeping genes, were both expressed to similar levels within samples, and *GAPDH* was therefore taken forward for normalisation for the target genes. Values were displayed as relative quantification (RQ) values, normalised to the vehicle control.

All four genes show an upregulation in expression following Gc addition, and this response is dose- and affinity- dependent. A small increase in expression is seen following 50nM HC, with a larger response following 500nM HC. The largest response is seen with a dose of 100nM Dex for all 4 GR target genes. Whilst the doses of 500nM HC and 100nM Dex are potency matched, the response appears to be more pronounced with Dex addition. This correlates with the response seen within the RNA-seq, in which both doses appeared to regulate a similar gene signature, as seen by the large overlap between the treatments, however, more genes were regulated by Dex. This response was similar in both M059J and M059K cells, suggesting that DNA-PK deficiency has no inherent effect on the GR transcriptional response.

4.2.7 Pathway analysis reveals anti-inflammatory, cell cycle, and DNA repair gene signatures

Through pathway analysis software, it is possible to predict the cellular effects of a group of differentially expressed genes. Using two example pathway analysis databases from Enrichr, this identified a large number of anti-inflammatory related pathways which were upregulated in M059K cells (Table 4.1 and 4.2, pathways indicated in green, DE genes indicated in the final column). Many of these pathways contain common GR target genes, such as *NFKBIA, JUN, IL6* and *IL1B*. These results may indicate a direct anti-inflammatory effect of Gc on GBM cells. This is interesting, as the Gc are presumed to act through anti-inflammatory effects on immune cells within the tumour microenvironment. In addition, dysregulation of the inflammatory response has been widely investigated within GBM progression.

The pathway analysis also revealed several other pathways which were differentially expressed in response to Gc (Table 4.1 and 4.2, pathways indicated in blue, DE genes indicated in the final column). These pathways included p53 effectors, and transcriptional misregulation in cancer. Again, several genes are common to both of these pathways, such as *CDKN1A, BCL2L1* and *BIRC3.* The p53 effector pathway (Table 4.2) also highlighted some unique but interesting genes, such as *DDIT4,* and *RGCC.* These genes have all been previously identified as Gc-regulated, but there has been no previous research suggesting that these genes in combination could drive a phenotype. Many of these genes, such as *DDIT4* and *CDKN1A* are directly involved in the repair of DNA damage, whilst others, such as *RGCC, BIRC3* and *BCL2L1* are known to control cell cycle and apoptosis. Therefore, the regulation of these genes could lead to functional effects on cell survival following therapy-induced DNA damage.

Table 4.1: KEGG 2016 pathway analysis indicates a strong anti-inflammatory phenotype, and cancer-relevant gene expression. Using the total differentially expressed gene lists across all 3 Gc treatment groups from the RNA-seq results, predicted pathways were analysed by Enrichr. KEGG database gene ontology analysis is used as a representative database, and the 15 most significantly affected pathways are shown. The majority of pathways are related to the differential expression of inflammatory genes (green), however, several cancer-related pathways were also affected (blue).

Term	Adjusted P-value	Z-score	Genes
NFκB signaling pathway	0.00044498	-1.767052	NFKBIA; VCAM1; CXCL12; CXCL8; GADD45B;PLAU;IL1B;BCL2L1;BIRC3
Transcriptional misregulation in cancer	0.00044498	-1.7261862	IL6; CEBPB; CDKN1A; MAF; CXCL8; BCL6; PLAU; PLAT; RUNX2; FOXO1; BCL2L1; BIRC3
FoxO signaling pathway	0.00063455	-1.7754276	CDKN2D; IL6; CDKN1A; GADD45B; BCL6; TNFSF10; IRS2; FBXO32; SGK1; FOXO1
Chagas disease (American trypanosomiasis	0.00305584	-1.7517404	NFKBIA; JUN; IL6; CXCL8; IFNGR1; IL1B; SERPINE1; TLR6
TNF signaling pathway	0.00363135	-1.8069505	NFKBIA; SOCS3; JUN; IL6; CEBPB; VCAM1; IL1B; BIRC3
AGE-RAGE signaling pathway in diabetic complications	0.01090477	-1.9191657	JUN; IL6; VCAM1; CXCL8; IL1B; SERPINE1; FOXO1
Toll-like receptor signaling pathway	0.01252075	-1.739436	NFKBIA; TLR1; JUN; IL6; CXCL8; IL1B; TLR6
NOD-like receptor signaling pathway	0.01932834	-1.5305636	NFKBIA; L6; CXCL8; IL1B; BIRC3
Pathways in cancer	0.03318759	-1.7894583	JUN; EGLN3; CDKN1A; CXCL8; PTGER2; FOXO1; FGF5; NFKBIA; IL6; CXCL12; RARB; BCL2L1; BIRC3
Inflammatory bowel disease (IBD)	0.0279876	-1.6250097	JUN; IL6; MAF; IFNGR1; IL1B
Influenza A	0.03318759	-1.7104063	NFKBIA; SOCS3; JUN; IL6; CXCL8; IFNGR1; IL1B; TNFSF10
Rheumatoid arthritis	0.02306148	-1.5456471	IL11; JUN; IL6; CXCL12; CXCL8; IL1B
HIF-1 signaling pathway	0.03318759	-1.5474484	IL6; EGLN3; CDKN1A; IFNGR1; SERPINE1; IL6R
Non-alcoholic fatty liver disease (NAFLD)	0.03727156	-1.5240211	SOCS3; JUN; IL6; CXCL8; IL1B; IRS2; IL6R
Insulin resistance	0.03424632	-1.4638882	NFKBIA; SOCS3; IL6; PPP1R3C; IRS2; FOXO1

Table 4.2: NCI-Nature pathway analysis indicates a strong anti-inflammatory phenotype, and DNA damage related genes. Using the total differentially expressed gene lists across all 3 Gc treatment groups from the RNA-seq results, predicted pathways were analysed by Enrichr. NCI-Nature 2016 gene ontology analysis is used as a representative database, and the 15 most significantly affected pathways are shown. The majority of pathways are related to the differential expression of inflammatory genes (green), however, several cancer-related pathways were also affected (blue).

Term	Adjusted P-value	Z-score	Genes
IL6-mediated signaling events	2.0198E-05	-1.7496001	SOCS3; JUN; IL6; CEBPB; CEBPD; LMO4; IL6R; FOXO1
AP-1 transcription factor network	0.00024854	-1.8217483	JUN; ELF1; IL6; MT2A; CXCL8; MAF; DUSP1; PLAU
Direct p53 effectors	0.00048606	-1.5591152	JUN; CDKN1A; RGCC; BCL6; DUSP1; SERPINE1; DDIT4; SNAI2; ARID3A; DKK1
ATF-2 transcription factor network	0.00048606	-1.5168433	SOCS3; JUN; IL6; CXCL8; DUSP1; PLAU; JDP2
LPA receptor mediated events	0.00435184	-1.5974491	NFKBIA; JUN; IL6; CXCL8; ADRA1B; HBEGF
C-MYB transcription factor network	0.00300692	-1.4168659	CEBPB; CDKN1A; MAF; CEBPD; ATP2B1; ETS2; BIRC3
Regulation of retinoblastoma protein	0.00435184	-1.4717314	JUN; ELF1; CEBPB; CDKN1A; CEBPD; RUNX2
Glucocorticoid receptor regulatory network	0.0107024	-1.4201121	JUN; IL6; CDKN1A; CXCL8; SGK1; FKBP5
Regulation of nuclear beta catenin signaling and target gene transcription	0.0107024	-1.3457413	TLE4; JUN; CXCL8; SNAI2; KLF4; DKK1
Regulation of nuclear SMAD2/3 signaling	0.0107024	-1.2364245	JUN;CEBPB;CDKN1A;SERPINE1;RUNX2;FOXO1
IL4-mediated signaling events	0.01366148	-1.1813556	SOCS3;CEBPB;BCL6;IRS2;MYBL1
Angiopoietin receptor Tie2-mediated signaling	0.03008389	-1.0900195	ELF1;CDKN1A;ITGA5;FOXO1
Validated transcriptional targets of AP1 family members Fra1 and Fra2	0.01366148	-0.8589402	JUN;IL6;CXCL8;PLAU
IL23-mediated signaling events	0.01389722	-0.7906358	NFKBIA;SOCS3;IL6;IL1B
FoxO family signaling	0.03008389	-0.8304554	BCL6;FBXO32;SGK1;FOXO1

4.2.8 Genes regulated by Gc appear to show differential expression in GBM tissue

In order to investigate the possible clinical relevance of these genes within GBM patients, expression of a selection of GR target genes was analysed using transcriptional data from patient samples. Data from TCGA was analysed using the GlioVis database, as used previously (220). Only transcriptome data obtained through RNA-seq was analysed.

Firstly expression of genes upregulated in response to Gc treatment was analysed (Fig. 4.8). These genes were selected due to their established link to DNA repair, and were linked to this phenotype in the previous Enrichr analysis. All four genes showed a trend towards increased expression in GBM, compared with normal brain tissue, reaching significance for *DDIT4, BCL2L1* and *CDKN1A.* This did not correlate with a difference in survival depending on expression of these genes as high *BIRC3* expression was associated with significantly shorter patient survival.

The expression of four genes downregulated in response to Gc treatment were then analysed (Fig. 4.9). *IL1B* expression was significantly reduced in GBM tissue compared with normal tissue, however, there was no significant difference in expression of *IL6, IL11*, or *CXC L12.* High expression of *IL11* was associated with reduced survival of GBM patients, however, none of the other genes rendered an effect on patient survival.
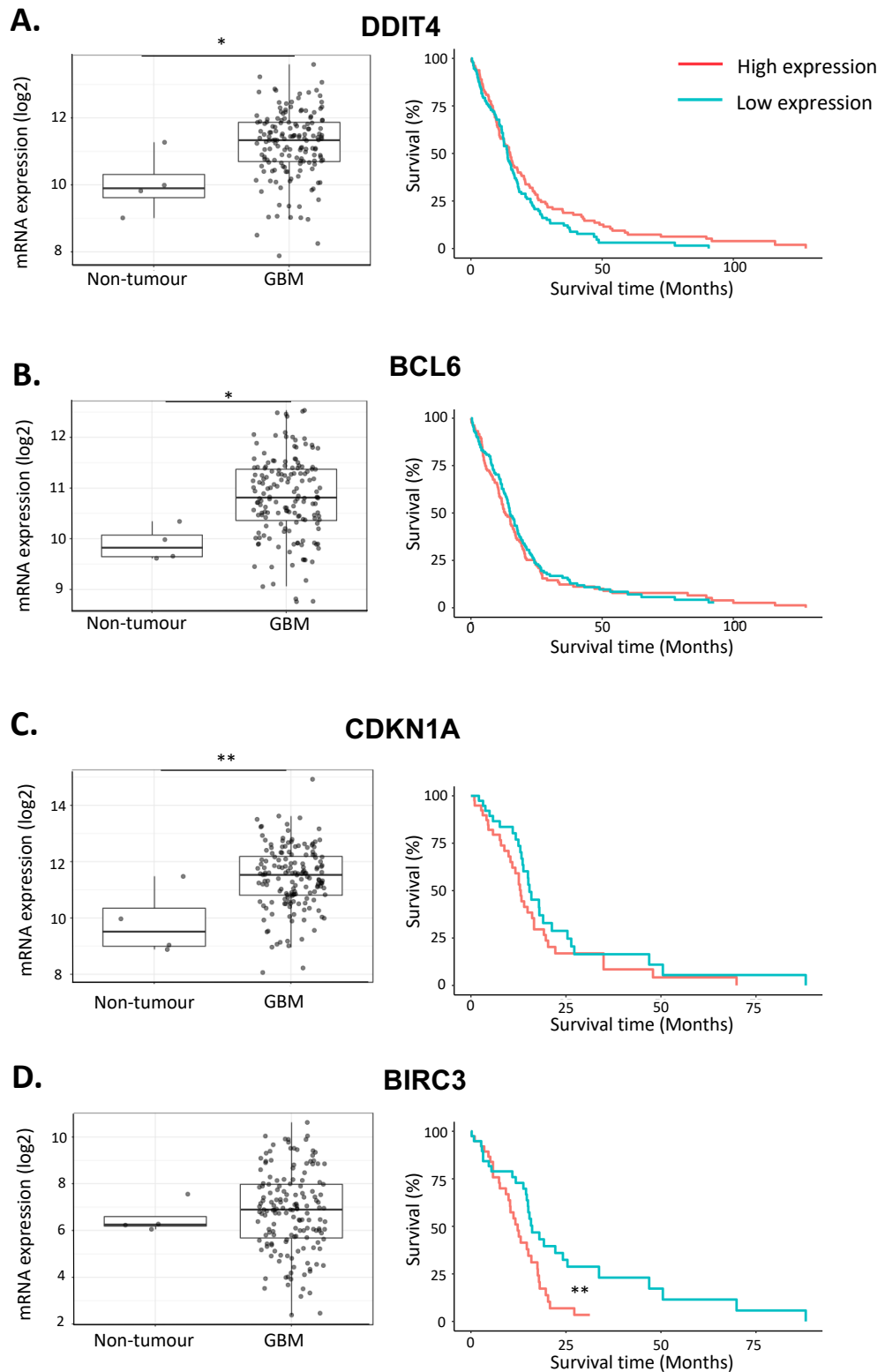
Figure 4.8: Genes upregulated in response to Dex treatment are also upregulated in GBM primary tissue. TCGA-GBM expression data was analysed compared with normal brain tissue using GlioVis. Expression levels are shown, and survival for patients with high and low expression are shown. Differences in expression were analysed with Tukey's Honest Significant Difference Test, and survival was analysed using a Hazard Ratio, and log p-value. * = $p \leq 0.05$, ** = $p \leq 0.01$.
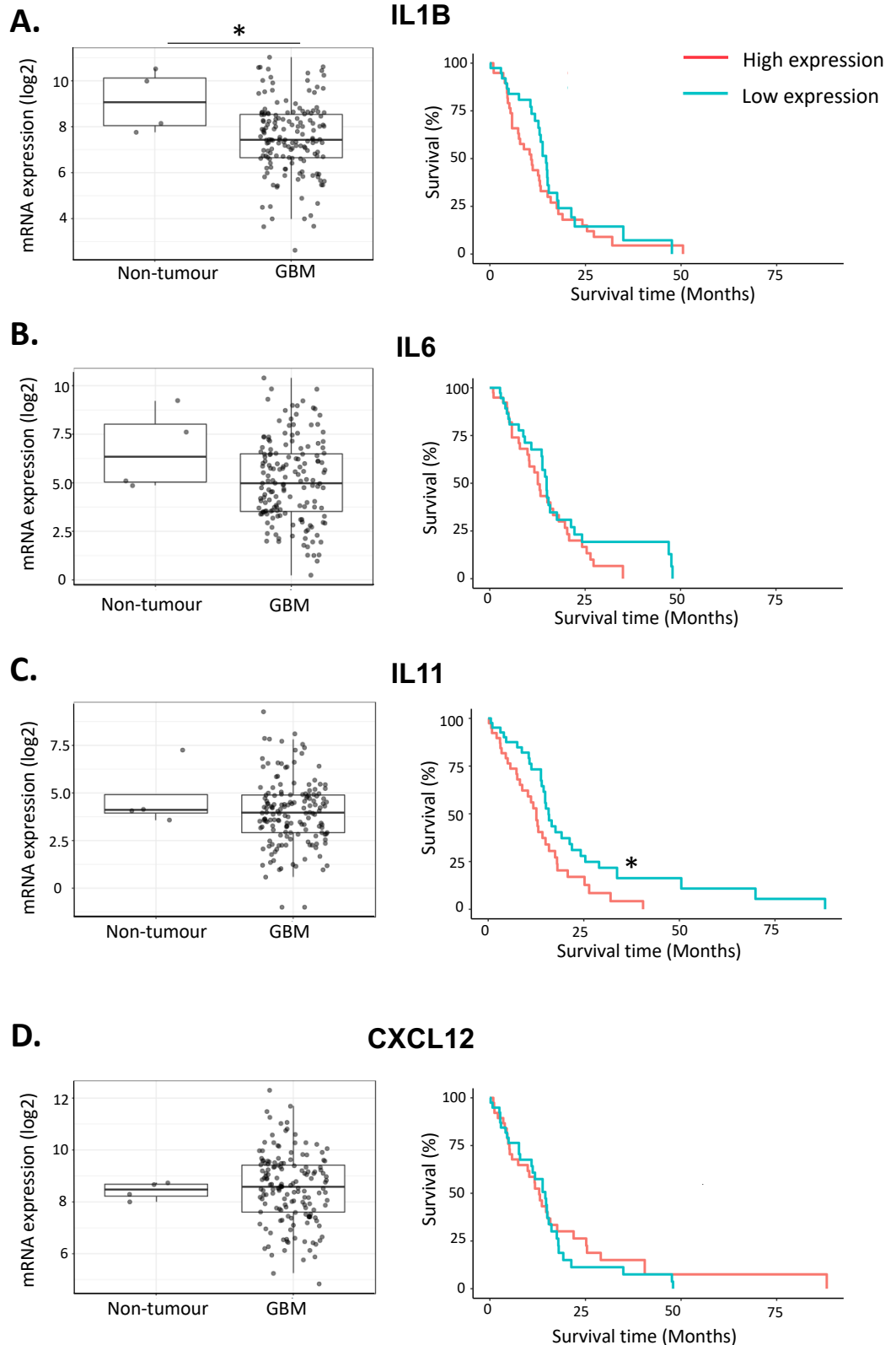
Figure 4.9: Genes downregulated in response to Dex are also downregulated in GBM primary tissue. TCGA-GBM expression data was analysed compared with normal brain tissue using GlioVis. Expression levels are shown, and patient survival for patients with high and low expression are shown. Differences in expression were analysed with Tukey's Honest Significant Difference Test, and survival was analysed using a Hazard Ratio, and log p-value. * = p ≤ 0.05, ** = p ≤ 0.01.

Whilst these results are only dependent on a small selection of genes, it does suggest that Gc driven gene signatures could lead to changes in GBM transcriptional outcome. As the data is from a publicly available source, there is no information provided regarding treatment prior to sampling, however, given the prevalence of Dex usage, it is likely that many of the patients were treated with Dex.

There were relatively few genes which showed direct correlation with expression and survival, however, it is possible that, if a Gc-mediated, multi-gene signature was analysed, this could show a predictive effect on patient outcome. This analysis was not carried out within the scope of this thesis, but would be an important component of any future work.

4.2.9 Gc partially reduces cell proliferation

Based on the results from the RNA-seq data, multiple mechanisms by which Gc could be reducing therapeutic efficacy, through DE genes were identified, namely;

- Inhibition of cell proliferation
- Cell cycle arrest
- Direct effects on DNA repair

The aim was therefore to investigate each of these effects in turn through a number of endpoint assays.
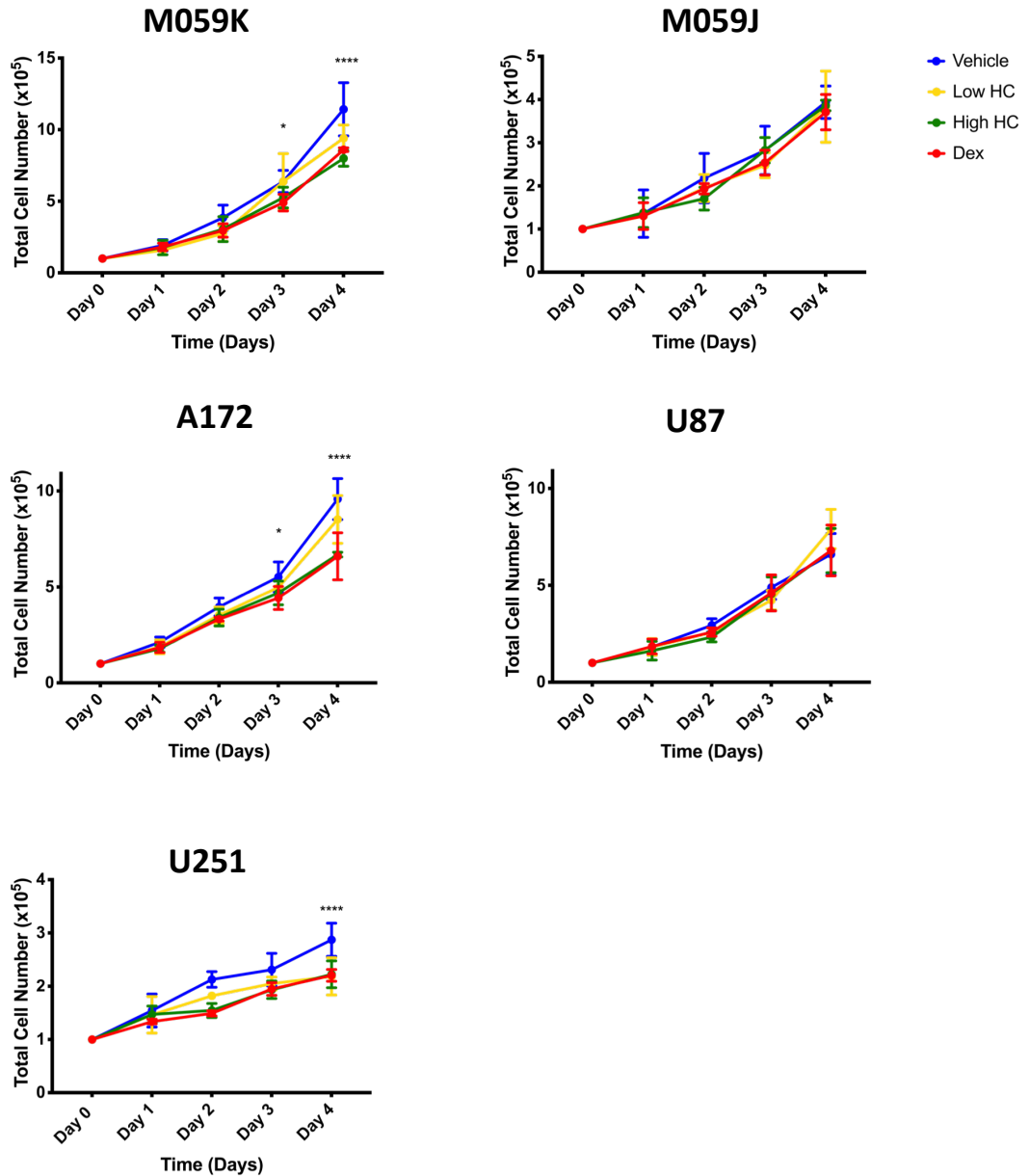
Figure 4.10: Gc do affect cell growth in some, but not all, GBM cell lines. GBM cell lines were incubated with 50nM HC, 500nM HC, 100nM Dexamethasone or a vehicle control. Cell counts were taken every 24 hours for 4 days. Results shown are n=3, and error bars denote SEM. Statistical significance was tested using 2-way ANOVA with Dunnett's multiple comparison test. Stars denote significance between Dex treated samples and the vehicle control. For simplicity, significance is not shown for 50nM and 500nM HC doses. * = $p \leq 0.05$, ** = $p \leq 0.01$, *** = $p \leq 0.001$.

Previous literature has suggested that Gc may affect therapeutic efficacy within GBM through the induction of growth arrest. Gc are known to induce cell cycle arrest and slow growth in other cancer types, such as lung cancer, however, this effect is controversial within GBM cells. To assess whether Gc were capable of reducing cell proliferation, A172, M059J, M059K, U87 and U251 cells were treated with a vehicle control, 50nM HC, 500nM HC, or 100nM Dex. Cell counts were performed every 24 hours for 4 days (Fig. 4.10). Growth rates were highly variable between cell lines. M059K cells had the largest increase in cell number, and the smallest increase was seen in U251 cells. A172, M059K, and U251 cells showed a significant inhibition of growth following Dex treatment, however, there was no significant difference in proliferation in the other three cell lines tested.

4.2.10   Gcs do not induce cell cycle arrest within GBM cells

To confirm if Gc could affect cell growth through cell cycle arrest, the cell lines were treated for 24 or 48 hours with Gc, then stained using propidium iodide as a marker for DNA content. Cells were analysed by flow cytometry (Fig. 4.11A), and Modfit software was used to calculate the proportion of cells in each cycle phase (Fig. 4.11B). None of the cell lines showed a significant accumulation of cells within any cell cycle phase following Gc treatment, confirming that Gc do not mediate their effects in GBM through induction of cell cycle arrest.

Within the M059J cell line, however, there was a robust and reproducible population which consisted of cells labelled as Sub-G0. When analysing the propidium iodide staining, the fluorescence intensity of this population was half that of G1 cells, suggesting that this population contained 50% of the DNA content of G0/G1 cells.
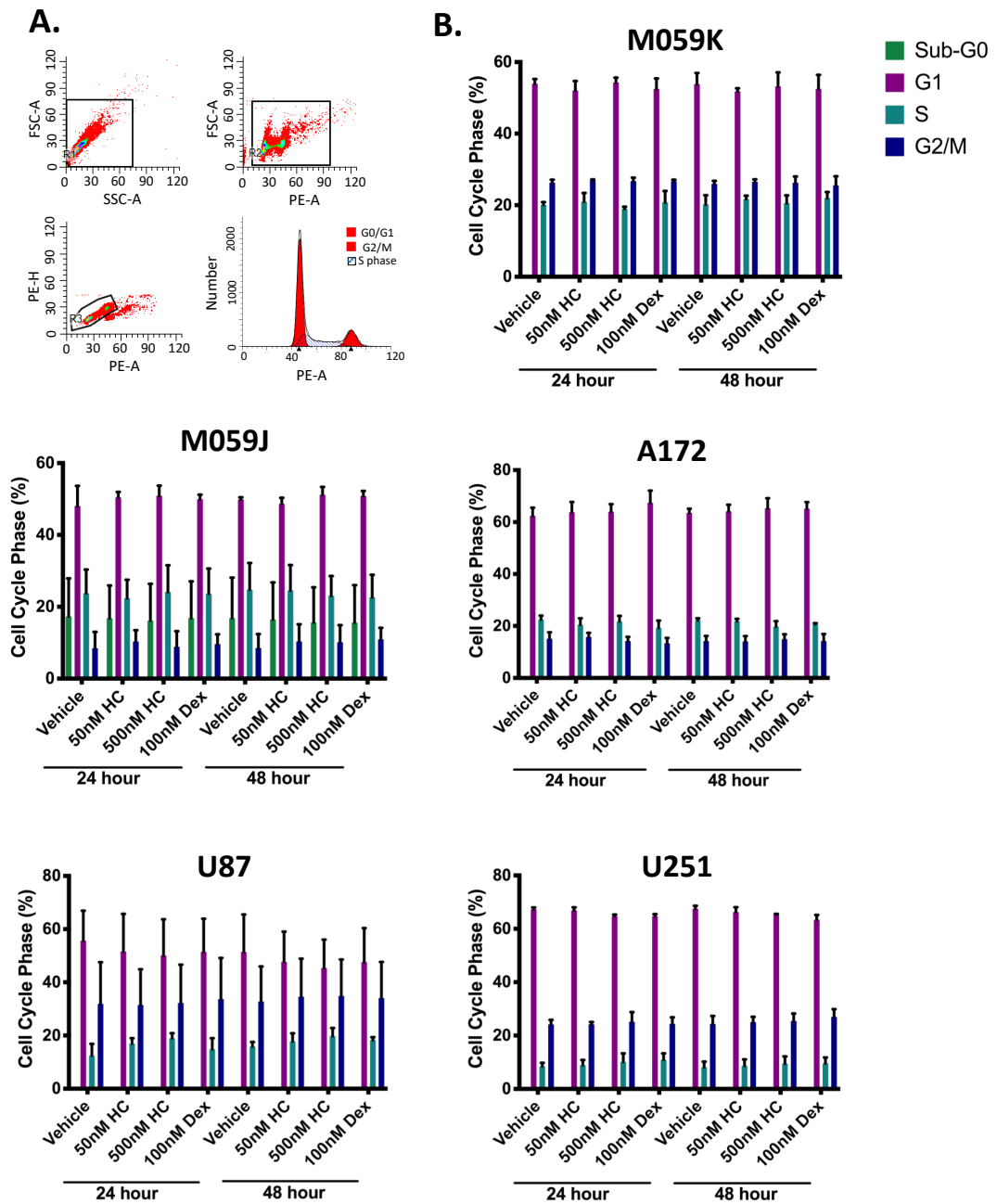
Figure 4.11: Gc treatment does not induce cell cycle arrest in GBM cells. GBM cells were treated for 24 or 48 hours with 50nM HC, 500nM HC, 100nM Dex or a vehicle control. Cells were fixed, then treated with propidium iodide. Propidium iodide staining was analysed by flow cytometry. Gating was used to remove debris, and remove doublets from further analysis. Modfit software was used to quantify each cell cycle phase according to PI staining, as a marker of total DNA content. A) Representative images of gating and Modfit software are shown. B) The cell cycle phase of each cell line was analysed. Results shown are n=3, and error bars denote SEM. Statistical significance was tested using 2-way ANOVA with Dunnett's multiple comparison test.

Work by others has also identified a similar population within this cell line, and has assumed the cells to be apoptotic. Cells undergoing apoptosis will present with reduced DNA, however, as the mean fluorescence intensity of these cells was consistently half of what was seen in the G0/G1 cells, it could be hypothesised that these cells were instead a haploid population.

Imaging of M059J cells throughout the work had not indicated a high proportion of apoptotic cells. In addition, as previously discussed, M059J cells contain a mutation within DNA-PKcs, a key component of the DNA repair machinery resulting in deletion. This was confirmed through western blotting and immunostaining of both M059J and M059K. DNA-PKcs was clearly expressed in M059K cells, but absent within M059J cells, and its expression was not induced through either IR or TMZ (Fig. 4.12A - B). Previous work has shown that DNA-PKcs is phosphorylated during mitosis, and DNA-PKcs siRNA knockdown leads to an increase in chromosome misalignment, and multipolarity during mitosis (239). It is therefore possible, that as a consequence of these aberrations, cells exiting mitosis may contain a haploid proportion of chromosomes. To test this, cells were treated with colcemid to increase the proportion of cells in metaphase. Metaphase spreads were carried out to visualise chromosomes and imaged. Example images are shown (Fig. 4.12C). The number of chromosomes in each cell was quantified for both M059J and M059K cells (Fig. 4.12D). M059J cells contained a mean of 79.85 chromosomes, and M059K cells contained a mean of 73.10 chromosomes. This is in line with previous ATCC data which has estimated the mean chromosome number in M059K cells as 75, however, there is no previous data to determine the mean chromosome number in M059J cells (ATCC).
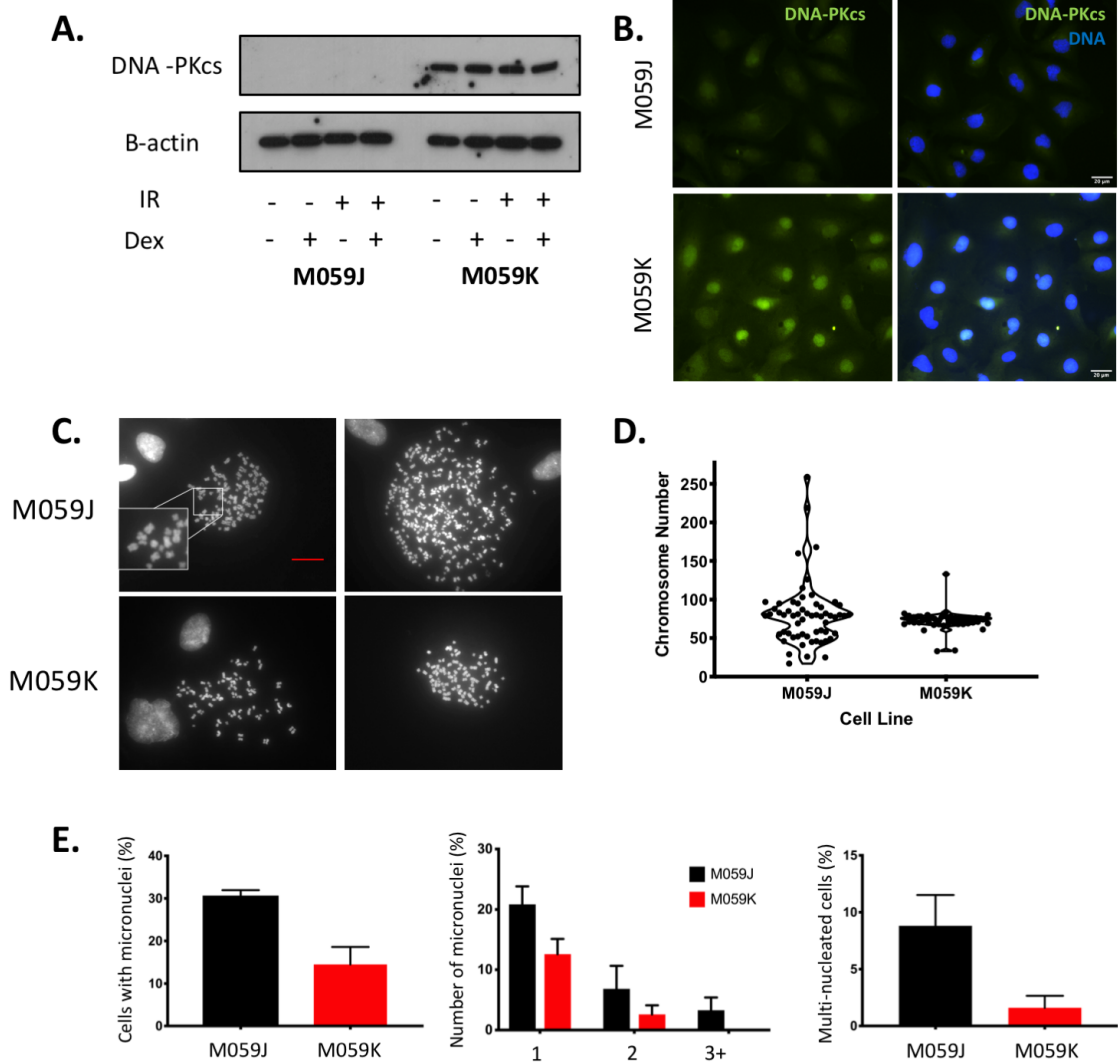
Figure 4.12: M059J cells contain a heterogenous number of chromosomes, and display multiple nuclear abnormalities. DNA-PK deletion was confirmed in M059J cells, but not M059K cells using western blot (A), and ouluorescent staining (B). M059J and M059K cells were treated with colcemid to induce metaphase arrest, then harvested, and dropped onto slides to produce metaphase drops. These were stained with Hoescht, coverslips added, and imaged. A selection of representative images are shown (C), and total chromosomes counted (D). Untreated cells were fixed and stained with Hoescht, and cells were quantified for micronuclei, multiple nuclei, and multiple nuclear lobes (E). Scale bar denotes 20μm. Results shown are n=3, and error bars denote SEM.

Whilst there was no significant difference in mean chromosome number between the cell lines, there was a marked difference in distribution. M059K cells showed very little aberration from the mean chromosome number, however, M059J cells varied widely from the mean, with chromosome content ranging from 17 to 259 chromosomes per cell. There also appeared to be a defined second cluster of M059J cells containing approximately 40 chromosomes. This population correlated with the sub-G0 peak seen in the cell cycle analysis, and confirmed this as a haploid population of cells, presumably produced through aberrant chromosome segregation during mitosis.

Further aberrations, such as micronuclei and multiple nuclei were analysed in M059J and M059K cells (Fig. 4.12E). Whilst there was no significant difference in the number of micronuclei between both cell lines, M059J showed a trend towards an increased number of cells with micronuclei, and more micronuclei in cells in which they were present. M059J cells also showed an increased number of cells containing multiple nuclei. Together, these results confirm that M059J cells exhibit aberrant chromosome numbers, and multiple nuclear abnormalities, presumably due to the DNA-PK deficiency previously reported.

Based on the cell growth and cell cycle analysis, it is possible that Dex is inducing a reduction in cell proliferation with long-term Gc treatment, however, on a short-term basis of up to 48 hours, there is no effect on cell cycle. This would suggest that the initial transcriptional response is not inducing an immediate cell cycle arrest, which is then reducing therapeutic efficacy.

The final option of DE genes from the RNA sequencing data was then investigated; namely, whether Gc could induce differences in the DNA repair response.

4.2.11   Gc treatment results in less DNA damage within GBM cells following treatment

It is clear that Gc could be reducing cell proliferation on a long-term basis, however, comet assays were used to investigate whether Gc could also be affecting DNA repair following more acute Gc treatments, through the upregulation of DNA repair genes seen within the RNA-seq data. Comet assays were used to measure the extent of DNA damage within individual cells, to investigate if less DNA damage was present within Dex-treated cells 24 hours after treatment. Comet assays, also known as single cell electrophoresis, allow the visualisation of shorter, broken lengths of DNA, relative to the nucleus as a whole. Representative images are shown in Fig. 4.13A. This "tail" of broken DNA can be quantified as a relative marker of DNA damage (Fig. 4.13B). The tail length, multiplied by the DNA content of the tail, relative to the head, is known as the tail moment. OpenComet, a freely-available plug-in for ImageJ, was used to quantify the tail moment in an unbiased manner (Fig. 4.13C). 24 hours after both irradiation and TMZ, and a combination of both, both M059J and M059K cells treated with a vehicle control exhibit increased tail moment compared with those not subjected to either treatment. This confirms that both IR and TMZ resulted in increased DNA damage, 24 hours after treatment.
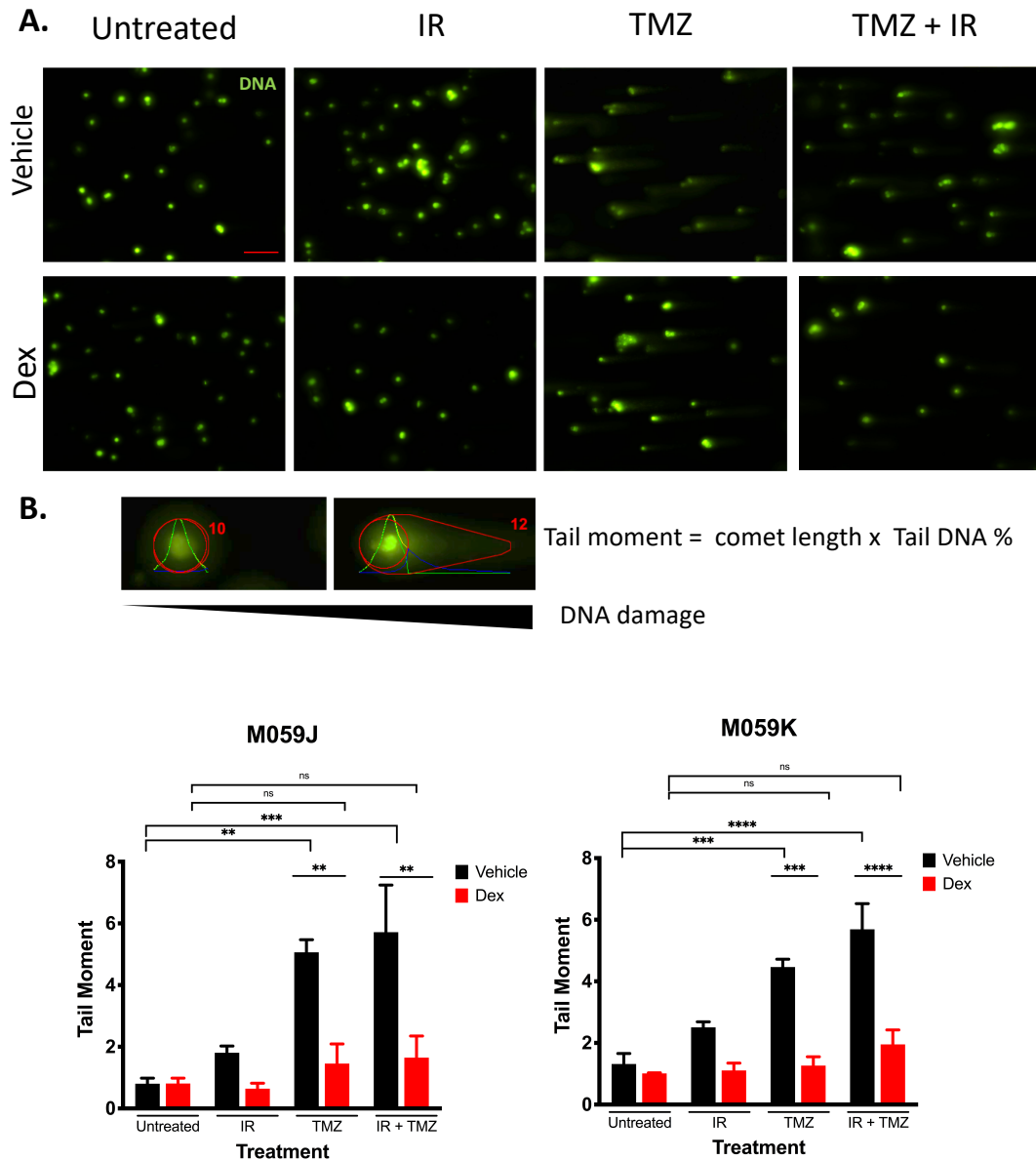
Figure 4.13: Dex induces active DNA repair in GBM cells following IR and TMZ, as measured by comet assay. A) M059J and M059K cells were subjected to irradiation (5Gy), TMZ (30µM), both, or left untreated, then incubated for 24 hours. B) DNA damage was quantified using a comet assay. Tail moment was used as a measure of DNA damage on a single cell basis. Average DNA damage for each treatment, measured as the tail moment, is shown in C). Scale bar denotes 100µm. Results shown are n=3, and error bars denote SEM. Statistical significance was tested using 2-way ANOVA with Dunnett's multiple comparison test. * = $p \leq 0.05$, ** = $p \leq 0.01$, *** = $p \leq 0.001$.

The largest amount of DNA damage was seen in cells treated with the combination therapy, which is to be expected. When cells were pre-treated overnight with Dex, however, there was a significant decrease in tail moment compared with the vehicle control across all treatments and across both cell lines. Further, there was no significant difference between the untreated Dex samples, and Dex samples following IR, TMZ or both. This suggests that, by 24 hours after IR or TMZ, cells pre-treated with Dex have significantly reduced DNA damage compared to those not pre-treated with Dex.

This effect could occur through either a reduction in the damage incurred following IR or TMZ, through some sort of protective mechanism, or through an increase in DNA repair following induction of DNA damage.

4.2.12   Selection of a robust, rapidly induced DNA damage marker

In order to test the first possibility, that Gc were reducing the amount of DNA damage induced by IR or TMZ treatment, a reliable, rapidly induced marker of DNA damage was required. Three common markers include increased intensity and presence of nuclear foci for RAD51, 53BP1 and phosphorylation of H2AX (γH2AX) (240-245). Each three of these markers were tested to determine which would produce the most robust signal after a short 2hr treatment.

As presented in Fig. 4.14 and 4.15, staining for all three markers was present. Staining for RAD51 was predominantly nuclear, with punctate staining evident in the absence of IR treatment (Fig. 4.14). Few cells stained for phosphorylated H2AX in the absence of IR, but there was a marked increase in staining intensity

in all cells following IR treatment (Fig. 4.14 and 4.15). 53BP1 staining, like RAD51 was present in control and IR treated cells (Fig. 4.15), however, staining appeared to localise to foci following IR treatment. These observations were supported by quantification of the images (Fig. 4.16). Based on its specificity, it was decided that γH2AX was the most reliable marker for rapidly induced DNA damage.
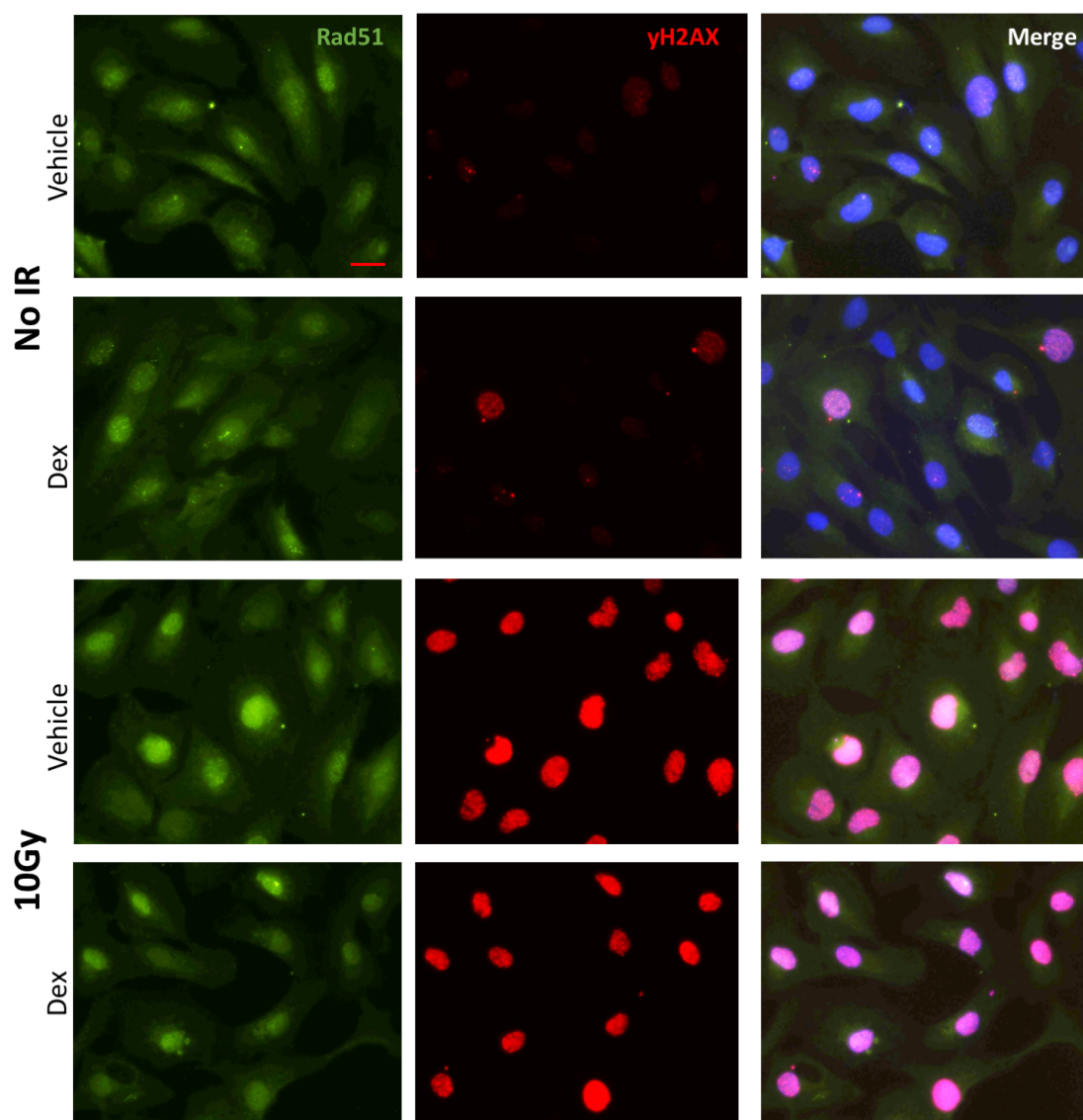
Figure 4.14: H2AX phosphorylation increases following IR within M059K cells. M059K cells were pre-treated overnight with 100nM Dex or a vehicle control, then subjected to 10Gy IR. After 2 hours, cells were fixed and stained for Rad51 (green) and γH2AX (red), and merged with Hoescht. Images shown are representative of one experiment.
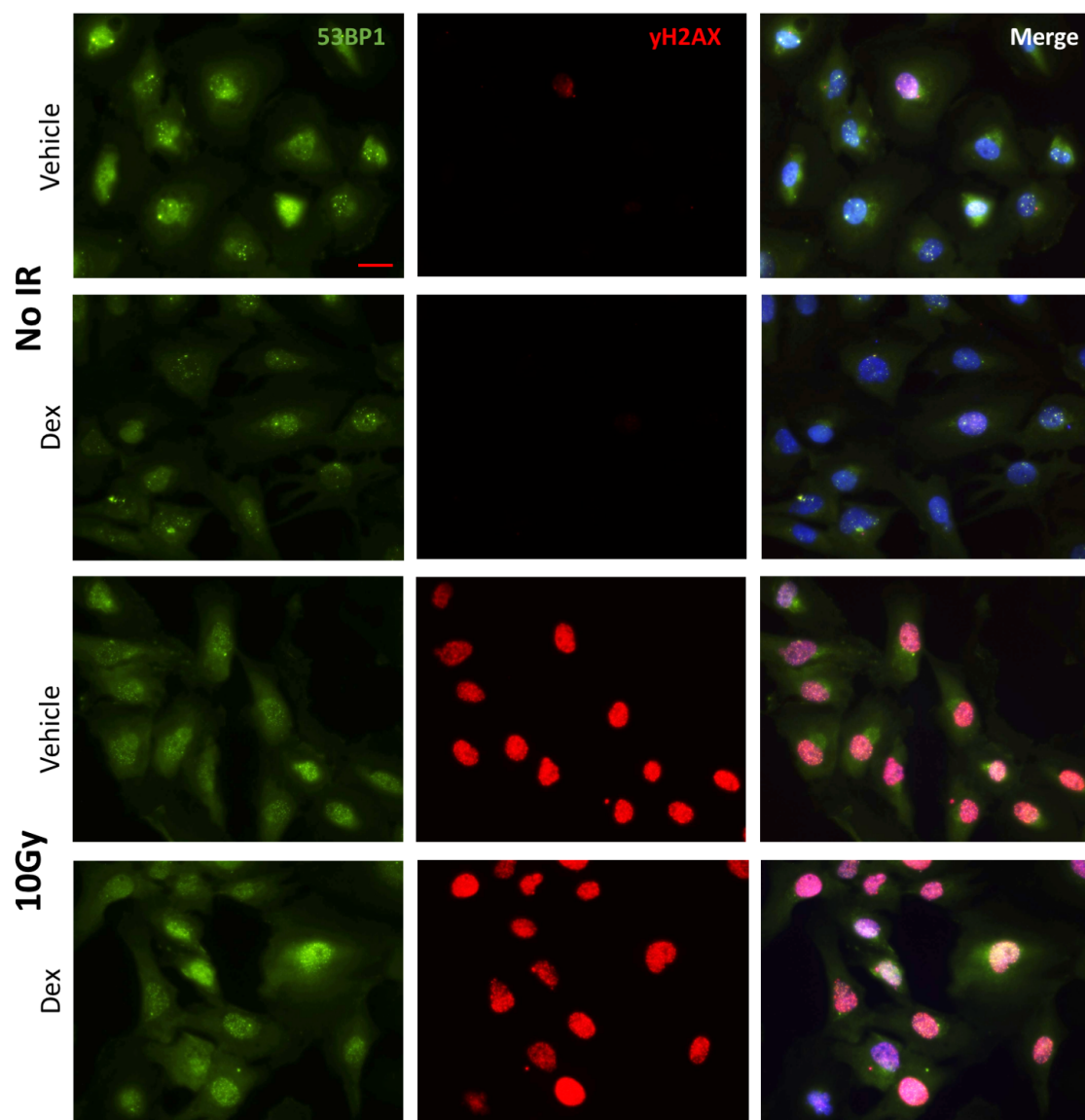
Figure 4.15: 53BP1 accumulates at nuclear foci following IR within M059K cells. M059K cells were pre-treated overnight with 100nM Dex or a vehicle control, then subjected to 10Gy IR. After 2 hours, cells were fixed and stained for 53BP1 (green) and γH2AX (red), and merged with Hoescht. Scale bar denotes 20µm. Images shown are representative of two independent experiments.

A.
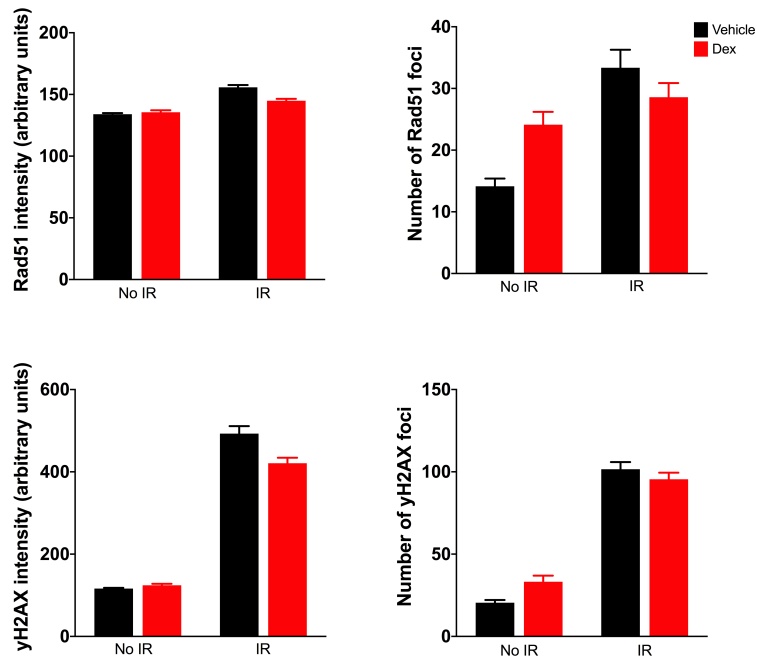
B.
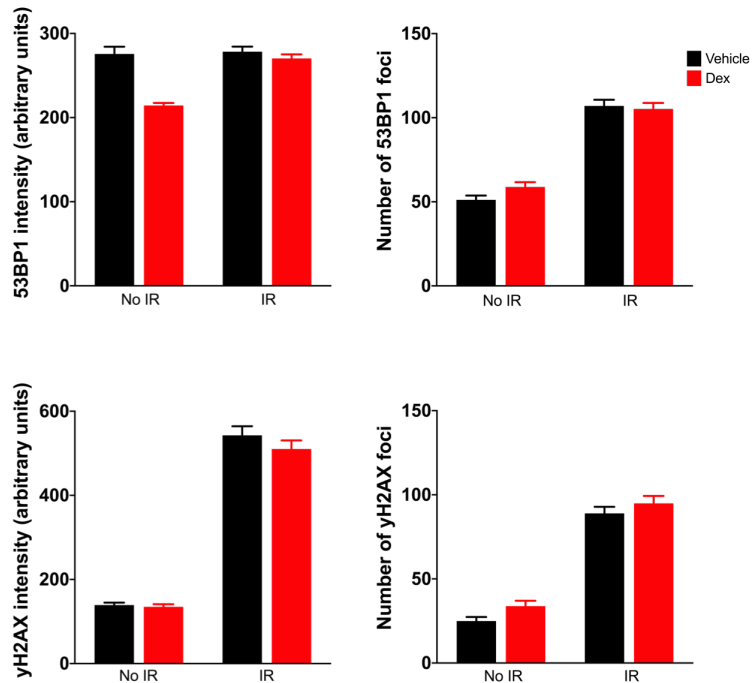
Figure 4.16: Phosphorylation of H2AX is a robust, rapid marker of DNA damage. M059K cells were pre-treated overnight with 100nM Dex or a vehicle control, then subjected to 10Gy IR. After 2 hours, cells were fixed and stained for Rad51 and γH2AX (A), or 53BP1 and yH2AX (B). Total intensity mean grey value (left) and number of foci (right) were quantified. 10 randomly selected fields of view were analysed for each condition. Results shown are the mean of 1 (A) or 2 (B) experiments. Error bars denote SEM.

4.2.13 Gc do not prevent induction of DNA damage within GBM cells

M059J (Fig 4.17) and M059K (Fig 4.18) cells were pre-treated with Gc, then subjected to 5Gy IR or 30µM TMZ, or a combination of both. Cells were fixed 2 hours after therapy, and stained using the antibody specific to phosphorylated H2AX, γH2AX. As one of the first responses to DNA damage, foci of γH2AX can be counted and used as an approximate readout for the number of breaks within the DNA of a cell. Representative images are shown (Fig 4.17A, 4.18A), and quantification of images have also been analysed (Fig. 4.17B, 4.18B). I carried out cell plating and treatment, and under my supervision, Sophie Williams fixed, stained and imaged samples as part of her undergraduate research project.

116
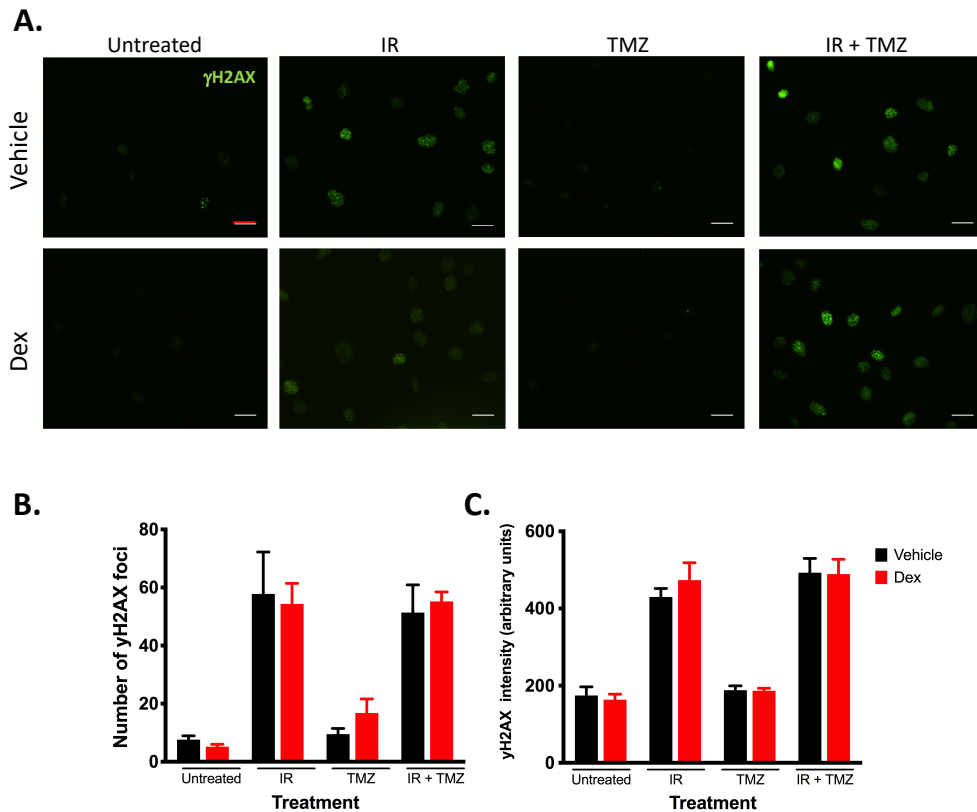
Figure 4.17: Dex pre-treatment does not alter γH2AX foci formation in M059J cells following IR, TMZ or both. M059J cells were pre-treated overnight with 100nM Dex or a vehicle control, then subjected to 5Gy IR, 30µM TMZ, or both combined. After 2 hours, cells were fixed and stained for YH2AX (green). Representative images are shown (A). The number of nuclear foci (B), and mean fluorescence intensity (C) were quantified. Scale bar denotes 20µm. Graphs show the average of 3 independent experiments, and error bars denote SEM. 5 fields of view were analysed within each experiment for each condition.

A.

B.   **C.**
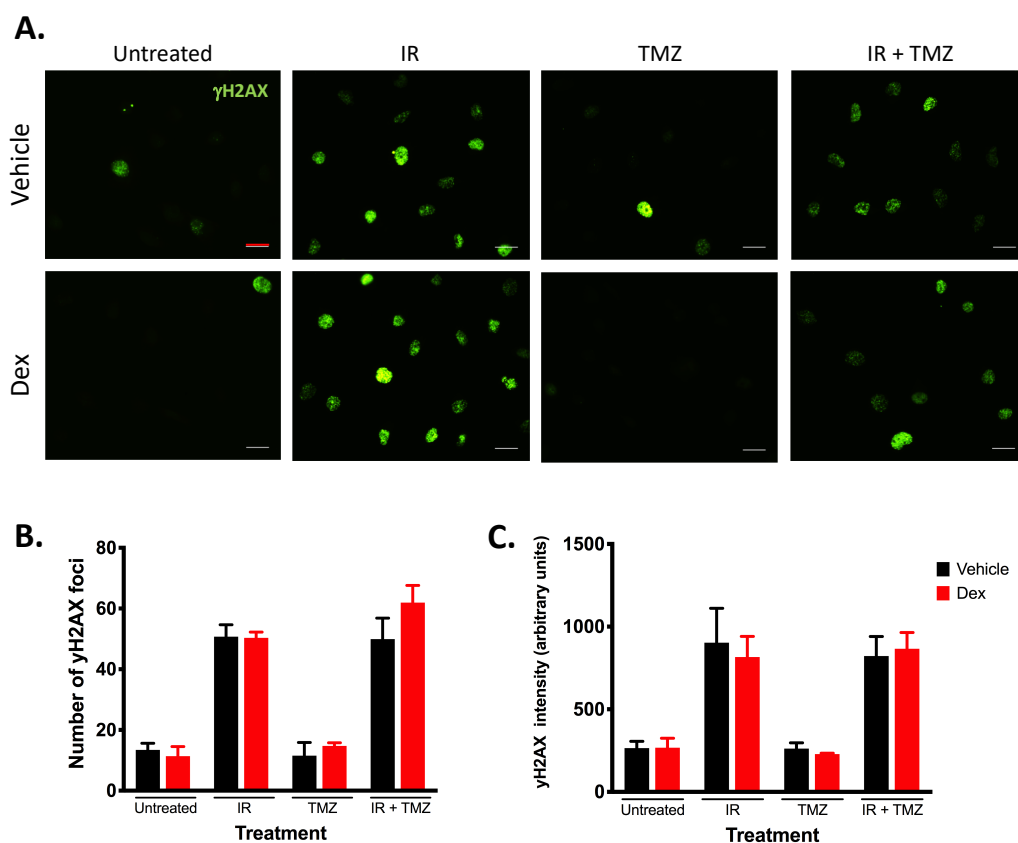
Figure 4.18: Dex pre-treatment does not alter γH2AX foci formation in M059K cells following IR, TMZ or both. M059K cells were pre-treated overnight with 100nM Dex or a vehicle control, then subjected to 5Gy IR, 30μM TMZ, or both combined. After 2 hours, cells were fixed and stained for YH2AX (green). Representative images are shown (A). The number of nuclear foci (B), and mean fluorescence intensity (C) were quantified. Scale bar denotes 20μm. Graphs show the average of 3 independent experiments, and error bars denote SEM. 5 fields of view were analysed within each experiment for each condition.

2 hours following IR, both M059J and M059K cells showed a significant increase in number of γH2AX foci, compared with the untreated control. There was no significant difference in staining between vehicle and Dex-treated samples following irradiation, suggesting Gc do not prevent the induction of DNA double stranded breaks. This was true for both the number of defined foci, and for the mean nuclear intensity of staining. TMZ treatment did not induce a significant increase in γH2AX foci, and IR + TMZ samples showed a small increase in number of foci compared with IR alone. H2AX is phosphorylated at sites of double

stranded breaks within DNA, however, TMZ primarily damages DNA through the addition of methyl groups. If unrepaired, this may ultimately result in formation of double stranded breaks after several rounds of unsuccessful cell division, but this damage would be expected to manifest later than the double stranded breaks directly caused by IR.

γH2AX staining was therefore repeated 24 hours following TMZ treatment to confirm that double stranded breaks were formed, albeit at a later time point (Fig. 4.19). 24 hours following 30µM TMZ treatment, there was an increase in both the number of foci, and the mean nuclear staining intensity of γH2AX. This confirmed that TMZ treatment did induce double stranded breaks, but at a later point than 2 hours. Similarly to the IR results at 2 hours, there was no difference in the number of γH2AX foci following either vehicle or Dex treatment. The mean fluorescence intensity of the nuclei, however, was significantly reduced in M059K cells following Dex treatment. There was also a trend towards a reduction in the mean fluorescence intensity of M059J cells however, this difference did not reach significance within this cell line. It may be possible that by 24 hours, a reduction in cells displaying pan-nuclear γH2AX staining could be seen, suggesting that cells with catastrophic DNA damage have been reduced following Dex treatment with TMZ, although the longer timepoint would also allow for a transcriptional response and subsequent DNA repair.
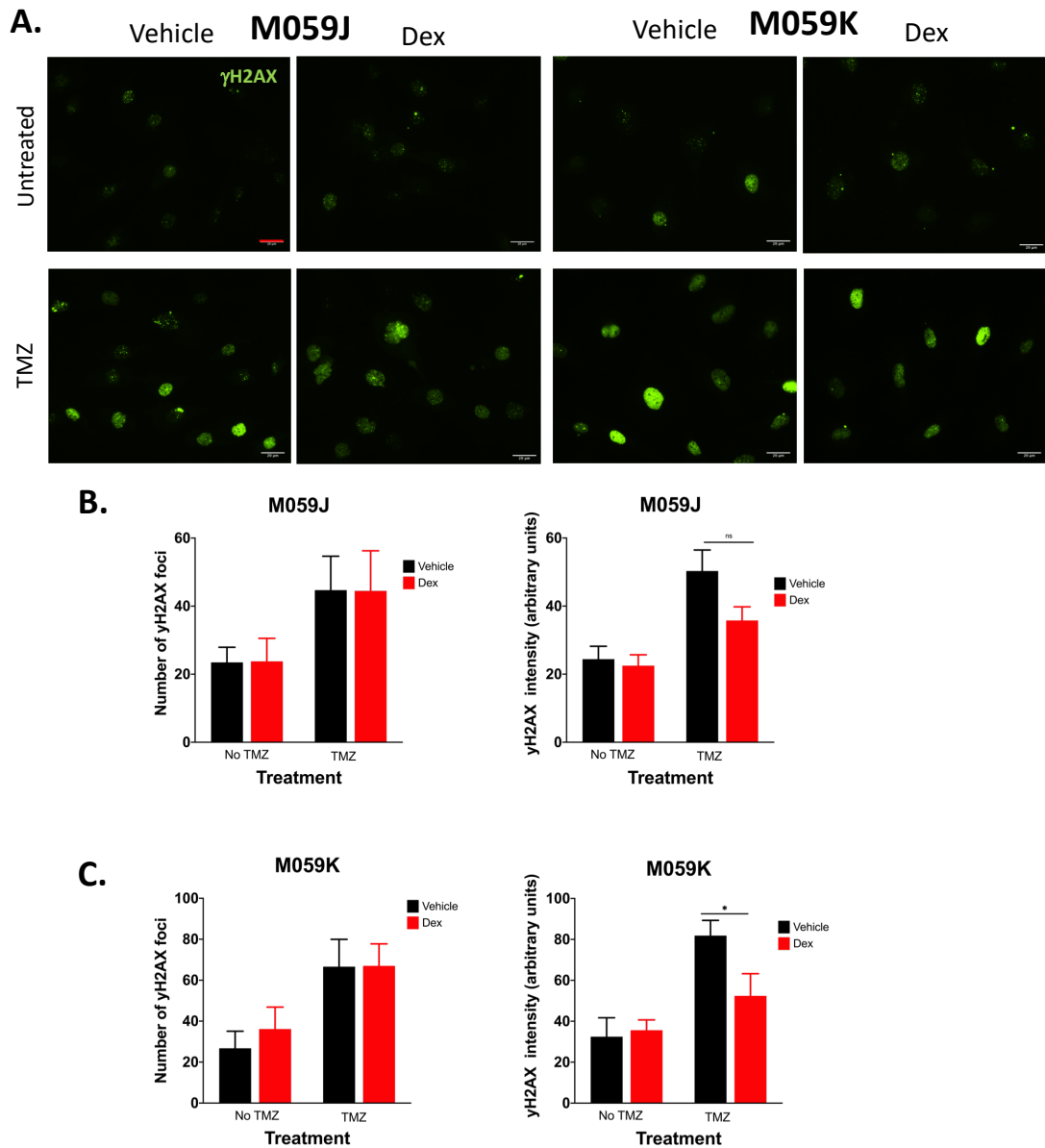
Figure 4.19: Dex pre-treatment does not alter yH2AX foci formation following TMZ treatment. M059J and M059K cells were pre-treated overnight with 100nM Dex or a vehicle control, then subjected to 30uM TMZ. After 24 hours, cells were fixed and stained for YH2AX (green). Representative images are shown (A). The number of nuclear foci, and mean fluorescence intensity were analysed for M059J (B) and M059K (C) cells. Scale bar denotes 20μm. Graphs show the average of 3 independent experiments, and error bars denote SEM. 5 fields of view were analysed within each experiment for each condition. * = p ≤ 0.05.

Taken together, these results indicate that Gc do not prevent both IR and TMZ from inducing DNA damage, but instead increase activity of DNA repair pathways, resulting in significantly increased DNA repair by 24 hours following IR or TMZ. There has previously been no publications to link Gc treatment and effects on DNA repair, so multiple pathways were investigated to determine how Gc may function.

4.2.14   Both GR and p53 regulate common genes

The original RNA-seq pathway analysis highlighted a possible role in coregulating p53 effectors. P53 is considered the key regulator of DNA repair, as it is activated downstream of multiple DNA repair pathways (246). As a transcription factor, it can induce cell cycle arrest, and prevent apoptosis whilst damage is repaired. It is possible that GR may modulate p53 effects directly through tethering, or through modulation of p53-mediated genes. In addition, p53 has been suggested to increase GR repression of NFkB, potentially through increased recruitment of cofactors (247). By accessing publicly available ChIP-seq data, the aim was to assess the overlap between p53- and GR-bound genes. One of the limitations of using publicly available data is that it was limited to the use of data that has been made available from other researchers. Therefore, it was not possible to directly compare GR and p53 binding within a GBM, or indeed a brain cell line. Instead, data pertaining to cell lines for bone, an osteosarcoma cell line (U20S), and MDA-MB-231, the triple-negative breast cancer cell line, were available. GR ChIP-seq data for both cell lines were acquired following treatment with 100nM Dex, for U2OS cells the treatment was for 1 hour, and MDA-MB-231 cells for 2 hours (234, 248). For p53 ChIP-seq data, both cell lines were untreated (249, 250).
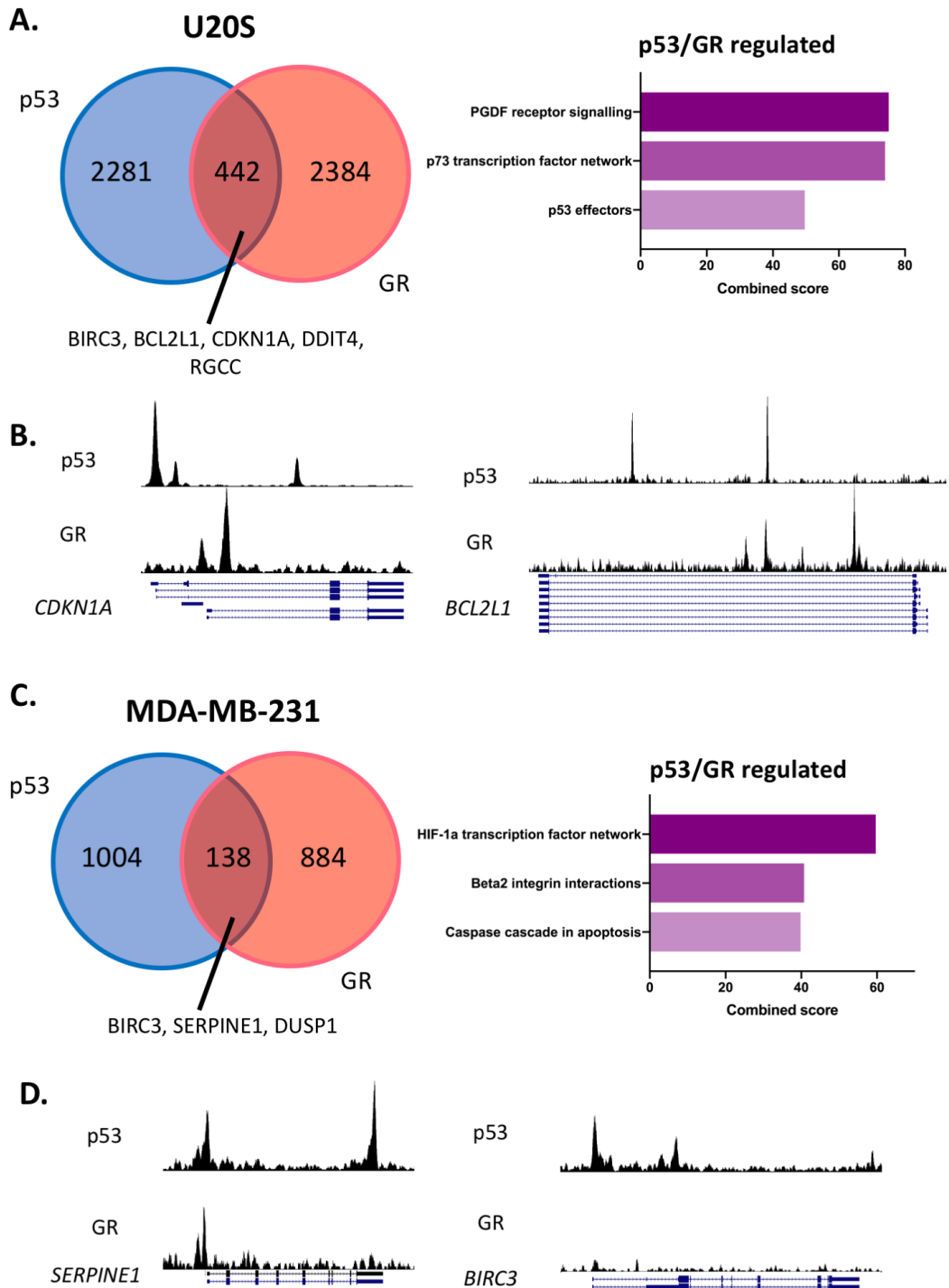
Figure 4.20: p53 and GR bind some common genes, based on ChIP-seq data. Using publicly available ChIP-seq data, GR and p53 binding sites were analysed within U20S cells (A-B), a bone cancer cell line, and MDA-MB-231 cells, a triple negative breast cancer cell line (C-D). GR and p53 genes were compared to find commonly bound genes (A & C).The genes identified within each subset were analysed for potential effects through Enrichr pathway analysis. The top 3 pathways for each common subset are shown. GR and p53 binding at commonly bound genes were visualised using the UCSC browser, and show GR and p53 are bound at different sites within the gene (B & D).

Within both cell lines, there was some overlap between GR and p53 bound genes (Fig. 4.20A &C). When GR and p53-bound genes were analysed using Enrichr pathway analysis, these genes were enriched for p53 effectors within both cell lines. This indicates that, rather than p53 regulating a small subset of anti-inflammatory or metabolic genes which are primarily regulated by GR, instead GR is binding a subset of p53, DNA repair-related genes. In both cell lines, these commonly bound genes include *DDIT4* and *CDKN1A*, which were both upregulated by Dex within M059K cells (section 4.2.7). Visualising gene tracks in UCSC for co-bound genes indicated that the two transcription factors were likely working independently at different regulatory regions (Fig. 4.20B & D). This suggested that GR perhaps is not working directly in cooperation with p53, but rather they are both regulating the same subset of genes independently.

4.2.15   GR effects on radioresistance and chemoresistance are not p53 dependent

It is clear that GR and p53 are both capable of altering expression of a common subset of genes. To test whether p53 expression is required to mediate the Gc effect on DNA repair, p53 was knocked down using 4 different targeting siRNAs (section 3.13), compared with the AllStars siNT control. Efficiency of the knockdown was evaluated using western blotting (Fig. 4.21A), alongside siRNAs to target DNA-PKcs and Rad51. These results were quantified (Fig. 4.21B). All 4 p53 siRNAs showed high level of knockdown, with expression ranging between 10.4% and 14.4% normalised against p53 expression in the siNT treated control cells.

123
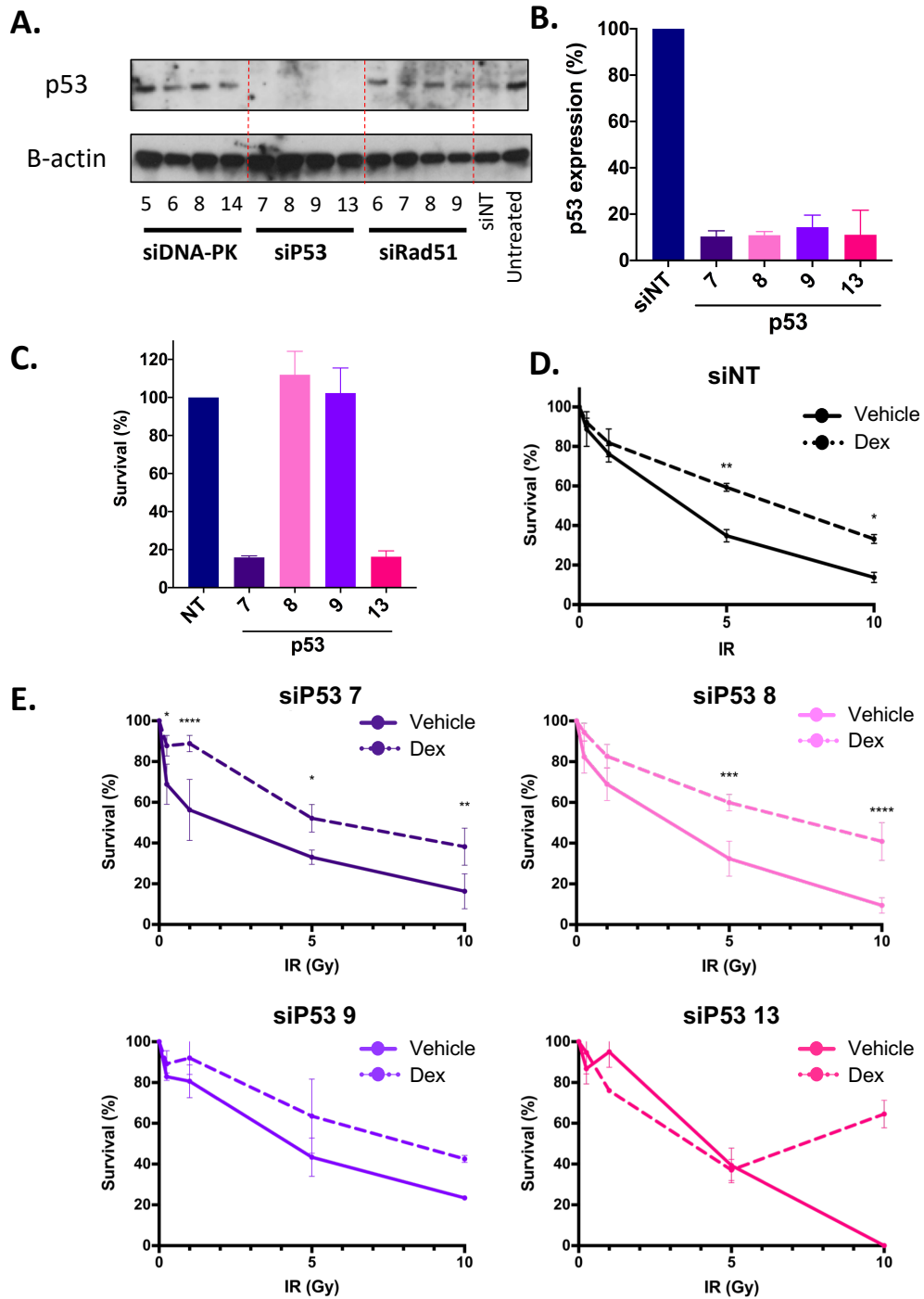
Figure 4.21: p53 knockdown does not remove the protective effect of Dex upon irradiation. Efficiency of knockdown was analysed using western blot (A). These results were quantified to determine efficiency (B). M059K cells were treated for 6 days using each siRNA then survival analysed by MTT assay (C). M059K cells were treated for 24 hours using siRNA, then treated overnight with Dex or vehicle. Cells were then subjected to IR, and survival analysed by MTT assay (D - E). Western blot images are representative of 2 independent experiments, and quantification indicates the mean of 2 independent experiments. MTT results for p53 7 and 8 are the mean of 3 independent experiments, and p53 9 and 13 are the results of 2 independent experiments. Statistical significance was tested using 2-way ANOVA with Dunnett's multiple comparison test. * = p ≤ 0.05, ** = p ≤ 0.01, *** = p ≤ 0.001.

Whilst the level of knockdown was consistent, survival of cells following treatment was variable between siRNAs. Both siRNA 7 and 13 led to low cell number survival, whilst treatment with siRNA 8 and 9 led to no difference in survival (Fig. 4.21C). Each siRNA was used to knock down p53 in M059K cells, cells irradiated, then survival was measured using MTT assay. P53 knockdown did not abrogate the protective effect of Dex, as Dex addition led to significantly increased survival following doses of 5 and 10Gy when treated with p53 7 and 8 (Fig. 4.21D – E). P53 9 and 13 siRNA were only tested twice, but siRNA 9 demonstrated a similar effect as siRNAs 7 and 8. This suggests p53 is not required for Gc to regulate DNA repair.

Therefore, the increase in survival caused by Dex addition was dependent on GR, but independent of p53. The genes regulated by both p53 and GR may contribute to a DNA repair phenotype, however, p53 is not required for this effect, suggesting GR does not affect transcription through tethering to p53 at gene promoters. Instead, based on the ChIP-seq data, it was hypothesised that GR was capable of directly binding to, and altering expression of DNA repair genes, which may also be modulated by p53 through independent mechanisms. By increasing expression of these genes, Gc may 'prime' cells to respond to DNA damage, allowing this damage to be repaired more quickly, and more effectively.

4.2.16 GR effects on radioresistance and chemoresistance are not DNA-PK dependent

The two main pathways of double strand break repair are NHEJ and HR. If, as shown, GR is able to increase active DNA repair within GBM cells, it may act through upregulation of one of these pathways. As a critical component of the NHEJ pathway, increased DNA-PK activity may lead to the increase in DNA repair seen with Gc addition. In contrast to this however, M059J cells showed the same protective effect of Dex treatment, suggesting DNA-PK was not required for Dex to increase survival. As single cell clones derived from the same tumour, M059J and M059K cells are suggested to be genetically identical except for the frameshift mutation within the DNA-PKcs gene, however, it is likely that through continued culture, one or both cell lines may have picked up other, unpublished mutations. In order to confirm that the protective effect of Dex is DNA-PK independent, siRNA was used to knock down DNA-PKcs expression within M059K cells. Four siRNA were used to knockdown DNA-PKcs, for 48 hours, and the efficacy of knockdown was analysed by western blot (Fig. 4.22A).

When targeting DNA-PKcs, siRNA 6 and 8 showed the highest knockdown efficiency (Fig. 4.22 A &B). Treatment with both siDNA-PKcs 6 and 8 lead to a reduction in M059K cell survival (Fig. 4.22C). Both DNA-PK siRNA-treated samples showed a similar pattern to the siNT control, with Dex leading to significantly increased survival (Fig. 4.22D - E). These results therefore confirm the results seen within M059J cells, that DNA-PK is not critical for Gc-controlled DNA repair.
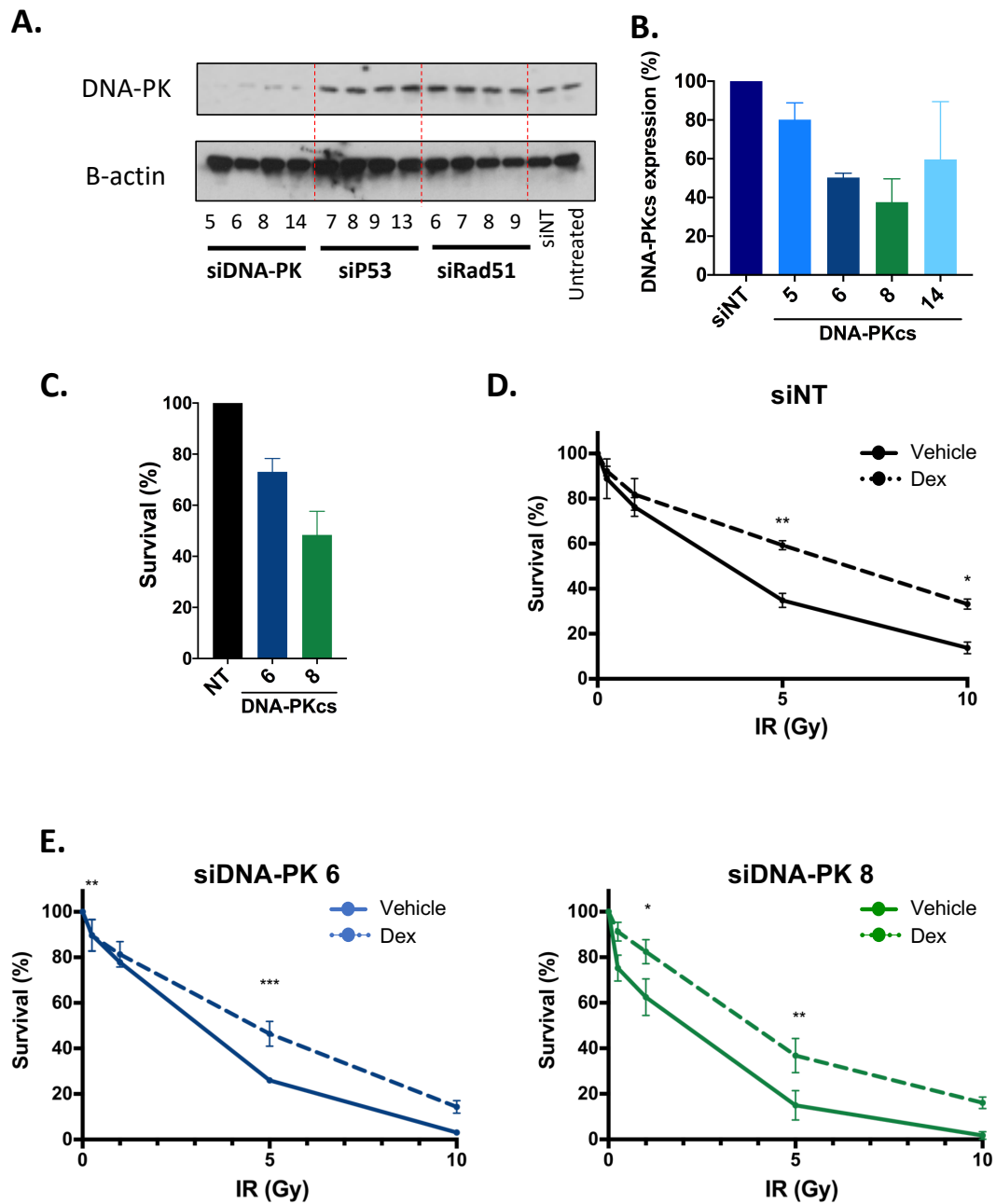
Figure 4.22: DNA-PKcs knockdown does not affect the protective effect of Dex upon irradiation. DNA-PKcs was knocked down using 4 targeting siRNA. Efficiency of knockdown was analysed using western blot (A). These results were quantified to determine efficiency (B). M059K cells were treated for 6 days using each siRNA then survival analysed by MTT assay (C). M059K cells were treated for 24 hours using siRNA, then treated overnight with Dex or vehicle. Cells were then subjected to IR, and survival analysed by MTT assay (D - E). Western blot images are representative of 2 independent experiments, and quantification indicates the mean of 2 independent experiments. MTT results shown are the average of 3 independent experiments. Statistical significance was tested using 2-way ANOVA with Dunnett's multiple comparison test. * = p ≤ 0.05, ** = p ≤ 0.01, *** = p ≤ 0.001.

4.2.17   Rad51 knockdown may affect radiosensitivity following Gc treatment

As the protective effects of Gc are unlikely to act through increased NHEJ, the next aim was to ascertain whether GR could act through HR, the other commonly used DNA repair pathway for double stranded breaks. To test this, siRNA was once again used to knock down Rad51, a key component of the HR pathway (Fig. 4.23). Several Rad51 antibodies were used to attempt to assess the efficacy of 4 Rad51 siRNA using western blotting, however, none of the antibodies tested produced a signal to quantify the efficacy (Fig. 4.23A). Therefore, all 4 siRNA were tested for an effect on survival following IR with and without Dex. All 4 siRNA produced a reduction in cell survival when compared with the siNT control (Fig. 4.23B). siRNA 8 treatment led to a survival of just 5.5% compared with control without IR. siRNA 7 and 9 reduced survival to 12.2% and 14.3% respectively. siRNA 6 had a survival of 40.7%, and, when Rad51 was knocked down with this siRNA, Dex did show a protective effect, however, this did not reach significance (Fig. 4.23D). This effect was not seen with the other siRNA tested, however, given the significant reduction in cell survival, it is not possible to determine if the lack of protective effect is due to affecting GR function, or due to the low proportion of surviving cells (Fig. 4.23B).
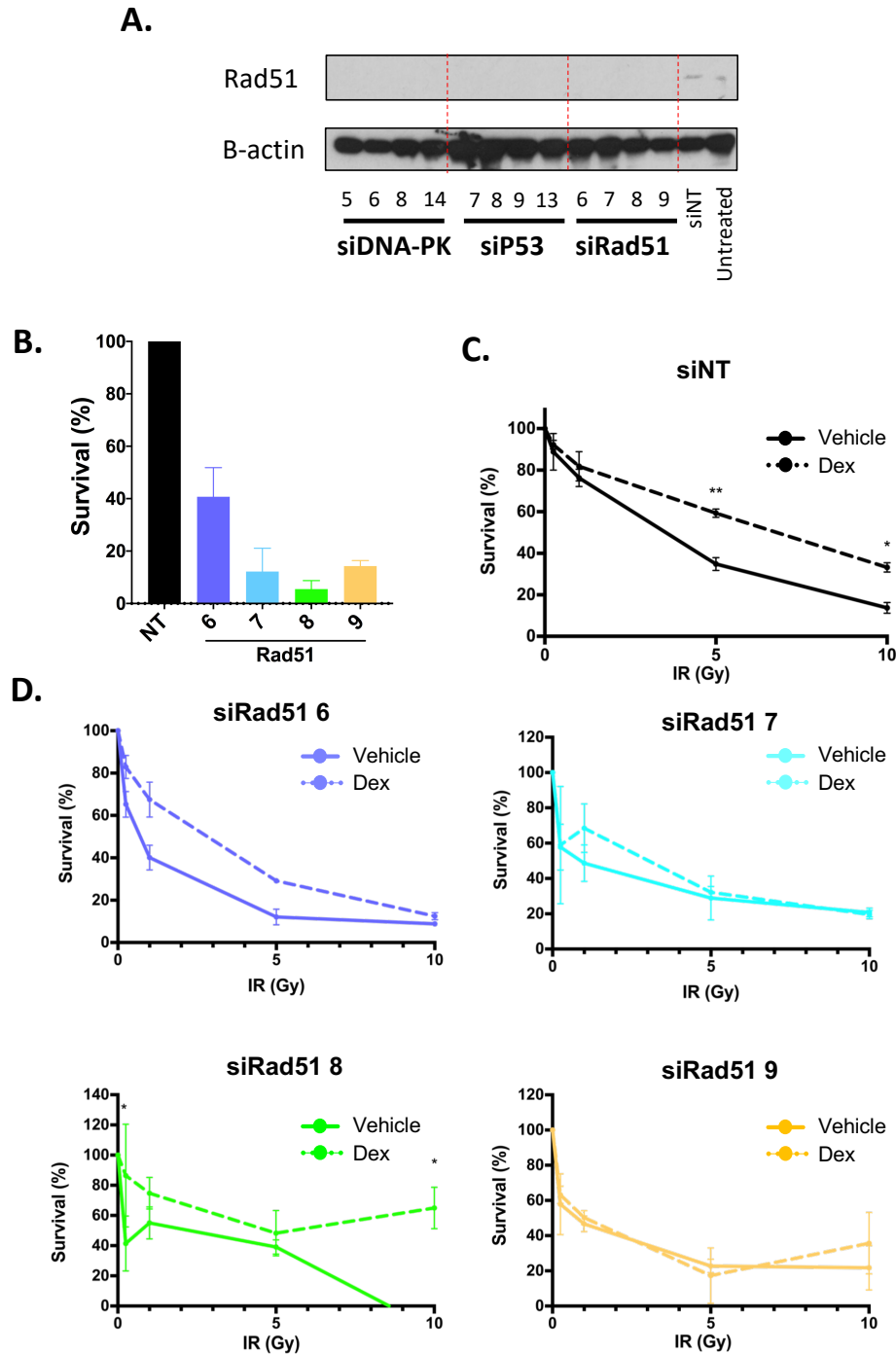
Figure 4.23: Rad51 knockdown does not affect the protective effect of Dex upon irradiation. Rad51 was knocked down using 4 targeting siRNA. Efficiency of knockdown was analysed using western blot (A). M059K cells were treated for 6 days using each siRNA then survival analysed by MTT assay (B). M059K cells were treated for 24 hours using siRNA, then treated overnight with Dex or vehicle. Cells were then subjected to IR, and survival analysed by MTT assay (C – D). Western blot results are representative of 2 independent experiments, and MTT results shown are the average of 3 independent experiments. Statistical significance was tested using 2-way ANOVA with Dunnett's multiple comparison test. * = p ≤ 0.05, ** = p ≤ 0.01.

Based on these results, it is possible that Rad51 may be involved in the effects of Gc treatment, however, the results are not reliable enough to confirm this. Further work is therefore required to investigate a potential relationship between GR and Rad51. A key limitation, however, has been the lack of a specific antibody for Rad51, so it will be necessary to use other mechanisms to try to investigate this.

4.2.18 Exploring non-transcriptional effects of Gc on DNA repair mechanisms

As previously discussed, GR is capable of altering cell phenotype through both genomic mechanisms, which require new transcription and non-genomic mechanisms which occur rapidly through direct protein-protein interactions. Previous work has investigated GR binding to other proteins using proteomics analysis (28). A549 cells were treated for 10 minutes with 100nM Dex, GR-protein complexes isolated and then analysed by mass spectrometry. Several DNA binding and repair pathways were highlighted within the analysis (Table 4.3). Of particular interest was the fact that GR can bind directly to DNA-PKcs, H2AX, and TRIM28, amongst other DNA repair related proteins. This suggests that GR is capable of binding in complex with proteins from DNA repair pathways.

Table 4.3: GR is capable of binding proteins relevant to DNA repair. Proteins bound to GR within proteomics analysis of A549 cells were entered into Enrichr. The proteins relevant to DNA repair are listed below.

Protein Name	Function
DDX3X	Associates with p53. Regulates apoptosis and cell cycle progression, but contradictory effects reported. Involved in promoter regulation of p21
DHX9	Unwinds RNA and DNA. Associates with yH2AX, BRCA1, EGFR and CBP and is involved in DNA replication
DNMT1	DNA methyltransferases. Involved in MMR - prevents p53-dependent apoptosis. Loss of DNMT1 activates ATMR/ATM -> accumulation of yH2AX and phosphorylation of Chk1/2. ATR is key
GTF2I	Regulates BRCA1-mediated HR, knockdown has reduced HR efficiency. Forms foci with yH2AX
H2AFX	H2AX – initial binding proteins at sites of double stranded breaks
HNRNPA1	Involved in telomere replication
HNRNPK	Involved in gene regulation by binding DNA and RNA. Cofactor of p53 - both phosphorylated by ATM/ATR and bind to p53 promoter regions, eg in p21. Knockdown - increased yH2AX
HNRNPU	Substrate for DNA-PK. Phosphorylated by DNA-PK following DNA damage. Recruited to the nucleus, then quickly excluded following damage. Function unclear.
HSPD1	Hsp60 - binds p53, can be considered both a tumour suppressor and promoter
KHDRBS1	Traffics DNA damage signals from the nucleus to the cytoplasm, ultimately resulting in NFkB activation and the activation of protective genes. Decreased levels results in increased radiosensitivity. Substrate of ATM/ATR and DNA-PKcs.
LRRFIP1	Promotes cancer metastasis, role in Wnt signalling. Senses DNA, resulting in IFNb production
MCM7	Involved in DNA unwinding. Suppression increases genomic instability
NCL	Involved in chromatin remodelling. Promotes HDM2 ubiquitination, disrupting its binding with p53. Also binds p53 mRNA to repress its translation
PRKDC	DNA-PKcs – part of the DNA-PK complex
RPL7	Little known
SFPQ	Along with NONO, promotes c-NHEJ DNA repair. Stimulates DNA-PKcs autophosphorylation. Works like XLF, redundant mechanisms
TRIM28	Phosphorylated by ATM following DNA damage. TRIM28 then migrates to the site of damage, where its function is unclear. Also binds MDM2, and marks p53 for degradation
XRCC5	Ku70 – part of the DNA-PK complex
XRCC6	Ku80 – part of the DNA-PK complex
YBX1	Colocalises with yH2AX at foci. Interacts with YBX1

To investigate whether these protein-protein interactions were related to the DNA repair genes indicated within the RNA-seq, GR interacting proteins, and GR target genes from the DNA damage/repair ontology were uploaded into String, a software tool which maps interactions between proteins (Fig. 4.24A) (251). There was no direct overlap between the genes regulated by GR and GR bound proteins, however, they did regulate closely related proteins. Both the transcriptomics and proteomics confirmed GR can increase expression of DNA repair genes, and may directly interact with DNA repair proteins. This may allow GR to alter DNA repair through a combination of rapid non-genomic mechanisms, and slower, but longer lasting genomic mechanisms.

As Rad51 was highlighted as a possible effector in Gc induced radioresistance, the DNA repair-related GR transcriptome and interactome were compared with the previously published RAD51 interactome (Fig. 4.24B). RAD51 itself was not bound by GR, and there were no overlaps between the RAD51 interactome and GR. Interestingly, however, the DNA-PK complex, of which all 3 components were bound by GR, can antagonise the action of Rad51. If GR were capable of using post-translational modifications to alter DNA-PK function, this would drive cells towards Rad51, and thus HR for DNA repair. Previously published work has indicated that DNA-PK inhibition can lead to an increase in Rad51 function (252). The possible interaction between Rad51 and GR therefore requires further investigation.
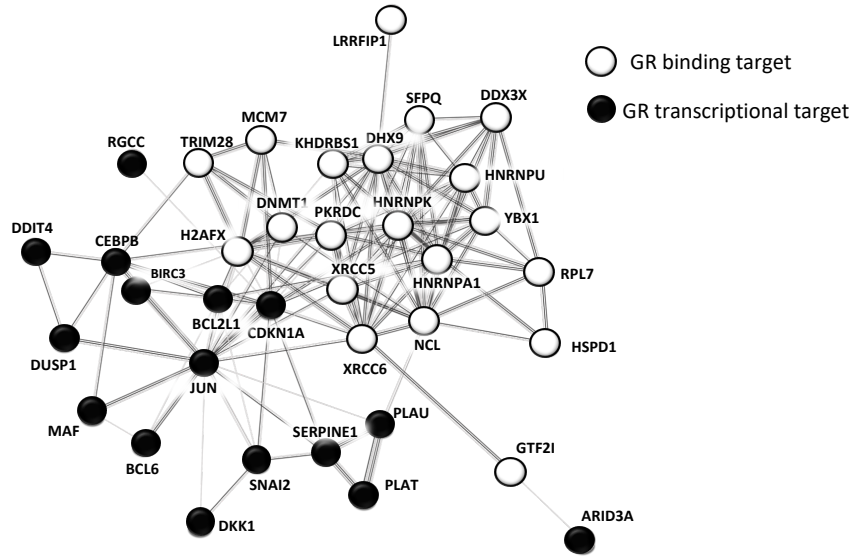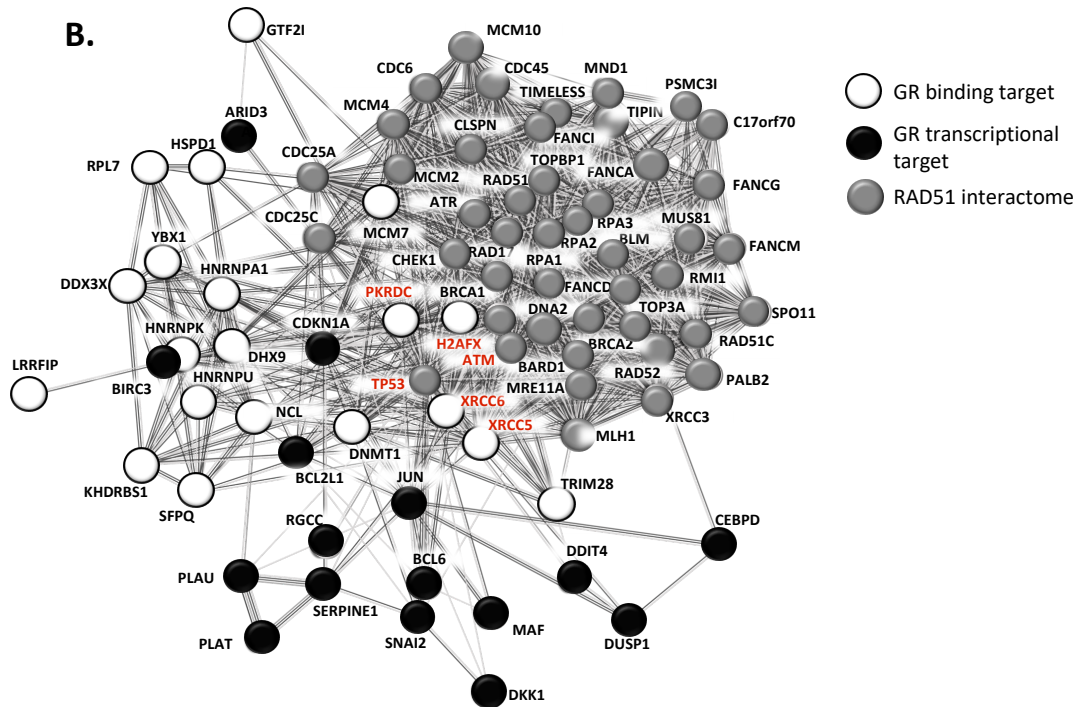
Figure 4.24: GR binds to, and alters expression of, 2 distinct subsets of proteins. A) Proteins bound by GR in A549 cells (white), and DE genes related to DNA repair (black), form 2 distinct clusters when analysed using String, a database which can map protein-protein interactions. Many of these proteins are closely related, shown as multiple joining lines. B) Both gene lists were then overlaid with the Rad51 interactome (grey).

4.2.19   Assessing the effects of selective GR modulators on GBM cell survival

For many years, there has been a popular concept that positive effects of Gc are mediated through repression of inflammatory genes, whilst activation of genes is responsible for potentially damaging side effects, such as metabolic effects. Through designing GR ligands which could maintain transrepressive effects, but limit transactivation, it would be possible to develop effective Gc, but with reduced side effects. This is, of course, a simplification of a complex signalling system, and selective GR ligands have yet to fulfil their initial promise. Within the context of DNA repair as a side effect, however, these ligands have not been tested.

Selective GR ligands were screened to determine if they could retain radiosensitivity in GBM, but still retain the anti-inflammatory effects. Three ligands were selected to test alongside Dex; these ligands were Compound A, Deflazacort and Loteprednol Etabonate.

The structures of each ligand are shown (Fig. 4.25A). CpA is perhaps the most well-characterised selective GR ligand. A synthetic analogue of a plant-derived compound, CpA has previously been shown to bind GR, and induce DNA binding, however CpA addition did not induce GR dimerization, and was shown to have a reduced ability to transactivate key GR target genes (253-255).

Deflazacort is similar in structure to prednisolone. *In vitro* studies have shown effective inhibition of cytokine release from immune cells, and efficacy has been shown in chronic inflammatory conditions, such as rheumatoid arthritis (256-258). On the other hand, Deflazacort has been shown to exhibit reduced effects on calcium and carbohydrate metabolism, suggesting specificity of its effects on GR

function (259, 260). Its precise mechanism of action, however, has not been studied to the same extent as CpA.

Finally, Loteprednol etabonate (LE) contains an ester at carbon-20, instead of the ketone found in prednisolone (261). This results in rapid de-esterification following application, resulting in a much lower half life. Within the clinic, LE is commonly used in the treatment of ophthalmic inflammatory conditions, due to its high efficacy, and low effects on circulating Gc levels (262).

The premise of selective ligands is to reduce the activation of GREs, such as TAT3-luciferase, whilst retaining the tethering effects of GR, such as reduction of NFκB binding sites, for example NRE-luciferase. Therefore, cells were transfected with a TAT3-luciferase, or NRE-luciferase, alongside Renilla as a housekeeping control.

Dex was included in both experiments as a positive control, and even at low doses of Dex treatment, there were large increases in TAT3 activation, indicating that GR is binding directly to DNA at the GRE, resulting in activation of GR target genes (Fig. 4.25B). This response was markedly reduced with Compound A addition, slightly reduced with Deflazacort, however, the response following LE addition was comparable to the Dex response. This suggested that Compound A was the most selective ligand, followed by Deflazacort.
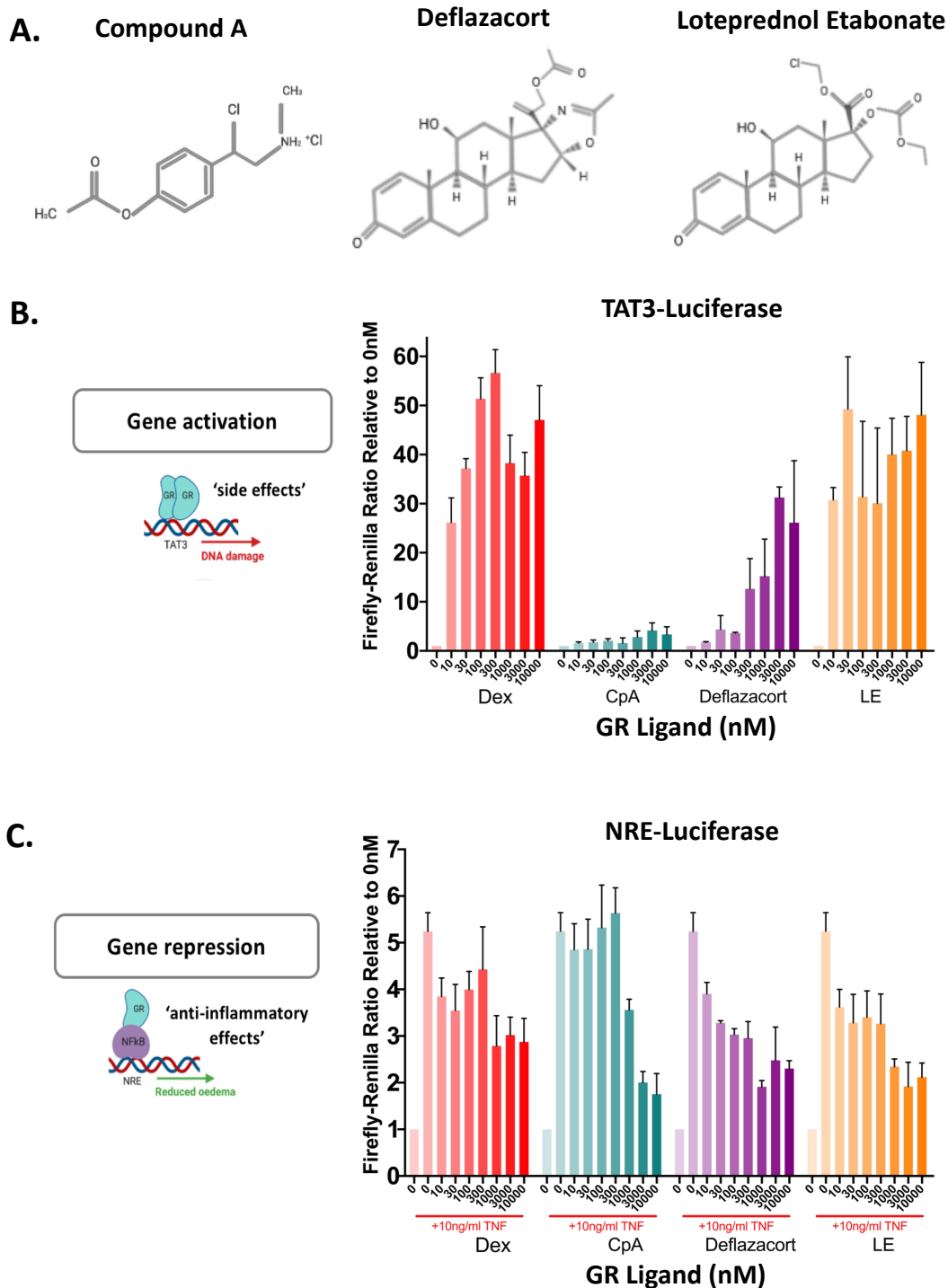
Figure 4.25: Selective GR ligands exhibit variable selective effects. A) Structures of 3 commercially available selective GR ligands (A). B) M059K cells were transfected with TAT3-luciferase and Renilla, then treated overnight with increasing doses of each ligand. TAT3 activation, measured as luciferase activity was analysed, relative to Renilla. C) Cells were pre-treated with selective ligands, then treated overnight with TNF to induce NRE activation. Luciferase activity was quantified, relative to Renilla. (C). Results shown are the mean of 3 independent experiments. Error bars denote SEM.

It was also important, however, to determine if the selective ligands also retained their transrepressive effects. Therefore, NFkB was activated through TNF addition, and cells were treated with selective ligands. As shown for Dex, the activation of NRE was reduced, suggesting that activated GR was capable of repressing NFκB activity (Fig. 4.25C). NFκB was activity was reduced following addition of each selective ligands, although higher doses were required of Compound A to supress NRE activity.

This system is clearly more basic than transcription under physiological conditions, as GR binding sites are under the control of multiple factors, such as chromatin availability, availability of transcriptional machinery, and the relative abundance of other transcription factors. As a broad initial assay, however, it does suggest that the selective ligands do show variability in the activation of TAT3, but all three ligands showed effective repression of NRE activation.

4.2.20 Compound A does not induce radioresistance within M059K cells

In order to determine if a reduction in transactivation could prevent the protective effects of Gc, M059K cells were treated with various doses of each selective ligand, alongside Dex as a positive control. Cells were then treated with 5Gy or 10Gy IR, and survival was analysed by MTT assay as previously described. Dex treatment led to significantly increased cell survival at doses of between 100nM and 10μM following 10Gy IR (Fig. 4.26A). Similarly, LE pre-treatment also resulted in increased cell survival, at each tested dosage (Fig. 4.26B), confirming it is not selective and would not be an appropriate ligand for future use.
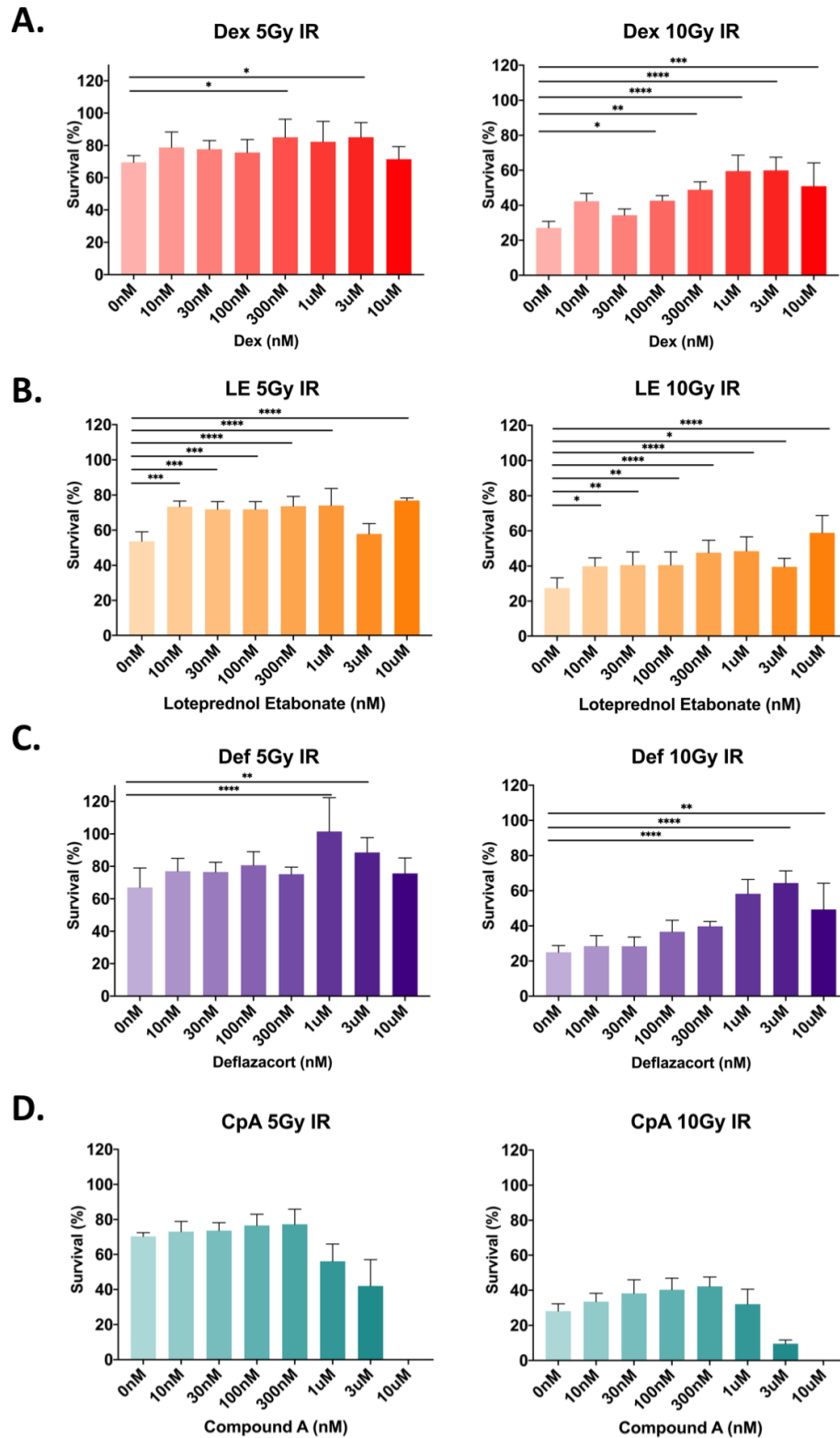
Figure 4.26: Selective GR ligands have variable effects on GBM cell survival following IR. M059K cell survival was analysed following treatment with doses of 10nM – 10µM of Dexamethasone (A), Loteprednol Etabonate (B), Deflazacort(C) and Compound A (D). Survival was assessed following doses of 0Gy, 5Gy and 10Gy IR. Results shown are the mean of 3 independent experiments. Error bars denote SEM. Statistical significance was tested using 2-way ANOVA with Dunnett's multiple comparison test. * = $p \leq 0.05$, ** = $p \leq 0.01$, *** = $p \leq 0.001$, and **** = $p \leq 0.0001$.

Deflazacort also showed increased survival, however, this occurred only at higher concentrations, above 1µM, suggesting it is weakly selective and does not induce radioresistance to the same extent (Fig. 4.26C). Finally, however, Compound A did not increase cell survival at any concentration, at either dosage of IR (Fig. 4.26D). This suggests that by reducing GR's transactivation function it is possible to prevent the resistance seen with Dex treatment. This is encouraging, suggesting that selective ligands may be a viable alternative to Dex treatment within patients.

4.2.21 Compound A does not induce resistance to TMZ in M059K cells

After determining how the selective ligands alter the response to radiation, it was then necessary to determine if they altered the response to TMZ. Cells were once again pre-treated with increasing doses of Dex as a positive control, and as expected, Dex pre-treatment led to significantly increased survival following both 30µM and 300µM TMZ (Fig. 4.27A). Once again, LE exhibited a very similar response to Dex, and increased survival with doses of both 30µM and 300µM TMZ (Fig. 4.27B). Pre-treatment of 100nM and 300nM Deflazacort resulted in significantly increased survival when treated with 30µM TMZ, however the effect was much more reduced than that seen with Dex and LE (Fig. 4.27C). Compound A resulted in no significant increase in cell survival, suggesting it does not exert chemoresistance (Fig. 4.27D).
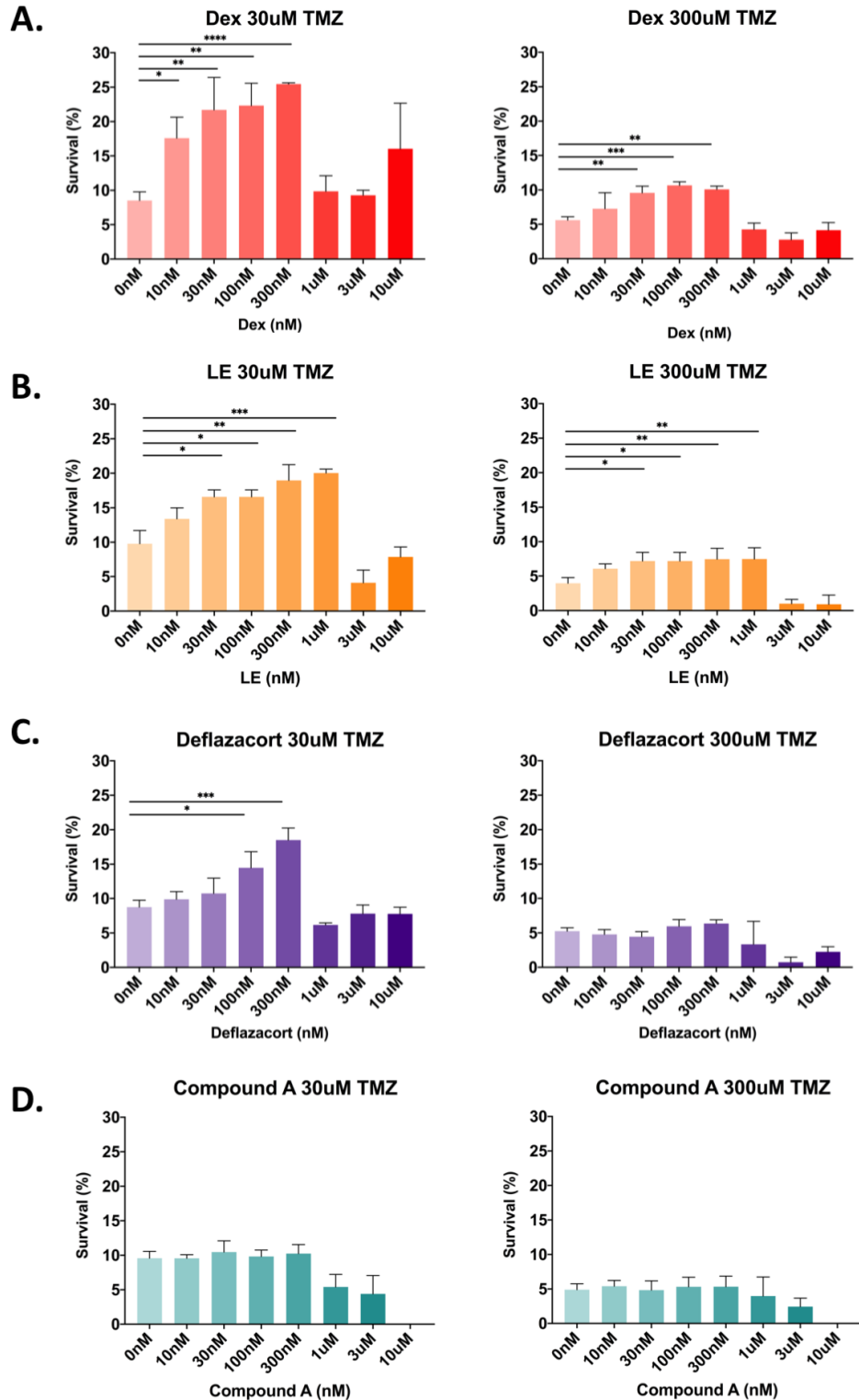
Figure 4.27: Selective GR ligands have variable effects on GBM cell survival following TMZ. M059K cell survival was analysed following treatment with doses of 10nM – 10µM of Dexamethasone (A), Loteprednol Etabonate (B), Deflazacort (C), and Compound A (D). Survival was assessed following doses of 30µM and 300µM. Results shown are the mean of 3 independent experiments. Error bars denote SEM. Statistical significance was tested using 2-way ANOVA with Dunnett's multiple comparison test. * = $p \leq 0.05$, ** = $p \leq 0.01$, *** = $p \leq 0.001$.

4.2.22   Selective ligands do not transactivate expression of DNA repair genes, but reduce expression of proinflammatory genes

The effects of selective ligands on expression of a number of GR target genes was then analysed through qPCR (Fig. 4.28). As LE had shown a protective effect on M059K cell survival, similar to that seen using Dex, it was not taken forward for further analysis. M059K were treated with doses of 100nM and 1µM of Dex, CpA, or Deflazacort, or a vehicle control, for 4 hours. Expression of *DDIT4* and *CDKN1A* was analysed, as both genes were upregulated within the RNA-seq data, and have both been linked to therapeutic resistance in GBM (Fig. 4.28A). Dex treatment led to an increase in expression of both genes, reaching significance at a dose of 1µM. *CDKN1A* expression was not increased compared to the vehicle control, following either CpA or Deflazacort treatment. *DDIT4* expression was increased following Dex treatment, however, this did not reach significance. Expression was also not significantly increased following either CpA or Deflazacort. A repeat of this experiment over a longer 6 or 8hr timepoint might generate more robust induction by Dex and therefore be a better comparison.

The ability of selective ligands to repress transcription was also tested through analysis of *IL6* and *IL8,* two genes previously demonstrated as being downregulated within the RNA-seq data. Expression of both *IL6* and *IL8* were not highly expressed, when CT values were analysed (data not shown). There was also little difference between the vehicle treated, and Dex treated samples when the samples were normalised (Fig. 4.28B). In order to induce sufficient expression in vehicle treated samples, cells were treated with TNF for 1 hour prior to ligand addition (Fig. 4.28C). Expression of both *IL6* and *IL8* were markedly increased following TNF addition. Expression was repressed following Dex

addition, and this reached significance for *IL6.* Both CpA and Delfazacort

repressed expression of *IL6* and *IL8,* however, this did not reach significance. It

is possible, however, that higher doses could reach significance.
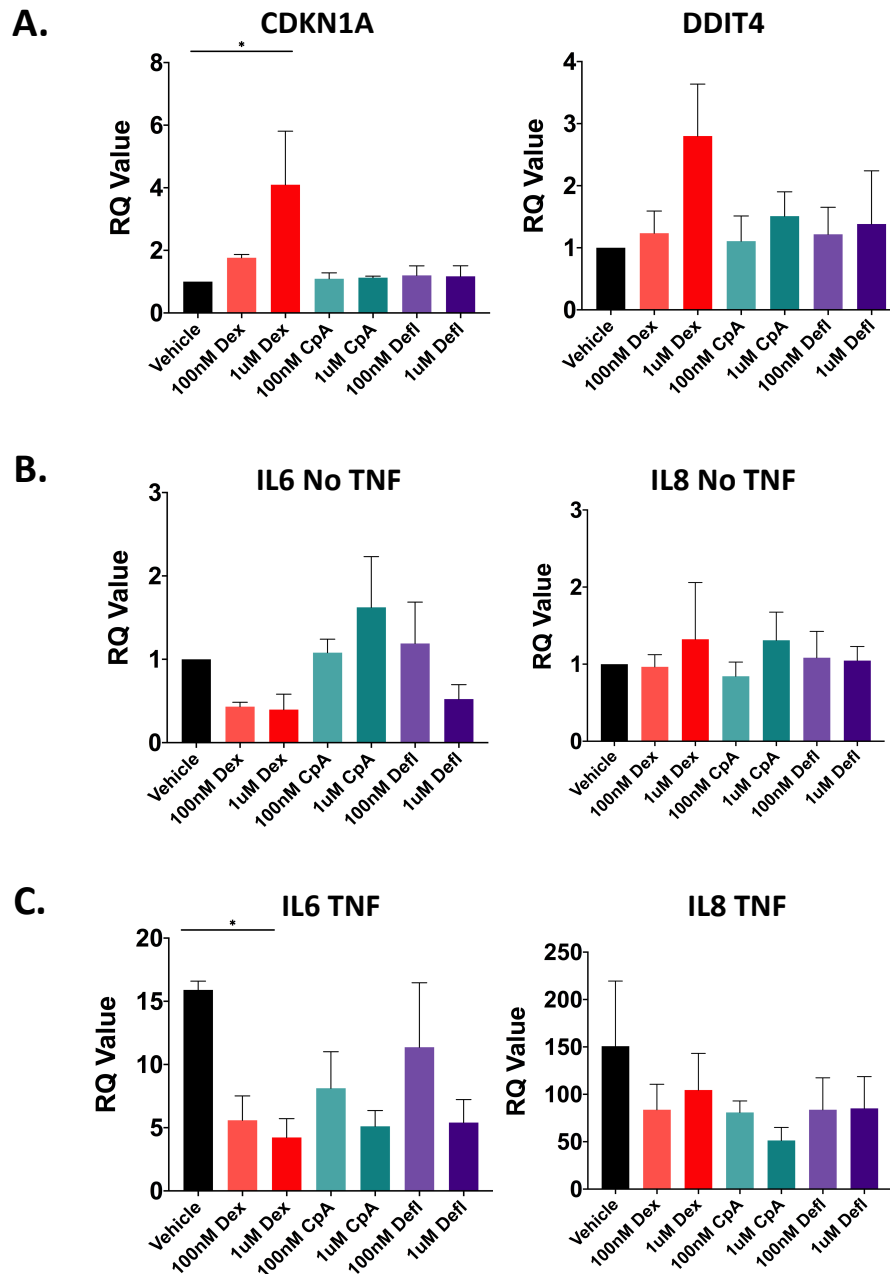
Figure 4.28: Selective GR ligands do not induce expression of DNA repair genes, but repress expression of TNF-induced *IL6* and *IL8*. M059K cells were treated for 4 hours with 100nM or 1µM of Dex, CpA, or Deflazacort, or a vehicle control. RNA was extracted and expression of upregulated (A), and downregulated (B) GR genes was analysed, relative to GAPDH. C) M059K cells were treated for 1 hour with TNF (10ng/ml) then treated for 4 hours with 100nM or 1µM of each ligand, or a vehicle control. Results shown are the mean of 3 independent experiments. Error bars denote SEM. Statistical significance was tested using 2-way ANOVA with Dunnett's multiple comparison test. * = $p \leq 0.05$.

The action of the selective ligands appear promising, as they appear to reduce expression of transactivation genes, many of which may be affecting treatment resistance, but appear to function similarly to Dex in repressing expression of pro-inflammatory genes. Clearly, these results are based on analysis of only 4 genes, and a much larger panel of genes would need to be analysed to confirm these effects. An RNA-seq experiment comparing genome wide responses is planned for future work. In addition, research will be required to investigate the effects of selective ligands on the tumour microenvironment as a whole to determine their efficacy in reducing oedema. Overall, however, this work has identified a novel mechanism of Gc action, and emphasises the complex mechanisms by which Gc can exert effects. Caution must therefore be taken with their use, until these effects can be fully understood.

4.3 Discussion

Within GBM, Gc have long been assumed to reduce inflammation through effects on the tumour microenvironment, and on the endothelial cells comprising the blood brain barrier (181). In light of this, the direct effects of Gc on the GBM cells themselves have perhaps been underestimated. Therefore, the aim of this research was to study the tissue-specific effects of Gc within GBM cells. To achieve this, a number of GBM cell lines were utilised. The use of cell lines within the study of GBM has been controversial, as GBM is, in itself, a highly heterogenous disease (263, 264). There is also an inevitable genetic and phenotypic drift when cells are maintained in culture over long periods. Within the context of our work, the aim was to investigate effects between Gc treatments, so a homogenous population was necessary to make differences between treatments clear. Any conclusions which appeared to suggest a functional effect could then be investigated using primary GBM cell lines, and primary tissue. The aim was to investigate the basic cellular biology of Gc within GBM cell lines, and given that Gc primarily affect cell function through the regulation of transcription, RNA-seq was used as an unbiased approach to identify pathways regulated by Gc within GBM.

The initial work confirmed that GR is expressed within both primary GBM tissue, and the GBM cell lines tested. Further, GR expression also appears to have a significant effect on cell survival within GBM, further confirming the importance of understanding GR function within GBM.

To elucidate the effects of Gc on GBM cell function, it was determined that within four of the five cell lines tested, Gc pre-treatment was able to induce resistance

to either IR, TMZ, or a combination of both. The effect was most pronounced within M059J and M059K cells, as the other three cell lines tested showed higher resistance to both radiotherapy and TMZ treatment, which made it difficult to identify any potential differences in survival. This protective effect has never previously been reported within GBM.

Within other cancer types, Gc have been suggested both as a radiosensitiser and a mechanism of inducing resistance (265). Many of these results may be due to differences in effects between tissues, but some conflict even within the same cancer type. Indeed, previous work within three murine astrocytoma cell lines suggested Dex increased cell death following IR, and increased γH2AX staining 30 minutes after 5Gy IR (266). Alternatively, however, earlier manuscripts had shown that within a human astroctyoma cell line, prior treatment with 100nM Dex for 8 hours was sufficient to reduce cell death caused by a variety of chemotherapeutics, although this did not include TMZ. This was suggested to act through upregulation of BCL-xL (267).

Once it was confirmed that Dex was having a protective effect, it was necessary to determine how these effects were being exerted. As previously mentioned, there is a complex network between nuclear receptors, and it cannot always be assumed that ligands are acting through their primary receptor. It was determined that MR, but not PR, was expressed within GBM cells. In light of the potentially harmful effects of Dex within GBM patients, recent research has been focused on investigating the effects of progesterone, and its receptor, PR (268, 269). Therefore, PR expression within glioma tumours and GBM cell lines was also assessed. Both glioma tissue, and all GBM cell lines tested, were uniformly

negative for PR expression. This does not rule out progesterone as a potential therapeutic; lack of expression on GBM cells may rule out potential side-effects on tumour cells, but expression within immune cells in the tumour microenvironment could allow for similar anti-inflammatory effects as seen with Gc treatment. Further work is ongoing to characterise the response of GBM tumours to progesterone treatment as part of an ongoing collaboration.

MR, meanwhile, is capable of binding some Gc, such as cortisol, with higher affinity than GR. Therefore, in studying GR action, it is necessary to identify any effects which may be mediated through MR binding. Both glioma tissue and all five GBM cell lines showed MR expression. Overall, this work suggests that glioma tissue, and our cell lines, may be classified as GR and MR positive, and PR negative.

RU486 was used to determine which nuclear receptors were necessary for Dex function within GBM. RU486 is an agonist for PR and antagonist for GR. As PR was not expressed within M059K cells, and progesterone treatment did not affect GBM cell survival, any effects of RU486 will likely be due to its antagonism of GR. Pre-treatment with RU486 reduced Dex-mediated survival, and it can therefore be concluded that the effects of Gc on GBM cell survival were GR-mediated. This was confirmed through the knockdown of GR expression through siRNA, which showed that GR expression was required for Dex to increase GBM cell survival.

As a final control, it would be important to antagonise MR action as a final confirmation that MR was not necessary for Gc-mediated therapeutic resistance.

This could be achieved through the use of spironolactone, an MR antagonist, which could be used as a pre-treatment in the same method as RU486.

It was necessary to narrow the 5 cell lines used until this point to one cell line for the RNA sequencing. M059K cells were chosen, as this cell line seemed representative of the other cell lines used, and by carrying out other experiments in parallel with M059J cells, it was still possible to continue work to investigate a possible role of DNA-PK in the GR response.

DNA-PKcs has also been shown to have functional relationships with a number of nuclear receptors. Androgen receptor (AR) can induce expression of DNA-PKcs following IR, and DNA-PKcs depletion led to a decrease in AR transcriptional activity (122, 270). Androgens also increased DNA-PK activity, allowing for a direct relationship between a nuclear receptor and DNA repair. DNA-PK also appears to have a relationship with the oestrogen receptor, initially indicated by the observation that DNA-PK was capable of phosphorylating ERα, resulting in increased ER activation (271). There is very limited evidence for a possible relationship between GR and DNA-PKcs, except that DNA-PK was shown to phosphorylate rat GR over 20 years ago (272). It is therefore entirely possible that a functional relationship may exist between the 2 proteins, however, this has yet to be investigated.

Bulk RNA-seq was originally intended to provide a population control for the single cell RNA-seq work described in the next chapter, but also to gain an unbiased overview of GR transcriptional function within GBM cells. There are a multitude of freely-available datasets analysing the genome-wide GR response within a large range of both primary tissue and cancer cell lines, however, none

yet exist within a GBM cell line. Given that GR function within cells is determined by the chromatin architecture of the tissue in question, and effects can be vastly different depending on the cell type, it was critical to investigate GR effects within GBM cells.

The bulk RNA-seq results were validated using qPCR for four Gc regulated genes. All four genes showed a dose- and affinity-dependent increase in expression following Gc treatment. Interestingly, although the 500nM HC and 100nM Dex doses were matched by potency, Dex still led to a larger increase in expression, suggesting that even when doses were matched, the higher affinity ligand still increased expression to a higher degree. Expression was tested in M059K cells, to validate the RNA-seq, but was also tested in M059J cells in parallel. Lack of DNA-PKcs expression does not appear to affect expression of GR target genes, suggesting that it is not required for genomic GR actions.

From the RNA-seq results, and the associated pathway analysis, it is clear that Gc induce a robust anti-inflammatory phenotype, through the downregulation of proinflammatory mediators, such as *IL6, IL11* and *IL1B,* and the upregulation of anti-inflammatory genes, such as *NFKBIA, IL6R,* and *GILZ.* These alterations in the cytokine milieu may result in the suppression of damage to the blood brain barrier. The literature surrounding the role of the immune system within GBM is plentiful, and beyond the scope of this thesis, however, IL6 and IL1β have both been associated with poor survival within GBM (273). IL6 expression is associated with increased macrophage activation within GBM, and a selective *IL6* knockout within endothelial cells led to increased survival *in vivo* (274). IL6 is also thought to support a cancer stem cell phenotype within GBM. Therefore, the

downregulation of these cytokines, and an upregulation of anti-inflammatory mediators may be considered beneficial within the GBM tumour (275). It is possible that Gc may reduce oedema within the tumour through direct action on GBM cells, alongside possible anti-inflammatory effects on immune cells within the tumour microenvironment and effects on the endothelial cells within the blood-brain barrier. Further work is clearly required in a more physiologically relevant system which can include the wider microenvironment, including endothelial cells and macrophages/microglia in order to ascertain the importance of these anti-inflammatory effects on the tumour cells themselves. It is possible that these effects are swamped by the effects on Gc on the other cell types, or indeed they may work in synergy to reduce inflammation and decrease the permeability of the blood-brain barrier.

The effects of Gc on the immune response within GBM are not surprising, however, the p53 effectors and prevalence of DNA repair and anti-apoptosis pathways were unexpected. All of the genes which made up this signature had previously been identified as differentially expressed in response to Gc, however, because of the complex levels of GR regulation, this does not necessarily mean that the gene is expressed within any particular tissue in response to Gc. A literature search did not indicate that this DNA repair signature had previously been identified within any other cancer cell line. The upregulation of these genes had a clear link to treatment sensitivity, and the role of these genes was therefore investigated further.

The expression of a number of the identified GR target genes was analysed using the GlioVis database, a freely available tool to analyse expression data from a

number of large datasets (220). Data from TCGA datasets was used, but limited to RNA-seq, rather than microarray data. This was used to limit samples to those with as high-quality data as possible, however, this was offset by a lower number of samples, particularly for the normal brain tissue. This is an important caveat for comparing expression data. It is also important to note that this expression data was derived from RNA from tumour sections, which may contain a variety of cells, including tumour cells, but also endothelial cells and immune infiltrates. This means it is not possible to determine if, for instance, the increased *NFKBIA* expression is within tumour cells, or within another population. Nonetheless, this analysis can indicate a potential protective or damaging effect.

Many of the genes analysed showed expression in line with the up- or down-regulation induced by Gc treatment. As mentioned, it was not possible to determine which patient samples had been treated with Dex before surgery, but it would suggest that Dex treatment may have induced a Gc-mediated gene signature. It is also important to note that whilst there was no significant difference in survival when each gene was looked at in isolation, a multi-gene signature, regulated by Gc, could ultimately result in altered survival. Such multi-gene signatures have previously been shown within GBM (276-278). This analysis was not possible using GlioVis software but could be an important aspect of future work.

Based on these results, Gc could be affecting treatment efficacy through a number of different mechanisms. Firstly, it could be acting through the induction of cell cycle arrest and inhibition of proliferation, as suggested by upregulated genes such as *RGCC* and *CDKN1A.* Alternatively, Gc could be altering the DNA

repair response following treatment, as suggested by upregulation of genes such as *DDIT4* and *BCL2L1.* Cell proliferation assays indicated variable effects of Gc on GBM cells. A172 and M059K cells both showed significantly reduced proliferation following Gc treatment, however, this effect was not seen in M059J, U87 or U251 cell lines.

As previously mentioned, A172 cells have been widely used previously to investigate effects of Dex on cell growth. Previous research has shown an inhibition of cell growth with continuous doses of 100nM - 100µM Dex for 3 - 5 days (223). Similarly, Kaup et al showed a significant decrease in cell proliferation in A172 cells after 4 days of treatment with 50nM Dex (222). Both of these studies showed no effect of Dex treatment on other cell lines, including U251 cells. Several papers have suggested that GBM cell growth is inhibited by Dex addition *in vitro*, however, many of these papers have used Dex dosages of up to 10µM Dex (222, 223). On the other hand, however, Fan et al suggested Dex could increase GBM cell growth in U251 cells, but inhibit growth in U87 cells (279). It should be noted, however, that this study used dose of between 1µg/ml to 200µg/ml, equivalent to 2.5µM – 509µM Dex. This is clearly far higher than the doses used within this work, and beyond the maximum 500nM found in GBM brain tissue. These results have therefore little relevance for clinical practice, and for understanding a mechanism of action for Dex function.

Our work showed a significant reduction in proliferation in A172 cells, and M059K cells, but not in the other 3 cell lines tested. Interestingly, however, this did not correlate with the induction of cell cycle arrest by 48 hours of Dex treatment in any of the 5 cell lines. Whilst the growth was inhibited by 4 days, it would be

expected that these effects should have manifested in cell cycle arrest by 48 hours. It is therefore likely, that whilst the induction of cell cycle arrest may contribute to the protective effects, this does not appear to be the primary mechanism of action.

Within M059J cells, a robust population of sub-G0 cells was apparent within each cell cycle experiment. This population has been previously noted within the literature, however, it has never been fully investigated. Previous work has identified that a stable DNA-PK inactivation within HeLa cells resulted in an increase in the number of cells with multipolar spindles during mitosis, and an increase in multinucleated cells (239). It stands to reason, then, that due to these dysregulations during mitosis, the result would be cells with an aberrant number of chromosomes. Indeed, this is what was observed within M059J cells, and this dysregulation of chromosome number may explain the third, haploid population seen within propidium iodide staining. This is an important factor to be considered for future work using M059J cells.

Given these results, it seemed unlikely that the effects on GBM cell survival were primarily driven by this difference in proliferation, especially given that this appeared to have manifested at some point between 48 hours, the timepoint of the cell cycle analysis, and 5 days, at which point the proliferation assays were carried out. Given the chronic nature of this effect, it seemed unlikely to be a primary transcriptional response. This made it likely to be a downstream effect on the DNA repair response.

Comet assays are a well-established, reproducible method of measuring the extent of DNA damage following exposure to a DNA damaging agent. They are extensively used within the literature to quantify damage induced by DNA damaging agents in a range of settings. In particular, it has the advantage of being a sensitive mechanism of measuring damage on a single cell basis. Tail moment is a commonly used measurement of quantifying DNA damage shown in comet assays (280). The tail moment incorporates both the length of the tail and the relative amount of damaged DNA. Both M059J and M059K cells showed increased damaged 24 hours after treatment with IR, TMZ or both combined, however, this damage was significantly reduced following Dex pre-treatment. Such a reduction in DNA damage suggests that DNA damage is either being repaired, or prevented from occurring.

Rapid phosphorylation of H2AX following the induction of double stranded breaks allows it to be used as a timely readout of points of DNA damage. Following IR there was no difference in DNA damage incurred following vehicle or Dex pre-treatment. As there was no significant increase in γH2AX foci following TMZ treatment at 4 hours, the γH2AX staining was repeated at 24 hours following TMZ addition. These results were conflicting, as there was no significant difference in the number of defined γH2AX foci, however, there was a significant reduction in the mean γH2AX staining in M059K cells. γH2AX staining is considered a standard, reliable marker of the induction of DSB, and is commonly used as a readout of both radio- and chemotherapeutic efficacy within clinical research. It can be considered a relatively direct functional readout, as it implies the activation of ATM, and downstream activation of the DNA repair pathways. In particular, immunofluorescence methods are preferred due to the ability to study the

formation of foci and nuclear localisation of staining (281). In particular, recent research has begun to differentiate between foci number and "pan-nuclear" γH2AX staining, such as that represented by the mean nuclear staining. As previously discussed, foci of phosphorylated H2AX occur at the sites of DSB, whereas this pan-nuclear staining occurs throughout the genome, even at sites of undamaged chromatin (282). This phenomenon has been observed in apoptotic cells, suggesting that DNA damage has resulted in mitotic catastrophe, which cannot be repaired and ultimately results in cell death (283). However, this phenomenon has also been observed in response to IR in cells which did not result in apoptosis. It has been suggested that this staining pattern may be associated with the activation of multiple kinases, including ATM, JNK and DNA-PK, however, the functional significance of this pan-nuclear staining is still very much under investigation. Overall, therefore Gc are not preventing DNA damage from being induced, however, a robust decrease in DNA damage at 24 hours post-treatment was observed. This would suggest that, at least following IR, Gc have induced active DNA repair within GBM cells.

When considering DNA repair, one of the most critical and common components of DNA repair pathways is p53 activation (148). P53 had been indicated in the pathway analysis from the RNA-seq work, and a relationship between GR and p53 could explain the increased treatment resistance within GBM cells following Dex treatment. ChIP-seq analysis of both GR and p53 binding indicated a common subset of genes bound by both transcription factors, however, visualisation of binding peaks indicate that GR and p53 were not bound at the same sites on commonly bound genes. This was therefore not conclusive evidence of a functional relationship. It could instead indicate two independent

pathways, resulting in expression of similar genes. Indeed, this appeared to be confirmed by p53 siRNA knockdowns, which indicated that knocked down p53 expression did not prevent the increased survival seen with Dex addition. Therefore, it seemed unlikely that there was any interaction between the two transcription factors.

Knockdown of several DNA repair proteins using siRNA was used to narrow down any potential interactions between the DNA repair pathways and GR. An effect on NHEJ was ruled out through the knockdown of DNA-PKcs, and previous work using M059J cells. An involvement of Rad51 could not be ruled out, due to differences in results seen with Rad51 knockdown. The efficiency of the knockdowns could not be determined using western blotting or IF due to poor signal from several Rad51 antibodies.

Both NHEJ and HR lead to the repair of DSB through different mechanisms. The interplay between the pathways is complex, as some proteins, such as ATM, the MRN complex and BRCA1 function within both pathways, whilst others, such as DNA-PK and RAD51 are pathway specific (284). Previous work has indicated that pathway choice is decided early within the repair process. The choice of pathway is highly dependent on cellular factors, the most obvious being cell cycle phase. An arrest in cell cycle phase within S or G2 phases may indirectly increase the proportion of HR repair, however, this was not seen within any of our GBM cell lines (135). Alternatively, relative abundance of 53BP1 and Rad51 are believed to drive cells towards NHEJ or HR respectively (285). 53BP1 prevents the DNA strand invasion, thus preventing end resection, which ultimately directs cells towards HR. M059K cells were stained for 53BP1 using IF techniques and

western blotting, however, neither yielded positive results due to lack of specificity in staining.

To investigate whether these effects on DNA repair may be due to direct interaction of GR with DNA repair proteins, proteomics data previously generated within the Matthews group was analysed. Direct protein-protein interactions, illustrated through proteomics data, would allow for rapid increase in DNA repair, without the requirement for genomic effects. For instance, GR can itself interact with H2AX, so by a theoretical increase in H2AX phosphorylation, it would be possible for GR to alter the subsequent downstream phosphorylation of DNA repair proteins, such as Chk1/2. This proteomics data suggests a previously unknown relationship between GR and DNA repair proteins, within minutes of Dex addition.

Comet assays showed that Dex pre-treatment led to a reduction in DNA damage by 24 hours after IR and TMZ. It is possible, however, that this resistance is mediated by different mechanisms. For IR damage repair, DNA is immediately damaged, then repair will begin. Alternatively, as TMZ required failed DNA replication, DSB formation is much slower. This is unlikely to have happened, and been repaired, by 24 hours following treatment. It was therefore possible that Gc increased repair before reaching the stage of DSB formation following TMZ treatment.

A previous publication has shown that Dex treatment led to the upregulation of MGMT expression within GBM cells (169). MGMT is a DNA repair enzyme which can rapidly repair damage caused by alkylating agents such as TMZ, thus

reducing treatment efficacy (156). Increased MGMT expression is a prognostic marker of poorer survival within patients (163). *MGMT* expression was tested within M059K cells at 4 and 24 hours post-TMZ treatment with and without Dex treatment, however, *MGMT* could not be detected in any of the samples tested. It is possible that *MGMT* expression may be aberrant within M059K cells, and further work is therefore necessary to confirm whether the Dex protective effects on GBM cell survival following TMZ treatment are related to *MGMT* gene expression.

As future work, it would be beneficial to knock out transcriptional targets of GR such as *BCL2,* to confirm that GR transcriptional effects are required for the protective effects. Such knockdowns are limited for many GR target genes, such as *RGCC* and *CDKN1A,* as knockdown is known to affect cell cycle and would therefore affect treatment sensitivity through a multitude of GR independent mechanisms. Alternatively, investigations could be carried out using stable transduction of GR containing a mutation within the DBD, or lacking the AF1 transactivation domain, allowing GR to continue its protein-protein interactions but preventing DNA binding. It would be important to test the response to both IR and TMZ to confirm if GR-mediated transcription is required for protection to one or both treatments.

Through the use of selective GR ligands, it is possible to retain the transrepressive effects of GR action within GBM, without retaining the potentially dangerous transactivation function. The more selective ligands, in particular CpA, did not show a protective effect on cell survival, following either IR or TMZ. It can be predicted, firstly, that the DNA repair effects are mediated through upregulated

genes, those such as *DDIT4* and *CDKN1A.* Secondly, this could raise a potential avenue of treatment, whereby a selective ligand could be used to maintain the anti-oedemic effects of Dex, but potentially without the side effects. Clearly, this would require a significant amount of work to determine appropriate dosages and safety.

Through the work described in this chapter, a previously unknown effect of Gc in GBM cells has been identified, which may add to previous work showing reduced survival in GBM patients receiving high doses of Dex. Our research has narrowed down the mechanism by which this increase in GBM cell survival is occurring to an increase in DNA repair, thus reducing the efficacy of both of the first-line treatments used within GBM. Further work is required to fully elucidate the precise method by which this occurs, but this should be carefully considered within the context of Gc administration in patients, and should further advance the case for alternative anti-oedemic treatments within GBM.

Chapter 5 Single cell RNA-seq unveils complex GR signalling within GBM cells

5.1 Introduction

For many years, transcriptional responses have been recognised as complex, highly regulated processes (286). Each stage of this process, is controlled by a multitude of factors, including abundance of transcription factors and cofactors, chromatin availability, and the recruitment of the basal transcriptional machinery. As our understanding of the transcriptional process becomes more layered and complex, attention has turned to understanding how this process occurs within individual cells. Mathematical modelling of transcription has highlighted that the process is inherently stochastic, meaning that it will occur at different rates within individual cells (188).

When we consider the response of specific transcription factors, biological context becomes more relevant, as it can further contribute to the heterogeneity seen within the system. Factors known to affect the transcriptional response at a cell population level, such as cell cycle phase, or inflammation, must also contribute to heterogeneity between individual cells in a population. Thanks to the emergence of single cell RNA-seq technologies, it is now possible to compare the transcriptional response within individual cells within a population, under different conditions. This technology has transformed many facets of basic science research, and has been particularly advantageous when attempting to identify small subpopulations based on their transcriptional output, notably within the fields of neurogenesis and immunology (196, 287-289). Single cell RNA-seq

(scRNA-seq) is far more sensitive than more traditional methods, such as fluorescence activated cell sorting (FACS), followed by bulk RNA-seq on the pre-sorted populations. These populations were sorted based on a selection of markers, then assumed to be homogenous. Instead, single cell RNA-seq may identify even a single cell with a different phenotype within a larger population.

Due to the relative novelty of these techniques, their use within the study of transcription factor dynamics has been limited. At the beginning of this project, there were no datasets investigating the glucocorticoid responses at a single cell level. We therefore aimed to use single cell RNA-seq to identify factors which affected GR transcriptional dynamics at a single cell level. These factors may be similar to those seen at a population level, such as cell cycle phase, or the activation of other transcription factors by inflammatory cues.

The aims of this chapter were therefore two-fold:

1) To complete single cell RNA-seq to examine heterogeneity in Gc responses in GBM cells.
2) To develop a high throughput assay to quantify transcript levels of a panel of genes and determine the effect of inflammation.

5.2 Results

5.2.1 Optimising conditions for single cell RNA-seq sample preparation

Single cell RNA-seq is a cutting edge technique, and as such, each experiment is costly, and it is therefore not possible to repeat. For this reason, appropriate steps were taken to confirm that cells were suitable for processing, and would remain viable following the possible lengthy preparation process. It is important to note that these optimisation experiments were only completed once, as we prepared for the single cell RNA-seq.

The single cell RNA-seq was carried out using an iCell 8 (Wafergen Biosystems). The iCell8 platform utilises a 5,184 well chip to potentially sequence thousands of cells within a single experiment (290-293).The system uses droplet technology, whereby cells stained with propidium iodide and Hoescht are diluted out such that a single droplet may contain a single cell. Each droplet is added to a well of a chip, then imaged to identify wells containing a single, live cell (propidium iodide positive and Hoescht negative). Individual wells can therefore be selected for library preparation and sequencing. This provides control in selecting equal numbers of cells between different conditions.

Success of using this platform requires an accurate estimation of cell number in the suspension, and that over 60% are single viable cells in order to maximise the number of droplets containing a single live cell (Fig. 5.1A). Using a cell strainer to remove potential doublets and larger clumps of cells was considered as part of the cell preparation process. This straining process, however, may significantly reduce the number of cells within the suspension, which is also very

important to optimally use the platform. To test the effects of cell straining on cell number, M059K cells were plated overnight, then trypsinised and counted before and after straining using either 40μm or 70μm strainers (Fig. 5.1B). Whilst the literature has not published a precise size for M059K cells, U87 cells, another GBM cell line, are estimated to be 12 – 14 μm when trypsinised (Merck). We would therefore expect M059K cells to pass easily through both of these strainer sizes. There was minimal difference in cell number both before and after straining, suggesting this does not have an effect on cell number. We also used flow cytometry to analyse the proportion of single cells compared with doublets (Fig. 5.1C). Cells were resuspended in FACS buffer following straining, then gated using forward and side scatter to identify a single cell population. There was no apparent effect of straining on the proportion of single cells within the suspension, and we therefore did not include a straining step within our protocol.

Secondly, we were made aware that, during the sample preparation process, samples may be required to be stored in PBS for up to 2 hours. We therefore tested the viability of M059K cells under these conditions, and samples were incubated at room temperature in either media or PBS for either 2 hours, then cell viability was analysed using flow cytometry (Fig. 5.1D – vehicle labelled samples). In order to test whether steroid treatment may alter viability, samples were also treated for 4 hours, then stored in either media or PBS under the same conditions. The results showed that storage within PBS led to a marked reduction in viability compared with cells stored in media, however, it does not appear that Gc treatment prior to sample processing led to any differences in cell viability.
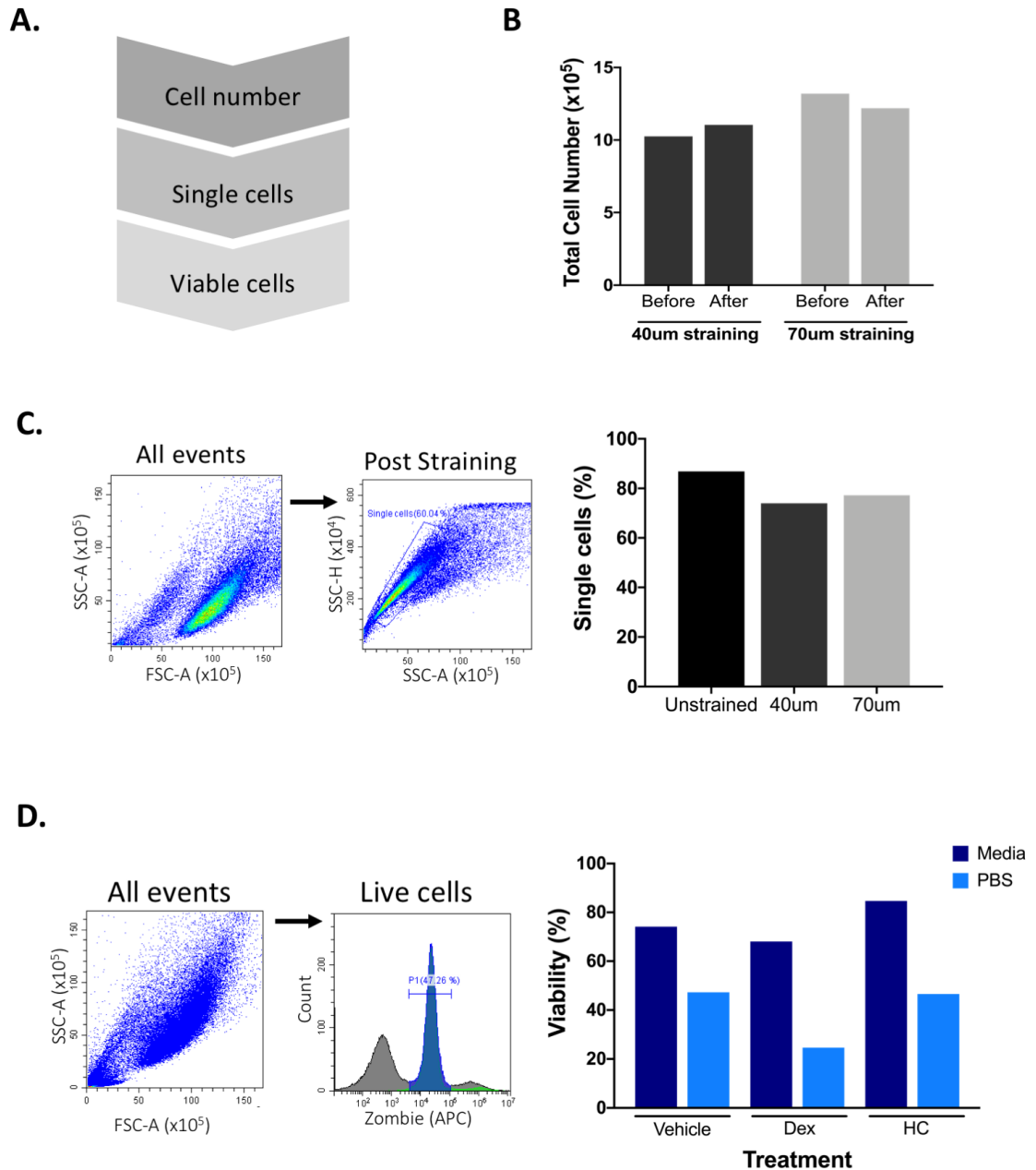
Figure 5.1: Cell number is not affected by cell straining, but cell viability is affected by incubation with PBS. Filtration method for the creation of a viable single cell suspension through the iCell8 platform. B**)** M059K cells were counted before and after straining through a 40µm filter, or a 70µm filter. C) Cells were analysed by flow cytometry and forward and side scatter were used to identify a population of single cells. The percentage of cells as single cells rather than doublets were quantified. D) M059K cells were treated for either 4 or 24 hours using a vehicle control, 100nM Dex, or 500nM HC. Cells were then incubated at room temperature in either culture media or PBS for 2 hours, then fixed. Cells were then stained with Zombie viability dye to quantify the relative number of live cells. HC – hydrocortisone; Dex – Dexamethasone.

Overall, our results raised concerns that sample storage in PBS during the preparation process could significantly affect viability. This was discussed with the core facility staff, and it was decided that samples would be stained in media, and only the final cell counting step prior to loading onto the machine in the core facility completed in PBS. As long term incubation in PBS was a concern, the core facility staff assured us that samples would be processed immediately to reduce sample storage time. As this would be the first experiment run on the iCell8 which was a new platform in the Manchester genomics facility, we were given the opportunity to complete a trial run. These samples would not be sequenced, but would be prepared as planned, then loaded onto the chip, and imaged to determine how many live, single cells could be detected.

5.2.2 Sample preparation for single cell RNA-seq

M059K cells were treated for 4 hours with a vehicle control, 50nM HC, 500nM HC or 100nM Dex. Cells were trypsinised, counted, then stained using propidium iodide and Hoescht. Cells were centrifuged and resuspended in PBS, and transferred to the Genomic Technologies Core Facility for a second cell count and then loading onto a chip for the iCell8. Optimally it is possible to generate 1,800 single viable cells, but realistically we expected that around 1,000 – 1,500 of the 5,184 wells should contain a single cell. For the 4 conditions, it was hoped that 200-250 cells could be sequenced for each condition.

In order to determine cell presence and viability, wells containing a single, Hoescht-positive, propidium iodide-negative cell are automatically identified using CellSelect software and taken forward for processing (Fig. 5.2A). This

enables sequencing only of wells containing live single cells, preventing potential doublets or dead cells from skewing the sequencing data. For the initial trial run, cells would be treated, stained and loaded onto a chip, then the number of viable candidate cells could be determined. Depending on the results, changes may then be made to the density of the cell suspension, or if capture rate was low, it may be necessary to reduce the number of conditions.

Following analysis of the results from the trial run, the chip contained over 250 viable candidate cells for the vehicle, 50nM and 500nM HC conditions, which was ideal for sequencing (Fig. 5.2B). For the 100nM Dex condition, however, we retained only 113 viable candidates. The previous work has indicated that Dex treatment is not capable of reducing cell viability, so we predicted that the difference in cell number must have been due to operational error during processing. As it was not possible to run another trial, we carried out the final run using the same protocol, but taking greater care over preparation of samples.

5.2.3 Single cell RNA-seq preparations enabled sequencing of 1000 cells

The single cell RNA-seq experiment was then carried out using the same protocol. All 4 treatment conditions resulted in over 250 wells containing viable candidates, and 250 cells were randomly selected from each condition for sequencing (Fig. 5.2C). Library preparation, quality control and bioinformatics analysis, as described below, were carried out by Syed Murtuza Baker at the University of Manchester, with input from myself and Laura Matthews regarding the biological interpretation of results, and what analysis would be appropriate given the biological context.

A.

| Vehicle | 50nM HC | 500nM HC | 100nM Dex |

○ Excluded
○ Suitable for sequencing

Multiple cells   Empty well   Live, single cell

B.

Trial summary

Sample	Wells	Empty Wells	Viable Candidates
Vehicle	1263	786	277
50nM HC	1272	790	269
500nM HC	1264	860	259
100nM Dex	1272	1101	113

C.

Run summary

Sample	Wells	Empty Wells	Viable Candidates
Vehicle	1263	668	325
50nM HC	1272	313	268
500nM HC	1264	341	294
100nM Dex	1272	493	342

Figure 5.2: A trial of single cell RNA-seq preparation showed an appropriate number of wells containing live, single cells. M059K cells were treated for 4 hours with a vehicle control, 50nM HC, 500nM HC, or 100nM Dex. Cells were stained using propidium iodide and Hoescht to identify live, single cells. Cells were dispensed onto an iCell8 chip, and imaged. Representative images for each condition are shown, alongside example images of positive and negative wells (A). Based on the PI and Hoescht staining, the number of wells containing viable candidates was then quantified for the trial (B), and also the sequencing run (C).

5.2.4 Quality control of single cell RNA-seq data

Initial quality control (QC) was carried out to remove any low quality cells from further analysis, as described below (Fig. 5.3). Initially, the total number of reads for each cell, known as the library size, were analysed. Cells in which RNA has not been efficiently converted to cDNA will contain a low number of reads, and should therefore be removed from further analysis. Any cells where the library size fell below the cut off (Fig. 5.3A, dashed line) would yield low quality data. These reads can be analysed further as an indicator of library quality. Uniquely mapped reads indicate reads which only map to a single gene of the reference genome, as a marker of the quality of the read. For most of the cells analysed, around 90% of the reads mapped to a single gene, indicating the data is of high quality (Fig. 5.3B).

Most of the cells sequenced also contained a high number of genes detected (Fig. 5.3C), suggesting that a large range of mRNA have been captured, rather than high volumes of the same transcript. This suggests that this data should more closely reflect the total transcriptome of the cell. Cells with few expressed genes again would reduce the quality of the data (Fig. 5.3C, dashed line).

Another commonly used method of determining the quality of the data is by analysing the percentage of genes which map to mitochondrial genes. The relative abundance of mitochondrial gene expression is variable between tissue types, but is also increased upon cellular stress (294). Therefore, if values are higher than expected, this may indicate that cell preparation has increased cellular stress prior to sequencing, or that the integrity of the cell was lost prior to lysis thus limiting the physiological relevance of the data. Within our data, our

cells showed around 10% of genes expressed to be mitochondrial in origin (Fig. 5.3D). Mitochondrial gene expression varies between 5% - 30% depending on the tissue, and previous data has indicated that mitochondrial contribution within normal brain tissue is 10 – 15% (295). These results again indicate the data is of good quality.
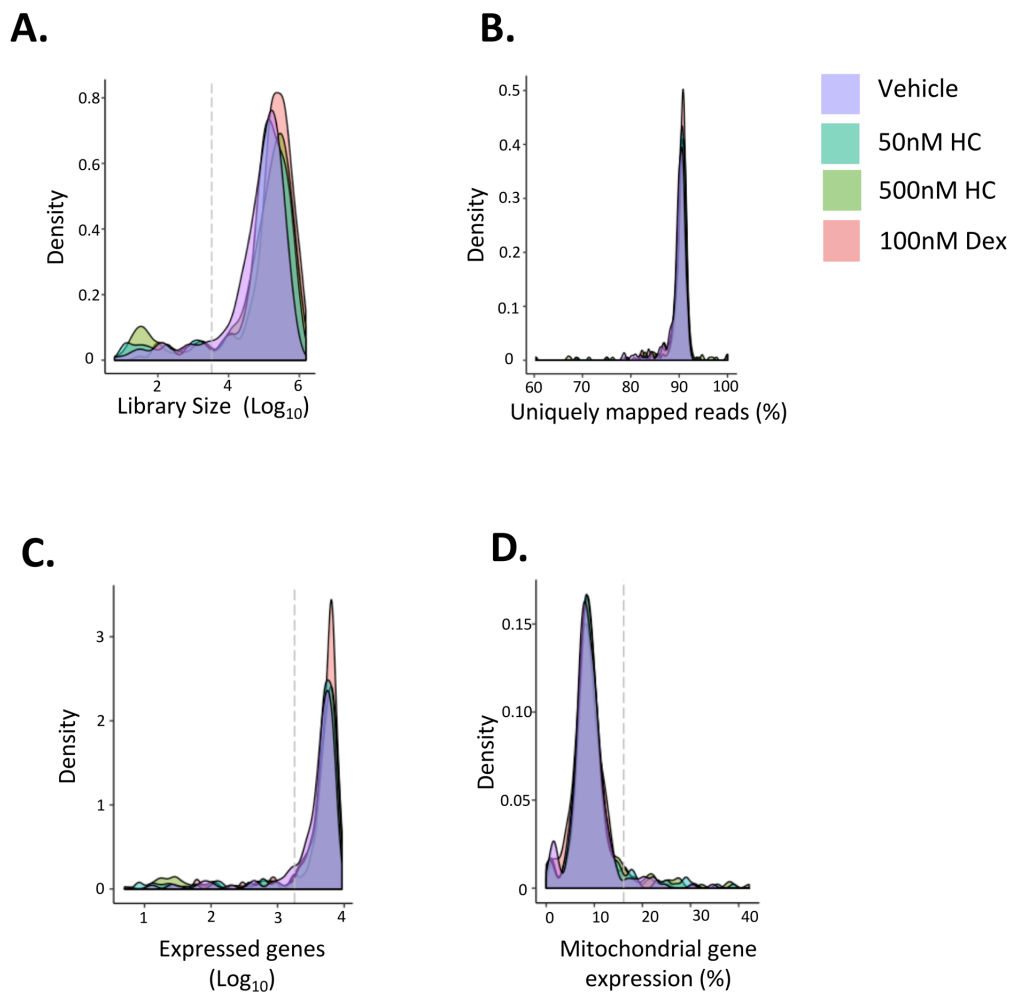
Figure 5.3: Single cell RNA-seq data indicated high quality reads. Following cell isolation and sequencing, a number of quality control matrices were analysed to confirm the quality of the reads from the sequencing. The number of total reads were quantified per cell (A). A high proportion of these reads correlated with a single gene (B), and most cells contain a high number of genes (C). The proportion of genes which were mitochondrial in origin were also quantified (D).

5.2.5 Filtering out low quality cells from further analysis

The library size, and the number of genes expressed, can both be used to estimate the quality of the reads, and can be used to filter out low quality cells from downstream analysis. Based on the distribution of cells using these features, Syed advised the following cutoffs. Cells which had a library size of below 3 Median Absolute Deviations (MAD) lower than the median log library size, or cells which expressed 3MAD fewer genes than the median number were filtered out. In short, this amounted to the removal of cells which had a library size below 3,321 reads, or fewer than 1,800 genes. As a further filtering mechanism, cells found to have over 16% mitochondrial gene expression were also removed. The number of cells filtered out from each treatment group are shown in Table 5.1. It is important to note that some cells were filtered out based on failing multiple thresholds. Overall, the number of cells filtered out within each treatment was consistent, with no major outliers. In addition, Gc are known to increase mitochondrial gene expression, however, there was no increase in cells filtered out based on high mitochondrial gene expression within Gc treated cells. The population before and after filtering are shown (Fig. 5.4 A – B).

Table 5.1: Cells removed from each treatment group based on filtering. Cells were filtered out from which fewer than 3,321 reads were gathered, in which fewer than 1,800 genes were detected, or in which over 16% of genes were mitochondrial in origin. The number of cells from each treatment group which failed these thresholds are shown, and the number of cells taken forward for further analysis.

Treatment	Removed by library size	Removed by total features	Removed by mitochondrial gene expression	Cells remaining
Vehicle	26	36	14	203
50nM HC	29	31	18	207
500nM HC	37	39	20	194
100nM HC	19	22	14	215

5.2.6 Library size and mitochondrial RNA proportion are unchanged across Gc treatment groups

The previous analysis had considered all 1,000 sequenced cells as a single group. Following filtering, we aimed to analyse the quality of data between the 4 treatment groups. The library size for each cell across all 4 conditions were plotted (Fig. 5.5A). There is a trend of decreasing library size across the treatment groups, however, this will be normalised during the following stages of analysis. The percentage of genes which were mitochondrial for each condition (Fig. 5.5B) were also quantified. There were no clear outliers, and the populations look similar for each condition. This suggested that Gc treatment had not induced stress within our cell populations, and thus could not account for any difference in response seen within our dataset.

A.

B.
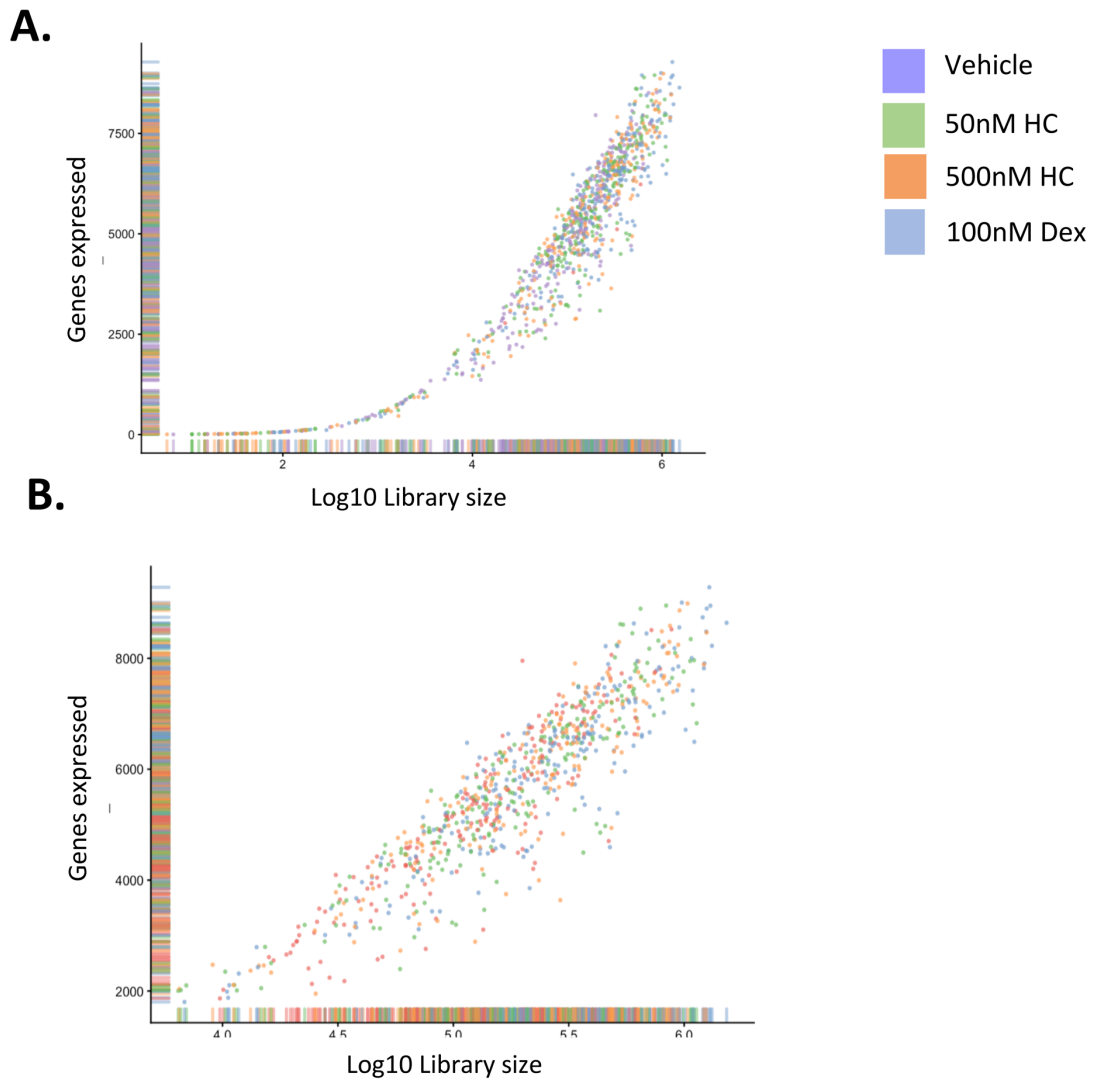
Figure 5.4: Low quality cells were filtered out from further analysis of single cell RNA-seq data. Low quality cells, were visualised by the number of genes expressed, and the total library size (A). Cells which expressed fewer than 1,800 genes, or which had a library size of 3,321 reads were filtered out, as these factors indicated low quality data from that cell. The distribution of cells which passed this quality control step are shown (B).

A.

B.
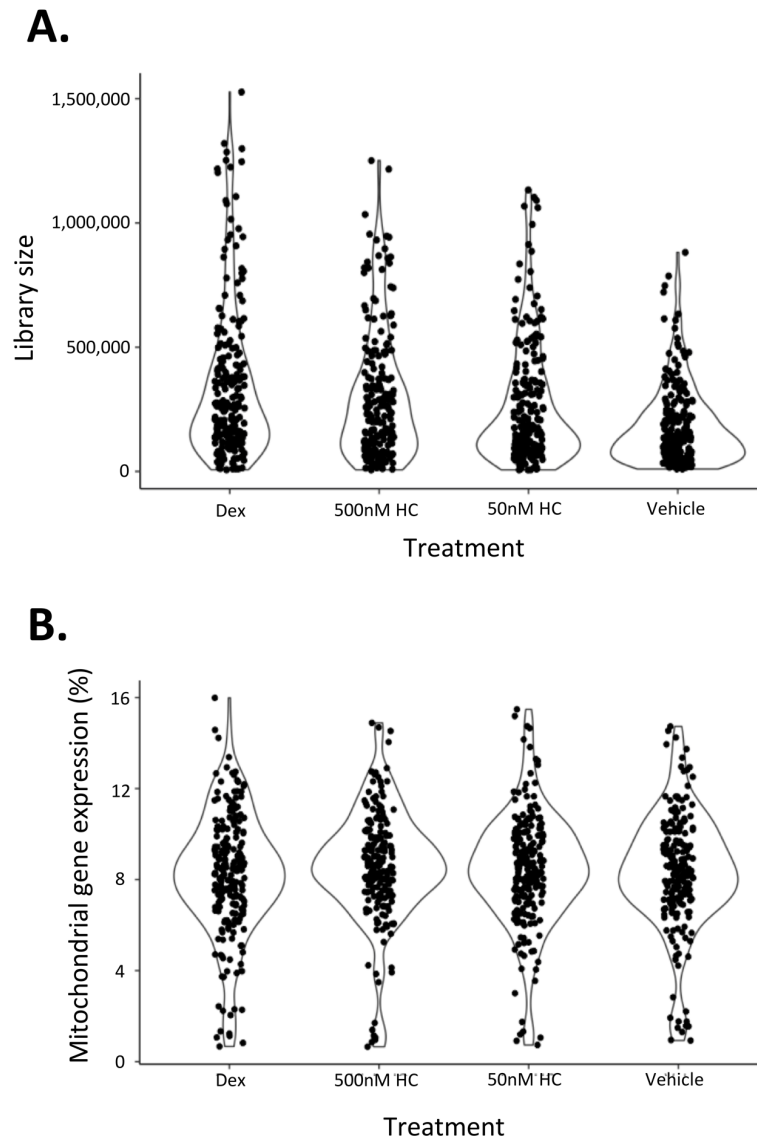
Figure 5.5: Gene analysis shows a consistent library size, and a similarly high proportion of mitochondrial genes, across the treatment groups. To confirm the quality of data for each cell, cells were divided into the 4 Gc treatment groups and plotted based on library size (A), and the percentage of mitochondrial gene expression (B).

Following filtering, of the 1,000 cells sequenced, data from 819 cells remained. The top 50 highly-expressed genes within the data were plotted (Fig. 5.6A). Many of these genes were mitochondrial in origin (indicated by the MT. prefix within gene name), or ribosomal proteins (indicated by the RP. prefix). High abundance of mitochondrial and ribosomal genes is expected, due to their relative abundance in within the transcriptome. Consistent with this GAPDH and ACTB, two well characterised high abundance, genes also featured in the top 50. Therefore, their high expression within this data indicated that the data reflects what is seen in a healthy cell population.

It was then necessary to determine the cut off to determine which genes were expressed. For single cell RNA-seq data, counts for genes are understandably low. It is therefore necessary to filter out genes with very low expression, as this could indicate poor capture efficiency, and lead to unreliable conclusions. It is important to consider, however, that genes which are downregulated by Gc treatment could show low expression in 3 of our 4 treatment groups (i.e. downregulated by Gc). This would skew results, and lead to the exclusion of many downregulated genes.

We then analysed how many genes were expressed (Fig. 5.6B). 43% of genes (4,312 genes) were expressed in at least 50% of cells. These included genes whose expression is required for basic cellular processes, such as so-called housekeeping genes, along with genes whose expression was upregulated by Gc treatment, which will be upregulated in 3 of 4 treatment groups. 72% of genes (7,914 genes) were expressed in at least 25% of cells. These may include genes which were downregulated by Gc addition.
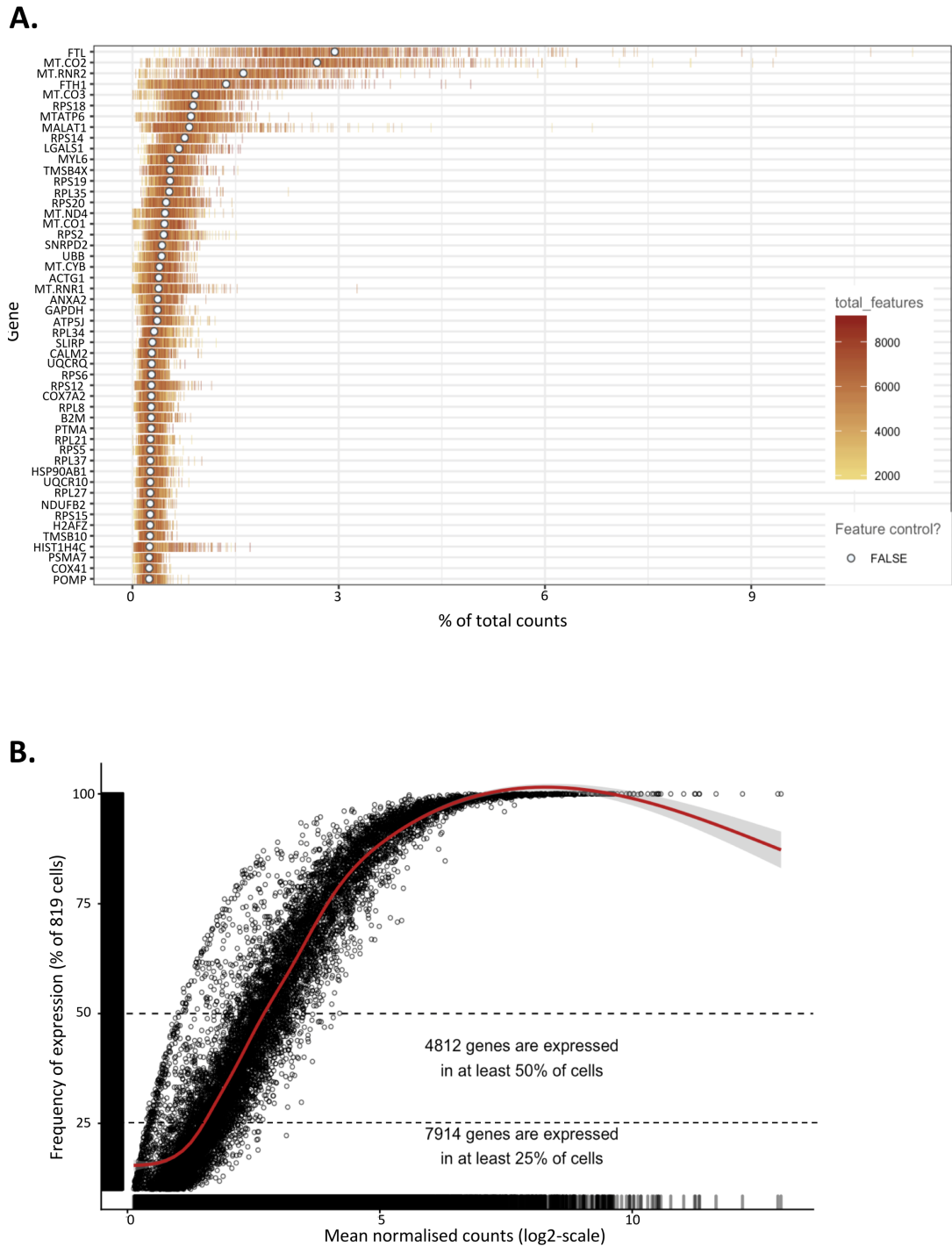
Figure 5.6: Gene analysis shows a high proportion of mitochondrial genes, and many genes with uniform expression across the population. A) The top 50 genes expressed across all 4 treatment groups within the single cell RNA-seq data were listed. Genes marked MT indicate mitochondrial genes, and RP indicated mRNA of ribosomal origin. B) The distribution of genes expressed within the population are shown to determine capture efficiency.

As we would be using scDE-seq2 to determine fold changes dependent on Gc treatment, a less stringent threshold for confirming expression of each gene was chosen. Initially, genes were removed which had a read count of less than 0.1 in less than 10% of cells. This filtering left 11,010 genes expressed in over 10% of cells.

5.2.7 Cell cycle phase of cells correlates with previous data

One of the possible factors which may contribute to heterogeneity in the GR response could be cell cycle phase. To investigate this, it was necessary to identify the position in the cell cycle of each individual cell, and determine if there were any differences between treatment groups. A previously described method was used (296), by which expression of cell phase-specific genes are used to estimate the phase of each cell within the dataset (Fig. 5.7A). This method utilises pairs of markers, one for G1M and one for G2. The score of each pair indicates whether the cell falls into one phase or the other, and by combining the results of multiple pairs, it is possible to build an effective marker profile and score for each individual cell. If the score for either G1M or G2 is above 0.5, the cell is considered to fall into this cycle phase. If the score is below 0.5 for both, the cell is clustered into S phase. This method is known to effectively sort G1M from G2 cells, however, S phase identification relies on, effectively, the absence of G1 and G2 markers. The phase of each cell was then quantified by treatment group (Fig. 5.7B). As discussed in Chapter 4, previous work has analysed the cell cycle phase of M059K cells at 24 and 48 hours following Gc treatment using propidium iodide staining to stain DNA content. Cells were analysed by flow cytometry, and Modfit software was used to quantify proportions of cells in each cell cycle phase.

A.

B.

	Total	G1 (%)	S (%)	G2/M (%)
Vehicle	203	166 (81.7)	13 (6.4)	24 (11.8)
50nM HC	207	165 (79.7)	11 (5.3)	31 (14.9)
500nM HC	194	168 (86.6)	10 (5.2)	16 (8.2)
100nM Dex	215	181 (84.2)	10 (4.7)	24 (11.2)

C.
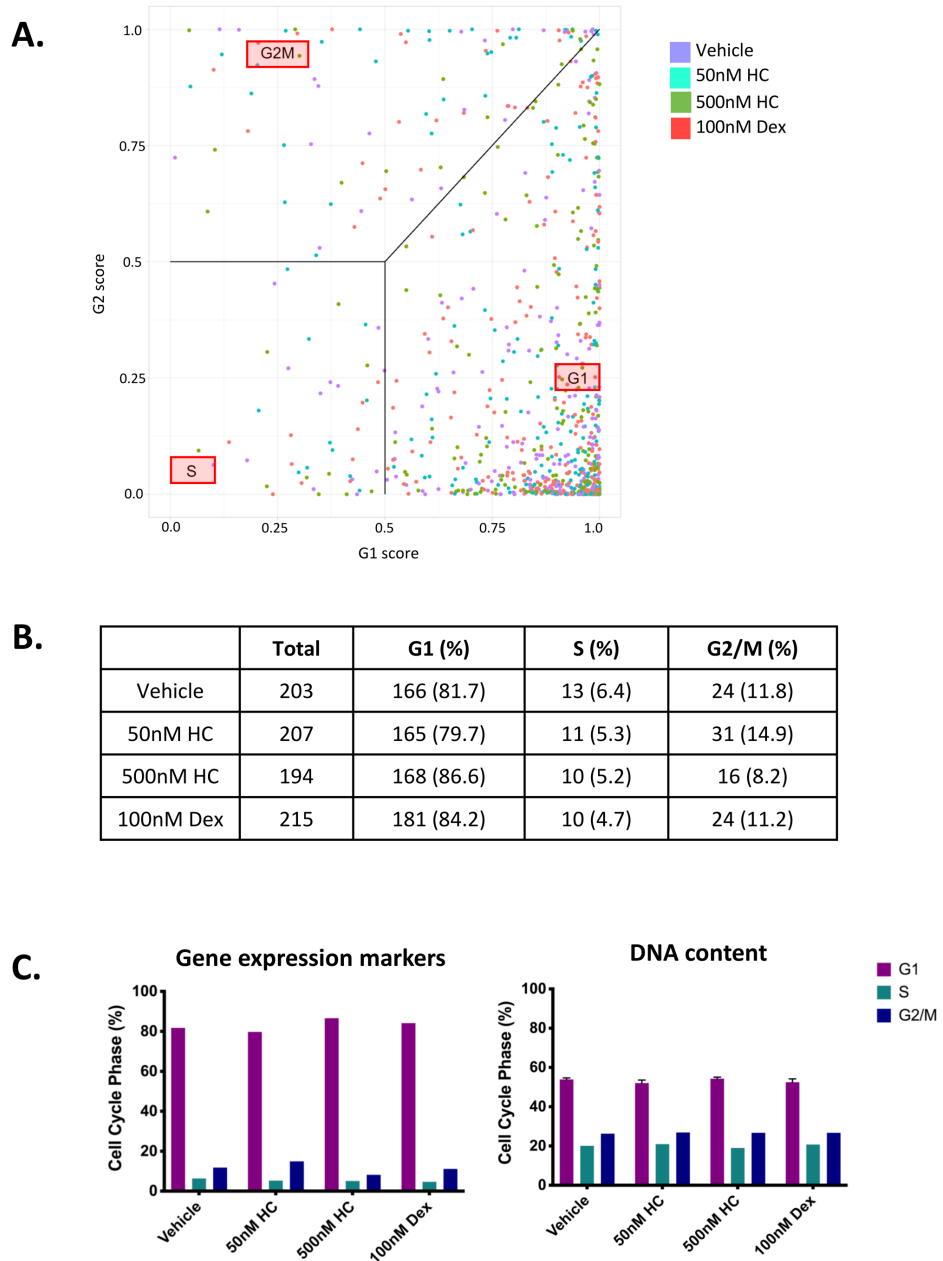
Figure 5.7: Cell cycle phase is unchanged with Gc treatment in scRNA-seq data, and correlates with previous data. A) Cell cycle phase was analysed in single cells through the expression of G1 and G2-specific markers. B) The number of cells within each cell cycle phase is shown for each Gc treatment. C) The proportion of cells in each phase was compared between the single cell RNA-seq data and propidium iodide staining previously shown in Figure 4.11

Cell cycle phase estimated through the bioinformatics analysis was compared with the cell cycle proportions seen at 24 hours following Gc treatment (Fig. 5.7C). The single cell RNA-seq did not show any difference in cell cycle phase following Gc treatment. This correlated with what was seen within the propidium iodide experiments, which also demonstrated that Gc treatment did not lead to cell cycle arrest, and that a representative population of cells had been analysed.

The main aim of classifying the cell cycle phase was to determine whether this was a major driver for heterogeneity within populations, and whether cell cycle phase was a determinant of the Gc response. Principal component analysis (PCA) was therefore used to visualise variation of the cell population (Fig. 5.8A). PCA analysis entails identifying sets of genes which contribute to the variation between different cells. These genes can then be combined into a larger gene subset, known as a principal component. The subset of genes which contribute the most to the variation in the population are assigned as PC1. PC2 is then assigned as the gene subset which has the second largest contribution to the variance of the population, and so on. PCA has been used commonly within single cell RNA-seq analysis as a tool to simplify the visualisation of large amounts of data, in order to make patterns of data more obvious, for instance in the study of cell lineage (195, 196, 297).
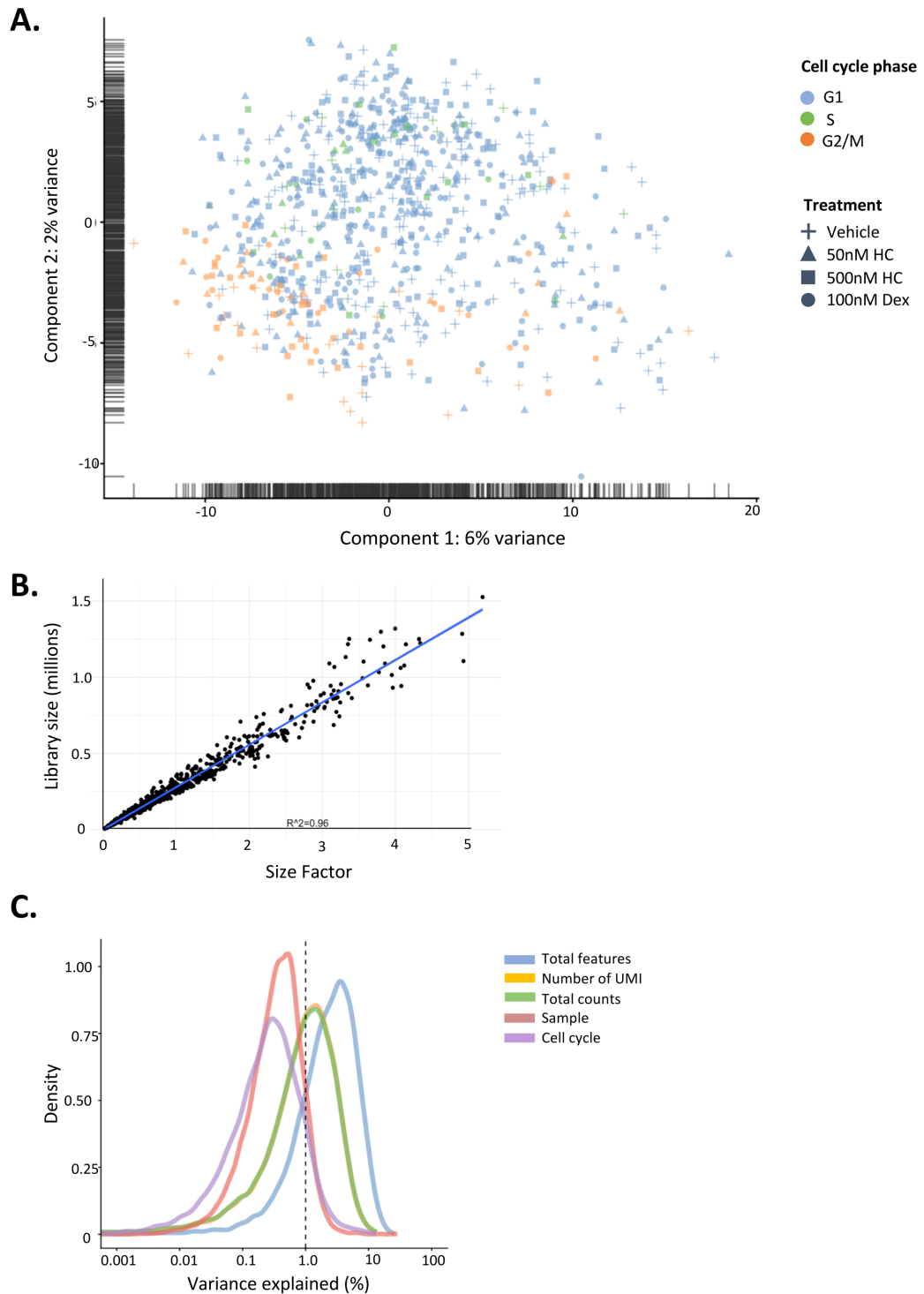
Figure 5.8: Cell cycle does not contribute to the variance between cells within single cell RNA-seq data. A) Principal component analysis shows slight clustering of cells according to cell cycle phase, however, this does not correlate with Gc treatment. B) Cells show a strong correlation between the computed size factor and the library size for each cell. C) The contribution of total features, UMI, total counts, sample type and cell cycle phase to the overall variance of the population was measured.

Cells were clustered, then visualised according to cell cycle phase (different colours) and Gc treatment (different shapes). There is some clustering of cells according to cell cycle phase, as seen by the clustering of G1(blue), and G2/M (orange) cells, with S phase cells (green) falling more broadly throughout G1 and G2/M populations (Fig. 5.8A). This suggested that cell cycle phase may contribute to variance within the population, however, there does not appear to be correlation between cell cycle phase and Gc treatment. For instance, vehicle treated cells (crosses), are broadly dispersed throughout the cell cycle phase clusters.

5.2.8 Normalisation to remove read depth bias

Previous research using single cell data has identified that differences in sequencing depth and the efficiency of library preparation within individual cells may lead to false results and inaccurate differential expression data (298). For instance, if one cell has twice the number of total transcripts than another, a gene may be considered differentially expressed, even if the relative number of transcripts compared with library size is the same. Therefore, it is necessary to normalise data from each cell and ensure the library size was as equal as possible between cells (212). To do this, a size factor is computed for each cell and applied. This factor is produced by assuming that differences in expression of a gene between cells are due to technical differences, rather than biological differences. Unfortunately, due to the low amount of starting material, scRNA-seq data contains many zero counts, which can reduce the accuracy of the size factor for each cell. Therefore, the size factor is computed by pooling data from across the population, and computing a mean size factor (299). This can then be deconvolved to produce an individual size factor for each cell.

Once a size factor has been computed for each cell, it is then possible to plot this size factor against the total number of reads, or library size, for each individual cell (Fig. 5.8B). If a cell has a high number of genes differentially expressed compared with the overall average across the population, the library size will not correlate with the size factor, and would sit as an outlier. Instead, we see a strong correlation between the library size and size factor, indicating that the cells are, overall, similar in expression for the majority of genes. This would suggest that the library size is the main driver of differences in expression. Through applying the size factor-based normalisation, we aim to limit the effect of the library size on differential expression.

As a final QC control, different features within the data were analysed, and their contribution to the heterogeneity within the data was quantified (Fig. 4.8C). Firstly, cell cycle phase does not contribute largely to variance within the data. The factor which appears to affect variance the most is the total features. This indicates that even after read depth normalisation, simply the number of genes detected within a cell contributed to the variance between cells. This is concerning, as this could enable false positives, wherein differences in the library sizes between cells could result in variability within expression, and therefore result in heterogeneity as an artefact of the system. Both number of uniquely mapped identifiers (UMI) and total counts also appear to contribute to the variance, however this also confirms that cell cycle does not contribute to the variance. By using the bulk RNA-sequencing data, we can limit analysis to genes which are variable due to Gc treatment.

5.2.9 The GR response leads to a distinct shift in phenotype

Before considering individual cells, it was first necessary to determine how large an effect Gc treatment may have on the phenotype of the population. Pooling all treatment groups together, the genes with the largest amount of variation between individual cells, known as the highly variable genes (HVG) were plotted (Fig. 5.9A). The top 15 HVG are shown. Of the 15 highest HVG genes, 8 genes (*PER1, FKBP5, CEBPD, DUSP1, GILZ, BIRC3, SNAI2* and *ANKRD1*) were also present in the top 25 most strongly regulated Gc responsive genes from the bulk RNA-seq data discussed in the previous chapter (indicated in bold in Fig. 5.9A).

While treatment group did not correlate with a shift in PCA, when the entire genome was considered, we next examined if using only the Gc responsive genes could distinguish treatment groups. Firstly, differences in the overall transcriptome of individual cells within each condition were analysed using PCA (Fig. 5.9B). scDE-seq2 was used to define differentially expressed genes between vehicle control and any of the three other treatment groups. Using this smaller gene set, after plotting PC1 and PC2, clustering of cells by condition can be observed. Interestingly, the clusters appear to move in a dose dependent manner, observed as a shift from left to right, from vehicle, to 50nM HC, followed by 500nM HC, and finally by 100nM Dex. This correlates with how the transcriptome would be expected to change, as the bulk RNA-seq showed the largest number of DE genes were seen with Dex treatment, compared with the vehicle control.
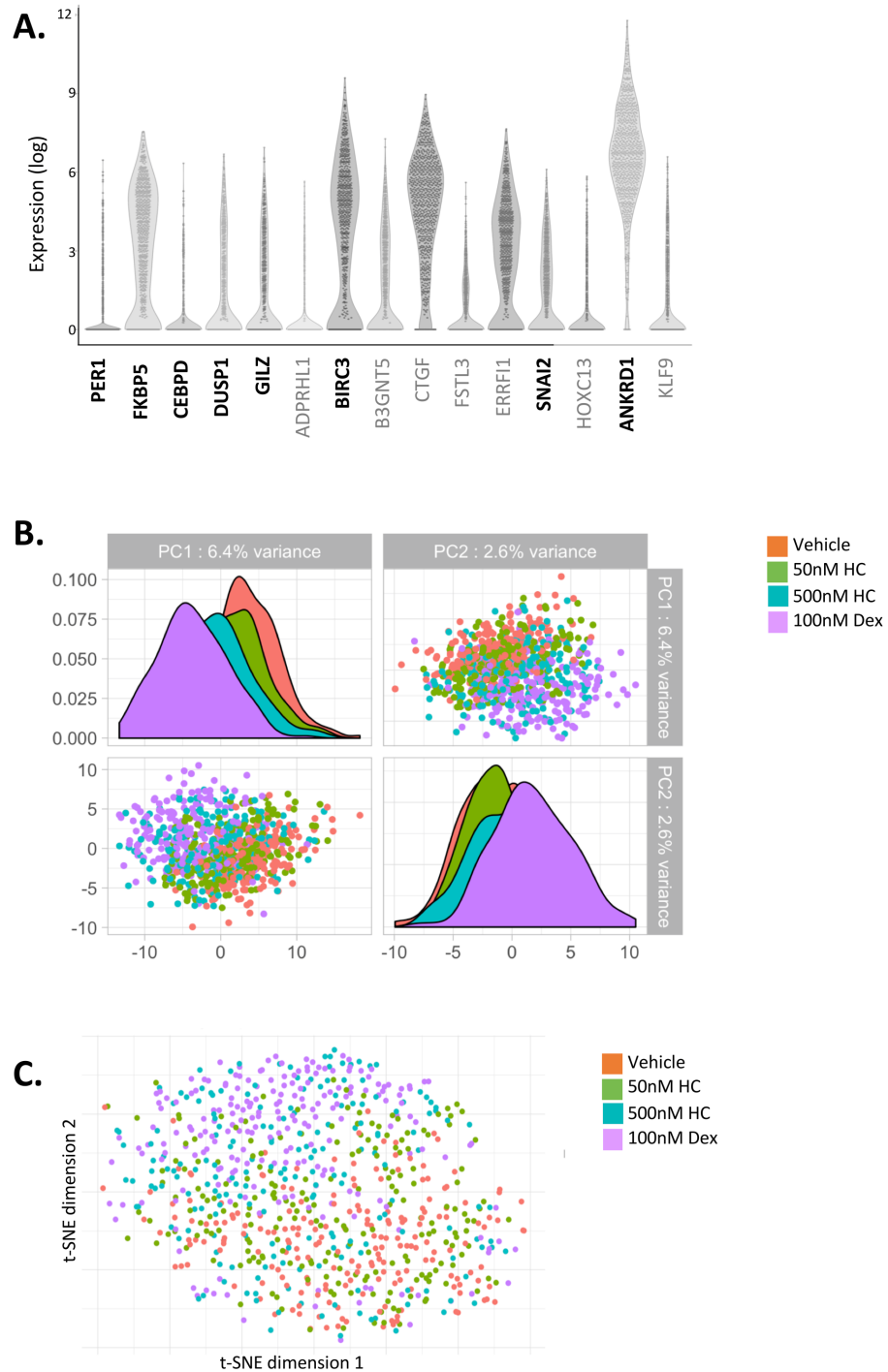
Figure 5.9: Gc treatment has a profound impact on phenotype within single cell RNA-seq. A) The top 15 most highly variable genes across all 4 Gc treatment conditions. Genes identified as DE in bulk RNA-seq analysis in response to Gc are indicated in bold. B) Cells clustered by the 4 largest principal component analyses show clustering according to Gc treatment. C) t-SNE analysis shows distinct clustering of cells according to Gc treatment.

PCA is a useful tool in plotting large differences within the population, however, it is often limited to large, very different clusters. Therefore, other mechanisms, may be used to visualise clustering within transcriptomic data. t-distributed stochastic neighbourhood embedding (t-SNE) is a commonly used mechanism of visualisation of single cell RNA-seq data. It allows for more subtle clustering of cells by pairing cells with their closest neighbours according to their transcriptional profiles (300, 301). When the data is analysed through t-SNE, the cells cluster more clearly according to treatment group (Fig. 5.9C). Once again, the 2 most distinct clusters comprise the vehicle and Dex treated cells, with HC-treated cells falling between these two extremes. These results suggest that even at a single cell level, Gc addition cause a robust change in transcriptome.

5.2.10   Using bulk RNA-seq to guide scRNA-seq analysis

Lists of DE genes for each Gc condition were created, relative to the vehicle control (Fig. 5.10A). A high degree of overlap between conditions was seen, but a higher number of genes which appear to be specific to each individual condition were observed in the scRNA-seq data, compared with those seen in the bulk RNA-seq. This is often seen within scRNA-seq data, as the data can be viewed as 200 replicates for each condition, compared with the triplicates run for bulk RNA-seq. This makes scRNA-seq on one hand more sensitive to small changes, but also more likely to identify noise as false positives (302, 303).

As the next stage would be to identify robust genes to develop a high throughput RNA FiSH assay, it was decided to only consider DE genes that appeared in both the single cell RNA-seq and bulk RNA-seq (Fig. 5.10B). There is an overlap of 99 genes between both datasets. This population contains many of the previously

analysed Gc-regulated genes, including *FKBP5, DUSP1, GILZ, PER1, CEBPB* and *CEBPD*. It is important to note that 76 Gc regulated DE genes from the bulk gene list were not present within the single cell data. VCAM, which is a well characterised Gc target gene provides a good example. VCAM has very low baseline expression, and is strongly downregulated by Gc which meant this gene was not included as an expressed gene during the early QC process.

Enrichr analysis of the pathways predicted to be controlled by the 99 Gc regulated genes showed inflammatory related terms, such as AP-1 transcription factor network, IL6 signalling, and response to cytokines. Direct p53 effectors and transcriptional misregulation in cancer was also identified (Fig. 5.10C). Finally, the Elsevier Pathway identified a signature entitled 'proteins in glioma'. These genes were then analysed using String to identify any possible protein-protein interactions between these targets and GR, labelled NR3C1 (Fig. 5.10C).
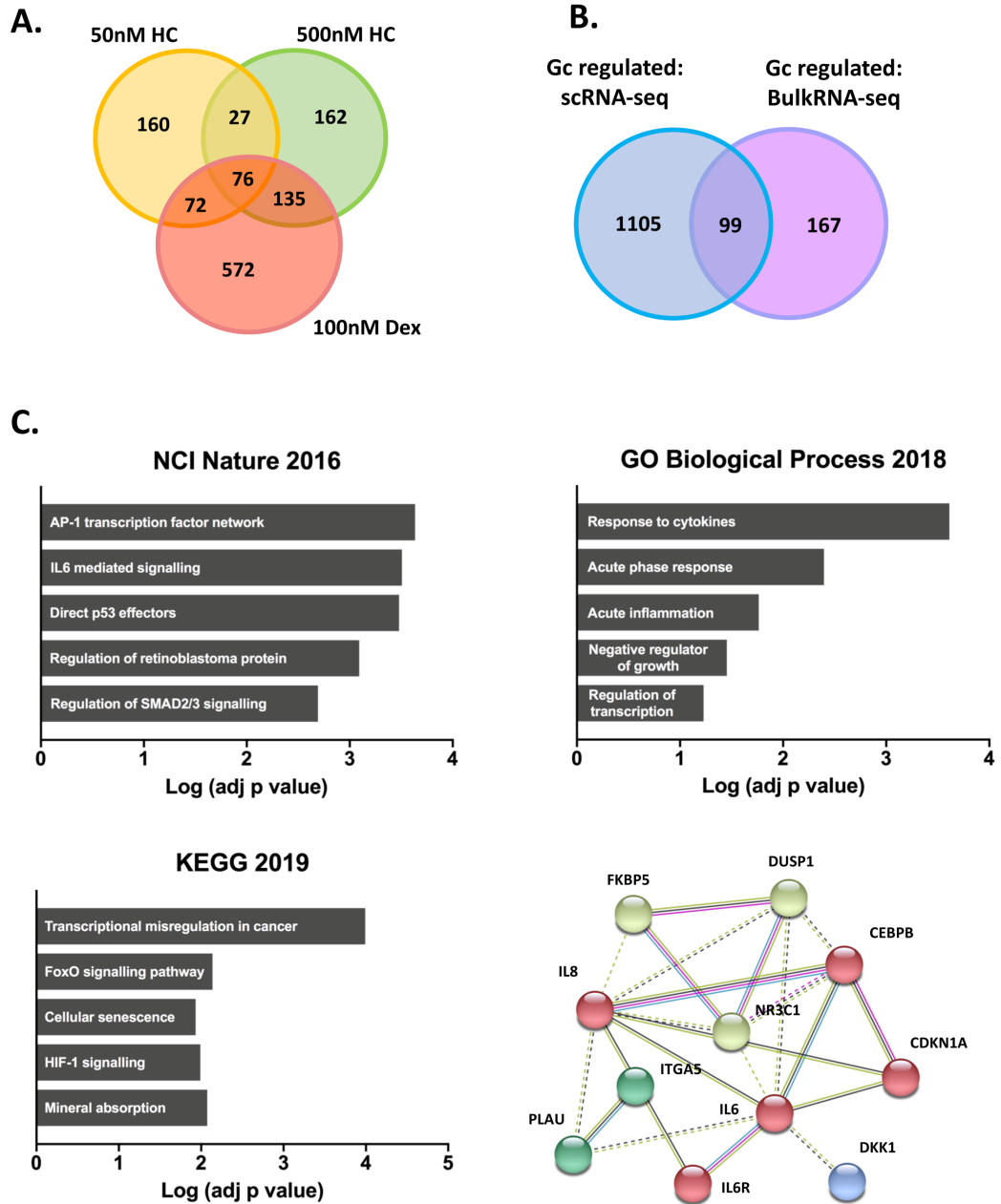
Figure 5.10: Overlaying single cell RNA-seq and bulk RNA-seq identifies a robust population of differentially expressed genes. A) Genes differentially expressed within the single cell RNA-seq between the vehicle control, and 50nM HC, 500nM HC and 100nM Dex. B) DE genes common between singe cell RNA-seq and bulk RNA-seq. Shown are the Enrichr predicted pathways for genes common to both datasets, and a string network showing protein interactions between proteins identified in glioma from the Elsevier Pathways collection, and GR (labelled NR3C1).

5.2.11   GR expression is variable

Our first gene of interest for further analysis is GR itself, gene name *NR3C1.* For simplification, *NR3C1* is referred to herein as *GR. GR* transcript expression is shown for all 4 conditions as a violin plot (Fig. 5.11A), and as a density plot (Fig. 5.11B). There is no significant difference in expression between conditions, which mirrors findings from the bulk sequencing. However, there is significant variability in *GR* expression within each sample. Differences in capture efficiency between cells may explain this variation, and so expression of *GR* was compared against two highly expressed, commonly used housekeeping genes, *GAPDH* and *ACTB* (Fig. 5.11C & D). It is clear that the variability of GR, plotted on the Y axis, has no correlation with expression of either *GAPDH* or *ACTB.* Lack of correlation between expression of either of the two housekeeping genes and *GR*, suggests that capture efficiency, or the total volume of RNA from each cell, cannot account for *GR* variability. Instead this suggests that biological factors must be responsible for the variation in *GR* expression. Immunofluorescent staining shows that GR protein expression and translocation show a high level of variability even within a clonal cell population (Fig. 5.12). Importantly, variation in *GR* expression may be a factor which determines the heterogeneity in expression of genes controlled by *GR* in response to Gc.
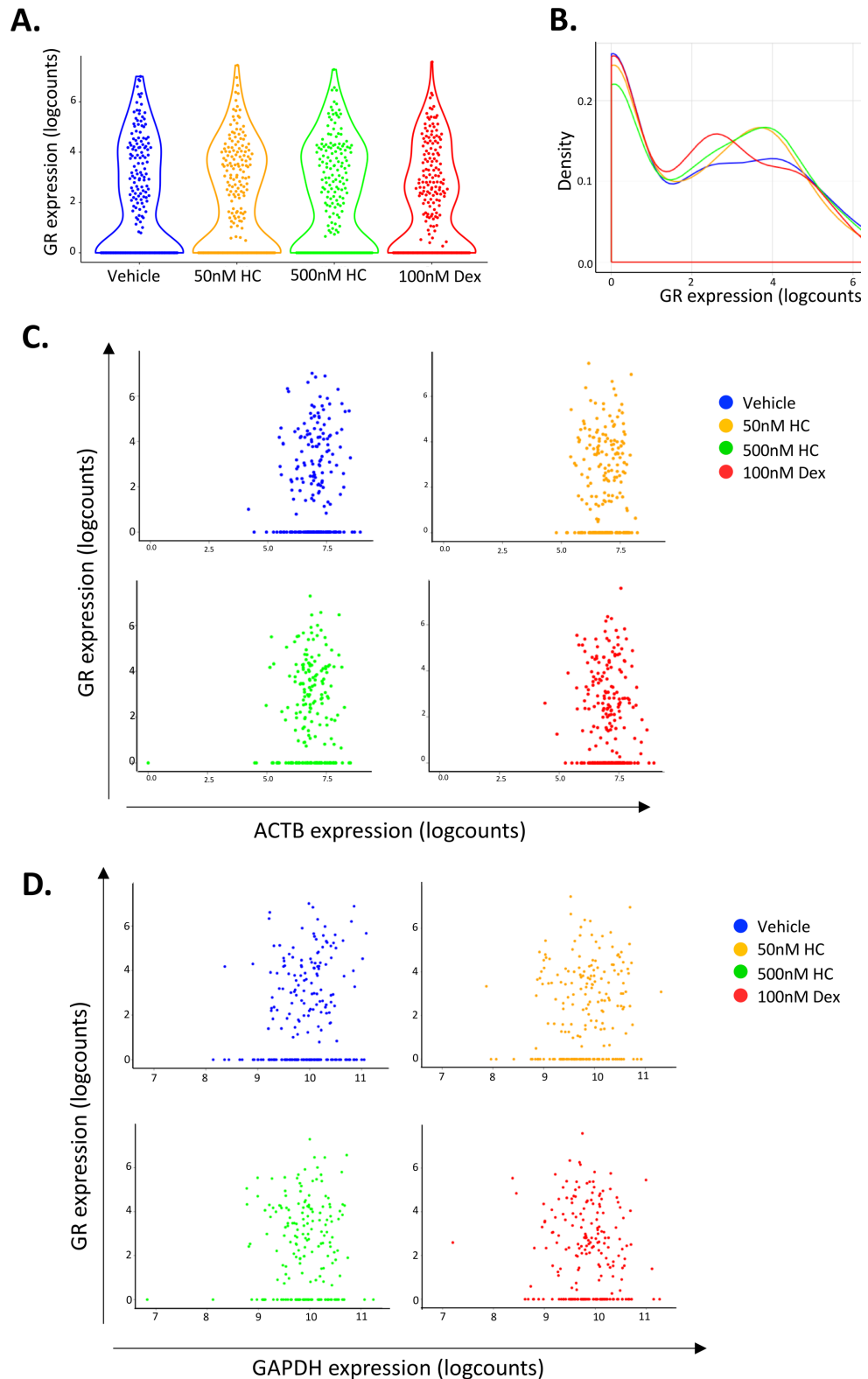
Figure 5.11: GR mRNA expression is variable between cells, but is unchanged following Gc treatment. A) Violin plot showing *GR* expression (log counts) across Gc treatment groups. Each individual dot represents expression within an individual cell. (B) Data is also represented as density plots, which enables better visualisation of cells lacking GR expression. *GR* expression was plotted against expression of *ACTB* (C), and *GAPDH* (D). Colour indicate treatment group.
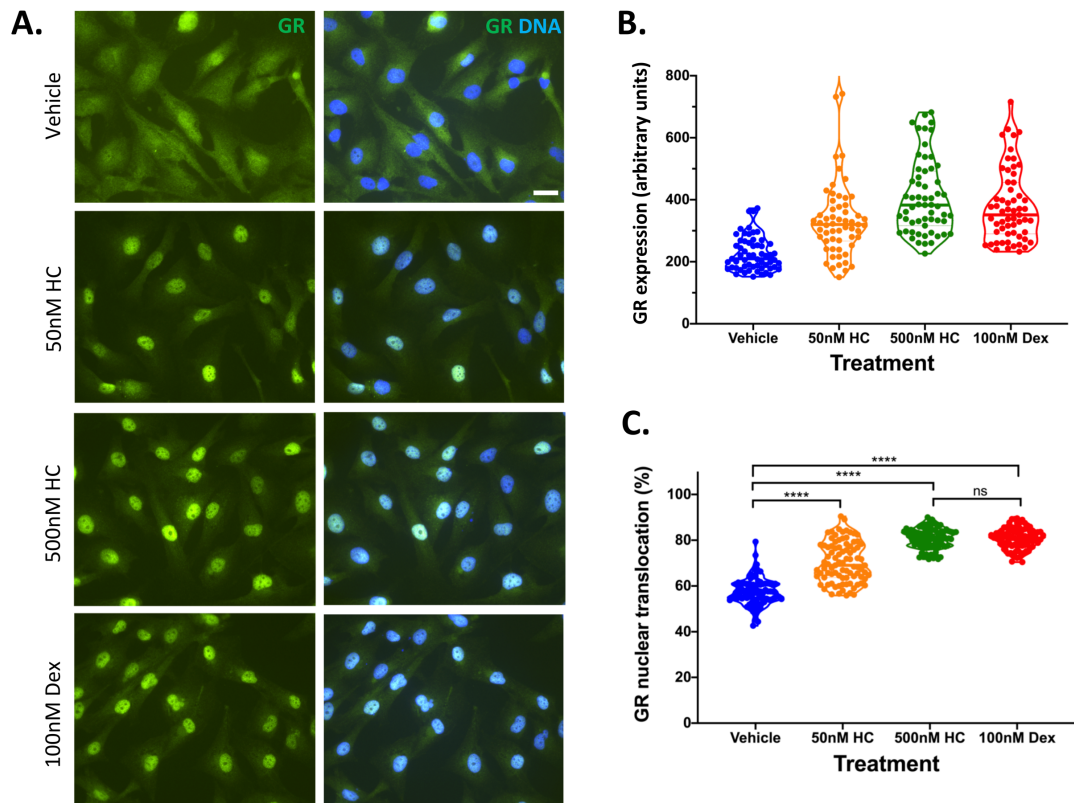
Figure 5.12: GR translocation is heterogenous across each condition. M059K cells were treated for 1 hour with a vehicle control, 50nM HC, 500nM HC or 100nM Dex. Cells were fixed and stained for GR (A). Images were analysed using ImageJ and GR expression within individual cells was quantified as the average signal intensity (mean grey value) within individual cells (B). Hoescht was used to demarcate the nucleus, and phalloidin for cytoplasmic area. The signal intensity in the nucleus, compared with the cytoplasm, was used to calculate the percentage of GR found within the nucleus (C). Scale bar denotes 20μm. Results shown are the mean of 3 independent experiments. A one-way ANOVA was carried out with a Dunn's multiple comparisons test. **** = $p \leq 0.0001$.

5.2.12 Expression of GR target genes is also highly variable

Next, it was explored how treatments influence the expression of Gc responsive target genes. A panel of genes where expression increased in a dose dependent manner following Gc addition is shown in Fig. 5.13. Some genes, such as *GILZ* showed a dose dependent increase in the maximum response as the dose and affinity of ligand increased. Alternatively, for other genes, such as *DUSP1* and *FKBP5,* the maximum response was unchanged, but more cells appeared to cluster toward the maximum response. Interestingly, across all genes, and all treatments, there was a high degree of variability. For *DUSP1,* for instance, there were some cells within the vehicle treated samples with the maximum expression level, whilst even with Dex treatment, there were still cells with no detectable expression of the analysed genes. Therefore, there must be cell intrinsic factors which determine the size of the response within individual cells within a population.

A similar picture emerged when examining downregulated genes (Fig. 5.14). *IL6* and *E2F7* both show a stepwise reduction in expression following Gc addition. While *IL6* was still expressed to the highest level in some cells, addition of Gc narrowed this population. For *E2F7* however, the entire population remained constant but shifted downward. Further work is needed to understand what factors could determine the strength of the Gc response in individual cells, and also how the population as a whole changes with Gc.
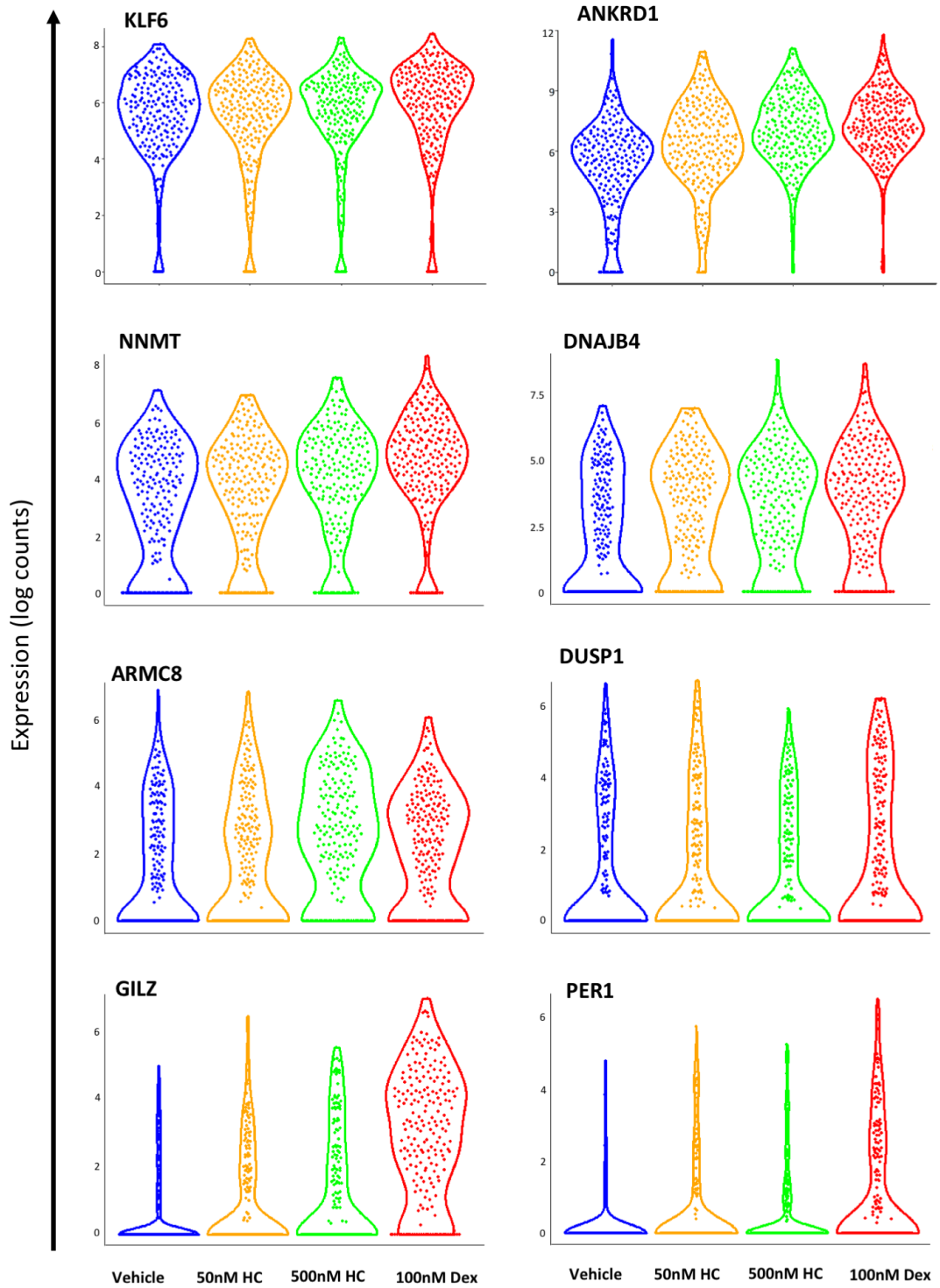
Figure 5.13: GR-dependent genes upregulated by Gc addition show a population-level increase in expression following Gc treatment, with high variability between cells. Violin plots to show expression of 8 genes significantly upregulated following Gc treatment, as determined by both bulk and single cell RNA-seq. Each individual dot represents a single cell.
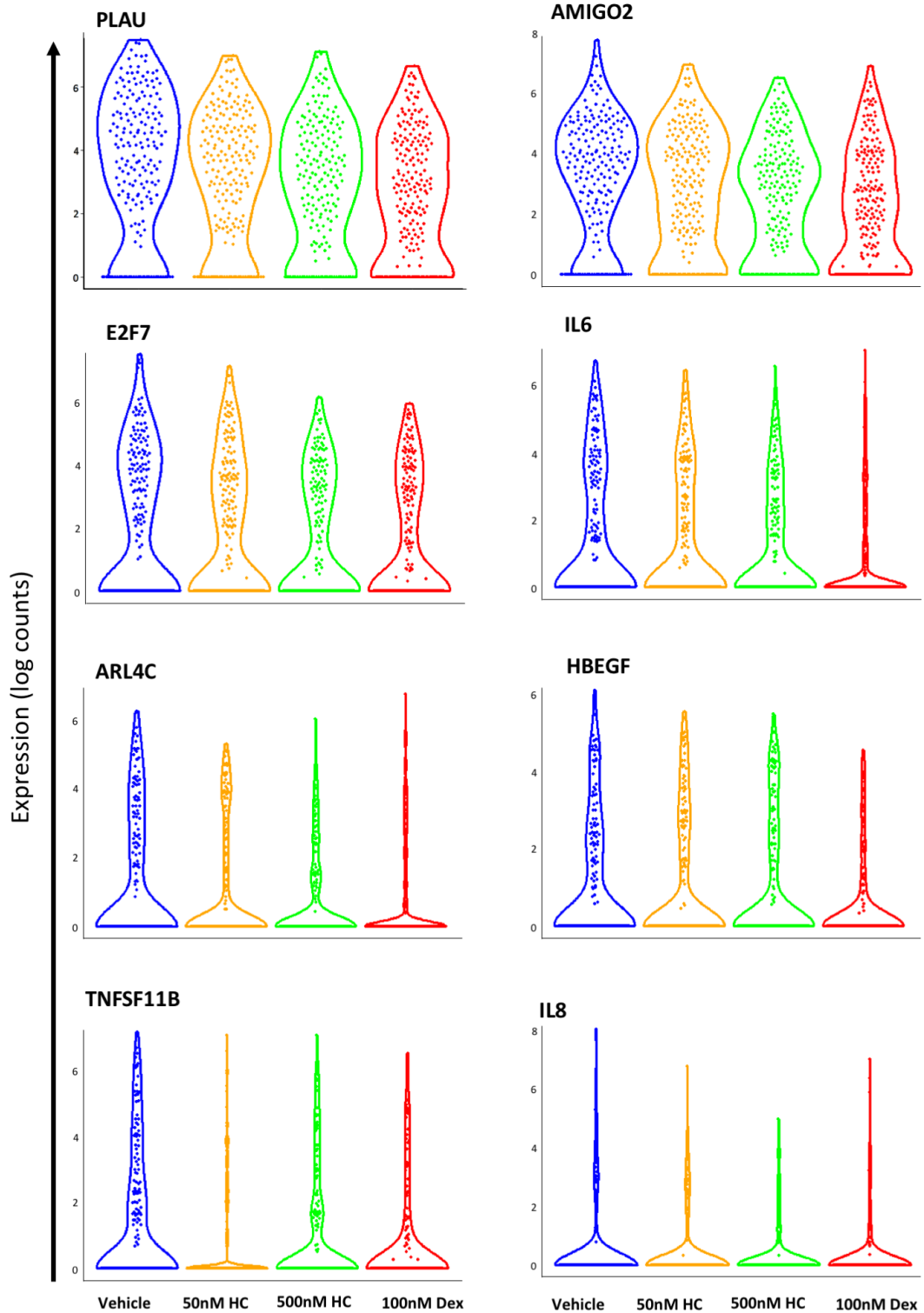
Figure 5.14: GR-dependent genes downregulated by Gc addition show a population-level decrease in expression following Gc treatment, with high variability between cells. Violin plots to show expression of 8 genes significantly downregulated following Gc treatment, as determined by both bulk and single cell RNA-seq. Each individual dot represents a single cell.

5.2.13 Gene expression patterns differ according to individual genes

We looked more closely at the expression pattern of each gene between individual cells within each condition. We initially predicted that we may see genes falling into two distinct populations – which could be explained by binary or rheostat-like responses.

To visualise the response more clearly, we plotted the expression data for each gene as density plots, rather than violin plots. This allows us to see distinct clusters of cells more clearly, as number of cells vs levels of gene expression. The x-axis shows the strength of the response, whilst the y-axis represents the relative proportion of cells responding at that level. For some genes, such as *ANKRD1*, which is upregulated by Gc, expression fits closely with what we would expect from a rheostat response (Fig. 5.15A). There is a single peak which simply shifts to the right in response to Gc, suggesting all of the cells respond to some degree. For some genes, such as *DNAJB4,* which is also upregulated by Gc, expression fits closely with what we expected to see from a binary response (Fig. 5.15A). Cells separate into a population of low expressing cells (left peak), and a second population of high expression cells (right peak). There are two distinct populations within the vehicle treated cells (blue line). Both doses of HC (yellow and green lines) increase the number of cells present in the higher expression population. This is even more prominent in Dex treated cells (red line). Expression of *GILZ* seems to be intermediate (Fig. 5.15A). There is a clear, narrow left peak of low expressing cells in the vehicle treated group. This is largely lost upon Gc treatment, but the higher expression peak is very broad, and right shifts with increasing dose or affinity.
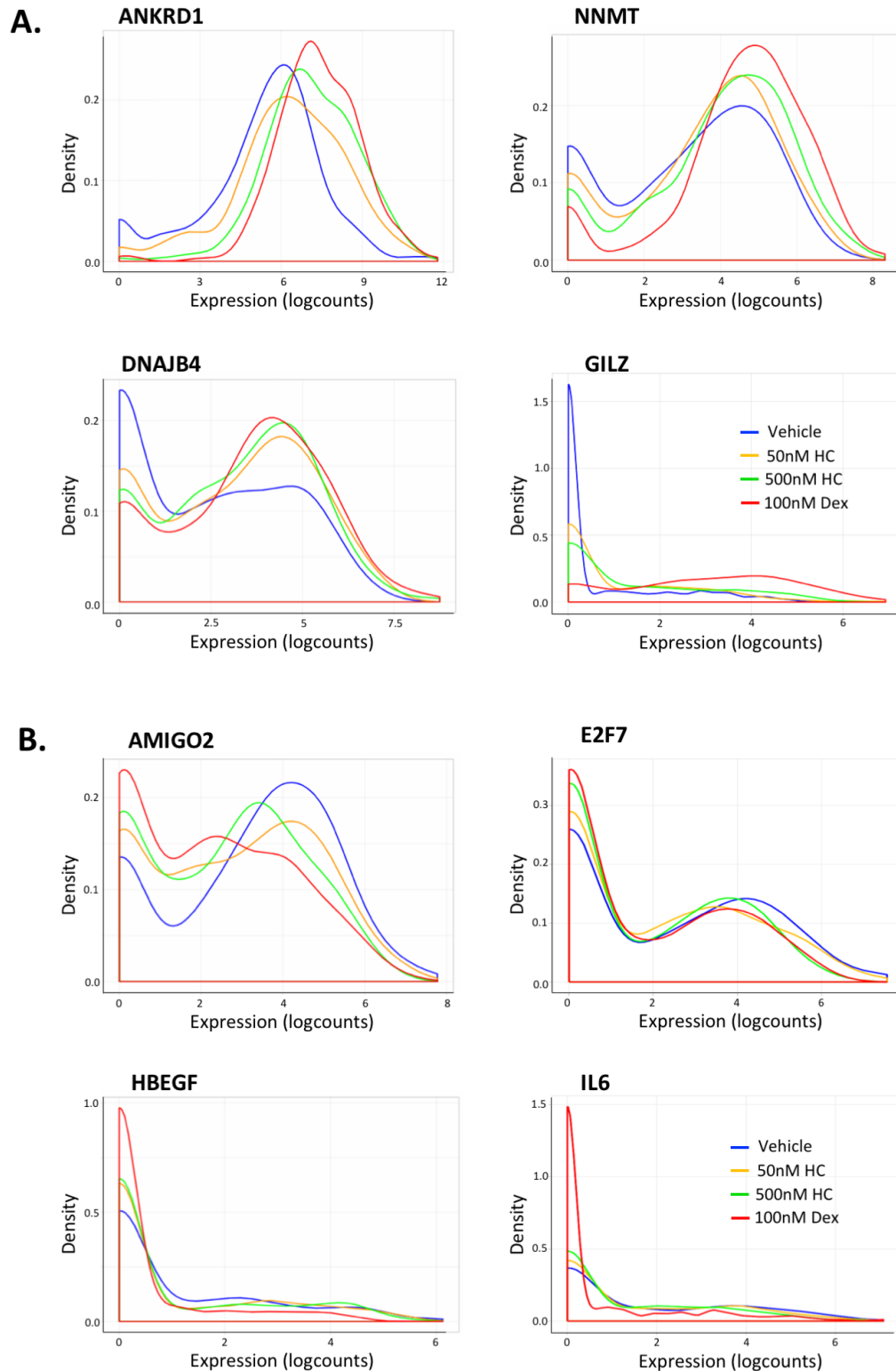
Figure 5.15: Single cell RNA-seq shows expression of GR target genes follow a binary or rheostat-type response following Gc treatment. Examples of upregulated (A) and downregulated (B) GR target genes, with expression shown as density plots. Expression is shown for each Gc treatment. Cells show a population of low-expressing cells (first peak), and a population of highly expressing cells (second peak). Differences in population expression are driven by changes in the number of cells in each peak.

This complex picture is also replicated in genes downregulated by Gc (Fig. 5.15B). *E2F7* for example shows binary expression, as evidenced by two cell peaks. However in this instance, Dex treatment reduces the number of high expressing cells, and increases the proportion of low expressing cells (Fig. 5.15B). The profile for *IL6*, is more comparable with *GILZ* expression, but inverted. Vehicle treated cells have a very broad range of IL6 expression, which left shifts in response to HC. Dex treatment pushes expression towards zero which is evidence as a large left peak (Fig. 5.15B).

These results suggest that both binary and graded responses can be seen within the Gc response. Mathematical modelling has focused on modelling either one type of response or the other, but this data instead illustrates a mixture of the two responses, depending on the gene in question.

It was noted that genes with lower expression tended to divide into two clear peaks. As the scRNA-seq results in relatively low read counts, then low expressed genes have a large proportion of cells where the gene is undetectable. This is also true of genes that are expressed to a higher level, but are downregulated by Gc to undetectable levels. Examples of genes with variant baseline expression have been shown (Fig. 5.15) in order to reflect this observation.

5.2.14 Gene regulation by Gc correlates with baseline gene expression

It was then necessary to examine other factors which might influence the magnitude of response, by separating the 99 genes into three groups – regulated by Dex alone (1 treatment), regulated by Dex and High HC (2 treatments), or

regulated by Dex, High HC and low HC (3 treatments). Given that baseline gene expression appeared to be a limitation in determining the type of response, base mean expression and transcript length were first analysed for each of the genes (Fig. 5.16A). While transcript length did not vary between genes regulated by low dose, low affinity HC or Dex, baseline expression did. Genes which were regulated by all three treatments – and therefore the most sensitive Gc target genes also had a higher baseline expression. The most obvious interpretation of this finding is not that Gc more reliably regulates highly expressed genes, but instead that the scRNA-seq platform is limited in detecting modest responses in genes expressed just at the limit of detection. It would be expected that Dex would induce the greatest response, and so this could explain why we would be able to detect a change in gene expression relative to a more modest response to low HC for example.

Another approach was to determine if the number of GR binding sites within genes could determine sensitivity to Gc. To investigate this, public GR ChIP-seq data from the cistrome database was analysed, using a dataset based on A549 cells, following treatment for 4 hours with 100nM Dex (304-306). The number of GR peaks, and the size of the peaks (peak score) was analysed for each of the 99 genes. Again, the genes were split into three groups dependent on whether they were regulated by one, two or all three treatments (Fig. 5.16B). There was no clear correlation between either the number or size of GR binding sites that could predict, or explain sensitivity to, low doses of Gc. Example of some gene tracks are shown in Fig. 5.16C. The ChIP-seq dataset used was based on a set of experiments, in which multiple doses of Dex were used to assess sensitivity of GR binding to GR target genes. Gene tracks with each dosage are shown for

both *IL6R* and *CDKN1A*. Binding is clearly increased in a dose-dependent

manner, suggesting Gc dose determines strength of GR-DNA binding.
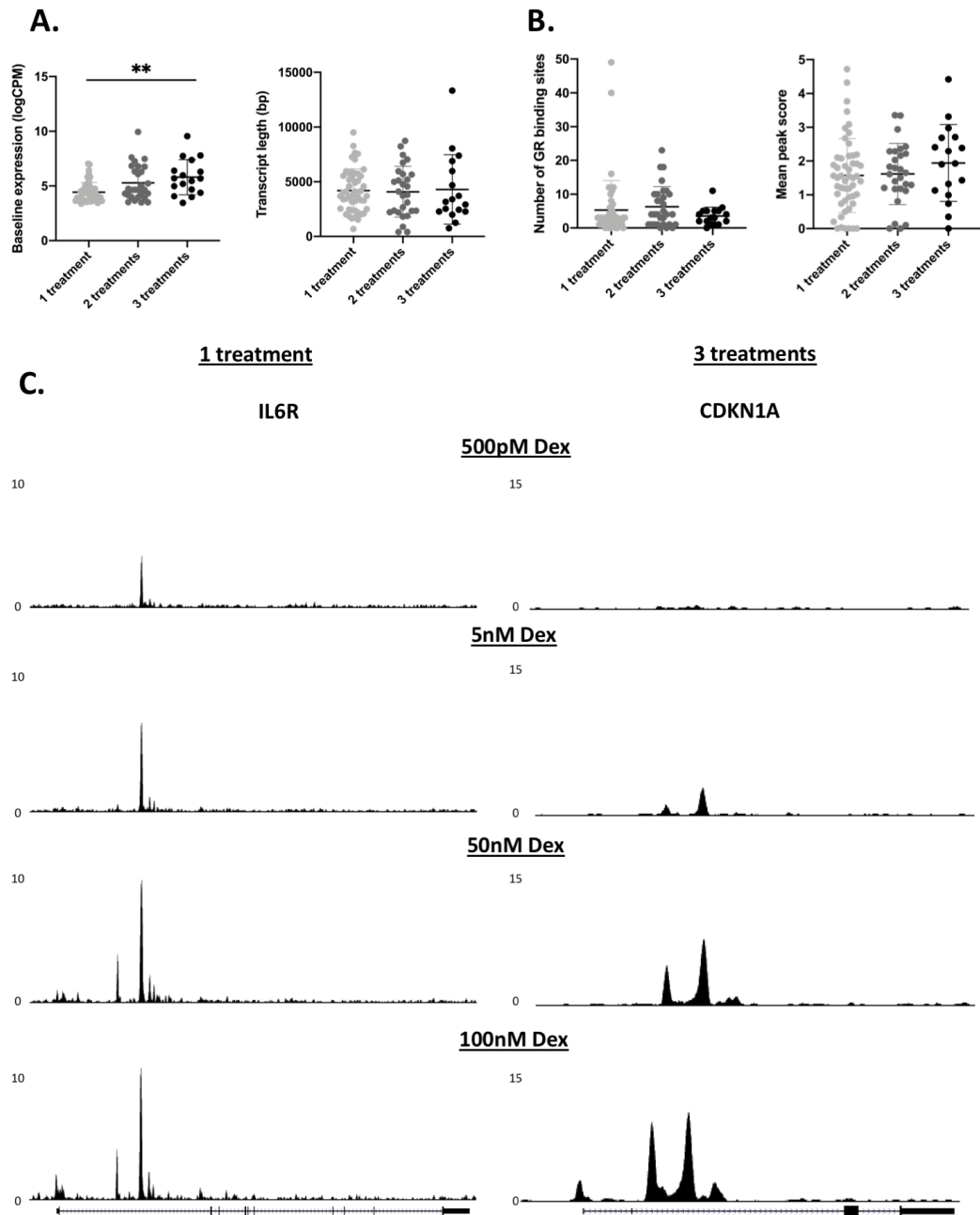
Figure 5.16: The baseline gene expression, but not number of GR binding sites, within GR responsive genes appears to correlate with sensitivity to Gc. A) Genes identified as differentially expressed in both the scRNA-seq and bulk RNA-seq were divided into categories, based on whether they were significantly differentially expressed in response to 1, 2 or all 3 Gc treatments. The baseline expression and transcript length were then analysed for each gene, according to their Gc sensitivity. B) Based on publicly available ChIP-seq data using A549 cells, the number of GR binding sites, and peak score were determined for each gene. These were then quantified according to treatment sensitivity. C) Example gene tracks for 2 genes (IL6R and CDKN1A) were analysed, at increasing concentrations of Dex, within the ChIP-seq dataset. Significance was tested using a one-way ANOVA with a Dunn's multiple comparison test. ** = $p \leq 0.01$.

As a complementary approach, these factors were also analysed to determine if they could explain any heterogeneity in the Gc response. The change in the coefficient of variation between vehicle and Dex treated cells was analysed for all 99 genes. A value that was between 0.75 and 1.25, suggested no change in heterogeneity in gene expression; if the value for the gene was greater than 1.25, this suggested reduced heterogeneity i.e. a stretching of the cell population following Gc treatment. Where the value was below 0.75, this suggested Gc increased heterogeneity in gene expression i.e. a contraction of the distribution of gene distribution. Genes with reduced heterogeneity following Dex addition (37 genes) included only upregulated genes, such as *GILZ*. Genes with increased heterogeneity (6 genes) included only downregulated genes, such as *IL6*. Genes with unchanged heterogeneity (56 genes) included a mix of upregulated and downregulated genes, such as *IL6R* and *E2F7*.

Higher baseline gene expression also correlated with a reduction of heterogeneity (Fig. 5.17A), but there was no effect on either the number of GR binding sites or strength of GR binding between groups (Fig. 5.17B). It should be noted that there is a trend towards more GR binding sites reducing heterogeneity, and fewer GR binding sites increasing heterogeneity but as so few genes fell into the increased heterogeneity group this did not reach significance (Fig. 5.17B). The small number of genes in the increased heterogeneity group is likely because many of the genes downregulated by Gc did not reach threshold of expression for inclusion during the QC stage. Given the clear divide between upregulated and downregulated genes to distinct groups, the number of binding sites could also reflect the mechanism of regulation, rather than inherent variability in response. Some example gene tracks are shown in (Fig. 4.17C).
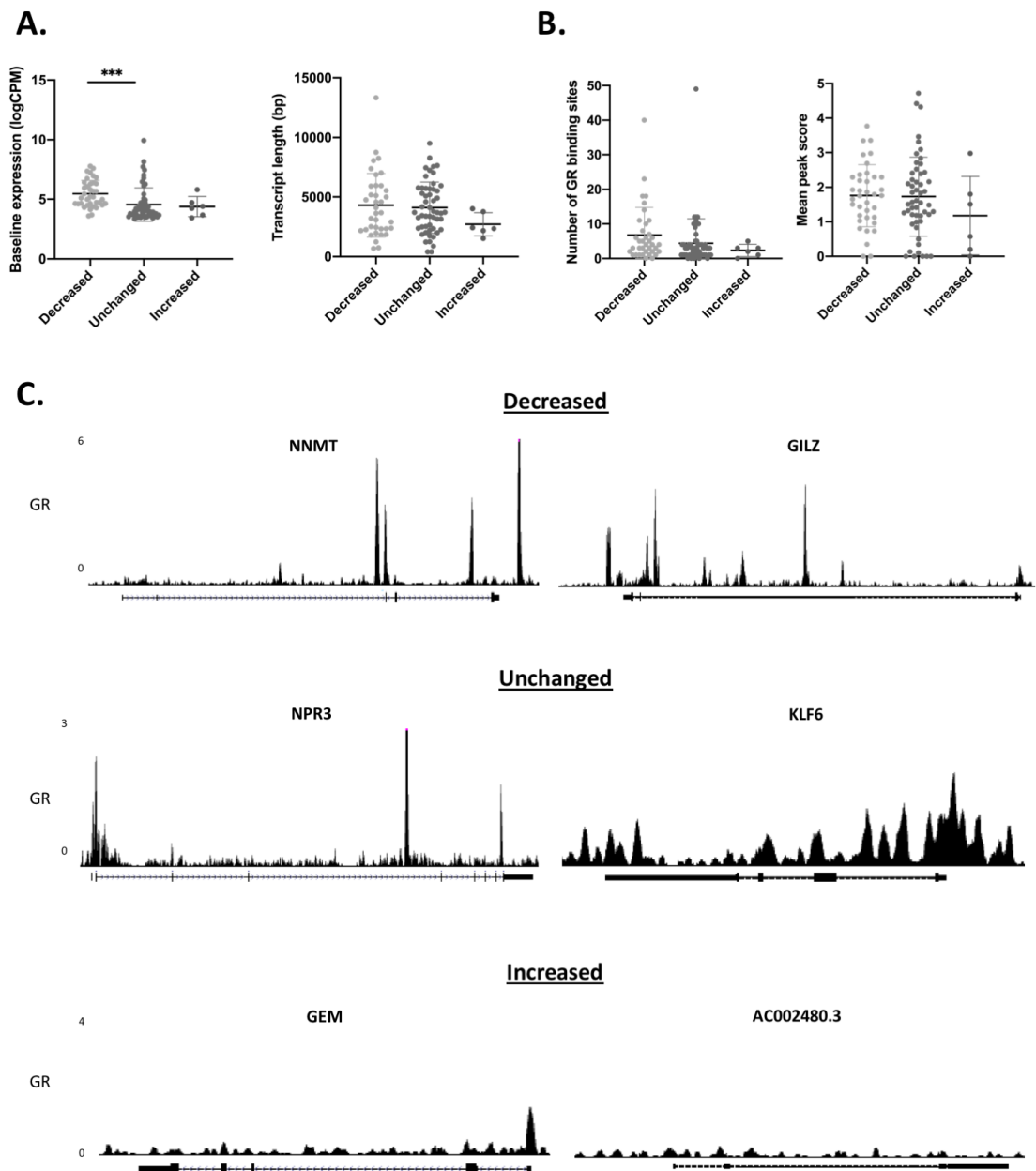
Figure 5.17: The baseline gene expression, but not number of GR binding sites, within GR responsive genes appears to correlate with heterogeneity in the Gc response. A) Genes identified as differentially expressed in both the scRNA-seq and bulk RNA-seq were divided into categories, based on the biological coefficient of variation. This was used to determine if the heterogeneity in response between cells was increased, decreased or unchanged upon Gc addition. This was compared with the baseline expression and transcript length of the mRNA produced. B) Based on publicly available ChIP-seq data using A549 cells, the number of GR binding sites, and peak score were determined for each gene. These were then quantified according to heterogeneity. C) Example gene tracks for genes which fell into each heterogeneity category, using the ChIP-seq dataset used within part B). Significance was tested using a one-way ANOVA with Dunn's multiple comparison test. ** = p ≤ 0.01.

5.2.15   smFISH was validated to ensure optimal quantification

Given the novelty of the technology used, it is necessary to confirm the results seen within scRNA-seq. The results correlate well with the bulk RNA-seq, which confirms the population level response, however, it was also necessary to confirm the patterns of expression seen within individual cells. To validate this, single molecule Fluorescence In Situ Hybridisation (smFISH) was utilised. smFISH is a ground-breaking technique which enables the visualisation of single mRNA molecules within individual cells, using either flow cytometry or immunofluorescence. The visualisation of mRNA expression through immunofluorescence was chosen, as it enables high sensitivity to count individual transcripts and also allows the simultaneous capture of other information, such as colocalization of transcripts. Each probe set, for a single mRNA, contains around 20 oligonucleotide pairs. These pairs bind to the target mRNA, and are then amplified through multiple steps, allowing the signal to be amplified enough to visualise a single bright dot, indicating a single mRNA molecule. These can then be imaged using microscopy.

The ViewRNA Cell Plus Assay (Thermo Fisher) was selected as the kit had been extensively validated, and probes were available for a wide range of genes (307). Initial testing focused on expression of *DUSP1, GILZ* and *GR* within M059K cells*,* following a 4 hour treatment using a vehicle control, or 100nM Dex, including *ACTB* as a positive control due to high expression and imaged using a widefield microscope*.*

As shown in (Fig. 5.18A), there was clear staining for *ACTB* (green) demonstrating the assay was working. *DUSP1* (green), *GILZ* (red) and *GR* (magenta) were also detected, and the expression of both *DUSP1* and *GILZ* appeared to increase after Dex treatment (Fig. 5.18B). No staining was evident when probes were not included suggesting specificity of the assay. A major concern however was the quality of the images, as it was difficult to identify (and therefore count) single transcripts. This was particularly evident in the GR labelled transcripts which appeared in large foci in the cells (Fig. 5.18B).

A.

B.
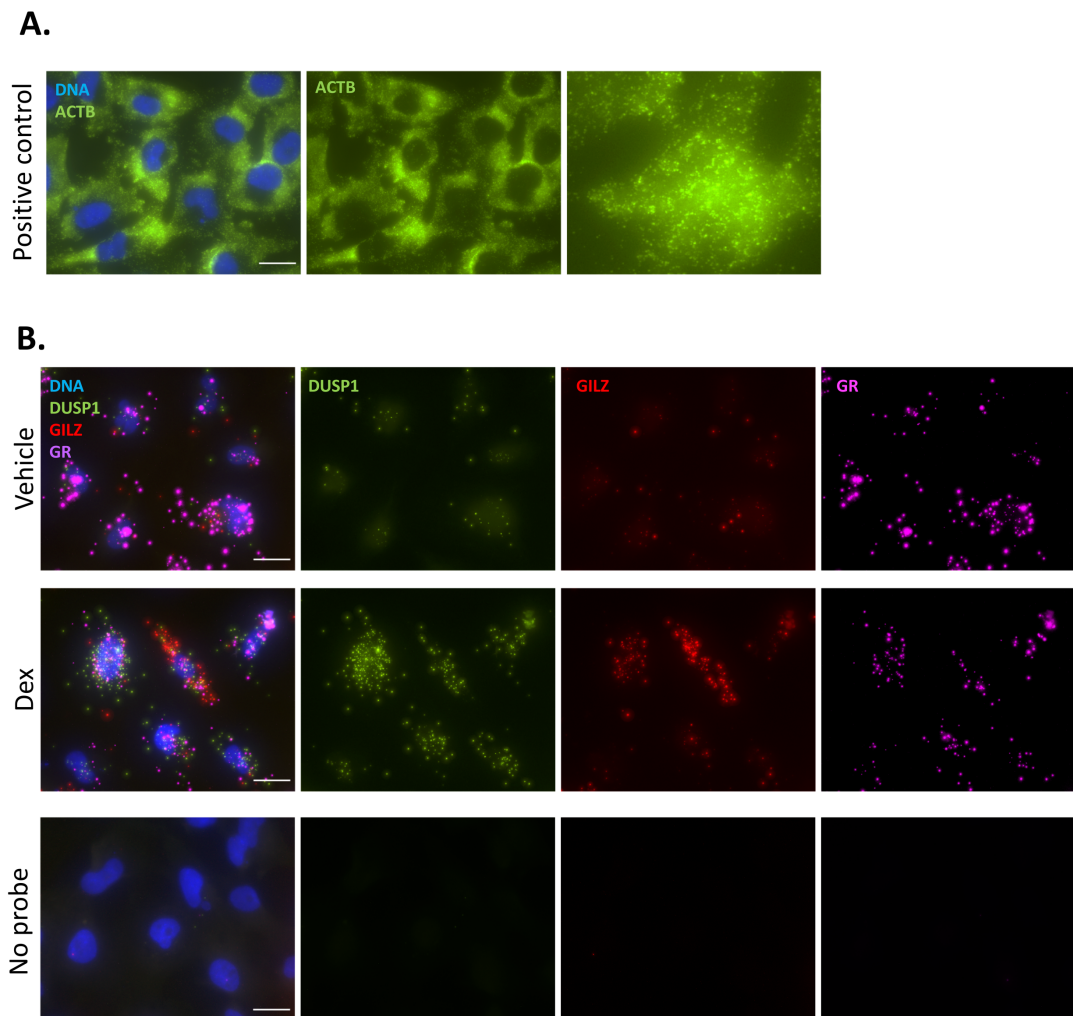
Figure 5.18: Widefield images were captured for smFISH. A) M059K cells were fixed and stained for *b-actin* mRNA using the smFISH assay. B) Cells were treated for 4 hours with a vehicle control or Dex, then stained for *DUSP2, GILZ* and *GR* mRNA, alongside Dapi to stain nuclei. Wells were imaged at x60 magnification. Scale bar denotes 20µm.

As an alternative, the Operetta system was tested, which uses widefield microscopy but also includes the option of image deconvolution to remove out of focus light (Fig. 5.19). An added advantage can is that this system can be programmed to take images at multiple sites within a well and also between wells and so offered a higher throughput option.
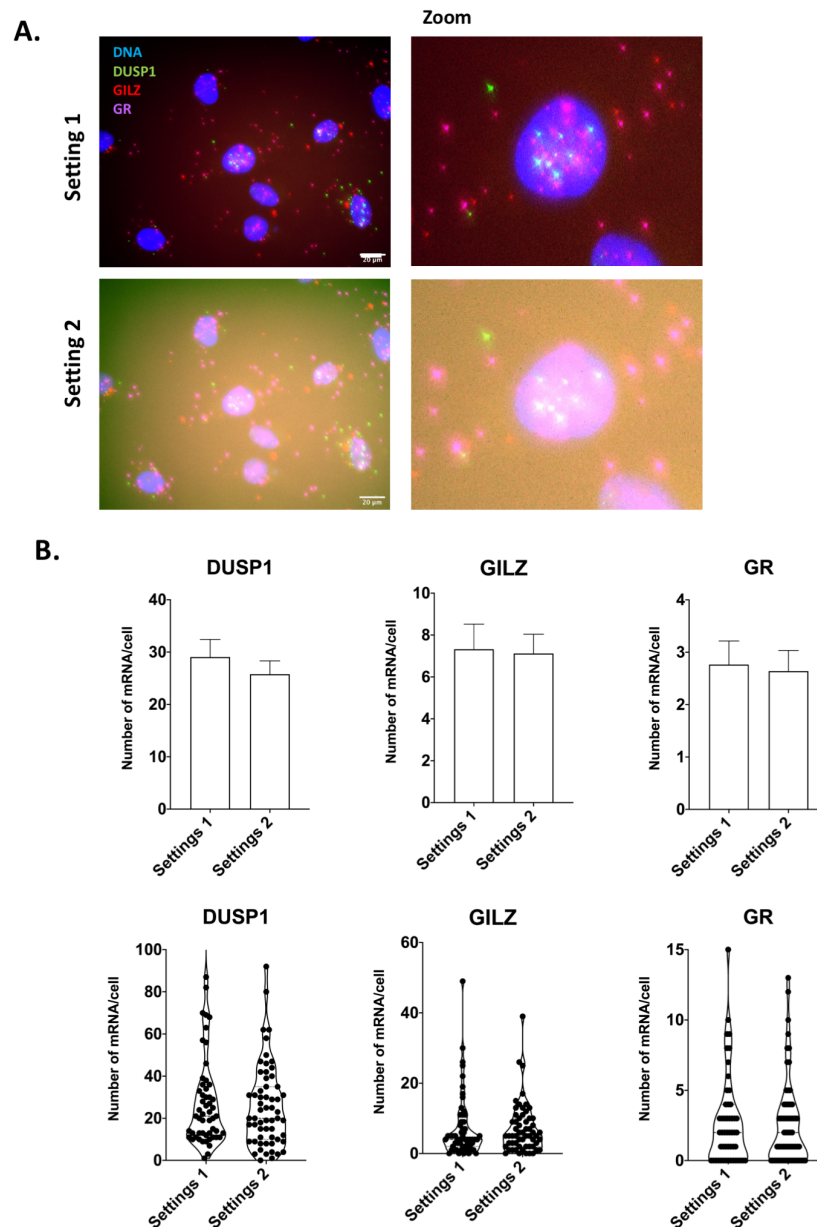
Figure 5.19: M059K cells were probed for *DUSP1*, *GILZ* and *GR* mRNA using smFISH following Gc treatment and imaged using the Operetta microscope. Cells were treated for 4 hours using 100nM Dex, then prepared for smFISH according to manufacturer's protocol. A) Cells were imaged using an Operetta widefield microscope. B) Images were quantified using FishQuant software. Scale bar denotes 20μm.

Images taken prior to deconvolution are shown in (Fig. 5.19A), in which two intensity settings were compared to determine if brightness influenced detection of transcript numbers. Again, there is some out of focus light, but individual spots can be identified. Quantification of the number of transcripts (spots) using the automated FiSHQuant software demonstrated that image intensity did not significantly affect the number of transcripts identified in each cell (Fig. 5.19B).

The assay was then repeated, labelling M059K cells treated with vehicle, 50nM HC, 500nM HC or 100nM Dex for four hours (Fig. 5.20A). The number of transcripts were then quantified using FiSHQuant software (Fig. 4.20B). Unfortunately, using this platform it was not possible to detect an increase in GILZ expression in response to Gc treatment, and the expression of GR was regulated by Gc, which does not reflect observations from the scRNA-seq. It is unclear what the underlying cause is, but it is possible that the Operetta is not sensitive enough to detect the low expression of *GILZ* and *GR.* Large foci could also still be seen in some images, suggesting the Operetta could still not effectively demarcate individual foci.
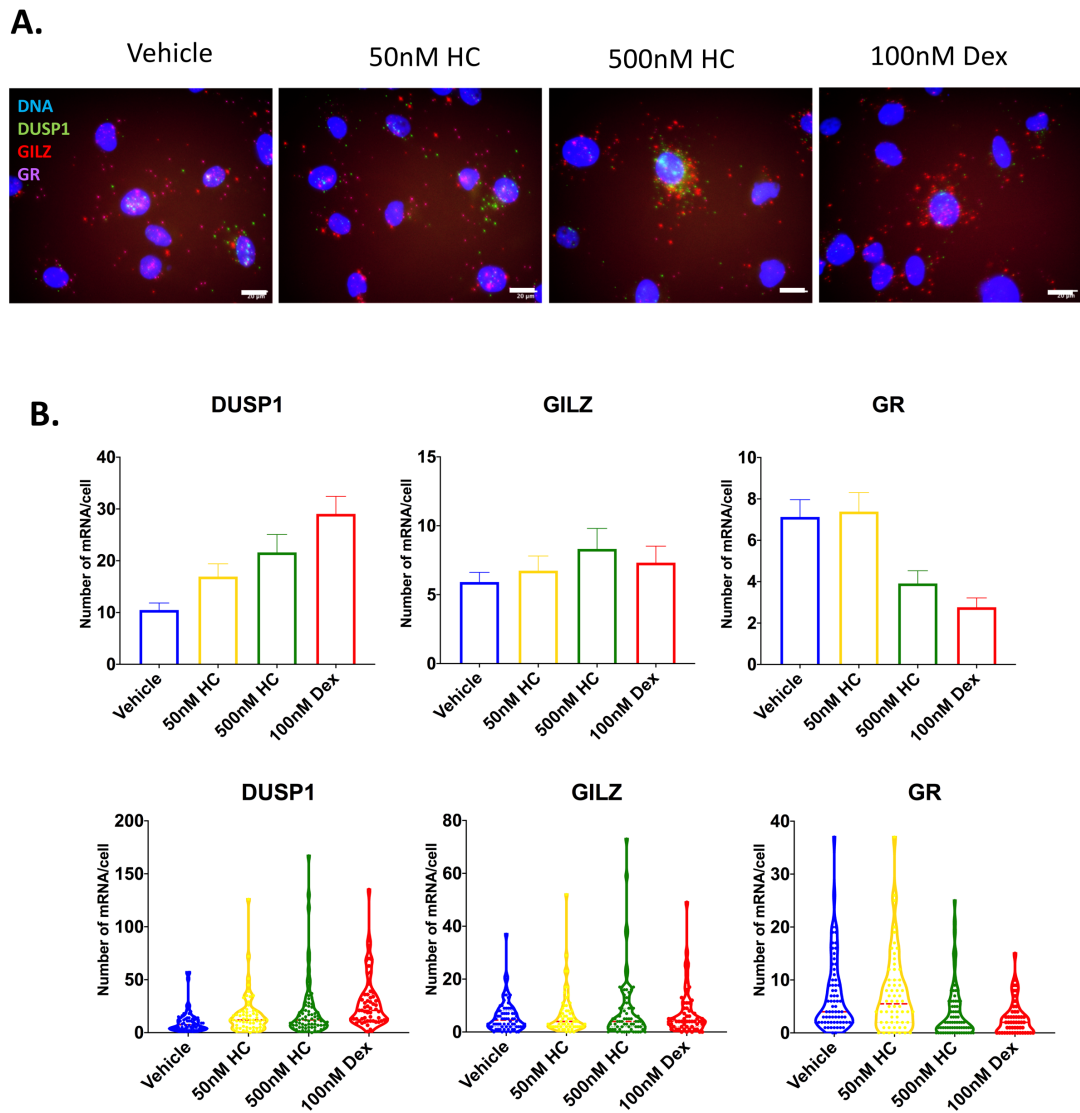
Figure 5.20: M059K cells were probed for DUSP1, GILZ and GR mRNA using smFISH following Gc treatment and imaged using widefield microscopy. Cells were treated for 4 hours using a vehicle control, 50nM HC, 500nM HC, or 100nM Dex, then prepared for smFISH according to manufacturer's protocol. A) Cells were imaged for each condition using an Operetta widefield microscope. B) Images were quantified using FishQuant software. Graphs show mean expression for each condition, and expression within individual cells was also shown. Error bars denote SEM, and scale bar denotes 20µm.

It was decided therefore to test using a confocal microscope, which although slower to acquire images and significantly more expensive to use might be the best option to enable this analysis. A pilot experiment testing imaging using the confocal in cells labelled either with actin, or without probe demonstrated that the quality of the images obtained were significantly better, with improved sensitivity and resolution (Fig. 5.21).
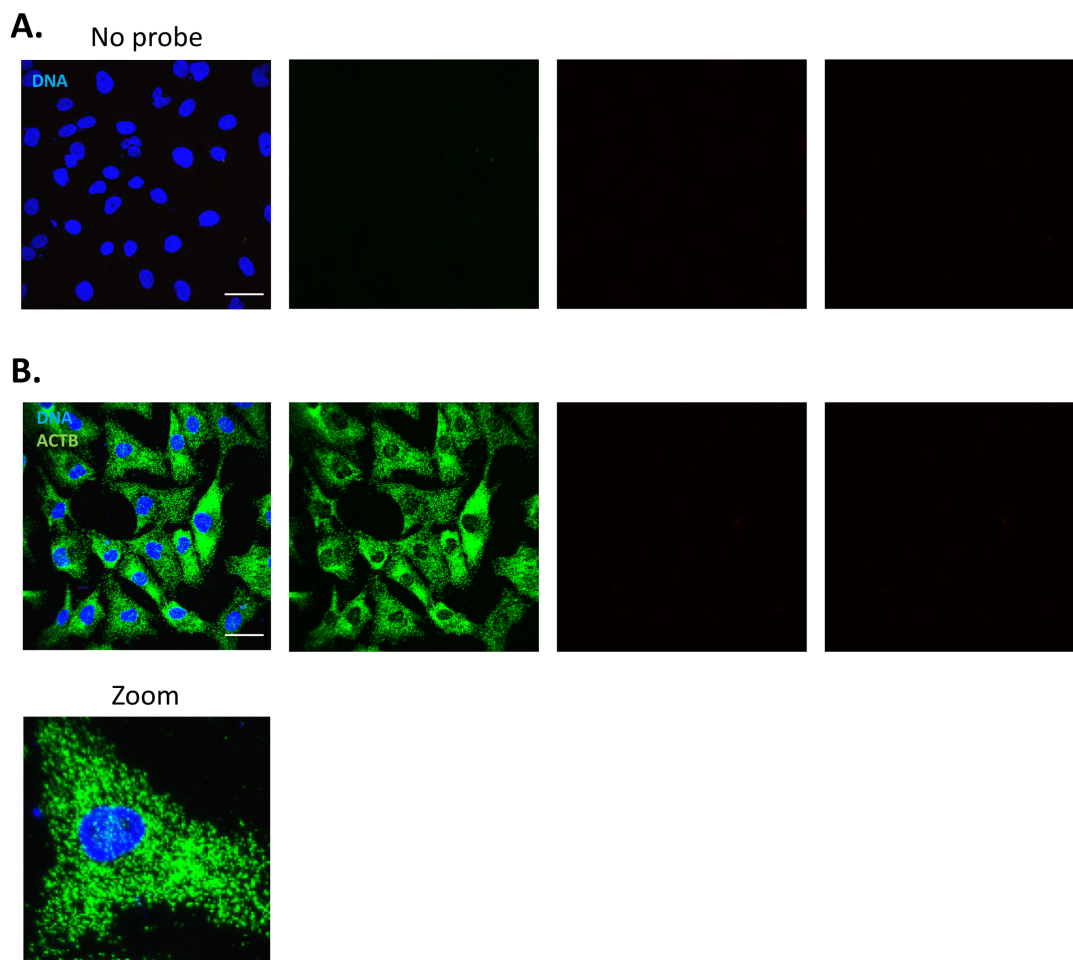
Figure 5.21: Confocal microscopy was tested using a no probe control and b-actin stained cells as a negative and positive control respectively. Cells were untreated with Gc, then stained without any probe sets (A), or for *ACTB* alone (B) and imaged in all four channels. Images were acquired using a Nikon confocal microscope at a 40x magnification. Sale bar denotes 50µm.

The confocal microscope was clearly the best imaging tool, and this also offered the option of taking a brightfield image to identify cell edges. This cannot be used to guide finding cells using FiSHQuant and so this was tested using ImageJ, using the brightfield to define the cells to determine if that was robust. Cells were treated with Gc for 4 hours, labelled with Dapi and the probes for *DUSP1, GILZ* and *GR*, then all 4 colour channels were imaged alongside a brightfield image (Fig. 5.22A). Unfortunately, the cell outlines were not detected reliably using the brightfield image and cell outlines were defined by freehand drawing around outlines (Fig. 5.22B). The find maxima tool was used to detect points of maximum staining compared with the background, and the number of these bright points within each outline was quantified for each condition (Fig. 5.22C). The number of spots did appear to increase for both *DUSP1* and *GILZ,* however, drawing around cell outlines did not appear to be a reliable method of analysis. In addition, image acquistion and analysis required approximately 16 hours of imaging when only imaging 5 images per condition. I therefore developed a program to enable automated image acquisition on the confocal microscope, and reverted to a modified pipeline for FiSHQuant analysis to quantify the confocal imaging data.

FishQuant is a free-to-use Matlab toolbox which can be used to automate analysis of smFISH images in an unbiased manner (308). FishQuant used the localisation of smFISH spots to predict a cytoplasmic mask for each cell. This software aims to detect mRNA across all 3 dimensions of the cell. It is also able to provide a quality score for each detected spot. This score indicates the certainty of the system that the foci indicates a positive signal, as opposed to autofluorescence or debris. FishQuant also includes a tool to create masks for

both the nuclear and cytoplasmic areas, based on the staining for Dapi and GR

staining respectively.
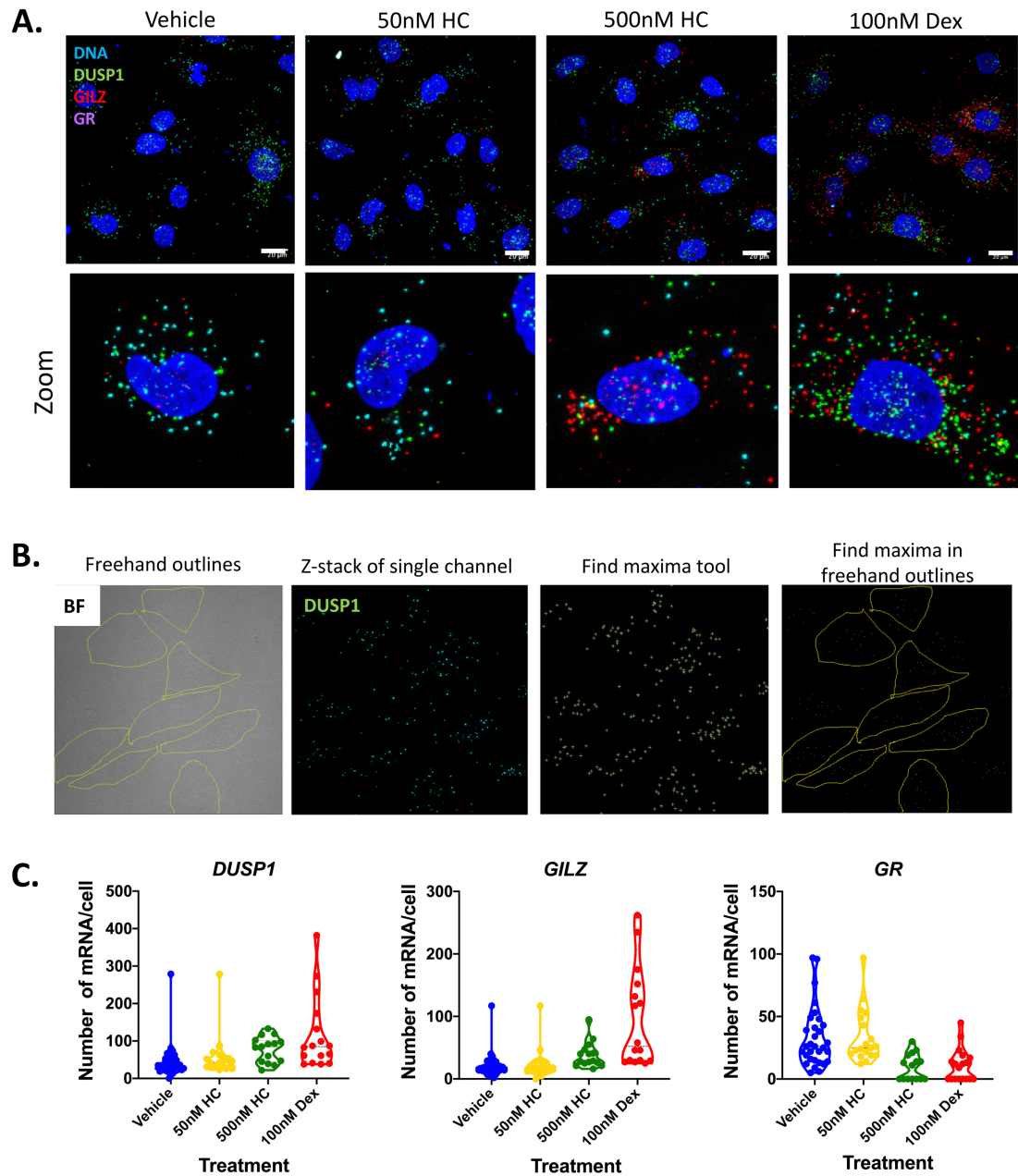
Figure 5.22: M059K cells were probed for *DUSP1*, *GILZ* and *GR* mRNA using smFISH following Gc treatment and imaged using confocal microscopy. M059K cells were treated for 4 hours using a vehicle control, 50nM HC, 500nM HC, or 100nM Dex, then prepared for smFISH according to manufacturer's protocol. A) Wells were imaged using a confocal microscope for each channel and a brightfield image. B) Cell outlines were drawn freehand using ImageJ. C) Spots were quantified using the find maxima tool to find points of maximum saturation. Images were acquired using a Nikon confocal microscope at a 40x magnification.

This entailed using a maximum projection of each image within a CellProfiler pipeline. These masks can then be added to the z-stack for each channel within each field of view. Based on this, the number of foci per cell may then be quantified, and each image can be manually checked for poor quality cell masks. By filtering out low quality cells and through the quality score for each mRNA, this allows for relative confidence in the system.

This system allows for high-throughput, unbiased quantification of foci, however a concern was whether the automated software was unable to distinguish between neighbouring cells or detect cell edges which may have lower numbers of GR transcript. A simple analysis was completed, subsampling across six different positions within 10 different cells to determine if variation in transcript numbers dependent on subcellular localisation (Fig. 5.23). While there was some variability in absolute transcript number from different regions within any cell, the largest variability came from differences in transcript abundance between cells. It was therefore determined that using automated confocal imaging coupled with the combined CellProfiler/FiSHQuant analysis was the most robust way to analyse the assay.
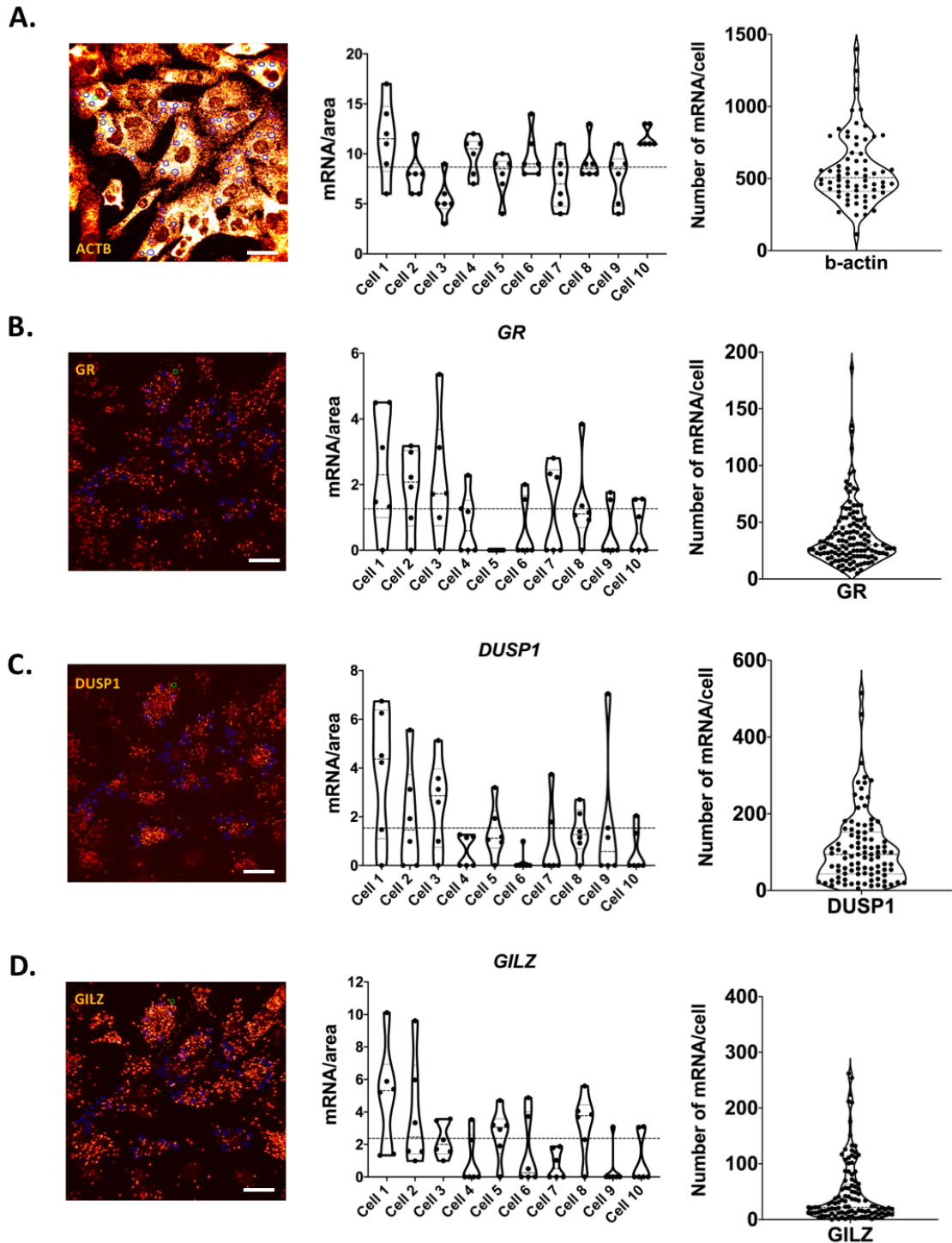
Figure 5.23: Subcellular sampling reveals heterogeneity between individual cells. Expression of mRNA transcripts were measured across 6 points within each cell, and normalised to area size. Variability within *ACTB* expression in untreated cells (A), and expression of *DUSP1, GILZ* and *GR* within Dex treated cells (B-D). Images show representative sampling. Dotted lines on graphs indicates mean expression. Scale bar denotes 50µm.

5.2.16 smFISH results show similar patterns to the scRNA-seq data

For each of the 4 experimental conditions, 5 fields of view were imaged at a 40x objective on an A1R confocal microscope, and images processed using CellProfiler and quantified using FishQuant. Example images for each condition are shown (Fig. 5.24). *GR* expression appeared relatively consistent across all 4 treatment groups, whilst both *DUSP1* and *GILZ* showed a dose-dependent increase in expression following Gc treatment.

The expression was quantified using FishQuant software. As was seen within the images, mean expression of *DUSP1* and *GILZ* showed significantly increased following Gc treatment (Fig. 5.25, upper). The number of mRNA molecules in each individual cell is presented as violin plots (Fig. 5.25, middle), which enable better comparison with the scRNA-seq data (Fig. 5.25, lower). The smFISH results do not correlate precisely with the scRNA-seq data, but the general outline of the data is very similar. For instance, for *DUSP1,* the maximal response did increase slightly in a small number of cells in response to the 100nM Dex. What is clear, however, is the increase in maximum response is much more pronounced for *GILZ. GILZ* expression within vehicle-treated cells is very low, and this entire population shifts upwards strongly in response to the 3 Gc doses. This highlights how the smFISH is so much more sensitive than the scRNA-seq and should be used as validation to ensure that limits of transcript detection are not interpreted as biological phenomena.
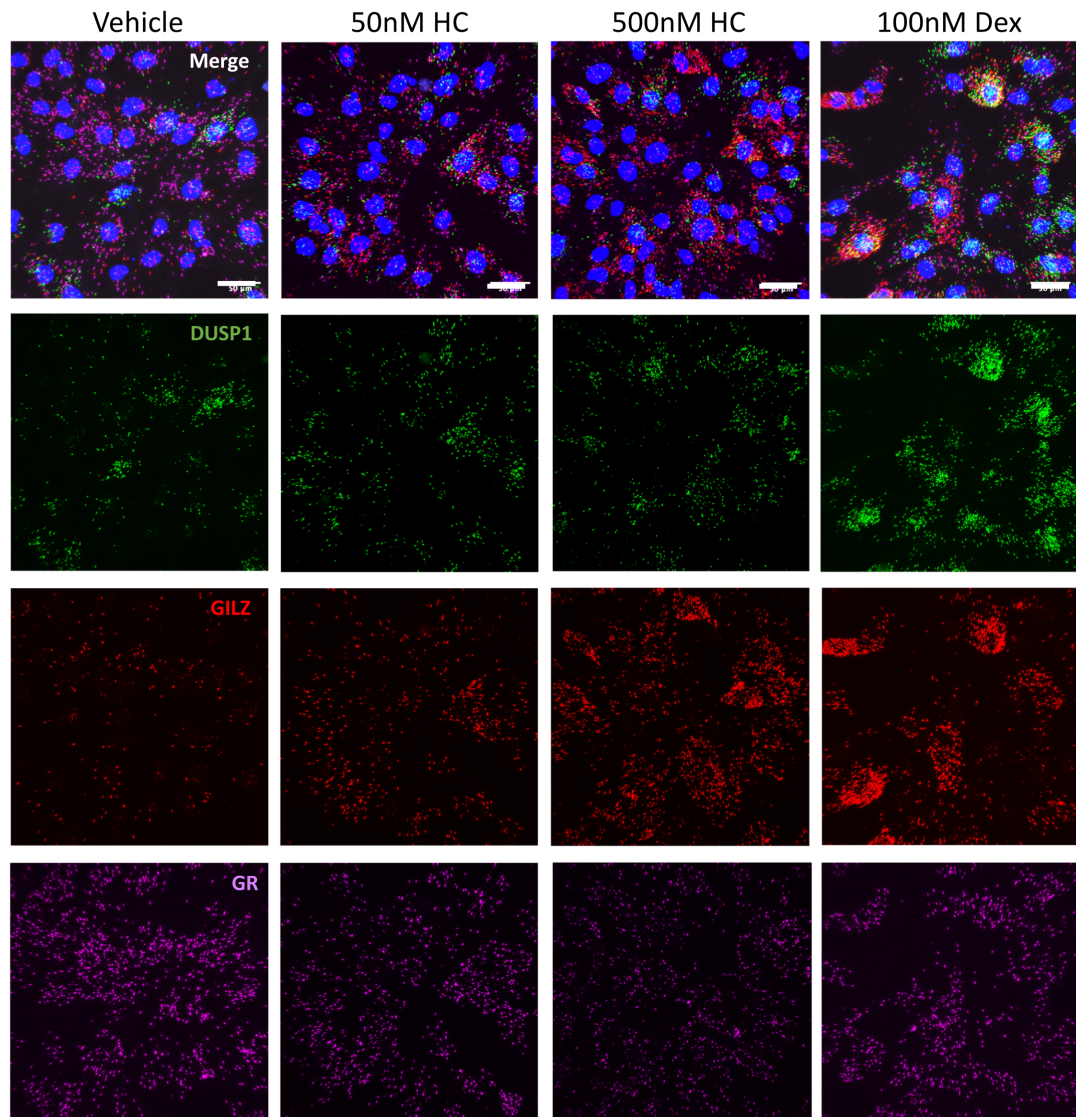
Figure 5.24: smFISH shows increased expression of DUSP1 and GILZ following Gc treatment. M059K cells were treated for 4 hours with a vehicle control, 50nM HC, 500nM HC, or 100nM, then probed in parallel for *DUSP1, GILZ,* and *GR*. Wells were imaged using a Nikon A1R confocal microscope at 40x objective. Images shown are representative of 3 independent experiments. Scale bar denotes 50um.
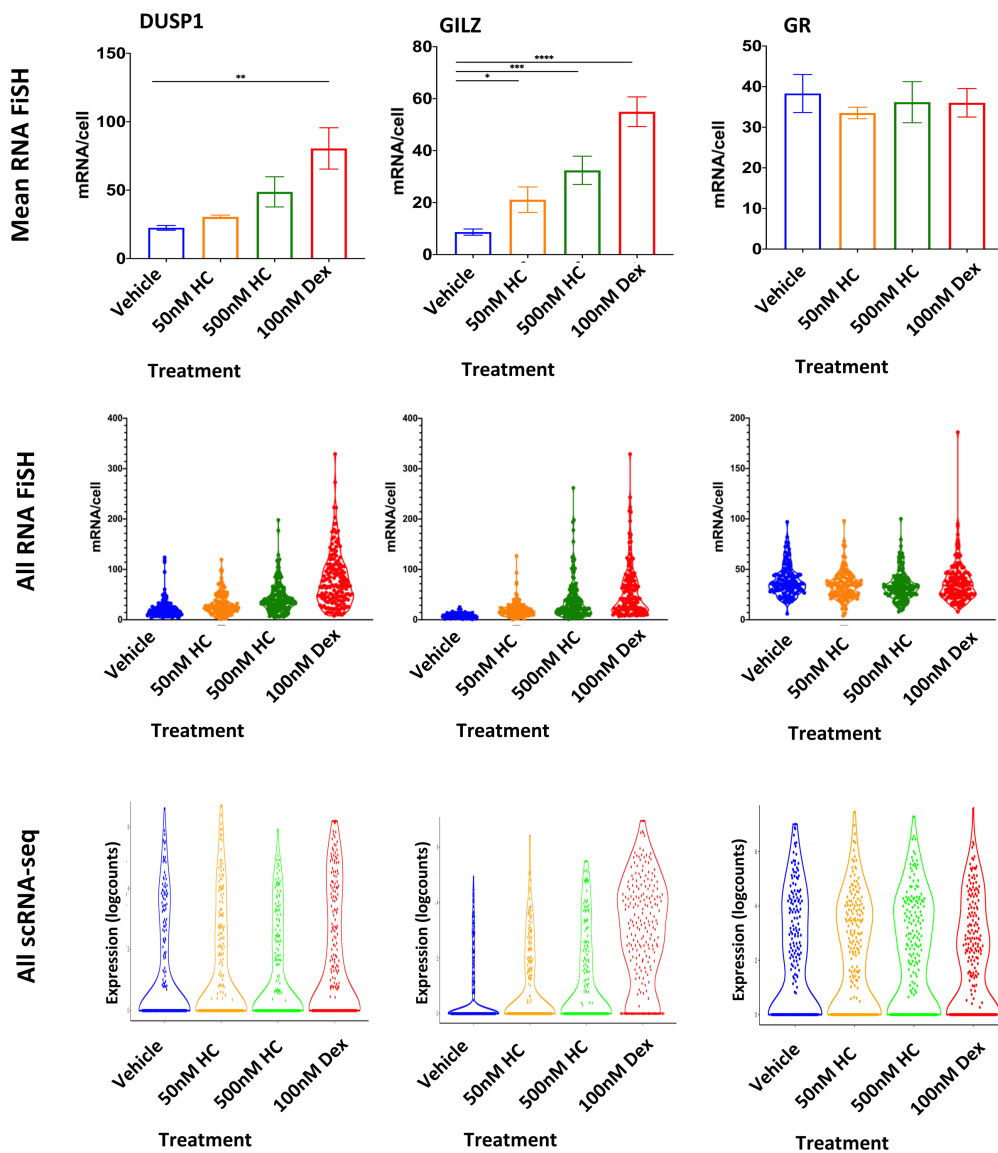
Figure 5.25: smFISH shows increased expression of DUSP1 and GILZ mRNA following Gc treatment. M059K cells were treated for 4 hours using a vehicle control, 50nM HC, 500nM HC, or 100nM Dex. Cells were stained for *DUSP1, GILZ* and *GR* mRNA, then imaged using confocal microscopy and quantified using FishQuant. A) Average expression for each mRNA probe is shown. B) Variability between expression within each gene is also shown as violin plots. Each dot represents expression within a single cell. C) This is compared to the expression data from the single cell RNA-seq data previously shown. Results shown are the average of 3 independent experiments. Shown are the mean +/- SEM.

5.2.17 smFISH suggests a correlation between expression of GR and Gc regulation of target genes

Given that GR expression shows such high variability between cells, it would therefore follow that cells with highest levels of GR expression would be the cells that show the greatest induction of Gc regulated genes. Expression of *GR* compared with either *DUSP1* (Fig. 5.26, left)*,* or *GILZ* (Fig. 5.26, middle) from the smFiSH data is shown for each treatment condition. For vehicle treated cells, expression of *DUSP1* and *GILZ* was low, and showed very little correlation with *GR* expression. There was a dose/affinity dependent increase expression of both genes following Gc treatment, and the stepwise increase in *DUSP1* and *GILZ* expression also increased correlation with GR expression in individual cells. Correlation between expression was quantified using a correlation coefficient, from which the R^2 value was calculated. An R^2 value of 1.0 would indicate that all of the variance of *DUSP1* expression, for instance, was explained by variation in *GR* expression. An R^2 value of 0, on the other hand, would indicate that variation in one variable was not related to variation in the other. For *DUSP1* and *GR*, R^2 was 0.1261 in vehicle treated cells, which increased to 0.4334 in Dex treated cells, and for *GILZ* and *GR*, R^2 was 0.1396 in vehicle treated cells, which increased to 0.3967 in Dex treated cells.

While this moderate positive correlation makes sense, it was surprising that the correlation was not stronger, suggesting other intrinsic factors that modulate the Gc response independently of *GR* expression. In support of this, despite good correlation of *GR* expression with *DUSP1* and *GILZ*, there was very little correlation between the expression between *DUSP1* and *GILZ* expression, even in the presence of Dex, with R^2 of 0.172.

This suggests that while GR expression is an important determinant in Gc sensitivity, which can account for some variability between cells, there are other factors that are important in modulating the Gc response on a gene by gene basis.
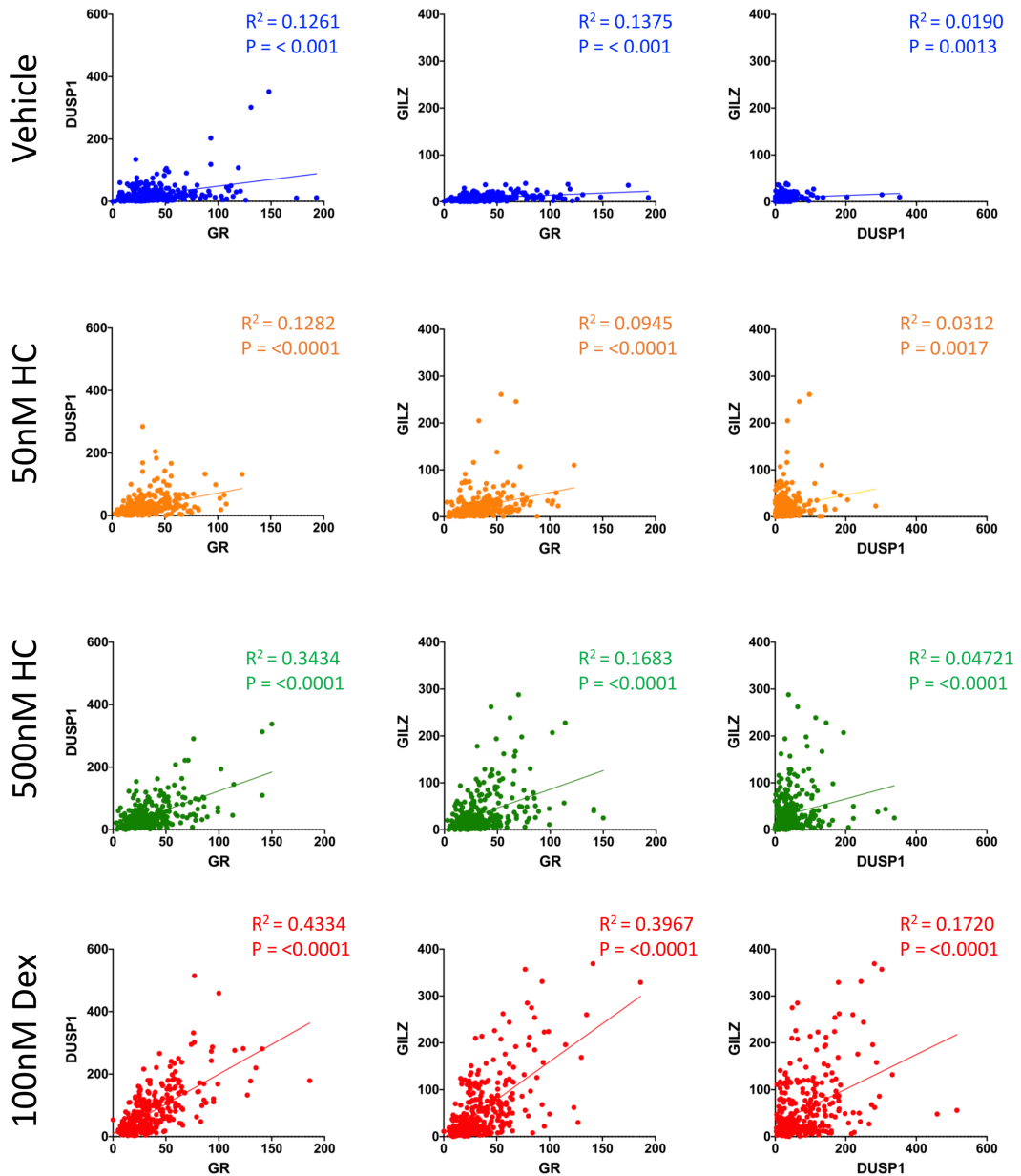
Figure 5.26: smFISH results show correlation between gene expression. Expression of *DUSP1* and *GR*, *GILZ* and *GR*, and *GILZ* and *DUSP1*. Correlation is shown between expression in the same cells for each of the 4 conditions; vehicle-treated cells, 50nM HC, 500nM HC, and 100nM Dex. Shown are the accumulated results across 3 independent experiments. R^2 value indicates the Pearson's coefficient to indicate correlation for each cell.

5.2.18   smFISH helps to elucidate effects of Gc on inflammation

In addition to providing further validation for the scRNA-seq results, downregulated GR target genes identified by the scRNA-seq were also analysed using smFISH, but in this case their expression was analysed within the context of an inflammatory cue, TNFα. To do this, two well characterised Gc target genes, *IL6* and *IL8 (CXCL8),* were chosen. Both are pro-inflammatory cytokines, are induced by TNFα and downregulated by Gc treatment.

Cells were pre-treated with TNFα for 1 hour prior to Dex addition, or pre-treated for 20 hours, to mimic the effects of acute and chronic inflammation respectively. Cells were then treated for 4 hours with a vehicle control, or 100nM Dex, then fixed and processed for smFiSH. Cells were then stained with probes for *IL6, IL8* and *GR.* Representative images are shown (Fig. 5.27). Images were then analysed using FishQuant to quantify transcript expression. Both *IL6* (Fig. 5.28A) and *IL8* (Fig. 5.28B) were increased following TNFα addition. Although, *IL6* showed a marked decrease in expression when then treated with Dex, this was not seen for *IL8,* which showed a marked increase in expression following Dex combined with acute TNF treatment. This response was not seen with chronic TNF treatment. It is important to note that these results are the mean of only two independent experiments. It is possible that these results may highlight the complex effects of Gc within the context of inflammation – Gc treatment can be proinflammatory in mild inflammation. This does, however, requires further validation.
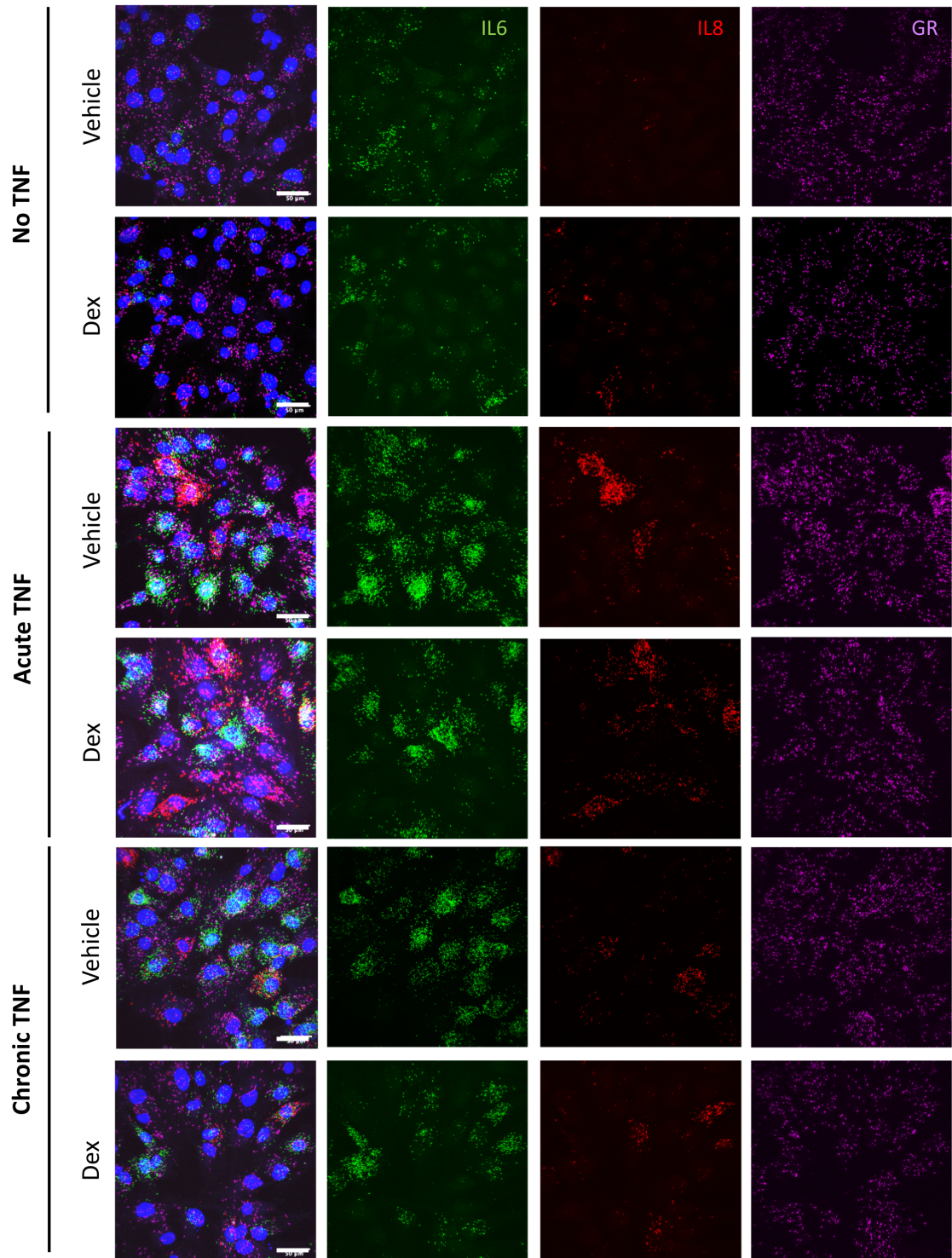
Figure 5.27: TNF treatment induces expression of IL6 and IL8, and this is abrogated by Dex treatment. M059K cells were pre-treated with 10ng/ml TNFα for 1 hour (acute TNF) or 20 hours (chronic TNF). Cells were then treated with a vehicle control, or 100nM Dex for 4 hours. smFISH was then used to probe for *IL6, IL8* and *GR* mRNA. Wells were imaged using a Nikon A1R confocal microscope at 40x objective. Scale bar denotes 50µm. Images shown are representative of 2 independent experiments.
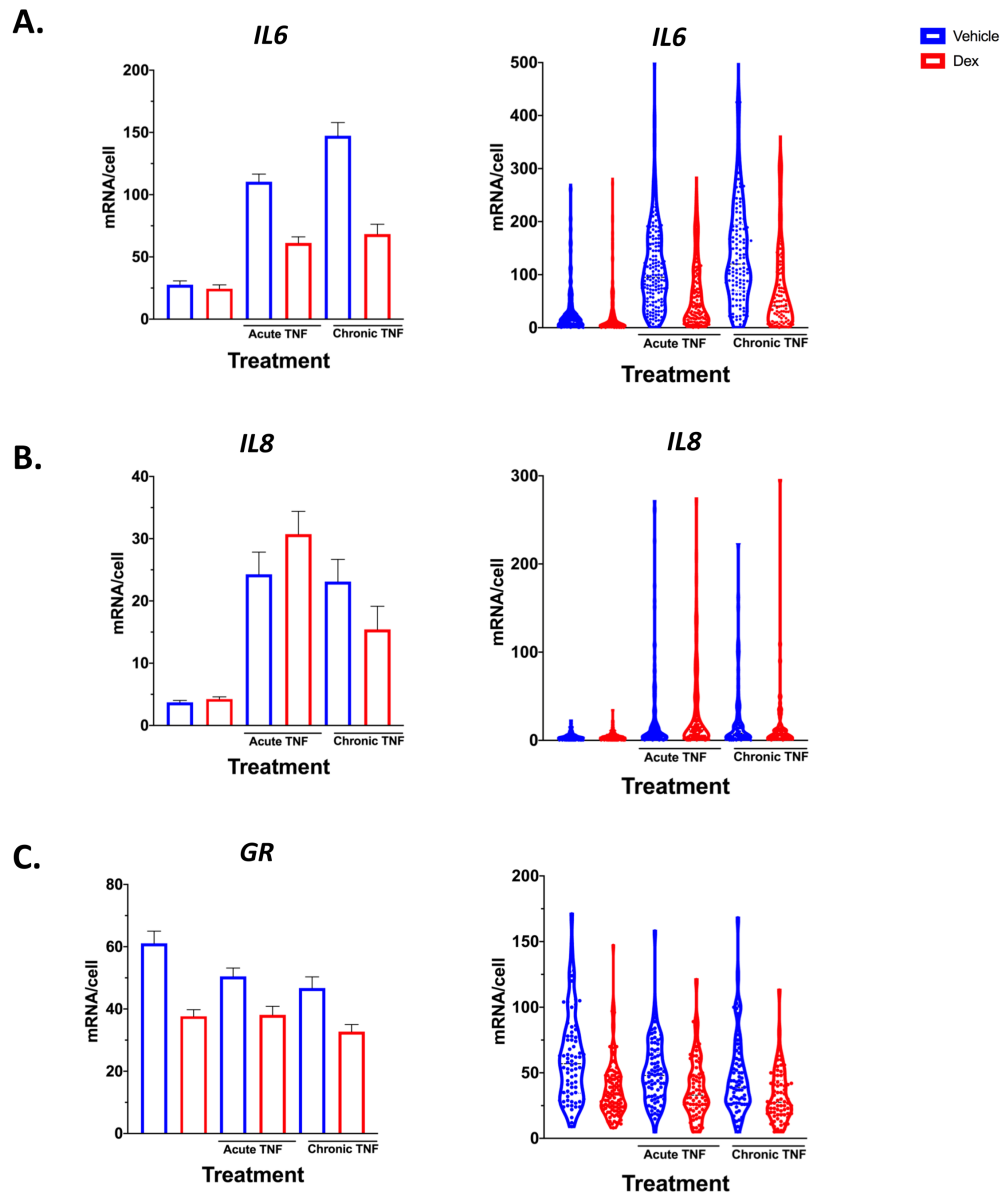
Figure 5.28: TNF treatment induces expression of IL6 and IL8, and this is abrogated by Dex treatment. M059K cells were pre-treated with TNF for 1 hour (acute) or 20 hours (chronic), then treated for 4 hours with a vehicle control (blue), or 100nM Dex (red). Cells were probed for *IL6, IL8* or *GR* transcripts. Average expression for each gene is shown (left), and violin plots of individual gene expression (right). For *IL6* and *IL8*, results are the sum of 2 independent experiments. For *GR*, results are the sum of 1 independent experiment. Error bars denote mean +/- SEM.

In contrast to observations with upregulated genes which showed positive correlation with GR expression, there was no negative correlation between *GR* and *IL6* expression (Fig. 5.29). This likely reflects the interaction of GR with other transcription factors such as AP-1 or NFkB in order to suppress *IL-6*.
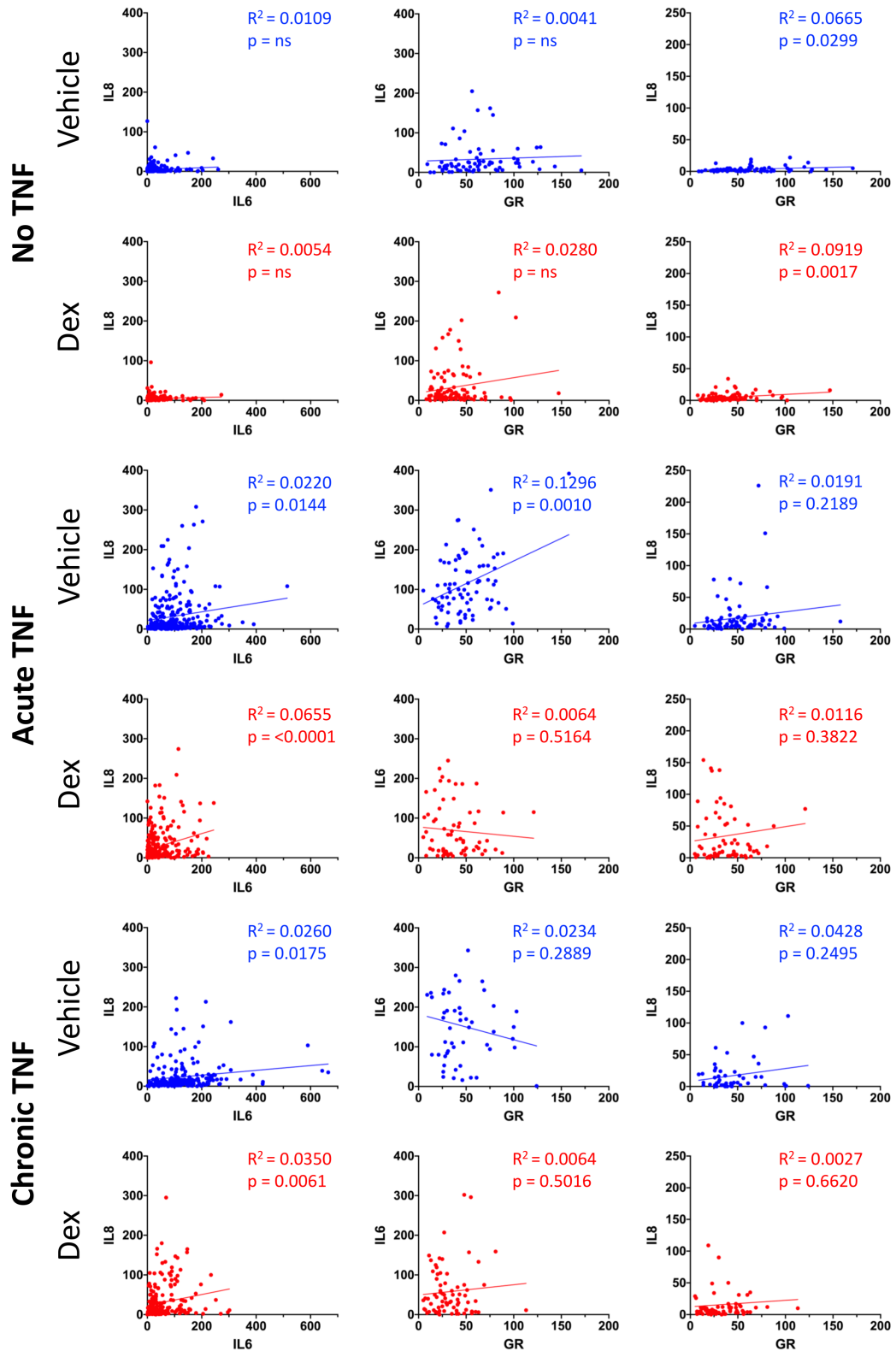
Figure 5.29: Expression of IL6 and GR shows no correlation in single cells. Cells pre-treated with TNF for 1 hour (acute) or 20 hours (chronic), then treated for 4 hours with a vehicle control, or 100nM Dex were probed for *IL6, IL8* or *GR* mRNA. Genes were paired, and correlation was tested using Pearson's tests, and the R^2 value was calculated. For *IL6* and *IL8* correlation, results are the sum of 2 independent experiments. For *GR* correlations, results are the sum of 1 independent experiment. At least 50 cells were analysed within each experiment.

The effect of acute and chronic TNFα treatment on Gc induction of *DUSP1* and *GILZ* was also analysed (Fig. 5.30 & 5.31). There was an increase in expression following Dex addition, and number of detected mRNA were consistent with previous experiments. The Dex-dependent increase in *DUSP1* expression was completely unaffected by TNFα pre-treatment (Fig. 5.31A), however, the Gc induced *GILZ* expression was abrogated following either acute or chronic TNF treatment, suggesting impaired Gc sensitivity (Fig. 5.31B).

This was also demonstrated by reduced correlation following Dex treatment, between *GR* and *GILZ* expression from R^2 in control treated cells of 0.6124, compared with R^2 of 0.1192 in acute TNF treated cells and R^2 of 0.2764 following chronic TNF treatment (Fig. 5.32). However, these experiments require additional repeats to enable statistical analysis.

Overall, further analysis of additional upregulated and downregulated genes will be required to determine whether the patterns seen within these genes are common within Gc-mediated transcription. Based on these results, however, the single cell RNA-seq data appears to provide a reliable measure of the heterogeneity within the GR response. Further analysis will aim to investigate other factors which could contribute to this heterogeneity, and could alter the GR response as a whole.
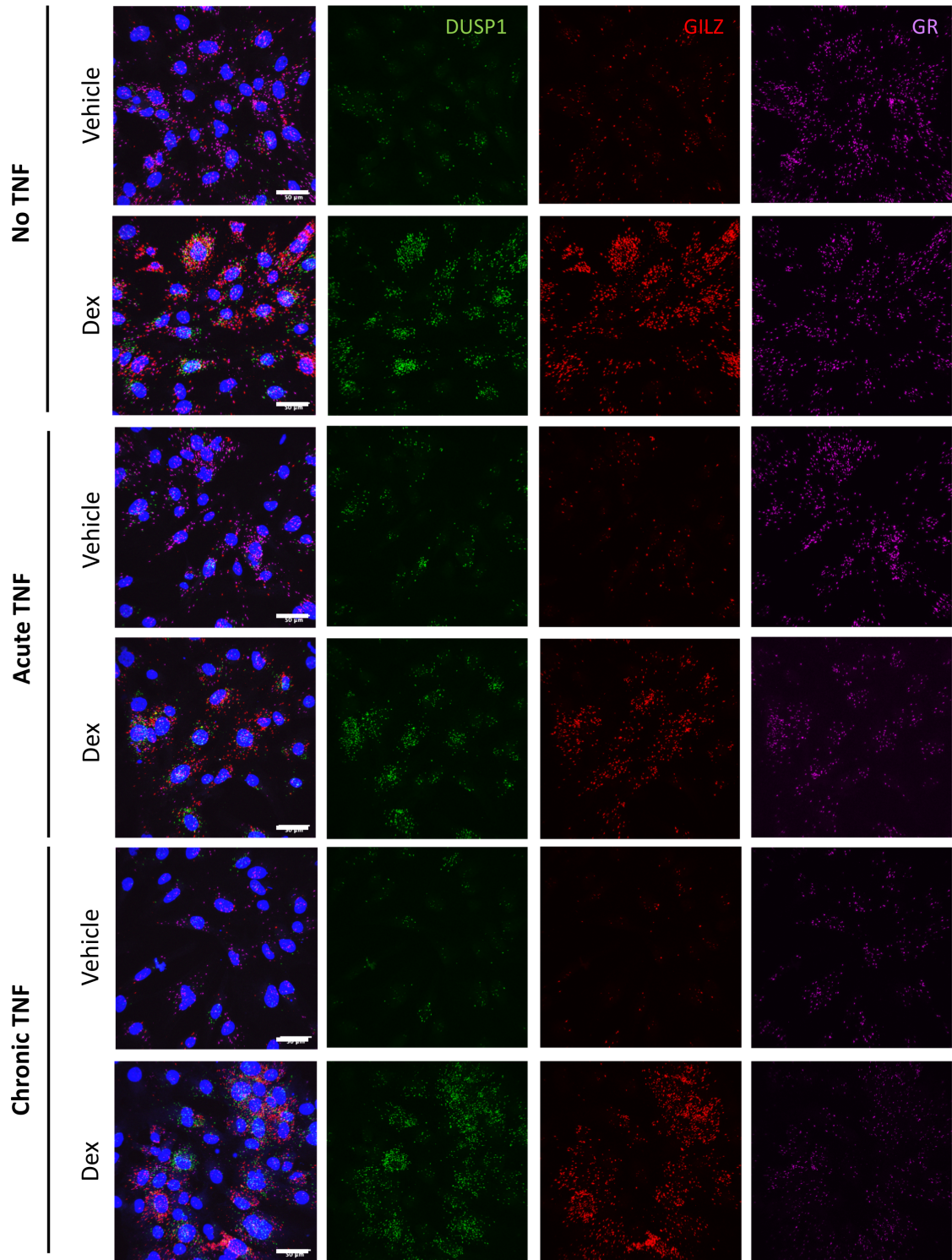
Figure 5.30: Effect of TNF treatment on Gc induction of DUSP1 and GILZ expression. M059K cells were pre-treated with 10ng/ml TNFα for either 1 hour (acute), or 20 hours (chronic), or left untreated. Cells were then treated for 4 hours with a vehicle control, or 100nM Dex. Cells were then probed using smFISH for *DUSP1, GILZ* and *GR* mRNA. Wells were imaged using a Nikon A1R confocal microscope at 40x objective. Images shown are representative of 2 independent experiments.
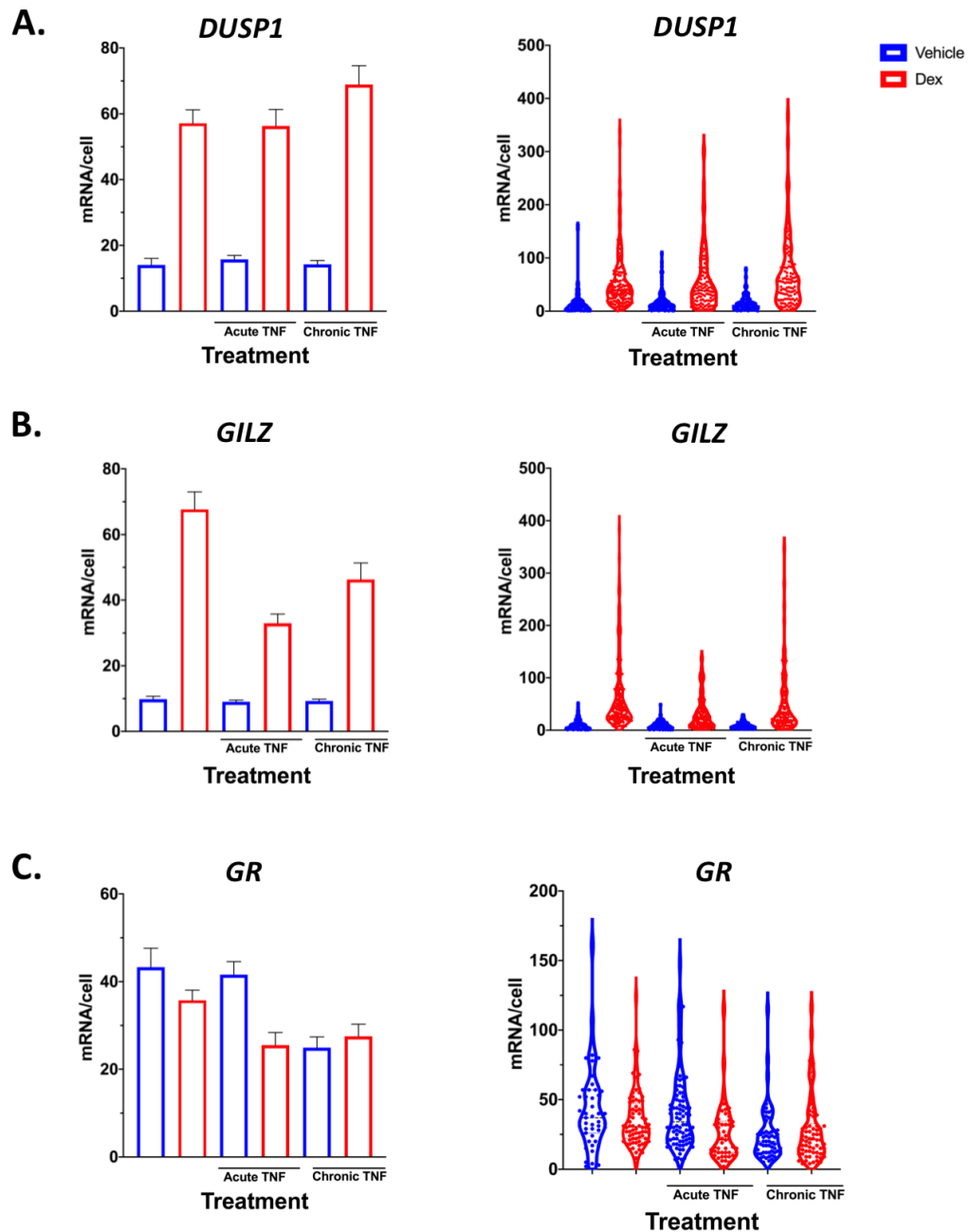
Figure 5.31: TNF treatment impairs Gc induction of GILZ but not DUSP1. M059K cells were pre-treated with TNF for 1 hour (acute) or 20 hours (chronic), then treated for 4 hours with a vehicle control (blue), or 100nM Dex (red). Cells were probed for *DUSP1, GILZ* or *GR* transcripts. Average expression for each gene is shown (left), and violin plots of individual gene expression (right). Results shown are the mean of 2 independent experiments. Error bars denote mean +/- SEM.
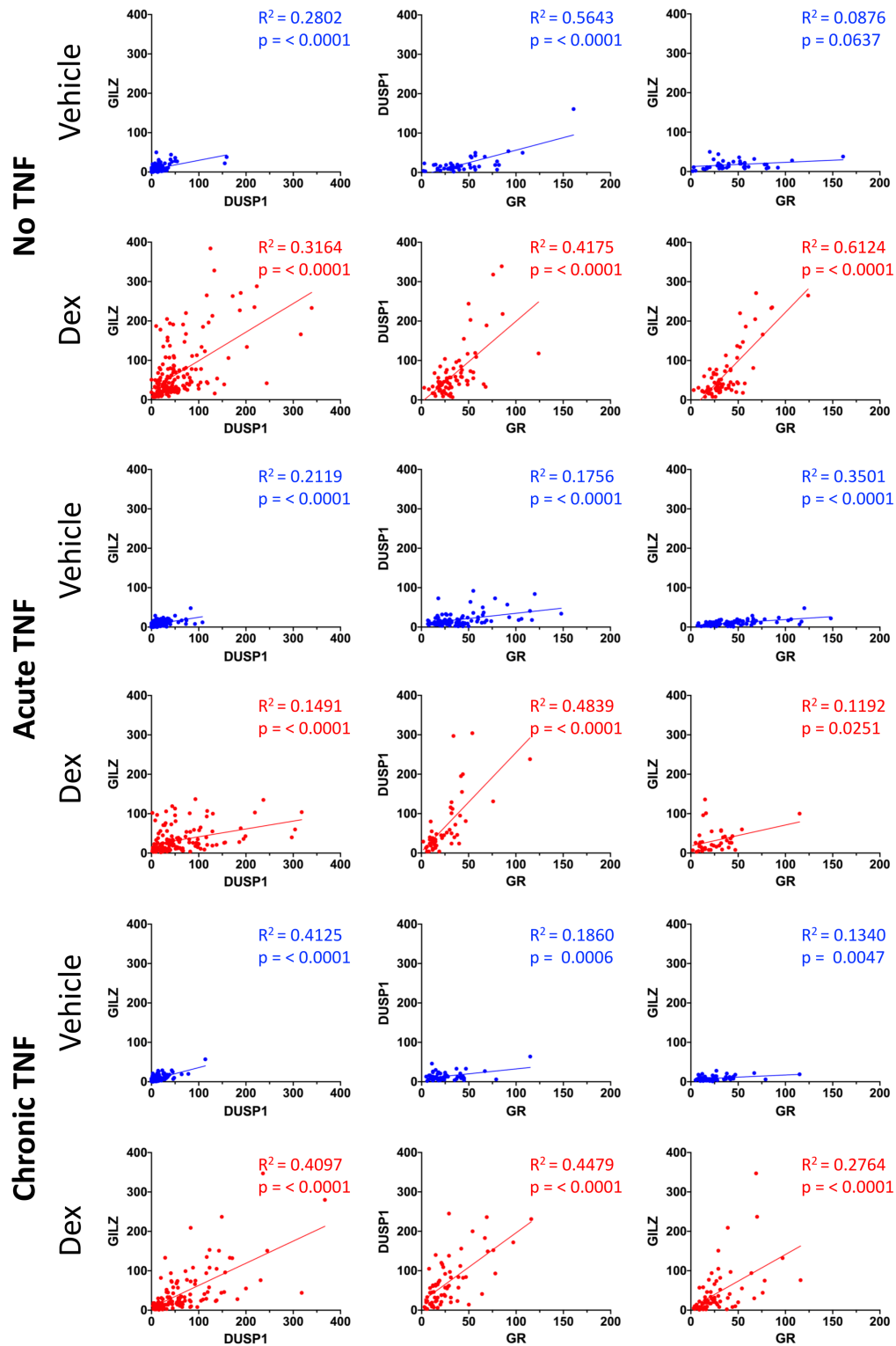
Figure 5.32: Expression of DUSP1, GILZ and GR do correlate, but this does not completely explain the heterogeneity in response. Cells were pre-treated with TNF for 1 hour (acute) or 20 hours (chronic), then treated for 4 hours with a vehicle control, or 100nM Dex. Cells were probed for *IL6, IL8* or *GR* mRNA. Expression of these genes were graphed, and correlation was tested using Pearson's tests, and the R^2 value was calculated. For *DUSP1* and *GILZ* correlation, results are the sum of 2 independent experiments. For *GR* correlations, results are the sum of 1 independent experiment. At least 50 cells were analysed within each experiment.

5.3 Discussion

Single cell RNA-seq is an exciting new technology which promises to unveil complex mechanisms of regulation within gene expression (303, 309). This technology has been used to increase understanding of the mechanisms by which the binding of Gc to its ligand leads to the transcription of GR target genes, and how this process can vary between individual cells.

The single cell RNA-seq preparation yielded a high number of viable single cells for each of the four conditions and the sequencing process was successful, as seen through the QC data. This has shown a large library size for each cell, with relatively few outliers. Cells with low number of transcripts can be indicative of cell death, or ruptured cells, resulting in low capture (294). It is therefore common to enforce a cutoff, such as that seen here (310, 311). The specific cutoff of 3 MAD has also been previously used within the literature (312). In addition, features such as the relatively low expression of mitochondrial genes indicates that cells were not under physiological stress (313). As a further control, cells with high mitochondrial gene expression were also filtered out. In addition, these quality matrices are unchanged across treatment groups, suggesting that Gc treatment does not affect the viability or stress of the cell population. Overall, these factors lend confidence to the quality of the data, and the conclusions drawn from it.

The first, and perhaps most obvious cellular feature to examine regarding variation in Gc responses was the cell cycle phase of individual cells. Using the transcriptional output to divide cells into estimated cell cycle phases has been

widely used within single cell RNA-seq analysis (292, 314, 315). Cell cycle phase has been shown to affect phenotypes within multiple single cell RNA-seq analyses of developmental populations (296, 316, 317). While cells in distinct cell cycle phases separate by PCA analysis, there appeared to be no relationship between the GR response and cell cycle phase. We had initially predicted that due to differences in chromatin condensation within cell cycle phase, GR binding might be altered, thus affecting the transcriptional output. This was not the case, and there appeared to be no significant difference in transcriptional output. This is confirmed by recent data, predicated on providing a model to combine single cell RNA-seq with a method of timing mRNA production. The assay consisted of A549 cells treated with Dexamethasone for time periods from 0 – 10 hours (318). 4-thiorudine was used to label newly synthesised mRNA for the final 2 hours of treatment. Cells were then prepared for single cell RNA-seq. When analysing the newly synthesised mRNA, rather than total mRNA content, overall mRNA output was reduced in early G1 and late G2M phases, however, there was no correlation between cell cycle phase and GR response. Applying this to our data, this may suggest that cells within these cell cycle phases would respond to a slightly lower level, but fall within the same population.

When comparing the single cell RNA-seq cell cycle phase data with the propidium iodide staining, the data correlated but did not precisely match. The single cell RNA-seq showed a much higher proportion of cells within G0/G1 compared with the PI staining. This may be due to differences in experimental procedure; the classification procedure may not be as effective as expected at identifying cells within G2. Alternatively, differences in experimental procedure may have altered the number of cells entering mitosis. Further, there also does not appear to be

any effect of Gc treatment on cell cycle phase within the single cell data, which further confirms the work in the previous chapter, which suggested that Gc do not affect GBM cells through the induction of cell cycle arrest.

At a population level, differential expression of genes in response to Gc treatment is well established, however, how this response manifests in individual cells is still unknown. More broadly, inherent variability in response to transcription factor activation has long been presumed, but the advent of technologies which allow us to analyse the response at a single cell resolution have finally allowed us to explore factors determining this variability (319, 320). Using PCA and t-SNE analysis, it was clear that Gc treatment led to a profound change in phenotype across the cell populations, however, there was also variability within this.

Bulk RNA-seq analysis was used to inform the downstream analysis of the data. As the bulk sequencing is limited to 3 technical repeats for each condition, and uses a larger volume of RNA for library preparation, results are more robust, with less noise within the system. This approach does have its disadvantages; principally, that by limiting analysis to genes which had sufficient differential expression to be found at a population level, we may be ruling out genes with more subtle differential expression between conditions, or for which high levels of heterogeneity within each condition could prevent differences between conditions from becoming significant at a population level. We concluded, however, that it was the only way to definitively confirm that the genes chosen for analysis further down the pipeline were not noise-induced artefacts within the system.

As previously discussed, we had predicted to see one of two types of response, either a binary or a rheostat response. Both models have been modelled within the literature, and are believed to show distinct transcriptional signatures. A binary response would indicate that expression of a gene could either be turned on or off. This means that the population would consist of two types of response, one with expression turned off, and one with expression turned on. These cells with expression turned on would all respond at the same maximal level. Alternatively, for rheostat genes, expression would form more of a spectrum, or graded, response. The population would gradually move up with increasing doses of ligand. Both types of response have been previously been modelled using fluorescent reporter genes, however the relevance of their results have been questioned. Such assays rely on the quantification of protein (e.g. GFP), rather than the quantification of mRNA levels. Models have shown that differences in mRNA and protein half-lives and translational efficiency can have marked effects on the model of response seen at a protein level (201). Therefore, by analysing the response at an mRNA level on a single gene basis, it is possible to determine which model fits the gene expression seen following GR activation.

Somewhat surprisingly, however, we found evidence for both types of response. Some of the density plots appeared to show that some genes consisted of a "binary" type response, whereby we saw two distinct populations of expression, and differences in proportions within these populations led to differences in the strength of the response at a population level. Alternatively, other genes consisted of a more graded response, whereby the entire population of cells showed a shift in expression in response to a ligand. We also saw a third response, which consisted of a widening of the response peak in response to

ligand, thus increasing the variability of the response. This population may consist of genes which fit somewhere between both responses, however, further work would be required to confirm this.

Analysis of GR binding in relation to sensitivity to Gc revealed that the number of binding sites did not reflect whether genes were responsive to low or high affinity Gc. It is important to note however, that genes that were downregulated tended to have fewer binding sites that upregulated genes, a difference that could be explained by mechanism of regulation – direct DNA binding versus tethering. The most important caveat to this work is that the ChIP-seq data is from a different cell line, which could potentially have a very different Gc response. Given how specific the Gc response is, depending on cellular clues and the microenvironment, it is probable that there are stark differences between A549 and M059K cells. Therefore, to fully relate the single cell data with GR binding data, it would be necessary to complete ChIP-seq analysis within M059K cells.

Further than this, GR binding sites are complex, and many of them may be found thousands of base pairs from the gene they regulate (321). Through the 3 dimensional architecture of the chromatin landscape, this binding site may be brought close to the gene, however, this information is not capable of being deduced through ChIP-seq analysis (322). Other new technologies, such as HiC, have begun to address these questions, and will hopefully be combined in the future with sequencing technologies.

Due to the novelty of single cell RNA-seq technology, it is still necessary to validate the results to confirm differences in response are not simply artefacts

introduced during sample preparation, or due to limits of detection sequencing technology. smFISH has been previously used within the literature to validate single cell RNA-seq data (323, 324). Our initial target genes consisted of *GR, DUSP1* and *GILZ.* Through the simultaneous use of three probes to these genes, we could confirm *GR* expression as relatively consistent across treatment groups, and could also directly compare expression of the two DE genes within the same cells. Once validated, this would provide a platform to test different drug treatments such as inflammatory cues, or chemotherapy to investigate how responses are altered.

smFISH staining required several stages of optimisation. Firstly, it was necessary to use an unbiased method of quantification of staining. Due to the use of three probe sets, it was not possible to include an additional cytoplasmic stain. Therefore, to create masks to analyse individual cells, it was initially necessary to manually demarcate each cell using freehand masks in ImageJ. This method is clearly not precise enough, and potentially subject to user bias. Therefore, FishQuant was identified as a promising tool for automated quantification of staining (325, 326). FishQuant allows the quantification of multiple colours within the same cell. In addition, it allows for the analysis across three dimensions to distinguish between debris and spots.

The second point of optimisation was image acquisition. Ideally, an automated system would be used in order to acquire an appropriate number of z-stack images for quantification. Unfortunately, the only fully automated system available was the Operetta, which employs a widefield microscopy system. Widefield microscopy conveys images of a lower resolution, and with a higher

risk of bleed through between planes within a z-stack of images. This leads to a reduction in the resolution of final images. When considering techniques, such as smFISH, which require high resolution to visualise small, defined spots, the resolution seen with the Operetta system was not sufficient. Therefore, it was necessary to use a confocal microscope system. Using confocal imaging, it is also possible to take z-stacks with slices much closer together, allowing the spots of staining to be more obvious. This process can also be partly automated, using Nikon software to automatically image several fields of view within each well.

The results from smFISH indicated that expression of *GILZ* and *DUSP1* genes was increased following Gc addition, and that the response was variable, in line with scRNA-seq data. The correlation seen between expression of Gc responsive genes and *GR* suggests that GR expression accounts for some of the variability observed, but that there must be additional regulatory factors involved. Consistent with this, there was weaker correlation between the two Gc target genes. Therefore, while *GR* expression imparts some effect on the magnitude of the response, *GR* can induce *GILZ* with little impact on *DUSP1* expression in the same cell. It can therefore be concluded that gene expression changes in response to Gc are controlled in both a cell-specific and a gene-specific manner. As a critical next step Dex treated cell populations from the scRNA-seq data could be separated into cell populations based on either high or low *GILZ* expression and determine which other genes/gene sets could predict a stronger *GILZ* response. This could also be repeated using *DUSP1* as a marker gene, and possibly others to identify master regulators of the Gc response. Of particular interest would be genes that predict good or poor responses, that were not themselves regulated by Gc. Once identified, these sensitivity marker genes

could be analysed alongside Gc responsive genes using the smFiSH assay to determine correlation and identify inherent, cell specific markers of Gc sensitivity.

In contrast to the Gc induced genes *GILZ* and *DUSP1*, there was no correlation between suppression of *IL6* and high *GR* expression. This is an interesting finding, since the mechanism by which *GR* regulates *GILZ* and *IL6* are different. While GR binds directly to regulatory sites to increase *GILZ* expression, GR tethers to NFkB and AP1 proinflammatory transcription factors and inhibits their function. In this context perhaps the expression of NFkB and AP1 in driving expression of IL6 is the most important factor. It would therefore be interesting to correlate *IL6* regulation in smFiSH assays alongside expression of GR in combination with p65 or AP1 gene expression. With this in mind, it would also be interesting to also analyse genes which are induced the proinflammatory transcription factors and potentially inhibited by Gc through direct DNA binding of GR, such as *PLAU, E2F7* or *AMIGO2*.

The work herein has described complex mechanisms of gene regulation, however, we have not discussed the levels of regulation at translation. Therefore, as an important piece of future work, it would be important to correlate mRNA and protein expression, for both GR, other transcription factors and for GR target genes. This could be achieved using the ViewRNA ISH kit used for the smFISH. Whilst the kit was used herein only to examine mRNA expression, it can also be used to compare mRNA and protein expression using an antibody specific to the protein of interest. Ideally, GR protein expression could be compared with *GR* gene expression, but also DE gene expression, to confirm a correlation.

Another interesting finding from the smFISH assay was that Gc induction of *GILZ* was impaired following acute or chronic Dex treatment. This experiment needs to be repeated, but the fact that the Gc induction of *DUSP1* was not impaired in the same cells, and under the same experiment conditions, suggests a technical issue is unlikely to account for this. Reports suggests that DUSP1 is transactivated through a mechanism of tethering, and the different effects of TNF may again reflect different mechanisms of GR action (238, 327). It would therefore be interesting to repeat this experiment including a broader panel of transactivated genes such as *PER1*, *FKBP5* or *SNAI2*. The use of GR modulators which favour transactivation or transrepression would provide interesting tools to interrogate this further pharmacologically.

The gene ontology analysis for the scRNA-seq, in addition to the bulk RNA-seq presented in the previous chapter, identified transcriptional misregulation in cancer and p53 effector pathways as terms, which includes genes that control DNA repair and stemness. While the smFiSH assay is useful to understand Gc responses at the single cell level in clonal cell populations, it also provides a cost effective way to explore how Gc may drive tumour evolution in more complex primary cultures and tissue sections. TNF treatment reflects one of the inflammatory cues in the brain tumour environment, but combining the 96 well smFiSH assay with transwell assays to coculture GBM cells with immune or stem cells could provide additional information on how Gc function within GBM.

In addition to examining how cells crosstalk within the tumour environment, it would also be important to track how Gc signatures change over time, and the impact of chemotherapy. Gc are known to be important regulators of epithelial-mesenchymal transition and so could link to cancer cell dormancy in addition to

chemoresistance. Repeating the smFiSH assays in cells that have been cultured for longer periods in Dex would be informative, although ideally another round of scRNA-seq would be preferable as the Gc response will likely evolve over time, and the previous scRNA-seq was only completed after 4hrs. The key limitation of single cell RNA-seq is that it captures a single snapshot of the Gc responses at one time. Analysing a time series would be a good option, but in addition access to new technology such as a nanobiopsy would permit longitudinal tracking of individual cells over time.

Through the combined scRNA-seq and bulk RNA-seq analysis, I have identified a panel of 99 genes that have been identified as robust markers of Gc action in GBM cells. A limitation of current sequencing data from GBM patients is that often, information relating to dose or even administration of Gc are not included. Moving forward it would be interesting to access public RNA-seq data from brain tumour patients and retrospectively identify tumours with high prevalence of Gc signatures and correlate this with patient outcome. This would be done by stratifying tumours into clusters based on the expression of the 99 genes (or possibly dividing into two signatures, one for upregulated genes and one for downregulated genes). A similar approach has been used by my supervisor to stratify triple negative breast cancer subtypes based on nuclear receptor expression.

This pilot dataset therefore provides some insight into how Gc responses of individual genes vary at the single cell level and provides exciting opportunities for further study. Already there are possible hints as to how the different mechanisms by which GR regulated genes might determine the robustness of the response, with distinct points for control. More work, using equally cutting-

edge technologies, and application to clinically relevant samples are needed. In addition to better understanding how Gc work, it is also hoped that this can feed into work presented in the previous results chapter to identify safer Gc to treat GBM.

Chapter 6 Discussion and Future Perspectives

Gcs are first line treatments for many inflammatory conditions. They are an essential means to limit the potentially damaging effects of inflammation, which if not properly controlled can cause serious long term consequences or even death (5). This is particularly important in the context of GBM, a highly aggressive form of brain cancer. Gc are used throughout GBM treatment, often from the point of diagnosis, to reduce oedema and its secondary side effects (328). Their use not only improves quality of life for patients, but also effectively reduces the risk of stroke. Unfortunately, patients prescribed higher doses of the potent synthetic Gc Dex also have reduced survival times (182). The reason for this remains controversial. Some believe that as the patients with most severe symptoms by definition also receive the highest doses of Gc, the corresponding correlation is merely a reflection of disease severity. However, growing evidence suggests that Gc directly reduce the efficacy of standard radiotherapy and chemotherapy (182, 185). Fully understanding the mechanism of Gc function in the context of GBM is critical to improve therapeutic options and help people live longer, with improved quality of life.

Despite over 60 years in clinical use, it is only over the last decade that we have gained real insight into mechanisms underlying Gc action. We now know that Gc responses are under multiple levels of control, which enables tissue and context specific responses. This is dependent on factors such as the chromatin availability, the presence of other transcription factors, and changes to the tissue microenvironment, such as the presence of inflammation (51, 329, 330). On one hand, this underlies their adaptability and consequently broad application to a

range of conditions as Gc exert effects on almost every cell type in the body. However, it also means that extrapolating information from, for example, a lung inflammation model, to make predictions for Gc action in GBM more challenging.

There are now an increasing number of studies investigating Gc action using *in vivo* models of GBM or in GBM cell lines (182, 331). These studies have been valuable in suggesting that Gc treatment does in fact increase either recurrence and aggressiveness of GBM and/or promotes treatment resistance. The mechanisms responsible, however, have not been clearly investigated. This is a major limitation of current studies and can be attributed, at least in part to the duration of Gc treatment which are typically longer and therefore identify secondary effects. These studies aim to recapitulate *in vivo* environment by using repeated, high doses of Gc over a period of several days. This approach has its merits, however, in this context cell cycle arrest (and little else) appears prominently in sequencing studies as the mechanism (222, 279). However, it is possible that in these conditions, with high doses and prolonged treatments, more subtle cellular effects, which occur earlier, may have been masked.

6.1 Primary Gc effects in GBM cells

To identify primary effects, GBM cells were subjected to an acute Gc challenge with Gc of different affinities and potencies and gene expression changes were analysed. This revealed a number of potential effectors – including other transcription factors known to regulate cancer, DNA repair pathways and stem cell regulators. Given that the two primary therapies used within GBM, namely radiotherapy and Temozolomide, rely on the induction of DNA damage, it was

hypothesised that Gc reduces the efficacy of both therapies by influencing the rate of DNA repair (104, 160).

Cell viability assays demonstrated that pre-treatment with Gc 24 hours prior to irradiation or chemotherapy treatment led to increased survival of GBM cells over the next few days. It is important to note, that Gc at these doses in the same cell line did not induce cell cycle arrest at the same timepoint, suggesting cell cycle effects at the time of radiotherapy or chemotherapy are unlikely to be a major determining factor in this context. Moreover, Gc treatment did not influence the amount of damage induced by chemotherapy or radiotherapy treatment, but instead reduced the level of damage over time. Overall, this suggests that the treatment of GBM cells with Dex leads to an increase in DNA repair responses, which in turn reduces therapeutic efficacy of radiotherapy and chemotherapy.

MGMT expression has been well-characterised as an indicator of treatment response in GBM. There has been previous research showing that Dex treatment is capable of increasing MGMT expression within GBM cells, including M059K cells, however, within our research, we were unable to detect MGMT expression within M059K cells using qPCR (171). MGMT has also previously been detected in M059K cells using western blotting, and a key priority of future work will be to test MGMT expression in M059K using this method, and in other cell lines, to determine if we can replicate these previously published results.

Further work will also be required to further investigate the roles of both Rad51 and p53 in relation to Gc-mediated therapeutic resistance. In particular, Rad51 knockdown showed mixed effects on GBM cell survival. It would therefore be

beneficial to quantify Rad51 foci formation following IR and TMZ, in order to determine if Dex could affect Rad51 activation, and thus lead to an increase in homologous recombination. To date, there has been no literature to suggest a functional relationship between Rad51 and GR, and these results could have implications in a wide range of conditions for which Gc are routinely prescribed.

GR is known to bind to tens of thousands of sites along the genome, recruiting large transcriptional regulatory complexes. Sites of active transcription accumulate damage and so given the role of GR in regulating transcription it is perhaps not surprising that GR can increase the expression of both DNA repair and cell cycle arrest genes as a safeguarding mechanism. Conceptually, this would buy time for any potential damage induced by the act of transcription to be actively repaired, and prevent any potentially damaging mutations from being replicated within the cell population. In the context of 'normal' biology this is an important feature. However, within the context of cancer therapeutics, which rely on inducing DNA damage and cell death it can lead to the unwanted reduction in efficacy seen within GBM cells. Alternative, more targeted therapeutics are therefore needed.

6.2 Increased safety using selective GR modulators

Despite these potentially damaging effects on therapeutic efficacy, care must still be taken when considering withdrawing Gc use within patients with severe inflammation. For many, Dex treatment leads to an invaluable increase in quality of life, and oedema itself may lead to premature death if not quickly and efficiently controlled (331, 332). Current guidelines recommend tapering of Dex following surgery, and prior to treatment with radiotherapy and chemotherapy (333, 334).

However, this is not always possible, as for some patients, removal of Dex treatment may lead to a recurrence in potentially fatal symptoms (335). For these reasons, care is needed to ensure that any alternatives are as rapid and effective as Dex, whilst reducing the possibility of the potentially damaging side effects on therapeutic efficacy. A selective GR ligand could be a promising alternative to Dex usage in GBM.

Gc are potent modulators of inflammation, but also control aspects of normal homeostasis, most notably metabolic functions. This means that patients taking Gc long term for rheumatic disease for example also develop a range of undesirable side effects such as osteoporosis and type 2 diabetes. There have been huge efforts by the pharmaceutical industry to develop a new generation of Gc that are equally efficacious to reduce inflammation, but have less impact on metabolic function (336). This has been challenging and has required innovative approaches to develop drugs with unique pharmacology and iteratively test them. The major premise for screening these novel compounds is based on theory that GR transactivation of genes leads to damaging side effects, such as effects on metabolism, and also potentially the effects on DNA repair reported herein (5, 337). Meanwhile, the transrepressive effects of GR primarily lead to the beneficial effects on reducing inflammation (338). By creating GR ligands which preferentially led to transrepression, with limited transactivation, many pharmaceutical companies had hoped to create effective Gc with reduced side effect profiles.

Needless to say, this has been to some extent an overly simplistic approach. Many of these ligands have not fulfilled their initial promise in initial laboratory

testing or within clinical trials. Despite several phase II and phase III trials of ligands such as Maprocorat and Fosdagrocorat, results have not been released, suggesting results may not have been positive (336). This is, in part, due to the unexpected complexity of genomic effects, which do not correspond to the simplistic dichotomy of transactivation/transrepression (336, 339). The work within this thesis, however, has suggested that within GBM, there is potential that some commercially available selective GR ligands repress expression of proinflammatory genes, without reducing the efficacy of IR or TMZ. This would suggest that these selective ligands may be a possible avenue of investigation for replacing Dex within the clinic.

Compound A, in particular, showed high efficacy in the reduction of inflammation, but did not increase GBM cell survival following IR. This is encouraging; however, previous research has indicated that its therapeutic window is limited, and high doses are toxic in mouse models, and due to these concerns, it is not approved for use in humans (336, 340). Therefore, whilst CpA has been beneficial as a proof of concept, other selective ligands must be investigated for potential therapeutic use. Many of these selective ligands have been through Phase I and II clinical trials as therapies for other conditions, so could be quickly repurposed. The next steps will be to expand the panel of compounds in testing to determine which have potential to reduce inflammation, but not impact efficacy of radiotherapy or chemotherapy, specifically using comet assays and yH2AX staining. Further work, using these assays, developed as part of this PhD, will clearly be required in collaboration with pharmaceutical companies before this can be trialled within patients.

Despite promise of testing compounds for effect on DNA repair and cell survival outcomes, it remains unclear exactly how this might occur. It is of critical importance to determine the underlying mechanism, both in order to characterise this novel mechanism of Gc action, but also to develop more specialised high throughput assays that could be used to screen compound libraries. As a continuation to this project M059K cells will be treated with radiotherapy and chemotherapy following 24hrs pre-treatment with either vehicle, Dex or compound A, then analysed by RNAseq. Genes differentially expressed between Dex or Compound A compared with vehicle will be identified, and those regulated by Dex, but not by compound A, will be a particular focus. Although compound A is a 'tool' compound and not a possible therapeutic, its use in this context provides the opportunity to determine mechanistically how differences in the cellular response to Dex and Compound A are determined at a transcriptional level, to guide new therapeutic screens.

The most likely candidate mechanism would be the transcription of DNA repair effectors *CDKN1A, BCL2L1* and *DDIT4,* but others such as *SNAI2, TBX2* and *CEBPB* are also plausible candidates. CDKN1A plays a key role in the regulation of cell cycle progression and apoptosis. Its roles are complex; for instance, through cell cycle arrest, CDKN1A may allow DNA repair to occur, however, nuclear CDKN1A is also known to induce apoptosis of damaged cells (341). Increased CDKN1A expression has been shown to increase resistance to both IR and TMZ within GBM (342, 343). DDIT4 also affects cell growth and apoptosis, in its role as an inhibitor of the mTOR signalling pathway (344). Increased DDIT4 expression has been shown to increase resistance to both IR and TMZ resistance in GBM, possibly due to its role in inhibiting hypoxia-induced cell death (345).

BCL2L1 prevents apoptosis directly through its binding of apoptotic pore-forming proteins, inhibiting their function (346). Therefore, through the upregulation of genes such as these, Gc can directly alter therapeutic efficacy.

In addition, our dataset also showed Gc upregulated stem cell-related factors, such as *SNAI2, DKK1* and *EFNB2.* Stemness is another route by which cells can evade treatments, and this relates to tumour cell plasticity *in vivo* (347). Stem cells are key in GBM recurrence; these cells are more resistant to treatment, and are capable of reconstituting the tumour once treatment has been completed. Therefore, an upregulation of these genes may increase the proportion of stem cells within the tumour environment, rendering a larger portion of the tumour resistant. This may also be linked to the changes in morphology seen within U87 cells following Dex treatment.

Looking to the future, it is also important to consider broader application. The majority of this work has been completed in one cell line. Of course, the reductionist approach of using monolayer cultures of cell lines has advantages as it permits controlled analysis of relatively homogeneous populations to determine direct action of Gc on GBM cells, and this system is also amenable to high throughput screening approaches for the same reason.

Firstly, it is still necessary to extend our findings to analyse a panel of primary cells, organoids or even tissue explants. GBM is a highly heterogenous disease, both between patients, and within the same tumour. Subpopulations can exist harbouring differing mutations and different resistances to therapy. It is therefore essential that this heterogeneity is reflected within our model systems. Our

analysis of Gc action in a clonal cell line provides the platform for this, as we identify a core module of Gc targets that can be specifically analysed in more complex systems.

Secondly, with the popularisation of organoid cell models has come an appreciation for the role of the surrounding tumour microenvironment in affecting tumour cell function (348, 349), and specifically the tissue microenvironment (350, 351). Communications between cells, both through direct cell-cell contacts, or through secreted factors, such as cytokines, can have a large impact on cell function and phenotype. It would therefore be important to identify cell types within tumour sections, in order to effectively recapitulate these cell types within an *in vitro* system. Through the use of tissue sections, it will also be possible to determine if other nuclear receptors, such as PR and MR, are expressed within the tissue microenvironment, and if they are expressed, what cells they are expressed within. It has previously been shown, for instance, that neurons exhibit high PR expression, compared with cells of glial origins (352, 353), and so PR modulators might represent an alternative therapeutic option.

6.3 Heterogeneity in Gc responses in GBM cells

The original RNA-seq analysis discussed in Chapter 4 investigated average Gc responses across large populations of cells. This type of data assumes that Gc addition results in identical responses in each cell within these populations. As our knowledge of single cell dynamics has broadened, it has seemed increasingly unlikely that this would be the case. If we start to consider how Gc might induce distinct transcriptional responses in heterogeneous cell populations, we first need

to consider how variable Gc responses are in homogeneous populations. In reality, Gc needs only to induce treatment resistance in a relatively small population of cells to evade death. Over time, these cells could expand, and cause the tumour to regrow.

Within the tumour environment there are multiple cell types present, but even within the tumour there are also potentially multiple clones. These tumour clones can expand and switch phenotype and therefore change tumour responses over time. Single cell RNA sequencing has enabled such concepts to come to the forefront of cancer research. Huge numbers of studies are revealing complex and dynamic changes to tumour populations. To date the majority of studies are defining different cell phenotypes, but is it possible to look at acute cell treatments in this context also? The disadvantage of single cell approaches is that the untreated and treated cells are – by definition - from different populations, so how can you determine which individual cells have responded or not? In addition what proportion of cells respond to Gc? We know that across the population level it is easy to observe transcriptional changes, but it is not clear whether this is represented by the majority with relatively modest and homogeneous response, or instead a large response by fewer cells.

To answer this question, single cell RNA-seq was completed on the M059K cell line, using the same concentrations and duration of Gc treatment as used in the bulk RNA-seq from the previous chapter. Using the same experimental system provides a means to compare single cell responses with population means, and also as the cell population is theoretically identical, provides the opportunity to determine variability in the Gc response without the confounding possibility of

multiple different cell types as might be predicted *in vivo*. Based on previous studies that employed mathematical modelling to predict transcriptional responses, we had hypothesised that the response would follow either a binary or graded response (188, 202). The binary response explains the average as a simple model where there are two thresholds of expression, and Gc treatment induces a proportion of cells to shift from the lower to the upper threshold of expression. The graded response is more complex, whereby expression of a gene has no lower threshold, and activation by Gc is variable in all cells which contribute to the population mean. The data showed that both responses could be observed to some degree, in a gene specific manner. Most genes such as *DUSP1* and *DNAJB4* appeared to exhibit a binary-type response, whilst others, such as *ANKRD1* and *MT2A* appeared to show a graded response. This seemed to be more of a reflection of baseline expression of the gene rather than a special mechanism of Gc action.

A limitation of the single cell RNA-seq was lack of read depth limiting detection of core Gc regulated genes. Genes with low baseline expression were not present in our dataset and so could not be explored – this was particularly evident with low expressed genes that were robustly downregulated by Gc such as ICAM and VCAM. Some of the genes previously linked to treatment resistance in GBM, such as *SNAI2, DDIT4, CEBPB*, and *CEBPD* were differentially regulated in the single cell dataset. Future work would further explore how these genes are changed within the population. For instance, are these genes upregulated within a small population of cells, corresponding to the creation of a treatment resistance subpopulation, which account for increased survival at a population level?

Aside from demonstrating that GR expression was a driving factor in the magnitude of response in an individual cell, the mechanism underlying the reason for a binary or graded response remains unclear. A pilot analysis indicated that there may be a link between the type of response and the baseline expression within the target gene. A major limitation was that some of these observations were based on the use of publicly available ChIP-seq data, which was carried out in an unrelated cell line – A549. Whilst the sequence of GR binding sites is unchanged between different cell types, the cellular context is crucial in determining which of these sites GR will bind under either resting conditions or following ligand addition, and this is dictated by chromatin architecture. It is therefore a priority that further unbiased, large scale ChIP-seq analysis is performed to confirm these observations and to try to determine what other cellular features, if any, could predict the strength of the response within individual cells.

As part of the validation process, single molecule FISH assays were optimised, and a high throughput image analysis pipeline was developed to quantify single transcripts in individual cells. Using a small gene panel with these assays, similar transcriptional signatures were shown compared with the single cell RNA-sequencing – in fact with greater sensitivity. These experiments also demonstrated that an inflammatory stimulus led to a robust increase in proinflammatory mediators across the cell population, and this was abrogated through Gc addition. This assay can therefore be used to analyse the effect of the selective GR modulators – to determine if there is a small response in a few cells or if they are truly selective across the entire cell population. This also allows

further investigation of potential environmental modifiers of the Gc response, both investigating further genes, and under different cellular contexts.

The benefit of the smFISH assay is that it can be applied to primary cell lines, spheroids or even cultured tissue sections to permit analysis of different cell populations in architectural context – for example analysing Gc responses in cells contacting other tumour cells vs immune cell populations, or adjacent to regions of necrosis. Additionally, expanding the panel to investigate some of the GR transcriptional targets implicated in stemness would be of particular interest. Evidence suggests that stem cell features induce dormancy for cells to evade treatment, and single cell RNA-seq has previously highlighted a continuum of expression of stem cell markers within GBM cells (197, 198).

One limitation to conducting single cell RNA-seq or indeed smFISH assays is that it only provides a snapshot in time. The vehicle and Gc treated cells are entirely separate, and so while we can evaluate treatment differences in clonal populations, this becomes more challenging in heterogeneous cell populations. Ideally, future work would track Gc responses longitudinally from individual cells over long periods of time to determine whether Gc can promote phenotypic switching and whether this could impact efficacy of radiotherapy or chemotherapy. A possible route to achieve this would be use of nanopipette technology. Nanopipettes are an exciting new technology, which will allow the sampling of mRNA from the same cell across multiple timepoints (354, 355), and will allow direct identification of a shifting phenotype within the same cell over time (356). These technologies are still in their infancy, but could revolutionise our understanding of how the Gc response changes over time within individual

cells, and in turn how this affects the population response as a whole. This is applicable not only to tumour evolution in the context of GBM, but also treatment resistance in inflammatory disease.

This project, like others, has highlighted even further levels of complexity in the GR response than had been predicted. As the technologies available to analyse genome wide responses are continuously improving, we would hope that they can be utilised for increasingly physiologically relevant observations. Overall, the work within this thesis has added to the understanding of Gc action, both from a basic science and a clinically relevant perspective. It is hoped that the discoveries of this project - relating to Gc selectivity and heterogeneity in Gc responses - will be the basis of future work to fully characterise Gc function, in order to ensure their safe usage, both within GBM and other inflammatory conditions.

Chapter 7 Summary

The data presented in this thesis explores how Gc, a main part of GBM standard therapy, influences GBM cell function, and efficacy of standard treatments. Through this, this work has identified a role in reducing the efficacy of chemotherapy and radiotherapy that cannot be explained simply through direct cell cycle effects, as others have reported. The role of Gc in controlling DNA repair is novel, and provides a platform to screen other selective Gc. Indeed, this work has identified a tool compound, compound A, which promotes beneficial anti-inflammatory effects without activating DNA repair.

This work has also considered how sensitivity to Gc might be altered in tumour cell populations, which are inherently heterogeneous. As a critical first step, Gc responses were examined at a single cell level to reveal heterogeneity of GR action in a clonal cell line. Core gene modules were identified in individual cells that could help stratify Gc responses in these systems. This analysis also identified that GR expression is highly variable even in clonal cell lines, and is the major driver of Gc sensitivity. While unravelling Gc actions in more complex heterogeneous tissues will be more challenging, a panel of genes could provide a benchmark to dissect future transcriptome data.

Future studies will build on this work to screen larger panels of selective GR modulators that have improved safety profiles in GBM. Tracking individual cells over time using nanopipette technology will provide much needed information on how Gc sensitivity, and the efficacy of radiotherapy and chemotherapy might evolve over time. It is hoped that this work can be used to improve therapeutic strategies within GBM.

References

1.   Hardy RS, Raza K, Cooper MS. Therapeutic glucocorticoids: mechanisms of actions in rheumatic diseases. Nat Rev Rheumatol. 2020;16(3):133-44.

2.   Chung S, Son GH, Kim K. Circadian rhythm of adrenal glucocorticoid: Its regulation and clinical implications. Biochim Biophys Acta Mol Basis Dis. 2011;1812(5):581-91.

3.   Lindenberg M, Kopp S, Dressman JB. Classification of orally administered drugs on the World Health Organization Model list of Essential Medicines according to the biopharmaceutics classification system. Eur J Pharm Biopharm. 2004;58(2):265-78.

4.   Miller WL, Auchus RJ. The molecular biology, biochemistry, and physiology of human steroidogenesis and its disorders. Endocr Rev. 2011;32(1):81-151.

5.   Ramamoorthy S, Cidlowski JA. Corticosteroids - Mechanisms of action in health and disease. Rheum Dis Clin North Am. 2016;42(1):15-31.

6.   Dineen R, Stewart PM, Sherlock M. Factors impacting on the action of glucocorticoids in patients receiving glucocorticoid therapy. Clin Endocrino. 2019;90(1):3-14.

7.   Mathieu M, Drelon C, Rodriguez S, Tabbal H, Septier A, Damon-Soubeyrand C, et al. Steroidogenic differentiation and PKA signaling are programmed by histone methyltransferase EZH2 in the adrenal cortex. Proc Natl Acad Sci USA. 2018;115(52):E12265-E74.

8.   Herman JP, McKlveen JM, Ghosal S, Kopp B, Wulsin A, Makinson R, et al. Regulation of the Hypothalamic-Pituitary-Adrenocortical stress response. Compr Physiol. 2016;6(2):603-21.

9.   Hammond GL. Plasma steroid-binding proteins: primary gatekeepers of steroid hormone action. J Endocrinol. 2016;230(1):13-25.

10.   Kuo T, McQueen A, Chen T-C, Wang J-C. Regulation of glucose homeostasis by glucocorticoids. Adv Exp Med Biol. 2015;872:99-126.

11.   Vgontzas A, Dijk D-J, de Kloet ER, Arvat E, Challet E, Oster H, et al. The functional and clinical significance of the 24-hour rhythm of circulating glucocorticoids. Endocr Rev. 2016;38(1):3-45.

12.   Fardet L, Petersen I, Nazareth I. Prevalence of long-term oral glucocorticoid prescriptions in the UK over the past 20 years. Rheumatology. 2011;50(11):1982-90.

13.   Paragliola RM, Papi G, Pontecorvi A, Corsello SM. Treatment with synthetic glucocorticoids and the Hypothalamus-Pituitary-Adrenal axis. Int J Mol Sci. 2017;18(10):2201.

14. Czock D, Keller F, Rasche FM, Häussler U. Pharmacokinetics and pharmacodynamics of systemically administered glucocorticoids. Clin Pharmacokinet. 2005;44(1):61-98.

15. Morin C, Fardet L. Systemic glucocorticoid therapy: risk factors for reported adverse events and beliefs about the drug. A cross-sectional online survey of 820 patients. Clin Rheumatol. 2015;34(12):2119-26.

16. Lovell AR, Ernst ME. Drug-Induced hypertension: Focus on mechanisms and management. Curr Hypertens Rep. 2017;19(5):39.

17. Patel GC, Millar JC, Clark AF. Glucocorticoid receptor transactivation is required for glucocorticoid-induced ocular hypertension and glaucoma. Invest Ophthalmol Vis Sci. 2019;60(6):1967-78.

18. Jozic I, Vukelic S, Stojadinovic O, Liang L, Ramirez HA, Pastar I, et al. Stress Signals, mediated by membranous glucocorticoid receptor, activate PLC/PKC/GSK-3β/β-catenin Pathway to inhibit wound closure. J Invest Dermatol. 2017;137(5):1144-54.

19. Rose AJ, Vegiopoulos A, Herzig S. Role of glucocorticoids and the glucocorticoid receptor in metabolism: Insights from genetic manipulations. J Steroid Biochem Mol Biol. 2010;122(1):10-20.

20. Jones CG, Hothi SK, Titheradge MA. Effect of dexamethasone on gluconeogenesis, pyruvate kinase, pyruvate carboxylase and pyruvate dehydrogenase flux in isolated hepatocytes. Biochem J. 1993;289:821-8.

21. Tanaka H, Shimizu N, Yoshikawa N. Role of skeletal muscle glucocorticoid receptor in systemic energy homeostasis. Exp Cell Res. 2017;360(1):24-6.

22. Coyne ES, Bedard N, Wykes L, Stretch C, Jammoul S, Li S, et al. Knockout of USP19 deubiquitinating enzyme prevents muscle wasting by modulating insulin and glucocorticoid signaling. Endocrinology. 2018;159(8):2966-77.

23. Morgan SA, Gathercole LL, Simonet C, Hassan-Smith ZK, Bujalska I, Guest P, et al. Regulation of lipid metabolism by glucocorticoids and 11β-HSD1 in skeletal muscle. Endocrinology. 2013;154(7):2374-84.

24. Peckett AJ, Wright DC, Riddell MC. The effects of glucocorticoids on adipose tissue lipid metabolism. Metabolism. 2011;60(11):1500-10.

25. Talabér G, Boldizsár F, Bartis D, Pálinkás L, Szabó M, Berta G, et al. Mitochondrial translocation of the glucocorticoid receptor in double-positive thymocytes correlates with their sensitivity to glucocorticoid-induced apoptosis. Int Immunol. 2009;21(11):1269-76.

26. Scheller K, Sekeris CE, Krohne G, Hock R, Hansen IA, Scheer U. Localization of glucocorticoid hormone receptors in mitochondria of human cells. Eur J Cell Biol. 2000;79(5):299-307.

27.	Lee S-R, Kim H-K, Song I-S, Youm J, Dizon LA, Jeong S-H, et al. Glucocorticoids and their receptors: Insights into specific roles in mitochondria. Prog Biophys Mol Biol. 2013;112(1):44-54.

28.	Morgan DJ, Poolman TM, Williamson AJK, Wang Z, Clark NR, Ma'ayan A, et al. Glucocorticoid receptor isoforms direct distinct mitochondrial programs to regulate ATP production. Sci Rep. 2016;6(1):26419.

29.	Petta I, Dejager L, Ballegeer M, Lievens S, Tavernier J, De Bosscher K, et al. The interactome of the glucocorticoid receptor and its influence on the actions of glucocorticoids in combatting inflammatory and infectious diseases. Microbiol Mol Biol Rev. 2016;80(2):495.

30.	Rao NA, McCalman MT, Moulos P, Francoijs KJ, Chatziioannou A, Kolisis FN, et al. Coactivation of GR and NFKB alters the repertoire of their binding sites and target genes. Genome Res. 2011;21(9):1404-16.

31.	Shah S, King EM, Chandrasekhar A, Newton R. Roles for the Mitogen-activated Protein Kinase (MAPK) phosphatase, DUSP1, in feedback control of inflammatory gene expression and repression by Dexamethasone. J Biol Chem. 2014;289(19):13667-79.

32.	De Bosscher K, Beck IM, Dejager L, Bougarne N, Gaigneaux A, Chateauvieux S, et al. Selective modulation of the glucocorticoid receptor can distinguish between transrepression of NF-κB and AP-1. Cell Mol Life Sci. 2014;71(1):143-63.

33.	Yang YH, Aeberli D, Dacumos A, Xue JR, Morand EF. Annexin-1 regulates macrophage IL-6 and TNF via glucocorticoid-induced leucine zipper. J Immunol. 2009;183(2):1435-45.

34.	Ricci E, Ronchetti S, Gabrielli E, Pericolini E, Gentili M, Roselletti E, et al. GILZ restrains neutrophil activation by inhibiting the MAPK pathway. J Leukoc Biol. 2019;105(1):187-94.

35.	Mitra R, Sapolsky RM. Acute corticosterone treatment is sufficient to induce anxiety and amygdaloid dendritic hypertrophy. Proc Natl Acad Sci U S A. 2008;105(14):5573-8.

36.	Rao RP, Anilkumar S, McEwen BS, Chattarji S. Glucocorticoids protect against the delayed behavioral and cellular effects of acute stress on the amygdala. Biol Psychiatry. 2012;72(6):466-75.

37.	Zohar J, Yahalom H, Kozlovsky N, Cwikel-Hamzany S, Matar MA, Kaplan Z, et al. High dose hydrocortisone immediately after trauma may alter the trajectory of PTSD: interplay between clinical and animal studies. Eur Neuropsychopharmacol. 2011;21(11):796-809.

38.	Koning A-SCAM, Buurstede JC, van Weert LTCM, Meijer OC. Glucocorticoid and Mineralocorticoid Receptors in the brain: A transcriptional perspective. J Endocr Soc. 2019;3(10):1917-30.

39.   Pereira AM, Tiemensma J, Romijn JA. Neuropsychiatric disorders in Cushing's Syndrome. Neuroendocrinology. 2010;92:65-70.

40.   Barthel A, Benker G, Berens K, Diederich S, Manfras B, Gruber M, et al. An Update on Addison's Disease. Exp Clin Endocrinol Diabetes. 2019;127(2-03):165-75.

41.   Mitchell AL, Pearce SHS. Autoimmune Addison disease: pathophysiology and genetic complexity. Nat Rev Endocrinol. 2012;8(5):306-16.

42.   Tam EWY, Chau V, Ferriero DM, Barkovich AJ, Poskitt KJ, Studholme C, et al. Preterm cerebellar growth impairment after postnatal exposure to glucocorticoids. Sci Transl Med. 2011;3(105):105.

43.   Huang P, Chandra V, Rastinejad F. Structural overview of the nuclear receptor superfamily: insights into physiology and therapeutics. Annu Rev Physiol. 2010;72(1):247-72.

44.   Leventhal SM, Lim D, Green TL, Cantrell AE, Cho K, Greenhalgh DG. Uncovering a multitude of human glucocorticoid receptor variants: an expansive survey of a single gene. BMC Genetics. 2019;20(1):16.

45.   Robinson-Rechavi M, Garcia HE, Laudet V. The nuclear receptor superfamily. J Cell Sci. 2003;116(4):585.

46.   Bookout AL, Jeong Y, Downes M, Yu RT, Evans RM, Mangelsdorf DJ. Anatomical profiling of nuclear receptor expression reveals a hierarchical transcriptional network. Cell. 2006;126(4):789-99.

47.   Kino T, Manoli I, Kelkar S, Wang Y, Su YA, Chrousos GP. Glucocorticoid receptor (GR) β has intrinsic, GRα-independent transcriptional activity. Biochemical and Biophysical Research Communications. 2009;381(4):671-5.

48.   Kelly A, Bowen H, Jee Y-K, Mahfiche N, Soh C, Lee T, et al. The glucocorticoid receptor β isoform can mediate transcriptional repression by recruiting histone deacetylases. J Allergy Clin Immunol. 2008;121(1):203-8.

49.   Lewis-Tuffin LJ, Cidlowski JA. The physiology of human glucocorticoid receptor β (hGRβ) and glucocorticoid resistance. Ann NY Acad Sci. 2006;1069(1):1-9.

50.   Beger C, Gerdes K, Lauten M, Tissing WJ, Fernandez-Munoz I, Schrappe M, et al. Expression and structural analysis of glucocorticoid receptor isoform gamma in human leukaemia cells using an isoform-specific real-time polymerase chain reaction approach. Br J Haematol. 2003;122(2):245-52.

51.   Ratman D, Vanden Berghe W, Dejager L, Libert C, Tavernier J, Beck IM, et al. How glucocorticoid receptors modulate the activity of other transcription factors: A scope beyond tethering. Mol Cell Endocrinol. 2013;380(1):41-54.

52.   Krett NL, Pillay S, Moalli PA, Greipp PR, Rosen ST. A variant glucocorticoid receptor messenger RNA is expressed in multiple myeloma patients. Cancer Res. 1995;55(13):2727-9.

53.   Taniguchi Y, Iwasaki Y, Tsugita M, Nishiyama M, Taguchi T, Okazaki M, et al. Glucocorticoid receptor-beta and receptor-gamma exert dominant negative effect on gene repression but not on gene induction. Endocrinology. 2010;151(7):3204-13.

54.   Oakley RH, Cidlowski JA. Cellular processing of the glucocorticoid receptor gene and protein: New mechanisms for generating tissue-specific actions of glucocorticoids. J Biol Chem. 2011;286(5):3177-84.

55.   Liu B, Zhang TN, Knight JK, Goodwin JE. The glucocorticoid receptor in cardiovascular health and disease. Cells. 2019;8(10):1227.

56.   Ricketson D, Hostick U, Fang L, Yamamoto KR, Darimont BD. A conformational switch in the ligand binding domain regulates the dependence of the glucocorticoid receptor on Hsp90: Regulating the dependence of GR on Hsp90. J Mol Biol. 2007;368(3):729-41.

57.   Kucera T, Waltner-Law M, Scott DK, Prasad R, Granner DK. A point mutation of the AF2 transactivation domain of the glucocorticoid receptor disrupts its interaction with Steroid Receptor Coactivator 1. J Biol Chem. 2002;277(29):26098-102.

58.   Cho S, Kagan BL, John A. Blackford J, Szapary D, S. Stoney Simons J. Glucocorticoid receptor ligand binding domain is sufficient for the modulation of glucocorticoid induction properties by homologous receptors, Coactivator Transcription Intermediary Factor 2, and Ubc9. Mol Endocrinol. 2005;19(2):290-311.

59.   Bledsoe RK, Montana VG, Stanley TB, Delves CJ, Apolito CJ, McKee DD, et al. Crystal structure of the glucocorticoid receptor ligand binding domain reveals a novel mode of receptor dimerization and coactivator recognition. Cell. 2002;110(1):93-105.

60.   Necela BM, Cidlowski JA. A single amino acid change in the first zinc finger of the DNA binding domain of the glucocorticoid receptor regulates differential promoter selectivity. J Biol Chem. 2004;279(38):39279-88.

61.   Tao Y, Williams-Skipp C, Scheinman RI. Mapping of Glucocorticoid Receptor DNA binding domain surfaces contributing to transrepression of NF-κB and induction of apoptosis. J BiolChem. 2001;276(4):2329-32.

62.   Kolodkin AN, Bruggeman FJ, Plant N, Moné MJ, Bakker BM, Campbell MJ, et al. Design principles of nuclear receptor signaling: how complex networking improves signal transduction. Mol Syst Biol. 2010;6:446.

63.   Khan SH, Awasthi S, Guo C, Goswami D, Ling J, Griffin PR, et al. Binding of the N-terminal region of coactivator TIF2 to the intrinsically disordered AF1 domain of the glucocorticoid receptor is accompanied by conformational reorganizations. J Biol Chem. 2012;287(53):44546-60.

64.   Lavery Derek N, McEwan Iain J. Structure and function of steroid receptor AF1 transactivation domains: induction of active conformations. Biochem J. 2005;391(3):449.

65.   Vandewalle J, Luypaert A, De Bosscher K, Libert C. Therapeutic mechanisms of glucocorticoids. Trends   Endocrinol Metab. 2018;29(1):42-54.

66.   Vandevyver S, Dejager L, Libert C. On the trail of the glucocorticoid receptor: into the nucleus and back. Traffic. 2012;13(3):364-74.

67.   Hornbeck PV, Zhang B, Murray B, Kornhauser JM, Latham V, Skrzypek E. PhosphoSitePlus, 2014: mutations, PTMs and recalibrations. Nucleic Acids Res. 2015;43:D512-20.

68.   Matthews L, Johnson J, Berry A, Trebble P, Cookson A, Spiller D, et al. Cell cycle phase regulates glucocorticoid receptor function. PLOS ONE. 2011;6(7):e22289.

69.   Carrigan A, Walther RF, Salem HA, Wu D, Atlas E, Lefebvre YA, et al. An active nuclear retention signal in the glucocorticoid receptor functions as a strong inducer of transcriptional activation. J Biol Chem. 2007;282(15):10963-71.

70.   Viengchareun S, Le Menuet D, Martinerie L, Munier M, Tallec LP-L, Lombès M. The mineralocorticoid receptor: insights into its molecular and (patho)physiological biology. Nucl Recept Signal. 2007;5(1):12.

71.   Gomez-Sanchez EP. Brain mineralocorticoid receptors in cognition and cardiovascular homeostasis. Steroids. 2014;91:20-31.

72.   Pascual-Le Tallec L, Simone F, Viengchareun S, Meduri G, Thirman MJ, Lombès M. The elongation factor ELL (eleven-nineteen lysine-rich leukemia) is a selective coregulator for steroid receptor functions. Mol Endocrinol. 2005;19(5):1158-69.

73.   Dittmar KD, Demady DR, Stancato LF, Krishna P, Pratt WB. Folding of the glucocorticoid receptor by the heat shock protein (hsp) 90-based chaperone machinery. J Biol Chem. 1997;272(34):21213-20.

74.   Li Z-y, Li Q-z, Chen L, Chen B-d, Zhang C, Wang X, et al. HPOB, an HDAC6 inhibitor, attenuates corticosterone-induced injury in rat adrenal pheochromocytoma PC12 cells by inhibiting mitochondrial GR translocation and the intrinsic apoptosis pathway. Neurochem Int. 2016;99:239-51.

75.   Kirschke E, Goswami D, Southworth D, Griffin Patrick R, Agard David A. Glucocorticoid receptor function regulated by coordinated action of the Hsp90 and Hsp70 chaperone cycles. Cell. 2014;157(7):1685-97.

76.   Panettieri RA, Schaafsma D, Amrani Y, Koziol-White C, Ostrom R, Tliba O. Non-genomic effects of glucocorticoids: An updated view. Trends Pharmacol Sci. 2019;40(1):38-49.

77.   Flaherty RL, Owen M, Fagan-Murphy A, Intabli H, Healy D, Patel A, et al. Glucocorticoids induce production of reactive oxygen species/reactive nitrogen species and DNA damage through an iNOS mediated pathway in breast cancer. Breast Cancer Res. 2017;19(1):35.

78.   Dimmeler S, Fleming I, Fisslthaler B, Hermann C, Busse R, Zeiher AM. Activation of nitric oxide synthase in endothelial cells by Akt-dependent phosphorylation. Nature. 1999;399(6736):601-5.

79.   Hafezi-Moghadam A, Simoncini T, Yang Z, Limbourg FP, Plumier JC, Rebsamen MC, et al. Acute cardiovascular protective effects of corticosteroids are mediated by non-transcriptional activation of endothelial nitric oxide synthase. Nat Med. 2002;8(5):473-9.

80.   Liu L, Wang YX, Zhou J, Long F, Sun HW, Liu Y, et al. Rapid non-genomic inhibitory effects of glucocorticoids on human neutrophil degranulation. J Inflamm Res. 2005;54(1):37-41.

81.   Kong F, Liu Z, Jain VG, Shima K, Suzuki T, Muglia LJ, et al. Inhibition of IRAK1 ubiquitination determines glucocorticoid sensitivity for TLR9-induced inflammation in macrophages. J Immunol. 2017;199(10):3654.

82.   Croxtall JD, Choudhury Q, Flower RJ. Glucocorticoids act within minutes to inhibit recruitment of signalling factors to activated EGF receptors through a receptor-dependent, transcription-independent mechanism. Br J Pharmacol. 2000;130(2):289-98.

83.   Ayroldi E, Cannarile L, Migliorati G, Nocentini G, Delfino DV, Riccardi C. Mechanisms of the anti-inflammatory effects of glucocorticoids: genomic and nongenomic interference with MAPK signaling pathways. The FASEB Journal. 2012;26(12):4805-20.

84.   Caratti G, Poolman T, Hurst RJ, Ince L, Knight A, Krakowiak K, et al. Caveolin1 interacts with the glucocorticoid receptor in the lung but is dispensable for its anti-inflammatory actions in lung inflammation and Trichuris Muris infection. Sci Rep. 2019;9(1):8581.

85.   Matthews L, Berry A, Ohanian V, Ohanian J, Garside H, Ray D. Caveolin mediates rapid glucocorticoid effects and couples glucocorticoid action to the antiproliferative program. Mol Endocrinol. 2008;22(6):1320-30.

86.   Manning BD, Toker A. AKT/PKB Signaling: Navigating the Network. Cell. 2017;169(3):381-405.

87.   Hynes D, Harvey BJ. Dexamethasone reduces airway epithelial Cl− secretion by rapid non-genomic inhibition of KCNQ1, KCNN4 and KATP K+ channels. Steroids. 2019;151:108459.

88.   Echeverría PC, Mazaira G, Erlejman A, Gomez-Sanchez C, Pilipuk GP, Galigniana MD. Nuclear import of the glucocorticoid receptor-hsp90 complex through the nuclear pore complex is mediated by its interaction with Nup62 and Importin β. Mol and Cell Biol. 2009;29(17):4788.

89.   Trebble PJ, Woolven JM, Saunders KA, Simpson KD, Farrow SN, Matthews LC, et al. A ligand-specific kinetic switch regulates glucocorticoid receptor trafficking and function. Journal of Cell Science. 2013;126(14):3159-69.

90.   Starick SR, Ibn-Salem J, Jurk M, Hernandez C, Love MI, Chung H-R, et al. ChIP-exo signal associated with DNA-binding motifs provides insight into the genomic binding of the glucocorticoid receptor and cooperating transcription factors. Genome Res. 2015;25(6):825-35.

91.   Uhlenhaut NH, Barish GD, Yu RT, Downes M, Karunasiri M, Liddle C, et al. Insights into negative regulation by the glucocorticoid receptor from genome-wide profiling of inflammatory cistromes. Mol Cell. 2013;49(1):158-71.

92.   Oh K-S, Patel H, Gottschalk RA, Lee WS, Baek S, Fraser IDC, et al. Anti-inflammatory chromatinscape suggests alternative mechanisms of glucocorticoid receptor action. Immunity. 2017;47(2):298-309.

93.   Paakinaho V, Presman DM, Ball DA, Johnson TA, Schiltz RL, Levitt P, et al. Single-molecule analysis of steroid receptor and cofactor action in living cells. Nat Commun. 2017;8(1):15896.

94.   Millard C, J., Watson PJ, Fairall L, Schwabe JWR. An evolving understanding of nuclear receptor coregulator proteins. J Mol Endocrinol. 2013;51(3):T23-T36.

95.   Surjit M, Ganti Krishna P, Mukherji A, Ye T, Hua G, Metzger D, et al. Widespread negative response elements mediate direct repression by agonist-liganded glucocorticoid receptor. Cell. 2011;145(2):224-41.

96.   Schiller BJ, Chodankar R, Watson LC, Stallcup MR, Yamamoto KR. Glucocorticoid receptor binds half sites as a monomer and regulates specific target genes. Genome Biol. 2014;15(7):418.

97.   Ramamoorthy S, Cidlowski JA. Exploring the molecular mechanisms of glucocorticoid receptor action from sensitivity to resistance. Endocr Dev. 2013;24:41-56.

98.   Kleiman A, Hübner S, Rodriguez Parkitna JM, Neumann A, Hofer S, Weigand MA, et al. Glucocorticoid receptor dimerization is required for survival in septic shock via suppression of interleukin-1 in macrophages. The FASEB Journal. 2011;26(2):722-9.

99.   Vandevyver S, Dejager L, Van Bogaert T, Kleyman A, Liu Y, Tuckermann J, et al. Glucocorticoid receptor dimerization induces MKP1 to protect against TNF-induced inflammation. J Clin Invest. 2012;122(6):2130-40.

100.   Rauch A, Seitz S, Baschant U, Schilling AF, Illing A, Stride B, et al. Glucocorticoids suppress bone formation by attenuating osteoblast differentiation via the monomeric glucocorticoid receptor. Cell Metab. 2010;11(6):517-31.

101.   De Bosscher K, Beck IM, Ratman D, Berghe WV, Libert C. Activation of the Glucocorticoid Receptor in Acute Inflammation: the SEDIGRAM Concept. Trends Pharmacol Sci. 2016;37(1):4-16.

102.   Souffriau J, Eggermont M, Van Ryckeghem S, Van Looveren K, Van Wyngene L, Van Hamme E, et al. A screening assay for Selective Dimerizing

Glucocorticoid Receptor Agonists and Modulators (SEDIGRAM) that are effective against acute inflammation. Sci Rep. 2018;8(1):12894.

103.   Ostrom QT, Gittleman H, Farah P, Ondracek A, Chen Y, Wolinsky Y, et al. CBTRUS statistical report: Primary brain and central nervous system tumors diagnosed in the United States in 2006-2010. Neuro Oncol. 2013;15:ii1-ii56.

104.   Stupp R, Mason WP, van den Bent MJ, Weller M, Fisher B, Taphoorn MJB, et al. Radiotherapy plus concomitant and adjuvant Temozolomide for Glioblastoma. N Engl J Med. 2005;352(10):987-96.

105.   Kazda T, Dziacky A, Burkon P, Pospisil P, Slavik M, Rehak Z, et al. Radiotherapy of Glioblastoma 15 Years after the landmark Stupp's trial: More controversies than standards? Radiol Oncol. 2018;52(2):121-8.

106.   Louis DN, Perry A, Reifenberger G, von Deimling A, Figarella-Branger D, Cavenee WK, et al. The 2016 World Health Organization classification of tumors of the central nervous system: a summary. Acta Neuropathol. 2016;131(6):803-20.

107.   Appay R, Dehais C, Maurage C-A, Alentorn A, Carpentier C, Colin C, et al. CDKN2A homozygous deletion is a strong adverse prognosis factor in diffuse malignant IDH-mutant gliomas. Neuro-Oncol. 2019;21(12):1519-28.

108.   Lee Y, Koh J, Kim S-I, Won JK, Park C-K, Choi SH, et al. The frequency and prognostic effect of TERT promoter mutation in diffuse gliomas. Acta Neuropathol Commun. 2017;5(1):62.

109.   Zhang Y, Dube C, Gibert M, Jr., Cruickshanks N, Wang B, Coughlan M, et al. The p53 pathway in Glioblastoma. Cancers. 2018;10(9):297.

110.   Everhard S, Tost Jr, El Abdalaoui H, Crinière E, Busato F, Marie Y, et al. Identification of regions correlating MGMT promoter methylation and gene expression in glioblastomas. Neuro-Oncol. 2009;11(4):348-56.

111.   Lacroix M, Abi-Said D, Fourney DR, Gokaslan ZL, Shi W, DeMonte F, et al. A multivariate analysis of 416 patients with glioblastoma multiforme: prognosis, extent of resection, and survival. J Neurosurg. 2001;95(2):190.

112.   Erasimus H, Gobin M, Niclou S, Van Dyck E. DNA repair mechanisms and their clinical impact in glioblastoma. Mutat Res. 2016;769:19-35.

113.   Curtin NJ. DNA repair dysregulation from cancer driver to therapeutic target. Nat Rev Cancer. 2012;12:801.

114.   Lamarche BJ, Orazio NI, Weitzman MD. The MRN complex in double-strand break repair and telomere maintenance. FEBS Lett. 2010;584(17):3682-95.

115.   Shamanna RA, Lu H, de Freitas JK, Tian J, Croteau DL, Bohr VA. WRN regulates pathway choice between classical and alternative non-homologous end joining. Nat Commun. 2016;7(1):13785.

116.   Ceccaldi R, Rondinelli B, D'Andrea AD. Repair Pathway Choices and Consequences at the Double-Strand Break. Trends Cell   Biol. 2016;26(1):52-64.

117.   Filippo JS, Sung P, Klein H. Mechanism of eukaryotic homologous recombination. Annu Rev Biochem. 2008;77(1):229-57.

118.   Beucher A, Birraux J, Tchouandong L, Barton O, Shibata A, Conrad S, et al. ATM and Artemis promote homologous recombination of radiation-induced DNA double-strand breaks in G2. EMBO J. 2009;28(21):3413.

119.   Spagnolo L, Rivera-Calzada A, Pearl LH, Llorca O. Three-dimensional structure of the human DNA-PKcs/Ku70/Ku80 complex assembled on DNA and its implications for DNA DSB repair. Mol Cell. 2006;22(4):511-9.

120.   Britton S, Coates J, Jackson SP. A new method for high-resolution imaging of Ku foci to decipher mechanisms of DNA double-strand break repair. J Cell Biol. 2013;202(3):579.

121.   An J, Huang Y-C, Xu Q-Z, Zhou L-J, Shang Z-F, Huang B, et al. DNA-PKcs plays a dominant role in the regulation of H2AX phosphorylation in response to DNA damage and cell cycle progression. BMC Mol Biol. 2010;11(1):18.

122.   Goodwin JF, Knudsen KE. Beyond DNA repair: DNA-PK function in cancer. Cancer Discov. 2014;4(10):1126-39.

123.   Gerodimos CA, Chang HHY, Watanabe G, Lieber MR. Effects of DNA end configuration on XRCC4-DNA ligase IV and its stimulation of Artemis activity. J Biol Chem. 2017;292(34):13914-24.

124.   Gustafsson A-S, Abramenkovs A, Stenerlöw B. Suppression of DNA-dependent protein kinase sensitize cells to radiation without affecting DSB repair. Mutat Res. 2014;769:1-10.

125.   Kase M, Vardja M, Lipping A, Asser T, Jaal J. Impact of PARP-1 and DNA-PK expression on survival in patients with glioblastoma multiforme. Radiother Oncol. 2011;101(1):127-31.

126.   Pilié PG, Tang C, Mills GB, Yap TA. State-of-the-art strategies for targeting the DNA damage response in cancer. Nat Rev Clin Oncol. 2019;16(2):81-104.

127.   Taccioli GE, Amatucci AG, Beamish HJ, Gell D, Xiang XH, Arzayus MIT, et al. Targeted disruption of the catalytic subunit of the DNA-PK gene in mice confers Severe Combined Immunodeficiency and Radiosensitivity. Immunity. 1998;9(3):355-66.

128.   Björkman A, Du L, Felgentreff K, Rosner C, Pankaj Kamdar R, Kokaraki G, et al. DNA-PKcs is involved in Ig class switch recombination in human B cells. J Immunol. 2015;195(12):5608.

129.   Kienker LJ, Shin EK, Meek K. Both V(D)J recombination and radioresistance require DNA-PK kinase activity, though minimal levels suffice for V(D)J recombination. Nucleic Acid Res. 2000;28(14):2752-61.

130.   Ju J, Naura AS, Errami Y, Zerfaoui M, Kim H, Kim JG, et al. Phosphorylation of p50 NF-kappaB at a single serine residue by DNA-dependent protein kinase is critical for VCAM-1 expression upon TNF treatment. J Biol Chem. 2010;285(52):41152-60.

131.   Kim Wiese A, Schluterman Burdine M, Turnage RH, Tackett AJ, Burdine LJ. DNA-PKcs controls calcineurin mediated IL-2 production in T lymphocytes. PLOS ONE. 2017;12(7):e0181608.

132.   Ghonim MA, Pyakurel K, Ju J, Rodriguez PC, Lammi MR, Davis C, et al. DNA-dependent protein kinase inhibition blocks asthma in mice and modulates human endothelial and CD4+ T-cell function without causing severe combined immunodeficiency. J Allergy Clin Immunol. 2015;135(2):425-40.

133.   Kotula E, Berthault N, Agrario C, Lienafa M-C, Simon A, Dingli F, et al. DNA-PKcs plays role in cancer metastasis through regulation of secreted proteins involved in migration and invasion. Cell Cycle. 2015;14(12):1961-72.

134.   Jackson SP, Bartek J. The DNA-damage response in human biology and disease. Nature. 2009;461:1071.

135.   Wei C, Li J, Li J, Xing P, Zheng S, Zhao X, et al. Cell cycle-dependent control of homologous recombination. Acta Biochim Biophys Sin. 2017;49(8):655-68.

136.   Luo K, Li L, Li Y, Wu C, Yin Y, Chen Y, et al. A phosphorylation–deubiquitination cascade regulates the BRCA2–RAD51 axis in homologous recombination. Genes Dev. 2016;30(23):2581-95.

137.   Jasin M, Rothstein R. Repair of strand breaks by homologous recombination. Cold Spring Harb Perspect Biol.5(11):012740-.

138.   Lee J-H, Paull TT. ATM Activation by DNA Double-Strand Breaks Through the Mre11-Rad50-Nbs1 Complex. Science. 2005;308(5721):551.

139.   Stiff T, Walker SA, Cerosaletti K, Goodarzi AA, Petermann E, Concannon P, et al. ATR-dependent phosphorylation and activation of ATM in response to UV treatment or replication fork stalling. EMBO J. 2006;25(24):5775.

140.   Maréchal A, Zou L. DNA Damage Sensing by the ATM and ATR Kinases. Cold Spring Harb Perspect Biol. 2013;5(9).

141.   Matsuoka S, Ballif BA, Smogorzewska A, McDonald ER, Hurov KE, Luo J, et al. ATM and ATR substrate analysis reveals extensive protein networks responsive to DNA damage. Science. 2007;316(5828):1160.

142.   Blackford AN, Jackson SP. ATM, ATR, and DNA-PK: The trinity at the heart of the DNA damage response. Mol Cell. 2017;66(6):801-17.

143.   Nepal M, Che R, Zhang J, Ma C, Fei P. Fanconi Anemia signaling and cancer. Trends Cancer. 2017;3(12):840-56.

144.	Serrano MA, Li Z, Dangeti M, Musich PR, Patrick S, Roginskaya M, et al. DNA-PK, ATM and ATR collaboratively regulate p53-RPA interaction to facilitate homologous recombination DNA repair. Oncogene. 2013;32(19):2452-62.

145.	Mantovani F, Collavin L, Del Sal G. Mutant p53 as a guardian of the cancer cell. Cell Death Differ. 2019;26(2):199-212.

146.	Muller PAJ, Vousden KH. Mutant p53 in cancer: new functions and therapeutic opportunities. Cancer Cell. 2014;25(3):304-17.

147.	Brennan CW, Verhaak RGW, McKenna A, Campos B, Noushmehr H, Salama SR, et al. The somatic genomic landscape of glioblastoma. Cell. 2013;155(2):462-77.

148.	Menon V, Povirk L. Involvement of p53 in the repair of DNA double strand breaks: multifaceted Roles of p53 in homologous recombination repair (HRR) and non-homologous end joining (NHEJ). Subcell Biochem. 2014;85:321-36.

149.	Ou Y-H, Chung P-H, Sun T-P, Shieh S-Y. p53 C-terminal phosphorylation by CHK1 and CHK2 participates in the regulation of DNA-damage-induced C-terminal acetylation. Mol Biol Cell. 2005;16(4):1684-95.

150.	Maya R, Balass M, Kim ST, Shkedy D, Leal JF, Shifman O, et al. ATM-dependent phosphorylation of Mdm2 on serine 395: role in p53 activation by DNA damage. Genes Dev. 2001;15(9):1067-77.

151.	Kim EM, Jung CH, Kim J, Hwang SG, Park JK, Um HD. The p53/p21 Complex Regulates Cancer Cell Invasion and Apoptosis by Targeting Bcl-2 Family Proteins. Cancer Res. 2017;77(11):3092-100.

152.	Chen J. The cell-cycle arrest and apoptotic functions of p53 in tumor initiation and progression. CSH Perspect Med. 2016;6(3):026104.

153.	Jiang P, Du W, Heese K, Wu M. The Bad guy cooperates with good cop p53: Bad is transcriptionally up-regulated by p53 and forms a Bad/p53 complex at the mitochondria to induce apoptosis. Mol Cell Biol. 2006;26(23):9071-82.

154.	Andrasi M, Bustos R, Gaspar A, Gomez FA, Klekner A. Analysis and stability study of temozolomide using capillary electrophoresis. J Chromatogr B Biomed Appl. 2010;878(21):1801-8.

155.	Zhang J, FG Stevens M, D Bradshaw T. Temozolomide: mechanisms of action, repair and resistance. Current Mol Pharmacol. 2012;5(1):102-14.

156.	Perazzoli G, Prados J, Ortiz R, Caba O, Cabeza L, Berdasco M, et al. Temozolomide resistance in glioblastoma cell lines: implication of MGMT, MMR, P-Glycoprotein and CD133 expression. PLoS One. 2015;10(10):e0140131.

157.	Thomas A, Tanaka M, Trepel J, Reinhold WC, Rajapakse VN, Pommier Y. Temozolomide in the era of precision medicine. Cancer Res. 2017;77(4):823.

158.   Roos W, Baumgartner M, Kaina B. Apoptosis triggered by DNA damage O6-methylguanine in human lymphocytes requires DNA replication and is mediated by p53 and Fas/CD95/Apo-1. Oncogene. 2004;23:359.

159.   Roos WP, Batista LFZ, Naumann SC, Wick W, Weller M, Menck CFM, et al. Apoptosis in malignant glioma cells triggered by the temozolomide-induced DNA lesion O6-methylguanine. Oncogene. 2006;26:186.

160.   Dresemann G. Temozolomide in malignant glioma. Oncotargets There. 2010;3:139-46.

161.   Hegi ME, Diserens A-C, Gorlia T, Hamou M-F, de Tribolet N, Weller M, et al. MGMT gene silencing and benefit from Temozolomide in Glioblastoma. New Engl J Med. 2005;352(10):997-1003.

162.   Gilbert MR, Wang M, Aldape KD, Stupp R, Hegi ME, Jaeckle KA, et al. Dose-Dense Temozolomide for Newly Diagnosed Glioblastoma: A Randomized Phase III Clinical Trial. J Clin Oncol. 2013;31(32):4085-91.

163.   Binabaj MM, Bahrami A, ShahidSales S, Joodi M, Joudi Mashhad M, Hassanian SM, et al. The prognostic value of MGMT promoter methylation in glioblastoma: A meta-analysis of clinical trials. J Cell Physiol. 2018;233(1):378-86.

164.   Uros S, Mara P, Matjaz Z, Emanuela B, Andrej Z, Viljem K, et al. Long-term survival in glioblastoma: methyl guanine methyl transferase (MGMT) promoter methylation as independent favourable prognostic factor. Radiol Oncol. 2016;50(4):394-401.

165.   Berberich A, Winkler F, Kessler T, Wick W, Wick A, Eisenmenger A, et al. N2M2 (NOA-20) phase I/II trial of molecularly matched targeted therapies plus radiotherapy in patients with newly diagnosed non-MGMT hypermethylated glioblastoma. Neuro-Oncol. 2018;21(1):95-105.

166.   Biswas T, Ramana CV, Srinivasan G, Boldogh I, Hazra TK, Chen Z, et al. Activation of human O6-methylguanine-DNA methyltransferase gene by glucocorticoid hormone. Oncogene. 1999;18:525.

167.   Boldogh I, Ramana CV, Chen Z, Biswas T, Hazra TK, Grösch S, et al. Regulation of expression of the DNA repair gene O6-Methylguanine-DNA Methyltransferase via Protein Kinase C-mediated Signaling. Cancer Res. 1998;58(17):3950.

168.   Lavon I, Fuchs D, Zrihan D, Efroni G, Zelikovitch B, Fellig Y, et al. Novel mechanism whereby Nuclear Factor κB mediates DNA damage repair through regulation of O6-Methylguanine-DNA-Methyltransferase. Cancer Res. 2007;67(18):8952.

169.   Shigeo U, Toshihiro M, Yukiko N, Hiroaki O, Tetsuya S, Kazuo T. Induction of the DNA repair gene O6-methylguanine—DNA methyltransferase by Dexamethasone in glioblastomas. J Neurosurg. 2004;101(4):659-63.

170. Sur P, Sribnick EA, Patel SJ, Ray SK, Banik NL. Dexamethasone decreases temozolomide-induced apoptosis in human gliobastoma T98G cells. Glia. 2005;50(2):160-7.

171. Aasland D, Reich TR, Tomicic MT, Switzeny OJ, Kaina B, Christmann M. Repair gene O6-methylguanine-DNA methyltransferase is controlled by SP1 and up-regulated by glucocorticoids, but not by temozolomide and radiation. J Neurochem. 2018;144(2):139-51.

172. Sun Y, Fang M, Davies H, Hu Z. Mifepristone: a potential clinical agent based on its anti-progesterone and anti-glucocorticoid properties. Gynecol Endocrinol. 2014;30(3):169-73.

173. Llaguno-Munive M, Romero-Piña M, Serrano-Bello J, Medina L, Uribe-Uribe N, Salazar A, et al. Mifepristone overcomes tumor resistance to Temozolomide associated with DNA damage repair and apoptosis in an orthotopic model of Glioblastoma. Cancers. 2019;11(1):16.

174. Llaguno-Munive M, Medina LA, Jurado R, Romero-Piña M, Garcia-Lopez P. Mifepristone improves chemo-radiation response in glioblastoma xenografts. Cancer Cell Int. 2013;13(1):29.

175. Dietrich J, Rao K, Pastorino S, Kesari S. Corticosteroids in brain cancer patients: benefits and pitfalls. Expert Rev Clin Pharmacol. 2011;4(2):233-42.

176. Ryken TC, McDermott M, Robinson PD, Ammirati M, Andrews DW, Asher AL, et al. The role of steroids in the management of brain metastases: a systematic review and evidence-based clinical practice guideline. J Neuro-Oncol. 2010;96(1):103-14.

177. Drappatz J, Schiff D, Kesari S, Norden AD, Wen PY. Medical management of brain tumor patients. Neurol Clin. 2007;25(4):1035-71.

178. Poungvarin N. Steroids have no role in stroke therapy. Stroke. 2004;35(1):229-30.

179. Förster C, Burek M, Romero IA, Weksler B, Couraud P-O, Drenckhahn D. Differential effects of hydrocortisone and TNFα on tight junction proteins in an in vitro model of the human blood–brain barrier. J Physiol. 2008;586(7):1937-49.

180. Engelhardt B. Molecular mechanisms involved in T cell migration across the blood–brain barrier. J Neural Transm. 2006;113(4):477-85.

181. Salvador E, Shityakov S, Förster C. Glucocorticoids and endothelial cell barrier function. Cell Tissue Res. 2014;355(3):597-605.

182. Pitter KL, Tamagno I, Alikhanyan K, Hosni-Ahmed A, Pattwell SS, Donnola S, et al. Corticosteroids compromise survival in glioblastoma. Brain. 2016;139(5):1458-71.

183. Millar BM, Bezjak A, Tsao M, Sturdza A, Laperriere N. Defining the impact and contribution of steroids in patients receiving whole-brain irradiation for cerebral metastases. Clin Oncol. 2004;16(5):339-44.

184.   Margolin K, Ernstoff MS, Hamid O, Lawrence D, McDermott D, Puzanov I, et al. Ipilimumab in patients with melanoma and brain metastases: an open-label, phase 2 trial. Lancet Oncol. 2012;13(5):459-65.

185.   Wong ET, Lok E, Gautam S, Swanson KD. Dexamethasone exerts profound immunologic interference on treatment efficacy for recurrent glioblastoma. Br J Cancer. 2015;113(2):232-41.

186.   Shields LBE, Shelton BJ, Shearer AJ, Chen L, Sun DA, Parsons S, et al. Dexamethasone administration during definitive radiation and temozolomide renders a poor prognosis in a retrospective analysis of newly diagnosed glioblastoma patients. Radiat Oncol. 2015;10(1):222.

187.   Grünberg S, Warfield L, Hahn S. Architecture of the RNA polymerase II preinitiation complex and mechanism of ATP-dependent promoter opening. Nat Struct Mol Biol. 2012;19(8):788-96.

188.   Kaern M, Elston TC, Blake WJ, Collins JJ. Stochasticity in gene expression: from theories to phenotypes. Nat Rev Genet. 2005;6(6):451-64.

189.   Soltani M, Vargas-Garcia CA, Antunes D, Singh A. Intercellular variability in protein levels from stochastic expression and noisy cell cycle processes. PLoS Comput Viol. 2016;12(8):e1004972.

190.   Bokes P, Singh A. Gene expression noise is affected differentially by feedback in burst frequency and burst size. J Math Biol. 2016;74:1483-509.

191.   Ozbudak EM, Thattai M, Kurtser I, Grossman AD, van Oudenaarden A. Regulation of noise in the expression of a single gene. Nat Genet. 2002;31(1):69-73.

192.   Elowitz MB, Levine AJ, Siggia ED, Swain PS. Stochastic gene expression in a single cell. Science. 2002;297(5584):1183.

193.   Silander OK, Nikolic N, Zaslaver A, Bren A, Kikoin I, Alon U, et al. A Genome-Wide Analysis of Promoter-Mediated Phenotypic Noise in Escherichia coli. PLOS Genet. 2012;8(1):e1002443.

194.   Evans CR, Fan Y, Weiss K, Ling J. Errors during gene expression: Single-cell heterogeneity, stress resistance, and microbe-host interactions. mBio. 2018;9(4):e01018-18.

195.   Artegiani B, Lyubimova A, Muraro M, van Es JH, van Oudenaarden A, Clevers H. A single-cell RNA sequencing study reveals cellular and molecular dynamics of the hippocampal neurogenic niche. Cell Rep. 2017;21(11):3271-84.

196.   Pandey S, Shekhar K, Regev A, Schier AF. Comprehensive identification and spatial mapping of habenular neuronal types using single-cell RNA-seq. Curr Biol. 2018;28(7):1052-65.e7.

197.   Patel AP, Tirosh I, Trombetta JJ, Shalek AK, Gillespie SM, Wakimoto H, et al. Single-cell RNA-seq highlights intratumoral heterogeneity in primary glioblastoma. Science. 2014;344(6190):1396-401.

198.   Meyer M, Reimand J, Lan X, Head R, Zhu X, Kushida M, et al. Single cell-derived clonal analysis of human glioblastoma links functional and genomic heterogeneity. Proc Natl Acad Sci. 2015;112(3):851.

199.   Yuan J, Levitin HM, Frattini V, Bush EC, Boyett DM, Samanamud J, et al. Single-cell transcriptome analysis of lineage diversity in high-grade glioma. Genome Med. 2018;10(1):57.

200.   Friebel E, Kapolou K, Unger S, Núñez NG, Utz S, Rushing EJ, et al. Single-cell mapping of human brain cancer reveals tumor-specific instruction of tissue-invading leukocytes. Cell. 2020;181(7):1626-42.

201.   Zhang Q, Andersen ME, Conolly RB. Binary gene induction and protein expression in individual cells. Theor Biol Med Model. 2006;3:18.

202.   Karmakar R, Bose I. Graded and binary responses in stochastic gene expression. Phys Biol. 2004;1(4):197-204.

203.   Fiering S, Whitelaw E, Martin DIK. To be or not to be active: the stochastic nature of enhancer action. BioEssays. 2000;22(4):381-7.

204.   Reddy TE, Gertz J, Crawford GE, Garabedian MJ, Myers RM. The hypersensitive glucocorticoid response specifically regulates period 1 and expression of circadian genes. Mol Cell Biol. 2012;32(18):3756-67.

205.   Gyori BM, Venkatachalam G, Thiagarajan PS, Hsu D, Clement M-V. OpenComet: An automated tool for comet assay image analysis. Redox Biol. 2014;2:457-65.

206.   Matthews L, Berry A, Tersigni M, D'Acquisto F, Ianaro A, Ray D. Thiazolidinediones are partial agonists for the glucocorticoid receptor. Endocrinology. 2009;150(1):75-86.

207.   Bolger AM, Lohse M, Usadel B. Trimmomatic: a flexible trimmer for Illumina sequence data. Bioinformatics. 2014;30(15):2114-20.

208.   Dobin A, Davis CA, Schlesinger F, Drenkow J, Zaleski C, Jha S, et al. STAR: ultrafast universal RNA-seq aligner. Bioinformatics. 2012;29(1):15-21.

209.   Anders S, Pyl PT, Huber W. HTSeq - a Python framework to work with high-throughput sequencing data. Bioinformatics. 2015;31(2):166-9.

210.   Love MI, Huber W, Anders S. Moderated estimation of fold change and dispersion for RNA-seq data with DESeq2. Genome biology. 2014;15(12):550-.

211.   McCarthy DJ, Chen Y, Smyth GK. Differential expression analysis of multifactor RNA-Seq experiments with respect to biological variation. Nucleic acids research. 2012;40(10):4288-97.

212.   Robinson MD, Oshlack A. A scaling normalization method for differential expression analysis of RNA-seq data. Genome Biol. 2010;11(3):R25.

213. Dyczynski M, Vesterlund M, Björklund A-C, Zachariadis V, Janssen J, Gallart-Ayala H, et al. Metabolic reprogramming of acute lymphoblastic leukemia cells in response to glucocorticoid treatment. Cell Death Dis. 2018;9(9):846.

214. Gomes LC, Ferrão ALM, Evangelista FCG, de Almeida TD, Barbosa RC, Carvalho MdG, et al. Advances in chronic lymphocytic leukemia pharmacotherapy. Biomed Pharmacother. 2018;97:349-58.

215. Kay P, Schlossmacher G, Matthews L, Sommer P, Singh D, White A, et al. Loss of glucocorticoid receptor expression by DNA methylation prevents glucocorticoid induced apoptosis in human small cell lung cancer cells. PLoS One. 2011;6(10):e24839.

216. Liang H, Kowalczyk P, Junco JJ, Klug-De Santiago HL, Malik G, Wei S-J, et al. Differential effects on lung cancer cell proliferation by agonists of glucocorticoid and PPARα receptors. Mol Carcinogen. 2014;53(9):753-63.

217. Sommer P, Cowen RL, Berry A, Cookson A, Telfer BA, Williams KJ, et al. Glucocorticoid receptor over-expression promotes human small cell lung cancer apoptosis in vivo and thereby slows tumor growth. Endocr-Relat Cancer. 2010;17(1):203-13.

218. Taylor KM, Ray DW, Sommer P. Glucocorticoid receptors in lung cancer: new perspectives. J Endocrinol. 2016;229(1):R17-R28.

219. Mattern J, Büchler MW, Herr I. Cell cycle arrest by glucocorticoids may protect normal tissue and solid tumors from cancer therapy. Cancer Biol There. 2007;6(9):1341-50.

220. Bowman RL, Wang Q, Carro A, Verhaak RGW, Squatrito M. GlioVis data portal for visualization and analysis of brain tumor expression datasets. Neuro Oncol. 2016;19(1):139-41.

221. Dostert A, Heinzel T. Negative glucocorticoid receptor response elements and their role in glucocorticoid action. Curr Pharm Des. 2004;10(23):2807-16.

222. Kaup B, Schindler I, Knüpfer H, Schlenzka A, Preiß R, Knüpfer M. Time-dependent inhibition of glioblastoma cell proliferation by dexamethasone. J Neuro-Oncol. 2001;51(2):105-10.

223. Kawamura A, Tamaki N, Kokunai T. Effect of dexamethasone on cell proliferation of neuroepithelial tumor cell lines. Neurol Med-Chir. 1998;38(10):633-40.

224. Xie Y, Bergström T, Jiang Y, Johansson P, Marinescu VD, Lindberg N, et al. The human glioblastoma cell culture resource: validated cell models representing all molecular subtypes. EBioMedicine. 2015;2(10):1351-63.

225. Anderson CW, Dunn JJ, Freimuth PI, Galloway AM, Allalunis-Turner MJ. Frameshift mutation in *PRKDC*, the gene for DNA-PKcs, in the DNA repair-defective, human, glioma-derived cell line M059J. Radiat Res. 2001;156(1):2-9.

226.   Allalunis-Turner MJ, Peter KYZ, Barron GM, Mirzayans R, Day RS. Radiation-induced DNA damage and repair in cells of a radiosensitive human malignant glioma cell line. Radiat Res. 1995;144(3):288-93.

227.   Nestler U, Winking M, Böker D-K. The tissue level of dexamethasone in human brain tumors is about 1000 times lower than the cytotoxic concentration in cell culture. Neurol Res. 2002;24(5):479-82.

228.   Wolfram B, Thomas R, Bernd Grosse O, Jürgen M. Factors responsible for the retention of fluid in human tumor edema and the effect of dexamethasone. J Neurosurg. 1987;67(2):250-7.

229.   Jessurun CAC, Hulsbergen AFC, Cho LD, Aglio LS, Nandoe Tewarie RDS, Broekman MLD. Evidence-based dexamethasone dosing in malignant brain tumors: what do we really know? J Neuro-Oncol. 2019;144(2):249-64.

230.   Rosso L, Brock CS, Gallo JM, Saleem A, Price PM, Turkheimer FE, et al. A new model for prediction of drug distribution in tumor and normal tissues: pharmacokinetics of Temozolomide in glioma patients. Cancer Res. 2009;69(1):120.

231.   Clark MJ, Homer N, O'Connor BD, Chen Z, Eskin A, Lee H, et al. U87MG decoded: the genomic sequence of a cytogenetically aberrant human cancer cell line. PLoS Gen. 2010;6(1):1000832.

232.   Uhlen M, Zhang C, Lee S, Sjöstedt E, Fagerberg L, Bidkhori G, et al. A pathology atlas of the human cancer transcriptome. Science. 2017;357(6352):2507.

233.   Matthews LC, Berry AA, Morgan DJ, Poolman TM, Bauer K, Kramer F, et al. Glucocorticoid receptor regulates accurate chromosome segregation and is associated with malignancy. Proc Natl Acad Sci USA. 2015;112(17):5479-84.

234.   Chen Z, Lan X, Wu D, Sunkel B, Ye Z, Huang J, et al. Ligand-dependent genomic function of glucocorticoid receptor in triple-negative breast cancer. Nat Commun. 2015;6:8323.

235.   Vockley CM, D'Ippolito AM, McDowell IC, Majoros WH, Safi A, Song L, et al. Direct GR binding sites potentiate clusters of TF binding across the human genome. Cell. 2016;166(5):1269-81.

236.   Binder EB. The role of FKBP5, a co-chaperone of the glucocorticoid receptor in the pathogenesis and therapy of affective and anxiety disorders. Psychoneuroendocrinology. 2009;34:186-95.

237.   Ronchetti S, Migliorati G, Riccardi C. GILZ as a Mediator of the Anti-Inflammatory Effects of Glucocorticoids. Front Endocrinol. 2015;6:170.

238.   Shipp LE, Lee JV, Yu C-Y, Pufall M, Zhang P, Scott DK, et al. Transcriptional regulation of human dual specificity protein phosphatase 1 (DUSP1) gene by glucocorticoids. PloS One. 2010;5(10):e13754-e.

239.   Shang Z-F, Huang B, Xu Q-Z, Zhang S-M, Fan R, Liu X-D, et al. Inactivation of DNA-Dependent Protein Kinase leads to spindle disruption and mitotic catastrophe with attenuated Checkpoint Protein 2 phosphorylation in response to DNA damage. Cancer Res. 2010;70(9):3657.

240.   Cruz C, Castroviejo-Bermejo M, Gutiérrez-Enríquez S, Llop-Guevara A, Ibrahim YH, Gris-Oliver A, et al. RAD51 foci as a functional biomarker of homologous recombination repair and PARP inhibitor resistance in germline BRCA-mutated breast cancer. Ann Oncol. 2018;29(5):1203-10.

241.   Gachechiladze M, Škarda J, Soltermann A, Joerger M. RAD51 as a potential surrogate marker for DNA repair capacity in solid malignancies. Int J Cancer. 2017;141(7):1286-94.

242.   Markova E, Vasilyev S, Belyaev I. 53BP1 foci as a marker of tumor cell radiosensitivity. Neoplasma. 2015;62(5):770-6.

243.   Bártová E, Legartová S, Dundr M, Suchánková J. A role of the 53BP1 protein in genome protection: structural and functional characteristics of 53BP1-dependent DNA repair. Aging. 2019;11(8):2488-511.

244.   Borràs M, Armengol G, De Cabo M, Barquinero JF, Barrios L. Comparison of methods to quantify histone H2AX phosphorylation and its usefulness for prediction of radiosensitivity. Int J Radiat Biol. 2015;91(12):915-24.

245.   Nagelkerke A, Span PN. Staining Against Phospho-H2AX (γ-H2AX) as a Marker for DNA Damage and Genomic Instability in Cancer Tissues and Cells. Adv Exp Med Biol. 2016;899:1-10.

246.   Williams AB, Schumacher B. p53 in the DNA-Damage-Repair Process. CSH Perspect Med. 2016;6(5).

247.   Murphy SH, Suzuki K, Downes M, Welch GL, De Jesus P, Miraglia LJ, et al. Tumor suppressor protein (p)53, is a regulator of NF-κB repression by the glucocorticoid receptor. Proceedings of the National Academy of Sciences. 2011;108(41):17117-22.

248.   Chodankar R, Wu D-Y, Gerke DS, Stallcup MR. Selective Coregulator Function and Restriction of Steroid Receptor Chromatin Occupancy by Hic-5. Mol Endocrinol. 2015;29(5):716-29.

249.   Gallenne T, Ross KN, Visser NL, Salony, Desmet CJ, Wittner BS, et al. Systematic functional perturbations uncover a prognostic genetic network driving human breast cancer. Oncotarget. 2017;8(13):20572-87.

250.   Menendez D, Nguyen T-A, Freudenberg JM, Mathew VJ, Anderson CW, Jothi R, et al. Diverse stresses dramatically alter genome-wide p53 binding and transactivation landscape in human cancer cells. Nucleic Acids Res. 2013;41(15):7286-301.

251.   Szklarczyk D, Gable AL, Lyon D, Junge A, Wyder S, Huerta-Cepas J, et al. STRING v11: protein-protein association networks with increased coverage,

supporting functional discovery in genome-wide experimental datasets. Nucleic Acids Res. 2019;47(D1):D607-d13.

252. San Filippo J, Sung P, Klein H. Mechanism of eukaryotic homologous recombination. Annu Rev Biochem. 2008;77(1):229-57.

253. De Bosscher K, Berghe WV, Beck IME, Van Molle W, Hennuyer N, Hapgood J, et al. A fully dissociated compound of plant origin for inflammatory gene repression. Proc Natl Acad Sci USA. 2005;102(44):15827.

254. Lesovaya E, Yemelyanov A, Swart AC, Swart P, Haegeman G, Budunova I. Discovery of Compound A--a selective activator of the glucocorticoid receptor with anti-inflammatory and anti-cancer activity. Oncotarget. 2015;6(31):30730-44.

255. Robertson S, Allie-Reid F, Vanden Berghe W, Visser K, Binder A, Africander D, et al. Abrogation of glucocorticoid receptor dimerization correlates with dissociated glucocorticoid behavior of compound a. J Biol Chem. 2010;285(11):8061-75.

256. Markham A, Bryson HM. Deflazacort. Drugs. 1995;50(2):317-33.

257. Parente L. Deflazacort: therapeutic index, relative potency and equivalent doses versus other corticosteroids. BMC Pharmacol Toxico. 2017;18(1):1-.

258. Del Rosso A, Cinelli M, Guiducci S, Pignone A, Fibbi G, Margheri F, et al. Deflazacort modulates the fibrinolytic pattern and reduces uPA-dependent chemioinvasion and proliferation in rheumatoid arthritis synoviocytes. Rheumatology. 2005;44(10):1255-62.

259. Pagano G, Bruno A, Cavallo-Perin P, Cesco L, Imbimbo B. Glucose intolerance after short-term administration of corticosteroids in healthy subjects: prednisone, deflazacort, and betamethasone. Arch Intern Med. 1989;149(5):1098-101.

260. Bruno A, Pagano G, Benzi L, Di Ciani G, Spallone V, Calabrese G, et al. Change in glucose metabolism after long-term treatment with deflazacort and betamethasone. Eur J Clin Pharmacol. 1992;43(1):47-50.

261. Pavesio CE, DeCory HH. Treatment of ocular inflammatory conditions with loteprednol etabonate. Brit J Ophthalmol. 2008;92(4):455.

262. Comstock TL, Sheppard JD. Loteprednol etabonate for inflammatory conditions of the anterior segment of the eye: twenty years of clinical experience with a retrometabolically designed corticosteroid. Expert Opin Pharmaco. 2018;19(4):337-53.

263. De Witt Hamer PC, Van Tilborg AAG, Eijk PP, Sminia P, Troost D, Van Noorden CJF, et al. The genomic profile of human malignant glioma is altered early in primary cell culture and preserved in spheroids. Oncogene. 2008;27(14):2091-6.

264.   Torsvik A, Stieber D, Enger PØ, Golebiewska A, Molven A, Svendsen A, et al. U-251 revisited: genetic drift and phenotypic consequences of long-term cultures of glioblastoma cells. Cancer Med. 2014;3(4):812-24.

265.   Lin K-T, Wang L-H. New dimension of glucocorticoids in cancer treatment. Steroids. 2016;111:84-8.

266.   Ortega-Martínez S. Dexamethasone acts as a radiosensitizer in three astrocytoma cell lines via oxidative stress. Redox Biol. 2015;5:388-97.

267.   Gorman AM, Hirt UA, Orrenius S, Ceccatelli S. Dexamethasone pre-treatment interferes with apoptotic death in glioma cells. Neuroscience. 2000;96(2):417-25.

268.   González-Orozco JC, Hansberg-Pastor V, Valadez-Cosmes P, Nicolas-Ortega W, Bastida-Beristain Y, Fuente-Granada M, et al. Activation of membrane progesterone receptor-alpha increases proliferation, migration, and invasion of human glioblastoma cells. Mol Cell Endocrinol. 2018;477:81-9.

269.   Atif F, Yousuf S, Espinosa-Garcia C, Sergeeva E, Stein DG. Progesterone Treatment Attenuates Glycolytic Metabolism and Induces Senescence in Glioblastoma. Sci Rep. 2019;9(1):988.

270.   Goodwin JF, Schiewer MJ, Dean JL, Schrecengost RS, de Leeuw R, Han S, et al. A hormone–DNA repair circuit governs the response to genotoxic insult. Cancer Discov. 2013;3(11):1254.

271.   Medunjanin S, Weinert S, Schmeisser A, Mayer D, Braun-Dullaeus RC. Interaction of the double strand break repair kinase DNA-PK and estrogen receptor-α. Mol Biol Cell. 2010;21(9):1620-8.

272.   Giffin W, Kwast-Welfeld J, Rodda DJ, Préfontaine GG, Traykova-Andonova M, Zhang Y, et al. Sequence-specific DNA binding and transcription factor phosphorylation by Ku autoantigen/DNA-dependent protein kinase: Phosphorylation of Ser-527 of the rat glucocorticoid receptor. J Biol Chem. 1997;272(9):5647-58.

273.   Prionisti I, Bühler LH, Walker PR, Jolivet RB. Harnessing microglia and macrophages for the treatment of glioblastoma. Front Pharmacol. 2019;10:506.

274.   Wang Q, He Z, Huang M, Liu T, Wang Y, Xu H, et al. Vascular niche IL-6 induces alternative macrophage activation in glioblastoma through HIF-2α. Nat Commun. 2018;9(1):559.

275.   a Dzaye OD, Hu F, Derkow K, Haage V, Euskirchen P, Harms C, et al. Glioma stem cells but not bulk glioma cells upregulate IL-6 secretion in microglia/brain macrophages via Toll-Like Receptor 4 signaling. J Neuropathol Exp Neurol. 2016;75(5):429-40.

276.   Hou Z, Yang J, Wang H, Liu D, Zhang H. A Potential Prognostic Gene Signature for Predicting Survival for Glioblastoma Patients. Biomed Res Int. 2019;2019:9506461.

277.	Cheng WY, Kandel JJ, Yamashiro DJ, Canoll P, Anastassiou D. A multi-cancer mesenchymal transition gene expression signature is associated with prolonged time to recurrence in glioblastoma. PLoS One. 2012;7(4):e34705.

278.	Chai R, Zhang K, Wang K, Li G, Huang R, Zhao Z, et al. A novel gene signature based on five glioblastoma stem-like cell relevant genes predicts the survival of primary glioblastoma. J Cancer Res Clin Oncol. 2018;144(3):439-47.

279.	Fan Z, Sehm T, Rauh M, Buchfelder M, Eyupoglu IY, Savaskan NE. Dexamethasone alleviates tumor-associated brain damage and angiogenesis. PLoS One. 2014;9(4):e93264.

280.	Kumaravel TS, Jha AN. Reliable comet assay measurements for detecting DNA damage induced by ionising radiation and chemicals. Mutat Res Genet Toxicol Environ Mutagen. 2006;605(1):7-16.

281.	Ivashkevich A, Redon CE, Nakamura AJ, Martin RF, Martin OA. Use of the γ-H2AX assay to monitor DNA damage and repair in translational cancer research. Cancer Lett. 2012;327(1):123-33.

282.	Meyer B, Voss K-O, Tobias F, Jakob B, Durante M, Taucher-Scholz G. Clustered DNA damage induces pan-nuclear H2AX phosphorylation mediated by ATM and DNA-PK. Nucleic Acids Res. 2013;41(12):6109-18.

283.	Moeglin E, Desplancq D, Conic S, Oulad-Abdelghani M, Stoessel A, Chiper M, et al. Uniform widespread nuclear phosphorylation of Histone H2AX is an indicator of lethal DNA replication stress. Cancers. 2019;11(3):355.

284.	Ceccaldi R, Rondinelli B, D'Andrea AD. Repair Pathway Choices and Consequences at the Double-Strand Break. Trends Cell Biol. 2016;26(1):52-64.

285.	Bunting SF, Callén E, Wong N, Chen H-T, Polato F, Gunn A, et al. 53BP1 inhibits homologous recombination in Brca1-deficient cells by blocking resection of DNA breaks. Cell. 2010;141(2):243-54.

286.	Shandilya J, Roberts SGE. The transcription cycle in eukaryotes: From productive initiation to RNA polymerase II recycling. BBA-Gene Regul Mech. 2012;1819(5):391-400.

287.	Dulken BW, Leeman DS, Boutet SC, Hebestreit K, Brunet A. Single-Cell Transcriptomic Analysis Defines Heterogeneity and Transcriptional Dynamics in the Adult Neural Stem Cell Lineage. Cell Rep. 2017;18(3):777-90.

288.	Nguyen A, Khoo WH, Moran I, Croucher PI, Phan TG. Single cell RNA sequencing of rare immune cell populations. Front Immunol. 2018;9:1553.

289.	Zhang L, Zhang Z. Recharacterizing tumor-infiltrating lymphocytes by single-cell RNA sequencing. Cancer Immunol Res. 2019;7(7):1040.

290.	Bergiers I, Andrews T, Vargel Bölükbaşı Ö, Buness A, Janosz E, Lopez-Anguita N, et al. Single-cell transcriptomics reveals a new dynamical function of transcription factors during embryonic hematopoiesis. eLife. 2018;7:e29312.

291. Gao R, Kim C, Sei E, Foukakis T, Crosetto N, Chan L-K, et al. Nanogrid single-nucleus RNA sequencing reveals phenotypic diversity in breast cancer. Nat Commun. 2017;8(1):228.

292. Goldstein LD, Chen Y-JJ, Dunne J, Mir A, Hubschle H, Guillory J, et al. Massively parallel nanowell-based single-cell gene expression profiling. BMC Genomics. 2017;18(1):519.

293. Kim C, Gao R, Sei E, Brandt R, Hartman J, Hatschek T, et al. Chemoresistance evolution in triple-negative breast cancer delineated by single-cell sequencing. Cell. 2018;173(4):879-93.e13.

294. AlJanahi AA, Danielsen M, Dunbar CE. An Introduction to the Analysis of Single-Cell RNA-Sequencing Data. Molecular Therapy - Methods & Clinical Development. 2018;10:189-96.

295. Mercer Tim R, Neph S, Dinger Marcel E, Crawford J, Smith Martin A, Shearwood A-Marie J, et al. The human mitochondrial transcriptome. Cell. 2011;146(4):645-58.

296. Scialdone A, Natarajan KN, Saraiva LR, Proserpio V, Teichmann SA, Stegle O, et al. Computational assignment of cell-cycle stage from single-cell transcriptome data. Methods. 2015;85:54-61.

297. Dulken BW, Leeman DS, Boutet SC, Hebestreit K, Brunet A. Single-Cell Transcriptomic Analysis Defines Heterogeneity and Transcriptional Dynamics in the Adult Neural Stem Cell Lineage. Cell Reports. 2017;18(3):777-90.

298. Stegle O, Teichmann SA, Marioni JC. Computational and analytical challenges in single-cell transcriptomics. Nat Rev Genet. 2015;16:133.

299. L. Lun AT, Bach K, Marioni JC. Pooling across cells to normalize single-cell RNA sequencing data with many zero counts. Genome Biology. 2016;17(1):75.

300. Lun A, McCarthy D, JC. M. A step-by-step workflow for low-level analysis of single-cell RNA-seq data with Bioconductor. F1000 Research. 2016;5(2122).

301. Kobak D, Berens P. The art of using t-SNE for single-cell transcriptomics. bioRxiv. 2019:453449.

302. Brennecke P, Anders S, Kim JK, Kołodziejczyk AA, Zhang X, Proserpio V, et al. Accounting for technical noise in single-cell RNA-seq experiments. Nature Methods. 2013;10:1093.

303. Marinov GK, Williams BA, McCue K, Schroth GP, Gertz J, Myers RM, et al. From single-cell to cell-pool transcriptomes: Stochasticity in gene expression and RNA splicing. Genome Research. 2014;24(3):496-510.

304. The EPC, Dunham I, Kundaje A, Aldred SF, Collins PJ, Davis CA, et al. An integrated encyclopedia of DNA elements in the human genome. Nature. 2012;489:57.

305.   Wang J, Zhuang J, Iyer S, Lin X, Whitfield TW, Greven MC, et al. Sequence features and chromatin structure around the genomic regions bound by 119 human transcription factors. Genome Research. 2012;22(9):1798-812.

306.   Wang J, Zhuang J, Iyer S, Lin X-Y, Greven MC, Kim B-H, et al. Factorbook.org: a Wiki-based database for transcription factor-binding data generated by the ENCODE consortium. Nucleic Acids Research. 2012;41(D1):D171-D6.

307.   Battich N, Stoeger T, Pelkmans L. Image-based transcriptomics in thousands of single human cells at single-molecule resolution. Nat Methods. 2013;10:1127.

308.   Mueller F, Senecal A, Tantale K, Marie-Nelly H, Ly N, Collin O, et al. FISH-quant: automatic counting of transcripts in 3D FISH images. Nat Methods. 2013;10:277.

309.   Iacono G, Massoni-Badosa R, Heyn H. Single-cell transcriptomics unveils gene regulatory network plasticity. Genome Biol. 2019;20(1):110.

310.   Ilicic T, Kim JK, Kolodziejczyk AA, Bagger FO, McCarthy DJ, Marioni JC, et al. Classification of low quality cells from single-cell RNA-seq data. Genome Biol. 2016;17(1):29.

311.   McCarthy DJ, Campbell KR, Lun ATL, Wills QF. Scater: pre-processing, quality control, normalization and visualization of single-cell RNA-seq data in R. Bioinformatics. 2017;33(8):1179-86.

312.   ATL L, DJ M, JC. M. A step-by-step workflow for low-level analysis of single-cell RNA-seq data with Bioconductor [version 2; peer review: 3 approved, 2 approved with reservations] . F1000 Research. 2016;5(2122).

313.   Zhao Q, Wang J, Levichkin IV, Stasinopoulos S, Ryan MT, Hoogenraad NJ. A mitochondrial specific stress response in mammalian cells. EMBO J. 2002;21(17):4411-9.

314.   Hsiao CJ, Tung P, Blischak JD, Burnett JE, Barr KA, Dey KK, et al. Characterizing and inferring quantitative cell cycle phase in single-cell RNA-seq data analysis. bioRxiv. 2020:526848.

315.   Luecken MD, Theis FJ. Current best practices in single-cell RNA-seq analysis: a tutorial. Mol Syst Biol. 2019;15(6):e8746.

316.   Li G, Tian L, Goodyer W, Kort EJ, Buikema JW, Xu A, et al. Single cell expression analysis reveals anatomical and cell cycle-dependent transcriptional shifts during heart development. Development. 2019;146(12):dev173476.

317.   Singh Amar M, Chappell J, Trost R, Lin L, Wang T, Tang J, et al. Cell-Cycle Control of Developmentally Regulated Transcription Factors Accounts for Heterogeneity in Human Pluripotent Cells. Stem Cell Rep. 2013;1(6):532-44.

318.   Cao J, Zhou W, Steemers F, Trapnell C, Shendure J. Characterizing the temporal dynamics of gene expression in single cells with sci-fate. bioRxiv. 2019:666081.

319.   Weikum ER, Knuesel MT, Ortlund EA, Yamamoto KR. Glucocorticoid receptor control of transcription: precision and plasticity via allostery. Nat Rev Mol Cell Biol. 2017;18(3):159-74.

320.   Zeng T, Dai H. Single-Cell RNA sequencing-based computational analysis to describe disease heterogeneity. Front Genet. 2019;10:629.

321.   Kuznetsova T, Wang S-Y, Rao NA, Mandoli A, Martens JHA, Rother N, et al. Glucocorticoid receptor and nuclear factor kappa-b affect three-dimensional chromatin organization. Genome Biology. 2015;16(1):264.

322.   Mishra A, Hawkins RD. Three-dimensional genome architecture and emerging technologies: looping in disease. Genome Med. 2017;9(1):87.

323.   Khong A, Matheny T, Jain S, Mitchell SF, Wheeler JR, Parker R. The Stress Granule Transcriptome Reveals Principles of mRNA Accumulation in Stress Granules. Mol Cell. 2017;68(4):808-20.e5.

324.   Hoa M, Olszewski R, Li X, Taukulis I, Gu S, DeTorres A, et al. Characterizing Adult Cochlear Supporting Cell Transcriptional Diversity Using Single-Cell RNA-Seq: Validation in the Adult Mouse and Translational Implications for the Adult Human Cochlea. Frontiers in molecular neuroscience. 2020;13:13-.

325.   Mueller F, Senecal A, Tantale K, Marie-Nelly H, Ly N, Collin O, et al. FISH-quant: automatic counting of transcripts in 3D FISH images. Nature Methods. 2013;10:277.

326.   Tsanov N, Samacoits A, Chouaib R, Traboulsi A-M, Gostan T, Weber C, et al. smiFISH and FISH-quant - a flexible single RNA detection approach with super-resolution capability. Nucleic Acids Res. 2016;44(22):e165.

327.   Krishan J-H, Elanchelian P, Sam O. Stimulation of MAPK-phosphatase 1 gene expression by glucocorticoids occurs through a tethering mechanism involving C/EBP. J Mol Endocrinol. 2008;41(4):239-49.

328.   Cenciarini M, Valentino M, Belia S, Sforna L, Rosa P, Ronchetti S, et al. Dexamethasone in Glioblastoma Multiforme therapy: mechanisms and controversies. Front Mol Neurosci. 2019;12:65.

329.   McDowell IC, Barrera A, D'Ippolito AM, Vockley CM, Hong LK, Leichter SM, et al. Glucocorticoid receptor recruits to enhancers and drives activation by motif-directed binding. Genome Res. 2018;28(9):1272-84.

330.   Bekhbat M, Rowson SA, Neigh GN. Checks and balances: The glucocorticoid receptor and NFκB in good times and bad. Front Neuroendocrin. 2017;46:15-31.

331.   Cenciarini M, Valentino M, Belia S, Sforna L, Rosa P, Ronchetti S, et al. Dexamethasone in Glioblastoma Multiforme therapy: mechanisms and controversies. Front Mol Neurosci. 2019;12:65-.

332.   Silbergeld DL, Rostomily RC, Alvord EC. The cause of death in patients with glioblastoma is multifactorial. J Neuro-Oncol. 1991;10(2):179-85.

333.   Wong ET, Swanson KD. Dexamethasone—Friend or Foe for Patients With Glioblastoma? JAMA Neurol. 2019;76(3):247-8.

334.   Kostaras X, Cusano F, Kline GA, Roa W, Easaw J, the Alberta Provincial CNSTT. Use of dexamethasone in patients with high-grade glioma: a clinical practice guideline. Curr Oncol. 2014;21(3):e493-e503.

335.   Faivre G, Pentsova E, Demopoulos A, Taillibert S, Rosenblum M, Omuro A. Clinical Reasoning: Worsening neurologic symptoms in a brain tumor patient. Neurology. 2015;85(7):57-61.

336.   Sundahl N, Bridelance J, Libert C, De Bosscher K, Beck IM. Selective glucocorticoid receptor modulation: New directions with non-steroidal scaffolds. Pharmacol Therapeut. 2015;152:28-41.

337.   Newton R, Holden NS. Separating transrepression and transactivation: a distressing divorce for the glucocorticoid receptor? Mol Pharmacol. 2007;72(4):799.

338.   Schäcke H, Schottelius A, Döcke W-D, Strehlke P, Jaroch S, Schmees N, et al. Dissociation of transactivation from transrepression by a selective glucocorticoid receptor agonist leads to separation of therapeutic effects from side effects. Proc Natl Acad Sci. 2004;101(1):227.

339.   Presman DM, Ogara MF, Stortz M, Alvarez LD, Pooley JR, Schiltz RL, et al. Live cell imaging unveils multiple domain requirements for in vivo dimerization of the glucocorticoid receptor. PLoS Biol. 2014;12(3):e1001813.

340.   Rauner M, Thiele S, Sinningen K, Winzer M, Salbach-Hirsch J, Gloe I, et al. Effects of the selective glucocorticoid receptor modulator Compound A on bone metabolism and inflammation in male mice with collagen-induced arthritis. Endocrinology. 2013;154(10):3719-28.

341.   Cazzalini O, Scovassi AI, Savio M, Stivala LA, Prosperi E. Multiple roles of the cell cycle inhibitor p21CDKN1A in the DNA damage response. Mut Res. 2010;704(1):12-20.

342.   Aasland D, Götzinger L, Hauck L, Berte N, Meyer J, Effenberger M, et al. Temozolomide induces senescence and repression of DNA repair pathways in Glioblastoma cells via activation of ATR–CHK1, p21, and NF-κB. Cancer Res. 2019;79(1):99.

343.   Kokunai T, Tamaki N. Relationship between expression of p21(WAF1/CIP1) and radioresistance in human gliomas. Jpn J Canc Res. 1999;90(6):638-46.

344. Tirado-Hurtado I, Fajardo W, Pinto JA. DNA Damage Inducible Transcript 4 gene: The switch of the metabolism as potential target in cancer. Front Oncol. 2018;8:106.

345. Foltyn M, Luger A-L, Lorenz NI, Sauer B, Mittelbronn M, Harter PN, et al. The physiological mTOR complex 1 inhibitor DDIT4 mediates therapy resistance in glioblastoma. Br J Cancer. 2019;120(5):481-7.

346. Michels J, Kepp O, Senovilla L, Lissa D, Castedo M, Kroemer G, et al. Functions of Bcl-XL at the interface between cell death and metabolism. Int J Cell Biol. 2013;2013:705294.

347. Pérez-Caro M, Bermejo-Rodríguez C, González-Herrero I, Sánchez-Beato M, Piris MA, Sánchez-García I. Transcriptomal profiling of the cellular response to DNA damage mediated by Slug (Snai2). Br J Cancer. 2008;98(2):480-8.

348. Fiorini E, Veghini L, Corbo V. Modeling cell communication in cancer with organoids: making the complex simple. Front Cell Dev Biol. 2020;8(166).

349. Hubert CG, Rivera M, Spangler LC, Wu Q, Mack SC, Prager BC, et al. A three-dimensional organoid culture system derived from human glioblastomas recapitulates the hypoxic gradients and cancer stem cell heterogeneity of tumors found in vivo. Cancer Res. 2016;76(8):2465.

350. Perrin SL, Samuel MS, Koszyca B, Brown MP, Ebert LM, Oksdath M, et al. Glioblastoma heterogeneity and the tumour microenvironment: implications for preclinical research and development of new treatments. Biochem Soc Trans. 2019;47(2):625-38.

351. D'Alessio A, Proietti G, Sica G, Scicchitano BM. Pathological and molecular features of Glioblastoma and its peritumoral tissue. Cancers. 2019;11(4):469.

352. Zhang Y, Chen K, Sloan SA, Bennett ML, Scholze AR, O'Keeffe S, et al. An RNA-sequencing transcriptome and splicing database of glia, neurons, and vascular cells of the cerebral cortex. J Neurosci. 2014;34(36):11929-47.

353. Piechota M, Korostynski M, Golda S, Ficek J, Jantas D, Barbara Z, et al. Transcriptional signatures of steroid hormones in the striatal neurons and astrocytes. BMC Neurosci. 2017;18(1):37.

354. Lu S-M, Long Y-T. Confined Nanopipette-A new microfluidic approach for single cell analysis. TrAC-Trend Anal Chem. 2019;117:39-46.

355. Bulbul G, Chaves G, Olivier J, Ozel RE, Pourmand N. Nanopipettes as monitoring probes for the single living cell: State of the art and future directions in molecular biology. Cells. 2018;7(6):55.

356. Cao Y, Hjort M, Chen H, Birey F, Leal-Ortiz SA, Han CM, et al. Nondestructive nanostraw intracellular sampling for longitudinal cell monitoring. Proc Natl Acad Sci USA. 2017;114(10):E1866-E74.